Characterising the effect of microwave treatment on bio-leaching of coarse, massive sulphide ore particles

by

Edson Charikinya

Dissertation presented for the Degree

of

DOCTOR OF PHILOSOPHY

(Extractive Metallurgical Engineering)

in the Faculty of Engineering
at Stellenbosch University

Supervisor
Prof S. M. Bradshaw

December 2015

Declaration

By submitting this dissertation electronically, I declare that the entirety of the work contained therein is my own, original work, that I am the sole author thereof (save to the extent explicitly otherwise stated), that reproduction and publication thereof by Stellenbosch University will not infringe any third party rights and that I have not previously in its entirety or in part submitted it for obtaining any qualification.

Date: 16-11-2015

Abstract

The aim of this work was to determine if microwave treatment of a typical massive sulphide ore, prior to bio-leaching would induce micro-cracks and enhance value mineral exposure resulting in improved bio-leaching metal extraction and kinetics. Using X-ray Computed tomography (XCT) and Quantitative Evaluation of Minerals by Scanning Electron Microscopy (QEMSCAN) image analysis techniques, the degree of microwave induced damage, and the effect of this damage on mineral exposure, was quantified directly for the first time, in this study. Ore sample preparation was carried out using a primary jaw crusher followed by secondary crushing by either high pressure grinding rolls (HPGR) or a cone crusher. Particles investigated consisted of small (-5+4.75) mm, medium (-16+9.5) mm, and large (-25+19) mm HPGR and cone crushed particles. XCT and QEMSCAN results showed the presence of microwave induced cracks within the cone and HPGR crushed particles, treated at a microwave power density of 1×10^9 W/m$^3_{abs}$ and exposure time 1.00 s. A qualitative analysis of the cracks, showed that the cracks consisted of both interphase trans-granular and grain boundary cracks. Both XCT and QEMSCAN analysis results showed that microwave treatment resulted in a significant increase of over 500% in crack volume for both modes of prior comminution at all particle sizes. Measurements of specific interfacial areas of particles before and after microwave treatment using XCT showed average losses in interfacial area of 31%, 23% and 16% for small (-5+4.75) mm, medium (-16+9.5) mm, and large (-25+19) mm particles. This demonstrated quantitatively for the first time, that microwave treatment of sulphide ores results in both grain boundary and trans-granular fracture. Value mineral grain exposure analysis was carried out on the XCT 3D data of particles before and after microwave treatment. The results showed an increase in the degree of sulphide grain exposure of 28%, 26% and 15% for small medium and large particles respectively. This is the first time that microwave particle damage and enhanced mineral exposure has been successfully quantified experimentally using XCT and image analysis techniques.

Column leaching experiments to simulate heap bio-leaching environment, were carried out over 350 days to assess the downstream benefits of microwave treatment of heap leaching feed. The results showed that microwave pre-treatment of crushed ore for bio-leaching, will lead to improved leaching recovery. Improvements in overall Zn metal recoveries of 26%, 24% and 23% were observed for small (-5+4.75) mm, medium (-16+9.5) mm, and large (-25+19) mm microwave treated particles. The enhanced metal recovery seen for microwave treated

material correlates well with the crack volume measurements and mineral exposure results. The column leaching results showed that medium (-16+9.5) mm sized microwave treated particles had a 10.1% higher metal recovery compared to small (-5+4.75) mm untreated particles. A comparison of overall metal recoveries of microwave treated cone and HPGR crushed ore particles showed that the mode of prior comminution gave no significant difference in recoveries at all sizes. This suggests that microwave treatment reduces the influence of mode of comminution on bio-leaching recovery. An investigation of the dissolution of sulphide grains in selected particles, using XCT 3D image analysis techniques over the course of 350 days of leaching, showed greater sub-surface conversion of minerals in microwave treated particles compared to untreated. Analysis of the cracks over the period of leaching using XCT data, showed a growth in microwave induced crack networks over 350 days of leaching. This suggest that microwave induced cracks accelerate reagent diffusion into the particles resulting in sub-surface conversion of minerals, during bio-leaching.

A bonded particle model (BPM) was developed to simulate a multiphase massive sulphide ore approximating the ore used in the physical experimental investigations. The developed ore model consisted of pyrite, sphalerite and quartz phases which were identified as the major phases in the ore used in the experiment. The resulting microwave induced crack patterns for different model resolution were compared against those obtained from physical experiments. The results showed that model resolution has a significant effect on observed microwave induced crack damage and patterns. It was observed that cracks in models with different resolution propagate in a different pattern despite having the same macro-mechanical properties. Crack patterns obtained for higher models were observed to compare well with crack patterns observed from physical microwave treatment experiments. It can be concluded that model calibration using the usual simulated UCS and Brazilian tests alone is not adequate to fix the model resolution, for simulations of thermal induced cracks. These results show that model specimen resolution has a significant effect on observed micro crack damage and that the minimum base material “particle” size is not a free parameter. The effect of absorbent phase content on microwave induced damage was investigated for the first time using a high resolution model. Damage maps which show the percentage of micro-cracks as a function of power density and exposure time for different ternary ores and absorbent phase content were constructed. It has been shown that for the same power density and energy input, the fraction of micro-fractures induced by microwave treatment considerably depends on absorbent phase grain content.

Opsomming

Die doel van hierdie studie was om te bepaal of mikrogolfbehandeling van ŉ tipiese massiewe sulfiederts, voor biologing, mikrokrake sal induseer en die waarde van mineraalblootstelling sal verhoog, wat sal lei tot verbeterde biologing-metaalwinning en -kinetika. Met behulp van die beeldontledingstegnieke X-straal-berekende tomografie (XBT) en kwantitatiewe evaluering van minerale deur skanderingelektronmikroskopie (KEMSKAN) is die graad van mikrogolf-geïnduseerde skade, en die uitwerking van hierdie skade op mineraalblootstelling, direk vir die eerste keer in hierdie studie gekwantifiseer.

Ertsmonstervoorbereiding is uitgevoer met behulp van primêre kakebrekermateriaal wat in twee dele verdeel is vir verdere vergruising deur óf ŉ hoëdrukmaalroller (HDMR) óf ŉ keëlbreker. Deeltjies wat ondersoek is, het bestaan uit klein (-5+4.75) mm, middelslag-

(-16+9.5) mm en groot (-25+19) mm HDMR- en keël-vergruisde deeltjies. XBT- en KEMSKAN-resultate het gewys op die teenwoordigheid van mikrogolf-geïnduseerde krake in die HDMR- en keël-vergruisde deeltjies wat teen ŉ mikrogolfkragdigtheid van 1× 109 W/m3abs en blootstellingstyd 1.00 s behandel is.

ŉ Kwalitatiewe analise van die krake het getoon dat die krake uit sowel interfase-transkorrel- as korrelgrenskrake bestaan. Die resultate van sowel die XBT- as die KEMSKAN-analises het getoon dat mikrogolfbehandeling tot ŉ aanmerklike toename van meer as 500% in kraakvolume vir albei middele van voorvergruising van alle deeltjiegroottes lei. Metings van spesifieke tussenvlakoppervlaktes van deeltjies voor en ná mikrogolfbehandeling met XBT het gemiddelde verliese in tussenvlakoppervlakte van 31%, 23% en 16% vir klein (-5+4.75) mm, middelslag- (-16+9.5) mm en groot (-25+19) mm deeltjies getoon. Dit het kwantitatief vir die eerste keer getoon dat mikrogolfbehandeling van sulfiederts tot sowel korrelgrens- as transkorrel-frakture lei.

ŉ Analise van die waarde van mineraalkorrelblootstelling is uitgevoer op die XBT 3D data van deeltjies voor en ná mikrogolfbehandeling. Die resultate het ŉ toename in die graad van sulfiedkorrelblootstelling van 28%, 26% en 15% vir onderskeidelik klein, middelslag- en groot deeltjies getoon. Dit is die eerste keer wat mikrogolfdeeltjieskade en versterkte mineraalblootstelling suksesvol eksperimenteel gekwantifiseer is met behulp van XBT- en beeldanalise-tegnieke.

Kolomlogingseksperimente om ’n stapelbiologingsomgewing te simuleer, is oor 350 dae uitgevoer om die stroomaf-voordele van mikrogolfbehandeling van stapellogingstoevoer te assesseer. Die resultate het getoon dat mikrogolf-voorbehandeling van vergruisde erts vir biologing tot verbeterde logingswinning sal lei. Verbeterings in algehele Zn-metaalwinnings van 26%, 24% en 23% is waargeneem vir klein (-5+4.75) mm, middelslag- (-16+9.5) mm en groot (-25+19) mm mikrogolfbehandelde deeltjies. Die verbeterde mineraalwinning vir mikrogolfbehandelde materiaal korreleer goed met die kraakvolumemetings- en mineraalblootstellingsresultate. Die kolomlogingsresultate het getoon dat die middelslaggrootte (-16+9.5) mm mikrogolfbehandelde deeltjies ’n 10.1% hoër metaalwinning het in vergelyking met klein (-5+4.75) mm onbehandelde deeltjies.

’n Vergelyking van algehele metaalwinning van mikrogolfbehandelde keël- en HPGR-vergruisde ertsdeeltjies het getoon dat die middel van voorvergruising geen aanmerklike verandering in winning teen alle groottes meegebring het nie. Dit doen aan die hand dat mikrogolfbehandeling die invloed van middel van vergruising op biologingswinning verminder. ’n Ondersoek na die oplossing van sulfiedkorrels in geselekteerde deeltjies, met behulp van XBT 3D beeldanalisetegnieke oor die verloop van 350 dae van loging, het groter suboppervlak-omsetting van minerale in mikrogolfbehandelde deeltjies getoon in vergelyking met onbehandelde deeltjies. ’n Analise van die krake oor die logingstydperk met behulp van XBT-data het ’n toename in mikrogolfgeïnduseerde kraaknetwerke oor 350 dae van loging getoon. Dit doen aan die hand dat mikrogolfgeïnduseerde krake reagensdiffusie in die deeltjies versnel, wat tot suboppervlak-omsetting van minerale tydens biologing lei.

’n Gebonde deeltjiemodel is ontwikkel om ’n veelfasige massiewe sulfiederts te simuleer wat soortgelyk is aan die erts wat in die fisiese eksperimente gebruik is. Die ontwikkelde ertsmodel het uit piriet-, sfaleriet- en kwarts-fases bestaan, wat geïdentifiseer is as die belangrikste fases in die erts wat in die eksperiment gebruik is. Die resultante mikrogolfgeïnduseerde kraakpatrone vir verskillende modelresolusies is met dié vergelyk wat uit die fisiese eksperimente verkry is. Die resultate het getoon dat die modelresolusie ’n aanmerklike uitwerking op waargenome mikrogolfgeïnduseerde kraakskade en -patrone het. Daar is waargeneem dat krake in modelle met verskillende resolusies in verskillende patrone propageer, ten spyte daarvan dat hulle dieselfde makromeganiese eienskappe het.

Kraakpatrone wat vir hoër modelle verkry is, het volgens waarneming goed vergelyk met kraakpatrone wat uit die fisiese mikrogolfbehandelingeksperimente waargeneem is. Die gevolgtrekking kan gemaak word dat modelkalibrasie met slegs die gewone gesimuleerde ODK- en Brasiliaanse toets nie genoegsaam is om die modelresolusie vir simulasies van

termies geïnduseerde krake vas te stel nie. Hierdie resultate toon dat modelmonsterresolusie ŉ aanmerklike uitwerking op waargenome mikrokraakskade het en dat die minimumbasismateriaal se ‘deeltjie’-grootte nie ŉ vrye parameter is nie.

Die uitwerking van absorbeerfase-inhoud op mikrogolfgeïnduseerde skade is vir die eerste keer met behulp van ŉ hoëresolusiemodel ondersoek. Skadekaarte wat die persentasie mikrokrake as ŉ funksie van kragdigtheid en blootstellingstyd vir verskillende ternêre ertse en absorbeerfase-inhoud toon, is saamgestel. Dit het getoon dat die fraksie mikrofrakture wat deur mikrogolfbehandeling geïnduseer is vir dieselfde kragdigtheid en energie-inset van absorbeerfase-korrelinhoud afhang.

Acknowledgements

The author wishes to acknowledge the following people and organisations that made this project possible. Prof Steven Bradshaw who supervised this research and provided all the necessary financial and technical support that was required to complete this research project. Staff in the Department of Process Engineering at Stellenbosch University. Dr Megan Becker from the Department of Chemical Engineering at the University of Cape Town, for her technical and material support and advice. Prof Jochen Petersen and Dr Yousef Ghorbani. Dr Anton du Plessis and staff at Stellenbosch XCT facility. South African Minerals to Metals Research Institute (SAMMRI) for funding. Lastly the author wishes to acknowledge Dr Margreth Tadie Charikinya for being a supportive wife, throughout the course of this project.

Statement of originality

This study developed a procedure to quantify the nature and extent of microwave induced cracks in coarse crushed ore particles (≥ 5 mm) using high resolution X-ray computed tomography (XCT). This is the first time that such quantification of microwave has been made. It provides a means for better understanding the characteristics of microwave induced cracks and how they can be best exploited in processing applications. This study has shown experimentally that microwave treatment results in enhanced value mineral exposure in coarse particles following microwave treatment. This enhanced mineral exposure is independent of prior mode of comminution of microwave treated particles.

This study has shown that microwave induced cracks enhance the recovery of value minerals from coarse particles in bio-leaching operations by creating new crack surface areas for lixiviant to access the value minerals within the particles. The significant enhancements in extraction of the metals during leaching have been achieved at economically viable energy inputs (2 to 3 kWh/t) and at microwave power densities (1×10^9 W/m$^3_{abs}$) that will minimise arcing in scaled up operation. This is particularly significant, as most previous work on microwave assisted mineral processing of ores, focused on microwave assisted comminution, with limited studies investigating the downstream processing benefits of microwave treating coarse crushed ore particles for bio-leaching at economical energy inputs.

This study examined whether bonded particle modelling (BPM) can provide qualitative and quantitative predictions of microwave induced cracks in a typical sulphide ore. This had not been possible previously, as experimental techniques to examine internal crack formation due to microwave treatment had not been applied to microwave treated particles. Therefore there was no experimental data to compare model results against. It was shown that BPM model scale effects have a significant influence on the prediction of microwave fracture in ore particles. The BPM model developed in this study offers a solution to challenges associated with experimentally investigating microwave induced fracture in minerals such as cost and time. Using BPM developed in this study it is possible to investigate a wide range of scenarios rapidly and at relatively low cost.

Table of Contents

List of Figures

List of Tables

Nomenclature

Abbreviations

2D	Two dimensional spaces
3D	Three dimensional spaces
Abs	microwave absorbent phase
Auto-SEM	Automated Scanning Electron Microscopy
BPM	Bonded Particle Modelling
BSE	Back Scattered Electron
BMA	Bulk Mineralogical Analysis
EDS	Energy Dispersive Spectrometry
FEG	Field Emission Gun
Ga	Galena
HPGR	High Pressure Grinding Rolls
Ka	Kaolinite
MT	microwave treated
MLA	Mineral Liberation Analysis
ORP	Oxidation Reduction Potential (mV)
Py	pyrite
PMA	Particle Mineral Analysis
PLS	Pregnant Leach Solution
QEMSCAN	Quantitative Evaluation of Minerals by Scanning Electron Microscopy
Qu	quartz
ROI	Region of interest
SMA	Specific Mineral Analysis
SEM	Scanning Electron Microscopy
Sph	sphalerite
T	treated
TE	transverse electric
TM	transverse magnetic
TIMA	Tescan Integrated Mineral Analyzer
TIMA	Tescan Integrated Mineral Analyzer
TMS	Trace Mineral Search

UCS	Uniaxial Compressive Strength (Pa)
UT	untreated
XCT	X-ray Computed tomography

Chemical formulas

Al	Aluminium
Ca	Calcium
Cu	Copper
Fe	Iron
Mg	Magneium
Mn	Manganese
Pb	Lead
S	Sulphur
Si	Silicon
Ti	Titanium
Zn	Zinc
Fe (III)	Ferric iron
Fe (II)	Ferrous iron
Fe^{2+}	Ferrous ion
Fe^{3+}	Ferric ion
H^{+}	Hydrogen ion
Me^{2+}	Metal ion
OH^{-}	Hydroxyl ions
S^{0}	Sulphur ion
$BaSO_4$	Baryte
CO_2	Carbon dioxide
$CuFeS_2$	Chalcopyrite
Cu_2S	Chalcocite
$FeCO_3$	Siderite
H_2O	Water
FeS_2	Pyrite
Fe_7S_8	Pyrrhotite
Fe_3O_4	Magnetite
Fe_2O_3	Hematite

$KAlSi_3O_6$	Othorclase
MeS	Metal sulphide
$MgCO_3$	Magnesite
$NaAlSi_3O_8$	Albite
O_2	Oxygen
PbS	Galena
SiO_2	Quartz
ZnS	Sphalerite

Symbols

α	coefficient of linear thermal expansion (1/°C)
α	Linear thermal expansion coefficient (1/°C)
$\bar{\alpha}$	expansion coefficient of the bond material (1/°C)
$\Delta\theta^s$	shear directed rotation increments (rad)
$\Delta\theta^n$	normal directed rotation increments (rad)
Δ R	increase in particle radius (mm)
Δ T	temperature change (°C)
ΔF^s	increment of shear force (N)
$\Delta\bar{F}^s$	shear directed forces (N)
$\Delta\bar{F}^n$	normal component of the force vector (N)
ΔU^n	normal displacement increment (mm)
$\Delta\bar{M}^n$	axial directed moments (Nm)
ΔU^s	shear displacement increment (mm)
ε	complex permittivity (F/m)
ε'	dielectric constant (F/m)
ε''	dielectric loss factor
ε_0	permittivity of free space (8.854×10^{-12} F/m)
λ	wavelength (m)
λ_0	free space wavelength (m)
$\bar{\lambda}$	radius multiplier used to set the parallel bond radii
μ	micro
μ_f	particle friction coefficient
μ^*	complex permeability
μ'	permeability (H/m)

μ''	magnetic loss factor
μ_i	attenuation coefficient
ρ	density of the material (kg/m^3)
ρ_b	ball density (kg/m^3)
$\bar{\sigma}_c$	normal (tensile) strength of the cement (MPa)
$\bar{\sigma}^{max}$	maximum tensile stresses acting on the parallel bond periphery (MPa)
$\bar{\tau}^{max}$	maximum shear stresses acting on the parallel bond periphery (MPa)
$\bar{\tau}_c$	shear strength of the cement (MPa)
ψ	bonded particle model resolution
$tan\delta$	loss tangent
C_p	specific heat (J/kgK)
C_t	Zn concentration in pregnant leach solution at time t (g/L)
C_0	Zn concentration in inlet leach solution (g/L)
D_p	Penetration depth (mm)
E_c	Young's modulus at each particle-particle contact (GPa)
$\bar{E}_c$	Young's modulus of each parallel bond (GPa)
E_0	electric field (V/m)
E	energy of the X-ray beam (J)
F_i	contact force vector (N)
$\bar{F}_i$	total force carried by the parallel bond (N)
F^n	normal force (N)
F_E	degree of exposure of the sulphide phase (%)
H_0	magnetic field (A/m)
K	thermal conductivity $(W/m.K)$
$\bar{L}$	bond length (mm)
$\bar{M}^s$	shear directed moments (Nm)
$\bar{M}_i$	moment carried by parallel bond (Nm)
P_d	power density (W/m^3)
R	particle radius (mm)
R_{min}	minimum radius of the ball (mm)
R_{max}	maximum radius of the ball (mm)
R_{avg}	average particle radius (mm)
$\bar{R}$	radius of the parallel bond (mm)

R^A	bonded particle radii (mm)
R^B	bonded particle radii (mm)
R_{Zn}	percentage Zn recovery from leaching (%)
$\mathbf{S_{internal\ grains\ int\ area}}$	Surface area of internal grains (mm^2)
$\mathbf{S_{exposed\ grains}}$	Surface area of exposed grains (mm^2)
S_{gangue}	Surface area of gangue (mm^2)
$S_{particle}$	Surface area of particle (mm^2)
U^n	normal displacement (mm)
V_t	volume of the pregnant leach solution at time t(L)
Wlx	model specimen width (mm)
Wly	model specimen length (mm)
Z_e	effective atomic number
b	is a constant
c	speed of light (299 792 458 m/s)
f	frequency (Hz)
f_i	fraction of the total number of electrons
k_n	particle normal stiffness (Pa/m)
k_s	parallel bond shear stiffness (Pa/m)
$\bar{k}_n$	parallel bond normal stiffness
$\bar{k}_s$	parallel bond shear stiffness
n	average porosity of the PFC^{2D}/ PFC^{3D} material
q_v	volumetric heat intensity (W/m^3)
q_i	is the heat flux vector governed by the Fourier's law in (W/m^2)
t	constant t=1 in 2D

CHAPTER 1

1. INTRODUCTION

1.1.Background

Society is economically, socially and culturally dependent on minerals and metals. The global demand for minerals and metals is rising however, the grade of minerals is decreasing and the costs required to produce minerals and metals is increasing (Krogscheepers and Gossel, 2015; Prior et al., 2012). The extraction of mineral values from ore requires liberation of the value minerals from the gangue followed by their separation. Liberation is achieved by size reduction operations that are energy inefficient and generally do not achieve significant selective breakage (Desmond, 2008; Fuerstenau and Abouzeid, 2002). It has been reported that size reduction operations consume about 3% of the world's electrical energy (Fuerstenau and Abouzeid, 2002; Sadrai et al., 2006). Size reduction operations remain by far the largest energy consumer on most mining sites (Morrison and Cleary, 2008; Tromans, 2008). The mining industry is coming under increased pressure to reduce the amounts of energy it consumes (Henckens et al., 2014). This clearly provides significant incentive to develop more efficient mineral beneficiation technologies.

For some years it has been suggested that microwave treatment of ores might result in thermal fracturing that would reduce subsequent comminution energy requirements and yield improved liberation (Kingman, 2006; Kingman et al., 2004c). It has been shown that microwave treatment of secondary crusher product at a specific microwave energy consumption of the order of 1 kWh/t reduces the work index of the ore and increases grade and recovery in batch flotation tests (Kingman et al., 2004c). However, the downstream processing benefits have been difficult to show either through physical experiments or theoretical modelling studies (Charikinya, 2011; Kobusheshe, 2010). Results of the work carried out so far suggests that the benefits of applying microwaves are strongly dependent on a number of factors such as ore type, design of the microwave treatment unit and the choice of downstream processing route (Ali and Bradshaw, 2010, 2011; Kobusheshe, 2010).

The most widely used processing steps in the recovery of value minerals from most ores are comminution followed by flotation. Most of the experimental work investigating the application of microwaves to mineral processing flow sheets has focused on assessing the benefits of applying microwave technology to flow sheets consisting of size reduction and mechanical flotation cells (Kingman et al., 2004c; Kingman et al., 2000b; Kobusheshe, 2010).

Experimental studies have shown that coarse crushing during tertiary grinding of microwave treated ore resulted in a better liberated coarser flotation feed (Scott et al., 2008). It has been suggested that improved liberation in milled flotation feed, was due to the presence of grain boundary fracture in microwave treated particles. However, this improvement in coarse particle liberation does not necessarily translate to a significant improvement in downstream flotation recovery (Kobusheshe, 2010). This is as a result of the size limit to the flotation of coarse material, due to detachment forces acting on particle-bubble aggregates, which increase as the particle size increases (Charikinya, 2011). Current conventional, mechanically agitated flotation cells are not designed to float coarse material (Jameson, 2012; Rodrigues et al., 2001). Hence it has been difficult to show the downstream processing benefits of applying microwaves to ores processed by comminution followed by flotation (Charikinya, 2011; Kobusheshe, 2010). Further modelling studies have shown that crushing velocity and hence mode of comminution could significantly affect the liberation properties of microwave treated ores (Scott et al., 2008). Numerical simulations that were carried out by Ali and Bradshaw (2011) showed that inter-particle breakage was the most appropriate comminution method of exploiting microwave induced cracks in microwave treated ores and could result in greater improvements in liberation.

It is clear from investigations carried out so far that inappropriate downstream exploitation of microwave treated ore would fail to realise a meaningful process benefit (Ali and Bradshaw, 2011; Kobusheshe, 2010; Scott et al., 2008). Conventional flow sheets consisting of size reduction and mechanical flotation cells do not effectively exploit the benefits of microwave induced damage (Charikinya, 2011; Scott et al., 2008). Charikinya (2011) investigated the effects of changes in liberation, as would be expected from microwave treatment of flotation feed, on recovery using a simulated flotation circuit. The results of the study showed that mechanically agitated froth flotation cells, can best exploit well-liberated material only if the material is coarser than a critical size. This suggests that the most appropriate way to exploit the benefits of microwave induced fracture would be to use coarse grinding, as can be achieved in high pressure grinding rolls (HPGR), following microwave treatment, followed by flash flotation of the coarsely liberated material.

Despite the presence of grain boundary fracture being important in realising downstream processing benefits such as improved liberation during crushing of microwave treated ore, the extent of grain boundary fracture in microwave treated particles has never been experimentally quantitavely determined. It remains unclear if microwave treating ores results in grain boundary fracture. The commercial development of microwave technology as an ore

preparation method depends on clear demonstration of the benefits on downstream processing in any proposed flow sheet. Investigations carried out to date suggest that the operating window for possible successful application of microwave pre-treatment of ores is relatively restricted but as yet poorly-quantified, hence further work is required to ascertain the value proposition of microwave treatment on different downstream processing routes (Ali and Bradshaw, 2011; Charikinya, 2011; Kobusheshe, 2010).

Heap leaching downstream operations could benefit from increased micro-fracturing, as the extent and kinetics of heap leaching processes depend on the accessibility of grains to lixiviants, which can potentially be improved through microwave treatment (Ghorbani et al., 2011a). However, the density and pattern of microwave induced cracks and how these cracks might subsequently affect recovery during heap leaching has not been investigated. Heap leaching studies have shown that the extent and kinetics of heap leaching processes depend on the accessibility of grains to lixiviant (Ghorbani et al., 2013a; Pradhan et al., 2008). The major drawback of heap leaching is low mineral recovery as compared to milling followed by flotation, since heap leaching is characterised by poorly liberated relatively coarse particle sizes (Ghorbani et al., 2011a; Pradhan et al., 2008). Heap leaching of too finely crushed ore may result in solution percolation and air flow problems. Studies have shown that the fluid flow dynamics in a heap can be enhanced by inducing cracks during ore preparation, which leads to enhanced ore permeability (Kodali et al., 2011). Thus accessibility and recovery of heap leaching operations can potentially be improved through microwave induced particle fracture.

In order to assess whether microwave treatment of coarse particles followed by heap leaching is an appropriate way to exploit microwave induced cracks, an understanding of microwave induced crack characteristics and properties in coarse particles is required. Due to the difficulties associated with analysing microwave induced cracks, the nature and characteristics of microwave induced cracks is not well understood (Ali and Bradshaw, 2010). Further there are no existing quantitative methods for measuring the amount of induced microwave cracks and determining if such cracks result in enhanced mineral exposure, in coarse particles. Previous studies quantifying microwave induced crack damage have been limited to numerical models with no physical experimental studies having been conducted (Ali and Bradshaw, 2009; Jones et al., 2005; Whittles et al., 2003). By applying a combination of high resolution 3-D X-ray Computed Tomography (XCT) and Automated Scanning Electron Microscopy and Energy Dispersive Spectrometry (Auto-SEM /EDS) conventional techniques this study attempts to measure and characterise microwave induced cracks.

Predicting the microwave treatment conditions (exposure time and power density) that will result in optimal formation of cracks for heap leaching is an important step towards evaluating and assessing the processing limits of microwave preparation of heap leach feed. Physical experiments alone are not sufficient in determining these processing limits, as they do not offer the possibility of investigating a large number of case studies at a reasonable cost and in a reasonable time period. Bonded particle modelling (BPM) offers a partial solution to these challenges due to the fact that a wide range of scenarios can be investigated rapidly and at relatively low cost. Ali and Bradshaw (2009, 2010) carried out numerical simulation investigations into the mechanism of microwave induced micro fracture using BPM. However, the models were not validated. Hence, the improvement of these existing models and their validation is a necessary step towards gaining a fundamental understanding of the optimal microwave treatment conditions for different ore types and how to best exploit the induced microwave fracture.

As the commercial development of microwave ore preparation depends on clear demonstration of the benefits on downstream processing there is a need to determine the value proposition for heap leaching of microwave treated ores. Quantification of the process economic benefit is critical in allowing the mineral processing industry to assess the so-called value proposition of microwave preparation of heap leach feed. This could be achieved through the use of traditional column heap leach experiments to ascertain the benefits of microwave assisted heap leaching ore feed. A study of the progression of leaching in microwave treated material will aid in giving better understanding to the possible role of microwave induced cracks in heap leaching operations.

1.2.Research aims and objectives

The aim of this work was to determine if microwave treatment of a typical massive sulphide ore, prior to bio-leaching would induce micro-cracks and enhance value mineral exposure resulting in improved bio-leaching metal extraction and kinetics. Thus the objectives of this study were:

1. To characterise and quantify microwave induced particle cracks through the use of high resolution XCT and Auto-SEM /EDS techniques;
2. To determine if microwave treatment results in enhanced value mineral exposure in coarse particles and to determine the mode of fracture during microwave treatment;
3. To determine the effect of microwave induced cracks on the dissolution kinetics of bio-leaching processes of a typical massive sulphide ore;
4. Use XCT and QEMSCAN experimental data to improve on and to validate numerical models for predicting microwave induced damage.

.

1.3.Key questions

The objectives of this work were met by addressing the following key questions:

1. Does microwave treatment result in significant crack damage in sulphide ores?
2. Is it possible to quantify microwave induced damage and enhanced value mineral exposure in coarse particles?
3. Is boundary crack fracture the dominant form of crack propagation in microwave treated sulphide ores?
4. Is there a size relation between the amount of microwave induced damage and particle size?
5. What are the process benefits of microwave treatment of heap leach feed ore?
6. Will microwave treatment of heap leach feed ores alter the progression of leaching in individual microwave treated particles?
7. Does microwave treatment reduce the effects of mode of comminution on overall heap leaching recovery?
8. Are microwave induced cracks of sufficient size to act as attachment sites for microbes during bio-leaching?
9. How do numerically modelled crack damage patterns in multiphase ore particles compare against crack patterns observed from physical experiments?
10. Is there a difference between experimentally measured crack damage density and numerically modelled crack damage density?

1.4.Scope and limitation

This study covers the following areas of mineral processing and beneficiation: microwave treatment of ores, bonded particle discrete element modelling, mineralogy and hydrometallurgy. It consists of investigations on the microwave treatment of a single ore type representing a massive sulphide ore and the effect of microwave treatment on downstream heap leach processing. A comparison of the column bio-leaching response of microwave treated ore is made against that of microwave untreated particles from typical conventional impact and compression breakage crushers (HPGRs). The influence of textural variation in the ore and how it influences crack formation during the microwave treatment experiments is not considered.

The ore sample used in the study consists of HPGR and cone crushed sphalerite ore from the Gamsberg Zinc mine in South Africa. Ore sample preparation was carried out using a primary jaw crusher product that was split into two parts for further crushing by either HPGR or cone crusher. Low zinc prices coupled with the difficulties associated with applying conventional methods in recovering zinc from the deposit has led to other alternative recovery techniques being considered such as heap leaching (McClung and Viljoen, 2011). A recent study investigated the effect of mode of comminution on heap leaching of Gamsberg zinc ore (Ghorbani et al., 2013b; Ghorbani et al., 2012). The results of the investigation showed greater mineral recovery in HPGR crushed coarse particles compared to cone crushed particles. Conducting the current study using the same bulk ore sample, allows for a direct comparison to be made between leaching recovery of, microwave treated and untreated HPGR and cone crushed particles.

The microwave induced crack characterisation and analysis is carried out using a combination of high resolution X-ray computed tomography and Auto-SEM/EDS (QEMSCAN) techniques. Image analysis and processing is carried out using algorithms in existing commercial software package. The development of new algorithms for image processing and analysis was not considered in this study.

The numerical modelling work focuses on developing and improving existing BPM for simulating microwave induced fracture in different materials. It is a continuation of previous work by Ali and Bradshaw (2010) to develop a model for investigating the microwave response of materials. The ore used in the experimental study is simulated and the crack pattern results from the model are validated.

Bio-leaching is investigated and the micro-organisms used consist of mixed culture of mesophilic bacteria. The study focuses only on the effect of microwave cracks on value mineral dissolution kinetics during bio-heap leaching. The study does not investigate the influence these cracks might have on attachment of micro-organisms during the bio-leaching process. Figure 1-1 and Figure 1-2 are schematic illustrations of differences between this work and previous work by done Ghorbani et al.(2012), using the same bulk ore sample.

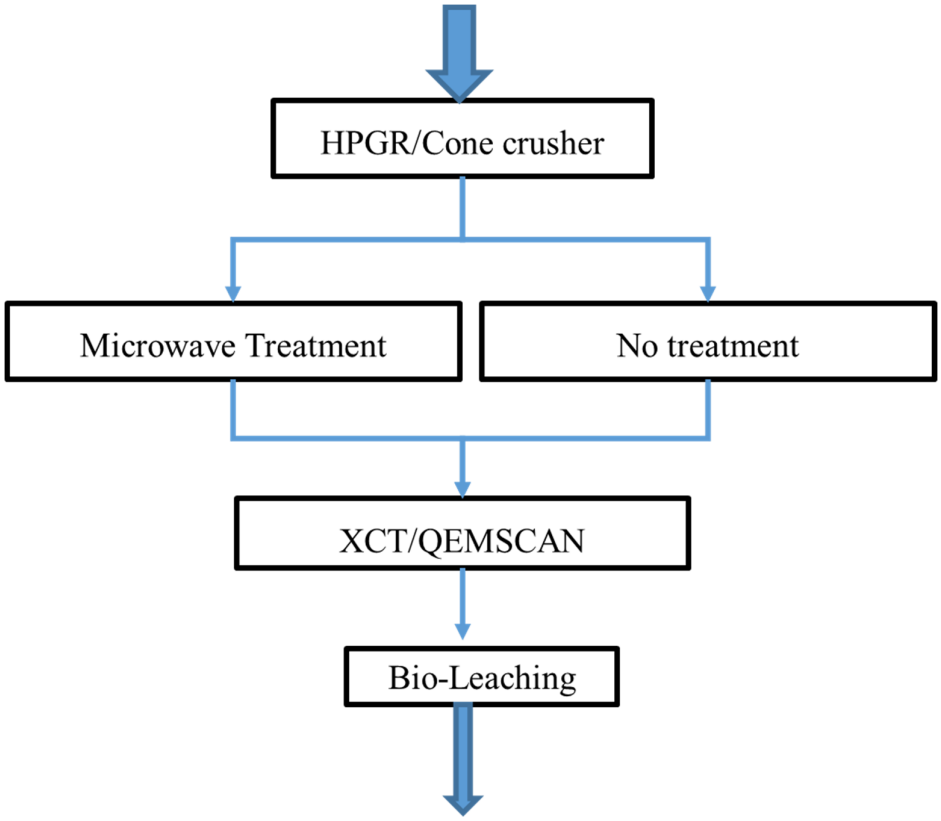

Figure 1-1: Schematic of the scope of research in this study

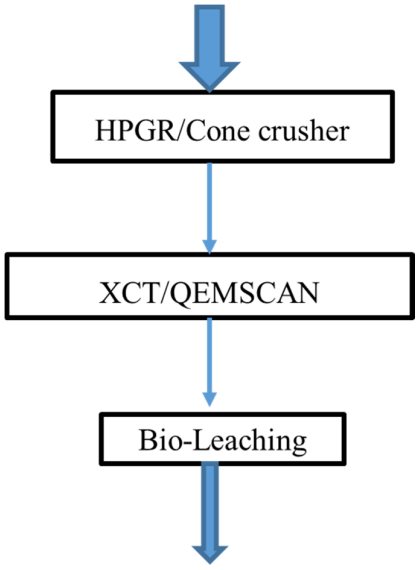

Figure 1-2: Scope of previous work investigating coarse particle heap leaching of Gamsberg ore by Ghorbani et al.(2012)

1.5.Organisation of thesis

Chapter 2 is a literature review covering the areas of microwaves theory and application in mineral processing, comminution, ore characterisation techniques and heap leaching. This chapter aims to provide the reader with a sufficient background to the study necessary for understanding the primary objectives of the body of work presented in this thesis.

Chapter 3 details the materials and methods used in this study. It describes ore preparation methods used along with a description of the microwave treatment experimental set up. This is followed by a description of XCT and QEMSCAN analysis techniques that were applied to characterise and quantify microwave crack induced damage. Lastly details of the column heap leach experimental set up and microbial cultures preparation are provided. The presentation of the results and their discussion is presented in three separate chapters; Chapters 4, 5 and 6.

Chapter 4 details results along with their discussion, of characterising and quantifying microwave induced crack damage using XCT and QEMSCAN analysis. This chapter also details results along with their discussion, of interfacial area measurements and mineral exposure analysis carried out on microwave treated particles.

Chapter 5 describes and discusses the leaching process in the leach reactors and selected ore particles. Mineral conversion in microwave treated and untreated single ore particle is investigated and conclusions are drawn on the influence of microwave induced cracks networks on metal recovery.

Chapter 6 details the methodologies used to simulate a macroscopic behaviour of ore models and the specification of the microscopic properties that are required in the models, to BPM. The influence of absorbent phase content on crack propagation under different microwave treatment conditions is elucidated in this chapter.

Chapter 7 presents the conclusions made from the physical microwave treatment experiments, column leaching test work and BPM. The practical implications of the results on the application of microwave technology in heap leach feed ore preparation are also addressed. The chapter also presents the scope for future work.

CHAPTER 2

2. LITERATURE REVIEW

Chapter 2 begins with a brief discussion of the fundamental nature of microwave, how microwaves are generated, and their interactions with materials, the different microwave heating mechanisms and microwave system components. Brief notes concerning dielectric properties measurements, power density, and penetration depth are also included. Finally a review of the major experimental and theoretical studies carried out to date on microwave assisted comminution and liberation of minerals. This chapter aims to provide the reader with sufficient background to the study of microwave assisted comminution and to understand the intentions of the body of work presented in this thesis. This research work will only be limited to the use of microwaves for industrial heating in the mineral processing industry.

2.1.Electromagnetic spectrum

Microwaves are a form of electromagnetic energy with a wide range of scientific and industrial applications. Microwave energy offers efficient, cost-effective methods of drying, heating, curing, and sterilizing products in industrial manufacturing. Microwaves form part of a continuous electromagnetic spectrum that extends from low frequency alternating currents to cosmic rays. Microwave energy is a nonionizing electromagnetic radiation that obeys the general wave formula given by:

$$\boldsymbol{c = \lambda . f} \qquad \text{2-1}$$

where c is the speed of light (299 792 458 m/s), λ is the wavelength (m), f is the frequency (Hz). Microwaves occupy the part of the electromagnetic spectrum from 300 MHz to 300 GHz with wavelengths ranging from 1 mm to 1 m. Microwave heating is usually applied at the most popular of the frequencies allowed for industrial, scientific and medical applications, namely 915 (896 in the UK) and 2450 MHz (Bradshaw et al., 1998; Meredith, 1998). Domestic microwave ovens are a familiar example operating at 2450 MHz.

2.2.Microwave heating mechanism

The response of material when exposed to high frequency electromagnetic waves varies. In general material response to microwave heating can be classified under three main categories: conductors, insulators (transparent) and dielectric (absorber) materials. Material can be heated using high frequency electromagnetic waves provided that the material is neither a perfect electrical conductor nor a perfect insulator. When conductors are exposed to an electric field electrons move freely in the material and an electric current results. Metals are typical example of conductors because of their high conductivity (Metaxas and Meredith, 1983; Sutton, 1993). Conductors largely reflect microwaves and thus, conductors are not effectively heated by microwaves. Conductors are often used as conduits (waveguide) for microwaves (Clark and Sutton, 1996; Haque, 1999). In insulators, electrons do not flow freely, but electronic reorientation or distortion of induced or permanent dipoles can give rise to heating (Courtney, 1970; Sutton et al., 1988). Insulators are transparent to microwaves and are often used in microwave ovens to support the material to be heated. A dielectric material has ability to absorb and store energy through polarisation when an external electric field is applied. Thus dielectric (absorbers) materials are excellent absorbers of microwave energy and are easily heated when exposed to microwaves. Microwaves cause molecular motion by migration of ionic species and/or rotation of dipolar species (Haque, 1999). Heating under microwave exposure may result from one of three main mechanisms. These are the conduction mechanism, ionic or dipolar polarisation, and interfacial polarisation.

2.2.1. Conduction mechanism

When microwaves interact with an electrical conductor, the charge carriers (electrons, ions, etc.) are moved through the material under the influence of an electric field, resulting in a polarisation. The induced current causes heating due to electrical resistance (Von Hippel, 1954). This heating mechanism is significant in conducting solid materials and ionic solutions. But as stated before, in high conducting materials such as metals, there is inadequate microwave penetration; rather microwaves are reflected at the surface which may lead to arcing (Metaxas and Meredith, 1983). In liquids, ionic conduction heating may dominate dipolar heating as the conductivity of the liquid is increased either by addition of ions or increase in temperature (Al-Harahsheh and Kingman, 2004).

2.2.2. Dipolar polarisation

In polar molecules, the different electro-negativities of individual atoms results in the existence of a permanent electric dipole on the molecule due to the asymmetric distribution of charge around the molecules. Under an oscillating electric field these molecules rotate continuously in an attempt to align with the field giving rise to orientation polarisation. This realignment is rapid for a free molecule, but in liquids instantaneous alignment is prohibited by the presence of other molecules (Meredith, 1998; Metaxas and Meredith, 1983). It is this motion that gives rise to frictional losses and subsequent increase in temperature during microwave heating. Thus the interaction of an electric field with molecular dipoles results in rotation of the dipoles, and energy is dissipated as heat from internal resistance to the rotation (Meredith, 1998; Metaxas and Meredith, 1983).

2.2.3. Interfacial polarisation

Electronic, atomic and dipolar polarisation all occur when charges are locally bound in atoms, molecules or structures of solids or liquids. Charge carriers also exist that can migrate over a distance through the material and polarisation occurs when this motion is impeded. Interfacial polarisation is most easily viewed as a combination of the conduction and dipolar polarisation effects (Metaxas and Meredith, 1983). This mechanism mostly occurs in systems comprised of conducting inclusions in a second, non-conducting material. An example would be a dispersion of metal particles in sulphur. Sulphur is microwave transparent and metals reflect microwaves however, the combination of the two forms a good microwave absorber (Cumbane, 2003; Jones, 2005).

2.2.4. Dielectric properties

Dielectric properties are the physical properties of materials that can be measured and used to predict material response to microwave treatment. The knowledge of the dielectric properties of materials to be processed is essential for the efficient design of microwave applicators (Cumbane et al., 2008). The property that describes the behaviour of a dielectric under the influence of high frequency is known as the complex permittivity. Microwave propagation in materials depends on the dielectric and magnetic properties of the medium. The electromagnetic properties of a medium are characterised by complex permittivity (ε) and complex permeability (μ^*) where:

$$\varepsilon = \varepsilon' - j\varepsilon'' \quad 2\text{-}2$$

$$\mu^* = \mu' - j\mu'' \quad 2\text{-}3$$

The real component of the complex permittivity, ε' is commonly referred to as the dielectric constant or permittivity while the imaginary part, ε'' is the dielectric loss factor. Real and imaginary components of the complex permeability, $\mu'$and $\mu''$are the permeability and the magnetic loss factor, respectively(Meredith, 1998; Zheng et al., 2005). The dielectric constant is a measure of the ability of the material to retard microwave energy as it passes through and the loss factor is a measure of the ability of the material to dissipate the energy. Loss factor represents the amount of input microwave energy that is lost in the material by being dissipated as heat. Therefore, a material with high 'loss' factor is easily heated by microwave energy. The ratio between the dielectric loss factor and the dielectric constant measures how well a material absorbs electromagnetic energy and dissipates it as heat in the material. The loss tangent $tan\delta$ is indicative of the ability of the material to convert absorbed energy into heat.

$$tan\delta = \frac{\varepsilon''}{\varepsilon'} \quad 2\text{-}4$$

The extent to which energy may be absorbed and dissipated in a material depends on its dielectric properties which include permittivity, permeability, conductivity and resistivity. Permeability is the degree of magnetization of a material that responds linearly to an applied magnetic field. Materials possessing poor thermal conductivity, heat generated due microwave heating does not rapidly dissipate into the surrounding non-heated regions of the material. The dielectric properties of a material vary with molecular structure, density, moisture content, temperature, frequency and orientation of the material. The main factors that affect dielectric properties of materials are frequency, temperature and moisture content (Meredith, 1998; Metaxas and Meredith, 1983; Pickles et al., 2005; Von Hippel, 1954). Industrial microwave applications use specified frequencies and therefore the variation of material dielectric properties with frequency is not as crucial as other factors such as temperature and moisture content. Previous studies have shown that the dielectric properties of metal oxides such as hematite, ilmenite and manganese oxide are strong functions of the frequency of radiation, while the dielectric properties of pyroxene and goethite is independent of frequency (Marland et al., 2001; Nelson et al., 1989). Liquid water is strongly polar in its structure, and is a good microwave absorber converting it to heat. The moisture content in a material has an effect upon its dielectric properties and consequently how the material responds under electric field (Metaxas and Meredith, 1983).

Some material exhibit an increase in loss factor with temperature. A material that is not a good absorber of microwave can become more absorbing if first pre-heated by other means. This is due to the dielectric properties of materials being dependant on temperature (Meredith, 1998; Metaxas and Meredith, 1983). The nature of the dependence is a function of the dielectric relaxation process operating under the particular conditions and the applied electric field frequency. Dielectric relaxation is defined as the time take for the dipoles to return to random orientation when the electric field is removed (Nelson et al., 1989). As temperature increases, the relaxation time decreases resulting in an increase in the dielectric constant (Böttcher et al., 1978; Holderfield and Salsman, 1992).

2.2.5. Microwave power dissipation

Microwave heating is a result of conversion of electromagnetic energy into heat. The former is generated by some source and transported through space or any other medium in form of an electromagnetic wave. In microwave engineering, the amount of thermal energy deposited in to a material due to microwave heating is called power density and given by:

$$P_d = 2\pi f \varepsilon_0 \varepsilon'' E_0^2 + 2\pi f \mu_0 \mu'' H_0^2 \qquad 2\text{-}5$$

Where P_d is the power density (W/m^3), f is the frequency of the microwave radiation (Hz), ε_0 is the permittivity of free space (8.854 × 10^{-12} F/m), $\varepsilon''$is the dielectric loss factor of the mineral, E_0 is the magnitude of the electric field of microwave energy inside the material (V/m), μ_0 permeability of free space (12.571× 10^{-7} H/m) μ'' is the magnetic loss factor and H_0 is the magnetic field (A/m) (Meredith, 1998; Metaxas and Meredith, 1983). The terms on the right hand side of the equation refers to electric and magnetic losses, respectively. It can be seen that the power density varies linearly with frequency, loss factor and square of electric field strength. Numerical methods are normally used for estimating the power density range that can be expected for a given applicator geometry, dielectric properties, microwave power and frequency of operation (Ali and Bradshaw, 2009; Jones, 2005; Whittles et al., 2003).

2.2.6. Microwave power penetration

When microwave energy is absorbed by materials, the amplitude of the wave decreases gradually as the wave propagates into the material. If any internally reflected waves are neglected, the power density (and therefore power absorbed) falls exponentially with depth. The field intensity and the associated power flux density fall exponentially with distance from the surface. The rate of decay of the power dissipation is a function of both the relative

permittivity (ε') and the loss factor (ε''). The penetration depth, D_p(m) is defined as the depth into the material at which the power flux has fallen to 1/e (0.368) of its surface value and is given as:

$$D_p = \frac{\lambda_0}{2\pi\sqrt{2\varepsilon'\left\{\sqrt{1+\left(\frac{\varepsilon''}{\varepsilon'}\right)^2}-1\right\}}} \qquad 2\text{-}6$$

λ_0 is the free space wavelength (Meredith, 1998; Metaxas and Meredith, 1983). Table 2-1 shows that the penetration depth of most minerals is greater than 50 mm. Thus volumetric heating assumption is reasonable for small particle size (Harrison, 1997).

Table 2-1: Penetration depth of some minerals (Harrison, 1997)

Mineral	Penetration depth at 2.45 GHz (m)
Quartz	5.86
Hematite	0.21
Ilmenite	0.31
Chalcopyrite	0.33
Pyrite	0.11
Magnetite	0.06
Galena	0.84

2.3.Microwave systems

Microwaves systems usually consist of a microwave source, waveguides, and an applicator. The wave guides deliver the generated electromagnetic energy from the microwave source to the applicator. In the applicator, the energy is either absorbed or reflected by the material.

2.3.1. Waveguides

Waveguides are hollow tubes in which the electromagnetic waves propagate from the magnetron to the cavity with minimum loss. Waveguides have highly conducting surfaces such as brass or aluminium as to minimise attenuation losses. The most commonly used cross-sections are rectangular (Thostenson and Chou, 1999). The microwaves propagate through the waveguide, in the form of a sinusoidal wave, until it reaches the load. If the load absorbs the wave completely, then there is no reflection of the wave back down the waveguide. They are usually classed as either TE (transverse electric) mode or TM (transverse magnetic) mode. When in TE mode, the electric field vector is normal to the direction of propagation. Conversely, when in TM mode, the magnetic field vector is normal to the direction of propagation (Meredith, 1998; Metaxas and Meredith, 1983).

2.3.2. Microwave Sources

The magnetron belongs to a class of tubes termed "crossed-field" devices so named because their basic operation employs both magnetic and electric fields that are perpendicular to one another (Metaxas and Meredith, 1983). The magnetron consists of a cylindrical electron emitter, or cathode, surrounded by a cylindrical structure, or anode. Magnets are arranged to supply a magnetic field parallel to the axis and hence perpendicular to the anode cathode electric field. Magnetrons are almost exclusively used to generate microwaves in all domestic and industrial microwave appliances because of their higher power output and efficiency, frequency stability and lower capital cost (Meredith, 1998; Metaxas and Meredith, 1983). They are found in all kitchen type ovens, and are cheaply mass-produced for low power output units.

2.3.3. Microwave applicators

Microwave applicators are devices that are designed to heat a material by exposing it to a microwave field in a controlled environment. A common example of an applicator is the metallic box inside the domestic microwave oven where food to be heated is placed. Applicators are classified by the type of field pattern that exists inside them. The choice of applicator depends on many factors, such as size, shape and properties of the material to be

processed as well as the heating rate required. The design of the applicator is critical to microwave heating because microwave energy is transferred to materials through the applicator. The most common microwave applicators are the travelling wave, multi-mode and single-mode applicators (Thostenson and Chou, 1999).

In a travelling wave applicator, microwaves are fed into a chamber where they are absorbed by the workload with the residue being dissipated into a terminating load (Metaxas and Meredith, 1983). Travelling wave applicators are suitable for continuous flow processing with a conveyor belt but are not suitable for low loss materials. The heating efficiency depends on the permittivity and loss factor of the material to be heated and the cross sectional area of the applicator. These applicators have the advantage of simplicity and low cost (Meredith, 1998).

Multi-mode applicators consist of a metallic enclosure into which a microwave signal is coupled through a slot and suffers multiple reflections. The superposition of the incident and reflected waves gives rise to a standing wave pattern or mode. In a given frequency range such an applicator will support a number of resonant modes (Metaxas and Meredith, 1983). Multi-mode applicators are not suitable for use in industrial treating of minerals and ores. This is because that multi-mode cavity uses random heating patterns that create intense hotspots within the samples (Kingman and Rowson, 1998). Hot spots contribute to the phenomenon known as the thermal “runaway effect” (uncontrolled rise in temperature) (Metaxas and Meredith, 1983). They are also not best suited for applications where high temperatures are required, as the energy is dissipated throughout a relatively large volume. Therefore some low loss materials do not heat sufficiently in multi-mode cavities (Jones, 2005). An example of a multi-mode cavity is the home microwave oven.

In single-mode applicators the superposition of the incident and reflected waves gives a standing wave pattern which is very well defined in space. This enables the dielectric material to be placed in the position of maximum electric field for optimum transfer of the electromagnetic energy. The design of single-mode cavities is based on the solution of the Maxwell equations to support one resonant mode. Single mode applicators have one well defined ‘hot spot’ where microwave field strength is maximised (Thostenson and Chou, 1999). Since only one mode of propagation is permitted the field pattern is well defined in space, allowing for the target load to be positioned accordingly. The electromagnetic energy propagated through the applicator and reflects against a short circuit tuner. With careful tuning the incident and reflected waves achieve superposition, and power density is maximised. For the same power applied, a single-mode cavity will establish higher electric field strength than

other applicator types. Single-mode cavities are therefore preferred where high heating rates are required and are also suitable for low loss material processing (Metaxas and Meredith, 1983). Single-mode cavities has been recently shown to be suitable for microwave treatment of ore (Kingman et al., 2004a).

2.3.4. Microwave safety considerations

As microwave power levels for industrial processing systems increase, potential hazards associated with exposure to radiation become more important. The effects of microwaves on biological tissue from exposure to microwaves are thermal in nature. Unlike the higher energy, ionizing region of the electromagnetic spectrum, including X-ray and gamma rays, the nonionizing bands do not carry enough energy to break chemical bonds (Metaxas and Meredith, 1983).Microwaves are still potentially hazardous: their effect may not be noticed until damage to living organisms has been done. The body is designed to warn against excessive external heat not internally generated heat as would be the case if microwave radiation penetrates the skin causing internal heating. To minimise exposure, the microwave system needs to be designed with effective leakage suppression, viewing or ventilation screens, and an interlock system on doors and access apertures to shut off power when doors are opened (Metaxas and Meredith, 1983).

2.4.Experimental investigations

2.4.1. Microwave heating of minerals

The first attempt at applying microwave technology in mineral processing reported in literature was in 1967 (Ford and Pei, 1967). In this study microwaves were used to heat reagent grade powdered metal oxides and sulphides at energy inputs of between 50-200W and at a frequency of 2.45GHz. Temperatures were measured using an infrared radiation thermometer. Findings from these studies were that dark coloured compounds heated rapidly compared to light coloured compounds that heated at slower rates. A relationship between dielectric loss with temperature was reported, for example the loss factor for alumina was observed to increase with temperature (Ford and Pei, 1967).

A lot of preliminary research on microwave heating of minerals was reported between the late 60s and late 90s (Chen et al., 1984; Chunpeng et al., 1990; McGill et al., 1988; Parkash et al., 1979; Walkiewicz et al., 1988; Walkiewicz et al., 1991). The general conclusion from this early work was that microwave radiation had potential application in mineral processing as a majority of sulphide minerals heated well. Perhaps the most important of this early work to the mineral processing industry was by Chen et al. (1984). Chen et al (1984) exposed 40 minerals to microwave exposure in a waveguide applicator to ascertain their behaviour. It was observed from results of the study that microwave effects dependent on mineral composition, and thus, elemental substitutions would affect the behaviour of a mineral in an electric field For example high iron sphalerite was a good microwave absorber compared to would low iron sphalerite which did not heat readily. Chen et al. (1984) grouped the minerals according to their microwave treatment response. The minerals were divided into two general groups, minerals where no or very little heat was generated and minerals where heat was generated. The major findings from this study were that Silicates, Carbonate and Sulphates are transparent to microwave energy in contrast to metal sulphides and oxides that were easily heated (Chen et al., 1984).

The US Bureau of mines carried out detailed and qualitative studies on the characteristics of microwave heating of minerals and reagent grade inorganic compounds (McGill et al., 1988; Walkiewicz et al., 1988; Walkiewicz et al., 1991). All heating tests were conducted on a 25 g of powdered sample using a 1 kW and 3 kW power generator at a frequency of 2.45 GHz. The maximum temperature attained by the microwave heated material was recorded using a thermocouple. The results further confirmed that microwave heating was dependent on the mineral composition with the non-sulphur gangue minerals being transparent to microwave

heating. The study concluded that microwave treatment of ores had potential to improve grinding efficiency as well as leaching recovery (Walkiewicz et al., 1991). These studies became the basis of subsequent investigations that focused on microwave assisted comminution. Most of the early work on microwave heating minerals was carried out using modest power inputs (≤ 1 kW) and hence low heating rates. McGill et al. (1988) reported the effect of power level on mineral heating rate, using power levels of between 500W and 2000W at 2.45GHz. The results showed that an increase in microwave power led to an increase in the heating rate of the minerals however, low loss minerals such as quartz and orthoclase did not heat effectively regardless of the applied power. Table 2-2 shows the microwave heating response of some common minerals.

Table 2-2: Heating response of various minerals (Walkiewicz et al., 1988)

Mineral	Chemical Composition	Temperature (° C)	Time (min)
Sphalerite	ZnS	87	7
Pyrite	FeS_2	1019	6.76
Pyrrhotite	$Fe_{1-x}S$	886	1.75
Magnetite	Fe_3O_4	1258	2.75
Hematite	Fe_2O_3	182	7
Galena	PbS	956	7
Chalcopyrite	$CuFeS_2$	920	1
Chalcocite	Cu_2S	746	7
Quartz	SiO_2	79	7
Orthoclase	$KAlSi_3O_6$	67	7
Albite	$NaAlSi_3O_8$	82	7

2.4.2. Influence of microwave treatment on comminution of materials

Taveras and King (2013) investigated the effect of rapid microwave heating on single particle breakage of different ores using a Ultrafast Load Cell to measure fracture energy for untreated and microwaved ore samples. The results showed a reduction in fracture energy of iron, taconite and titanium ore samples (particles sizes 2.00 to 4.75 mm) microwave treated at exposure times of 30 seconds. It was concluded from the study that microwave pre-treatment had the effect of weakening multiphase particulate materials. Analysis of the crushed fragments of untreated and microwave ores showed that the progeny size distributions of microwaved products were finer than those of untreated ore (Saramak and Kleiv, 2013). Taveras and King

(2009) investigated the relationship between microwave induced apparent crack density and reduction in material stiffness. The apparent crack density was measured using an optical image analysis system. The results showed a good correspondence between measured material stiffness values and the apparent crack density(Bailey et al., 2009).

Kingman et al. (2000b) carried out studies on commercially exploited ores to investigate the influence of ore mineralogy on microwave assisted grinding. The ores investigated consisted of four different ores: massive ilmenite, refractory gold, carbonatite and massive sulphide were investigated. After conducting mineralogical analysis on the ores and establishing the textural relationship between the ore phases, each ore was microwave treated with varying exposure times for each sample. The results showed an increase in grindability of the ores after microwave treatment. This increase in grindability was related to minerology of the ore. It was observed that ores with consistent mineralogy and that contain a good absorber of microwave radiation in a transparent gangue matrix were more responsive to microwave radiation compared to ores with finely disseminated absorbent phase grains which were poorly heated. The results showed improvements in grindability at high microwave energy inputs of 14.3 kWh/t. This input was less than the grinding energy required input of 20 kWh/t. These results highlighted the possibility of carrying microwave assisted comminution at potentially viable microwave energy inputs (Kingman et al., 2000b).

In the same year, Kingman et al.(2000a) reported results of investigations on the effects of microwave treatment on the processing of Palabora ore. The studies not only showed enhanced grindability due to microwave treatment but also demonstrated that increases in recovery of copper after froth flotation could be obtained. Scanning Electron Microscopy analysis showed significant inter-granular fracture in the ore. At long exposure time reduction in copper grades were observed which suggested surface oxidation of the sulphides owing to high temperatures. The potential benefit of reduced Bond Work Index due to microwave treatment on a grinding circuit was also investigated in the same study. This was done by simulating a closed circuit ball mill grinding plant and reducing the Bond Work Index of the ore to a value less than the typical operating plant's value. The impact of the reduced work index value on the circulating load was then analysed. The simulations showed that microwave assisted comminution had the potential to reduce the grindability by as much as 2 kWh/t. It was concluded that the technical benefits were attractive but the economics were poor, as the reduction in work index was achieved at high microwave energy input (Kingman et al., 2000a). These studies further showed that the technical feasibility of microwave assisted comminution.

Rizmanoski (2011) investigated the influence of modulated microwave power on copper ore breakage. The particle sizes of the porphyry copper ore tested ranged between –11.2 + 9.5 mm to –31.5 + 26.5 mm. Comparative drop weight tests showed that material microwave treated for 5 s at 5 kW of modulated power was easier to break than untreated material. The change in strength of samples exposed to microwaves in the applicator were found to be related to the applied microwave power level. The investigation concluded that when using modulated microwave power high power levels were required to obtain significant improvements in liberation than using conventional methods of breakage. Modulated microwave power was found to use less energy to induce thermal stress between mineral species than continuous wave power.

2.4.3. Influence of microwave treatment on changes in magnetic properties

Magnetic separation has long been used to upgrade and beneficiate a wide variety of industrial minerals based on differences in their magnetic susceptibility. Magnetic separation processes utilise the differences in magnetic properties of different mineral phase components making up ores. The separation of weakly magnetic ores is limited by the magnitude of magnetic force that can be developed in high intensity magnetic separators. It has therefore been suggested that the magnetic properties of minerals can be improved by using microwave treatment. Kingman et al (1998 and 1999) investigated the effect of microwave radiation on a number of minerals, e.g., chalcopyrite, hematite and wolframite. The microwave treatment experiments were carried out for exposure times of up to 5 minutes using a 650 W kitchen type microwave heater. A magnetometer was used to determine the magnetic susceptibility of the minerals before and after microwave treatment. The results showed significant increases in magnetic susceptibility of chalcopyrite, ilmenite, hematite and wulframite.

Znamenáčková et.al. (2005) investigated the effect of microwave treatment on magnetic separation of siderite ore (0.5 – 1 mm). Microwave treatment was carried out in a microwave oven with a 900 W power supply at a frequency of 2.45 GHz. The magnetic separation of siderite ore specimens was carried out employing a roll-type electromagnetic separator. The results of the study showed improved Fe recovery with microwave treatment. This recovery was shown to increase with exposure time. Fe recovery of 84.4 % was reported at microwave treatment exposure times of 10 minutes, at higher exposure times of 15 minutes Fe recovery increased to 97.6 % (Znamenáčková et al., 2005).

Guo et al. (2011) investigated the influence of microwave treatment on the grinding and magnetic separation of ilmenite ore. The microwave treatment experiments were carried out

using a microwave oven with a 1 kW power supply at a frequency of 2.45 GHz. Ore samples were treated at microwave exposure times of 30 s followed by water quenching. SEM analysis of the microwave treated samples indicated evidence of microwave induced inter-granular and trans-granular fracture. Subsequent magnetic separation experiments showed increased recovery of magnetite after microwave treatment from 44% to 72%.

Omran et.al.(2014) investigated the effect of microwave radiation on the heating rate, magnetic properties and magnetic separation of iron ore was investigated. Samples were treated using a 2.45 GHz microwave oven with a maximum output power of 900 W. One hundred gram iron ore samples were microwave treated in the oven for varying power levels and exposure times in each test. Microwave treatment was found to be more efficient at larger particle sizes and longer exposure times for a fixed value of the applied power intensity. Magnetic separation of microwave treated and untreated iron ore indicated that iron recovery increased from 39.54% in the untreated sample to 97.95% in the microwave treated sample. This improvement in iron recovery after microwave treatment was due to enhanced magnetic properties of weak magnetic minerals in the ore by microwaves which resulted in altering of the mineral surface of the iron to more magnetic phases. The results indicated that microwave radiation has a significant effect on the magnetic properties of hematite through the formation of new and more magnetic phases that facilitate their separation from non-magnetic minerals, thereby obtaining high recovery (Omran et al., 2014).

2.4.4. Influence of microwave treatment on flotation recovery

There is a limited amount of studies that have investigated the downstream flotation of microwave treated ores. Vorster et al. (2001a) investigated the influence of microwave treatment on grindability and downstream flotation recovery of a massive sulphide copper ore using a 2.6 kW multi-mode cavity operating at 2.45 GHz at exposure times of up to 90 seconds. The results showed reductions in work index of up to 70 % in microwave treated ores. Subsequent flotation tests to investigate if microwave treatment would need to improved flotation recovery of the ore showed no improvements in copper recovery after microwave treatment. This results suggest that downstream processing benefits of applying microwave technology is dependent on the type of the ore.

Henda et al. (2005) investigated the influence of microwave treatment on the grindability and flotation recovery of a complex sulphide nickel-copper ore using a 2.45 GHz microwave oven with a 1.9 kW power supply. Results of the study showed that microwave treatment resulted in a 23 % reduction in work index of ore treated a microwave power of 1.406 kW and

after 10 s of exposure time. The flotation experiments showed enhanced concentrate recoveries and grades of nickel and copper for microwave treated ore. Relative increases in recovered concentrate, grade of nickel, and grade of copper of 26 wt.%, 15 wt.%, and 27%, respectively, were obtained for ore treated at a microwave power of 1,330 kW and after 30 s of exposure time and ground to 75 µm prior to flotation.

Further studies investigating the downstream flotation benefits of microwave treatment of a copper carbonite ore were carried out by Sahyoun et al. (2005). The ore samples were treated in a single-mode microwave cavity at power levels 5, 7.5,10 and 12 kW for exposure times of 0.1 and 0.5 s before grinding for flotation. The flotation experiments were carried out in a 3 litre Denver laboratory flotation cell. The results indicated a higher recovery in microwave treated samples for all power level and exposure time. Higher copper recoveries were obtained for ores treated at higher energy inputs compared to ores treated at lower inputs. There was no significant difference in cumulative grade between ore treated at lower power level and untreated ore. These results suggest that further benefits could be realised from microwave assisted comminution in the form of improved flotation recovery. These benefits besides being ore specific are also dependent on the microwave treatment conditions

Kobusheshe (2010) studied the downstream flotation benefits of microwave treated porphyry copper ores. The results showed improved liberation of secondary crusher product of up to 20% at typical flotation grind sizes. The ore was treated at energy input of about 2 kWh/t. Improvements in liberation were reported at coarser sizes between 212 µm to 425 µm. An increase in value mineral recovery of between 8 to 10% in coarse sizes and an overall grade increase of 1-2% were reported. These results showed the possible economic benefits of microwave pre-treatment of ore. Although the investigations were carried out in batch flotation tests, the results represent the first attempts at quantifying the benefits of microwave assisted comminution at economical energy inputs.

Charikinya (2011) investigated the effects of changes in liberation, as would be expected from microwave treatment of flotation feed, on recovery using a simulated flotation circuit. The investigation combined a fundamental model of froth flotation with the particle tracking capabilities of the mineral processing plant simulator HSC Chemistry 7. By doing so it was possible to investigate how differing degrees of mineral liberation, affect the grade and recovery achieved in flotation. The results of the study showed that mechanically agitated froth flotation cells can best exploit well-liberated material only if the material is coarser than a critical size (Charikinya, 2011). This suggests that the most appropriate way to exploit the benefits of microwave enhanced liberation would be to use coarse grinding following

microwave treatment, followed by flash flotation of the coarsely liberated material. Flash flotation is a relatively new method developed for floating coarse material that exceed the design limits of conventional, mechanically agitated flotation cells.The work carried out by Charikinya (2011) was limited to only the flotation section of the mineral processing flow sheet.

Irannajad et al. (2014) investigated the effect of microwave treatment on the flotation of ilmenite. Microwave pre-treatment was carried out in a 2.45 GHz microwave oven with a 1 kW power supply. The ore was microwave treated prior to grinding before flotation. The flotation experiments consisted of microflotation and batch flotation tests. The results from the microflotation experiments showed that the ilmenite surface irradiation converts Fe^{2+} to Fe^{3+} ions, leading to improved floatability. Microwave pre-treatment also resulted in a decrease in consumption of flotation reagents. Microwave treatment had no significant effect on surface properties and floatability of quartz particles. Results of the batch flotation experiments improvements in concentrate grade and recovery from 21.3% to 22.1% and 71% to 82.5%, respectively. The study concluded that microwave treatment results in improved selectivity and flotation recovery of ilmenite ore. The investigation was carried out at low energy inputs using multi-mode microwave heater. It is possible that higher recoveries could have been obtained at higher energy microwave treatment conditions.

2.4.5. Microwave assisted leaching

The application of microwaves to leaching processes can be divided into two main categories. The first involves the use of microwaves to enhance leaching kinetics, by carrying out leaching under the influence of microwaves. The second involves the use of microwave treatment during ore preparation stage to increase value mineral exposure and surface area by inducing cracks in ore particles. Most investigations reported in literature have focused on the former category. The latter category is of more interest in this study since the application of microwave treatment during ore preparation of heap leach feed as proposed in this study falls under that category. This review will therefore focus mostly on work that has been carried under the latter category.

Al-Harahsheh et al. (2005) investigated the effect of microwave treatment on leaching kinetics of a chalcopyrite ore. The chalcopyrite used in this study was in the form of natural crystals that were ground down to 100% passing 106 µm before being divided into different sub-fractions. Leaching experiments were carried out under conventional and microwave heat treatment conditions. Comparison of the amount of copper recovered from chalcopyrite under conventional and microwave heat treatment showed a marginal, but consistent, improvements

in copper recovery under microwave heat treatment conditions as opposed to conventional heating. It was suggested that the increase in copper recovery with microwave leaching was due to localized higher temperatures around the outer shell of the leaching solution as a result of the high dielectric loss factor (and thus low penetration depth) of the solution, and also selective heating of the outer skin of the chalcopyrite particles due to the high conductivity of this material. Al-Harahsheh et al. (2007) further investigated the leaching kinetics of pure sphalerite crystals in acidic ferric chloride under conventional- and microwave heated conditions. It was found that zinc recovery increased when leaching was carried out under microwave irradiation. It was suggested that this enhancement was due to the higher heating rates in the leaching solution. Other claims of improved value mineral recovery under microwave irradiation conditions during leaching has been reported by various authors (Hua et al., 2002; Hwang et al., 2002; Krishnan et al., 2007; Zhai et al., 2009).

Olubambi et al. (2007) investigated the influences of microwave irradiation on the heating characteristics, breakage response, mineralogy and the mechanisms of dissolution in sulphuric acid and hydrochloric acid. The ore used for the study was a complex sulphide ore and consisting of ferrous sphalerite, galena, pyrite and covelite. Microwave heating of the ore was carried out in a 2.45 GHz microwave oven with a 1.1 kW power supply at microwave exposure times of between 5 to 11 min. The results of the study showed that the application of microwave heating had a beneficial effect on the dissolution of a complex sulphide ore in sulphuric and hydrochloric acid. The increase in dissolution of the microwaved treated samples was attributed to an increase in electrochemical sites resulting from an increase in the number of cracks, and increased pyrite phases which promoted galvanic interaction within the system.

Olubambi (2009) further investigated the influence of microwave treatment on the bio-leaching behaviour of a low-grade complex sulphide ore in a mixed mesophilic bacterial culture through bio-leaching experiments and electrochemical techniques. Improved bio-leaching recovery was observed for the microwave treated ore. Both microwave treated and untreated samples showed similar electrochemical behaviour. Microwaved samples displayed higher reactivity, dissolution rates, dissolution currents, current densities and a decreased polarisation resistance. Results revealed that microwave treatment improved the bio-leaching of behaviour of the ore, with more effect on copper and iron dissolutions than on zinc and lead. It was suggested that the increase in dissolution of the microwaved treated samples was due to phase changes in the ore which promoted galvanic interaction within the system, and an increase in electrochemical sites resulting from an increase in the number of cracks induced by microwave heating.

Schmuhl et al. (2011) investigate whether heap leaching efficiency could be improved by introducing micro-fractures and cracks into the ore using microwaves. The investigation was conducted using a low-grade copper ore with finely disseminated sulphide mineral phases. The main copper-bearing mineral phases in the ore were chalcopyrite, chalcocite and bornite. The ore was crushed and screened to the following size fractions, +6.7-9.2 mm, +9.2-12.5 mm and +13-19 mm. The ore samples in each size fraction was then irradiated in a 2.45 GHz single mode microwave applicator coupled to a 3 kW switched mode power supply at microwave exposure times ranging from 5 to 120 s. Column leaching experiments were carried out over 30 days using sulphuric acid as a lixiviant. The results of the study showed an increase in copper yield with microwave pre-treatment of the particles. The increase in copper recovery was attributed to microwave pre-treatment inducing macro and micro-fracturing in the particles, resulting in a substantial increase in the internal surface area of the ore particles. Copper yield during leaching was observed to increase by between 10 to 20% after microwave pre-treatment. It was concluded that microwave pre-treatment of ores before heap leaching had the potential to significantly enhance the economics of heap leaching recovery. The microwave treatment conditions were observed to have a significant influence on the observed enhancement in metal recovery.

2.4.6. Numerical modelling studies on microwave heating of ores

Numerical simulations have been used to investigate the microwave treatment response of different materials. Continuum analyses and bonded particle modelling has been used to investigate the patterns of stresses generated inside microwave treated ore particles during microwave treatment in a number of studies (Ali and Bradshaw, 2009; Jones et al., 2005, 2007; Salsman et al., 1996; Wang and Djordjevic, 2014; Whittles et al., 2003).

Salsman et al.(1996) developed a finite element model to predict the thermo-mechanical response of a single spherical pyrite particle, locked in a calcite host rock, subjected to short-pulse microwave heating. The results from the model showed that the temperature gradient between the two phases increased with an increase in power density, with the resulting thermal stresses exceeding the strength of the materials. The simulation results showed that the temperature gradient was due to the selective heating of the value mineral phase by microwaves and that the temperature gradient increased with an increase in power density. It was concluded that the economics of microwave assisted grinding could be improved by using very high power density microwaves for at short exposure time. This was because the temperature gradient was observed to decrease with increasing exposure time.

Whittles et al.(2003) conducted studies to predict the influence of power density on strength reduction by using a finite difference numerical modelling. In the study, a binary phase ore was simulated which consisted of an absorbing phase and transparent host represented by pyrite and calcite respectively. Numerical simulations were then applied to assess the influence of applied power density on the strength of the simulated ore. The results showed that at higher power density and shorter exposure time heat lost by conduction was minimised. The major findings from this study was that by increasing the power density, significantly greater thermally induced stresses and strain were induced at lower microwave energy input. This was in agreement with results from the model developed by Salsman et.al. (1996).

Jones et al.(2005) developed finite difference quasi-static thermo-mechanical 2-D model of a theoretical 2-phase mineral. The model was used to simulate the thermal stresses generated and subsequent thermal damage in a rock particle exposed to high electric field strength microwave energy. In the study, a binary phase ore was simulated which consisted of a single circular pyrite grain in a calcite matrix. The diameter of the pyrite grain was varied so as to determine the influence of power density and grain size on thermal stress generation and thermal damage. Simulation results indicated that the stress regime inside the pyrite is compressive whereas outside boundary shear and tensile stress were predominant. These results showed that fractures originate at the grain boundary between heated and transparent phases, which once again illustrated the potential for increased liberation in addition to particle weakening. It was noted that the spherical nature of the microwave absorbing grains was responsible for the grain boundary fracture observed in the ore models. It was suggested that the symmetry of the pyrite grains ensured that compressive stresses were equal in all directions, reducing the likelihood of shear stresses developing thus, making the formation of trans-granular fracture unlikely. In real ores where particles deviate from spherical, trans-granular fracture is likely to be more prevalent.

Later Jones et.al. (2007) investigated the likely strength reduction over a wide range of power densities and exposure times, to determine the optimum operating range of future microwave comminution equipment. Using a quasi-static thermo-mechanical 2D model of a simplified pyrite/calcite system. The model ore comprised of a 1% pyrite particle randomly disseminated in a calcite matrix. After simulating the heating of the model ore by microwaves, the strength of the ore was quantified using a simulated unconfined compressive strength test. The exposure power times and the power densities were varied and the corresponding decrease in strength due to microwave treatment was measured. The results showed greater reductions in strength for a given total energy input at shorter exposure times. The model results showed

higher model ore strength reduction when the power density was very high and the exposure time was very short. The power density was varied between 1×10^{9} to 1×10^{15} W/m^3. Based on the model results, it was suggested that future microwave comminution equipment should be capable of generating power densities of between 1×10^{10} and 1×10^{12} W/m^3 with exposure times of between 0.2 and 0.002s.

Wang et al. (2008) studied the effect of microwave heating on thermal damage in a conceptual binary ore consisting of pyrite in a calcite matrix using a thermal-based particle model. The model was used to investigate the efficiency of fracturing and grinding on ores containing different calcite/pyrite ratios after microwave treatment. Simulations were performed using power densities of 1×10^{9} and 1×10^{11} W/m^3. Simulation results indicated a higher temperature gradient and thermal stress at the interface between the pyrite and calcite phases when the power density was high for the same exposure time. This was in agreement with modelling results from earlier studies that showed an increase in temperature gradient with increasing energy input. Wang et al. (2008) also showed that the fracture density (the ratio of number of broken bonds to original number of bonds) increased as the microwave exposure time (energy input) increased. An investigation of the effect of power density on stress distribution and fracture density for the same energy inputs was not carried out in this study. For microwave pre-treatment of ore to be economically viable, significant fracture should be achieved at economical energy inputs.

Ali and Bradshaw (2010) carried out bonded particle modelling investigations into the mechanism of microwave induced micro fracture. Computational simulations of microwave heating and thermal damage were carried out using two-phase conceptual ores. The results showed that microwave treatment at high power density offered the possibility of localizing induced damage around the grain boundaries. This followed on previous numerical modelling work by the author, where a continuum modelling approach was used to determine the most efficient method of maximising grain boundary damage in microwave treated ore particles (Ali and Bradshaw, 2009). The results of the study showed that operating at high microwave power density and decreasing exposure time offered the best energy efficiency with maximum grain boundary damage. The study also showed that the amount of damage incurred at a specific power density and energy input was dependent on the ore mineralogy and its texture. The modelling results showed that more grain boundary damage was induced in coarser textured ores for the same energy input and damage was maximised for ores with microwave absorbing grains with a large thermal expansion coefficient.(Ali and Bradshaw, 2009). These results further showed the feasibility of microwave treatment as substantial microwave induced

fracture was achieved at economical energy inputs. Ali and Bradshaw (2011) using bonded particle modelling investigated confined bed crushing of microwave treated ores. The study showed that crushing velocity could significantly affect the liberation properties of pre-treated ores. The work suggested inter-particle breakage as the most appropriate comminution method of exploiting microwave induced grain boundary fracture in microwave pre-treated ores (Ali and Bradshaw, 2011).

Wang and Djordjevic (2014) simulated the thermal cracking process around a single microwave absorbent phase inclusion using finite element method. The dependence of the failure mechanism on power density and exposure time was investigated. The simulated ore particle consisted of an absorbing phase and transparent host represented by pyrite and calcite respectively. The model ore measured 1 mm in radius with the pyrite grain size varying between 0.25 mm and 0.50 mm in radius. Results of the study showed that, initial breakage due to microwave treatment is caused by tensile thermal stresses therefore cracks propagate gradually in a radial direction from the calcite matrix. This was in agreement with results from an earlier study by Jones et al. (2005) that demonstrated that the stress outside the microwave absorbing pyrite phase grains was predominantly tensile. Wang and Djordjevic (2014) further reported that the cracks in the calcite matrix started close to the phase boundary interface but not right on it. The main factor affecting the location of maximum stress was observed to be the thermal expansion of the calcite matrix and exposure time. The longer the exposure time, the further away the peak stress was from the phase boundary interface of the different minerals. The thermal expansion of the different phases was observed to play a critical role in producing thermal stresses, this was in agreement with results from a study by Ali and Bradshaw (2009). The amount of absorbing phase was reported to have an effect on microwave induced breakage with large pyrite grains increasing the peak tensile stress. The study concluded that high power density combined with a short microwave heating exposure time was expected to offer the best energy efficiency for microwave heating of ore particles. This was consistent with previous findings from earlier modelling studies (Ali and Bradshaw, 2011; Jones et al., 2007; Salsman et al., 1996).

Meisels et al. (2015) investigated the influence of particle heterogeneity on the amount of diffuse scattering as well as the heating and the formation of microwave induced stresses using, finite element method. The size of the rectangular model particle was 50 cm in width and 30 cm in length and a simulated microwave source with width 8.6 cm (corresponding to the opening of the waveguide for 2.45 GHz) was used to simulate microwave heating of the rock model. The rock model was a two-component model, with circular discs measuring 0.467

cm in diameter, representing plagioclase distributed randomly in a matrix representing quartz. The results of the study showed that reflections at the discs/matrix interfaces and absorption in the discs lead to diffuse scattering with up to 20% changes in the intensity of the main microwave beam compared to a homogeneous ore model. In addition a high thermal gradients between the constituents were observed leading to high maximum principal stresses. Based on the results it was concluded that the thermal and mechanical material properties combined with selective absorption are essential for enhanced damage due to microwave treatment. In ore particles with strong heterogeneity thermal stresses can have short-range variations due to the different thermal expansion of the constituents. These results suggests that ore heterogeneity has an influence on the extent of crack damage during microwave treatment. Results of this study confirmed results from similar studies that showed that the extent of microwave induced damage was dependent on ore mineralogy and texture (Ali and Bradshaw, 2009, 2010; Wang and Djordjevic, 2014). Thus the heterogeneous nature (texture) of ores has to be considered when investigating microwave induced stress and damage.

2.5.Comminution

Typical heap leaching operations involve a crushing plant where ore from the mine is reduced in size, before it is placed in heaps for metal recovery (see Figure 2-1). Dump leaching is similar to heap leaching however, in the case of dump leaching ore is taken directly from the mine and placed in heaps without crushing. Typically, the feed size to the heaps is < 25 mm for crushed and agglomerated ores and as large as 500 mm for run of mine ore types found in dump leaching (Watling, 2006). The desired value metal is recovered from the heap liquor by solvent-extraction to produce high grade concentrates.

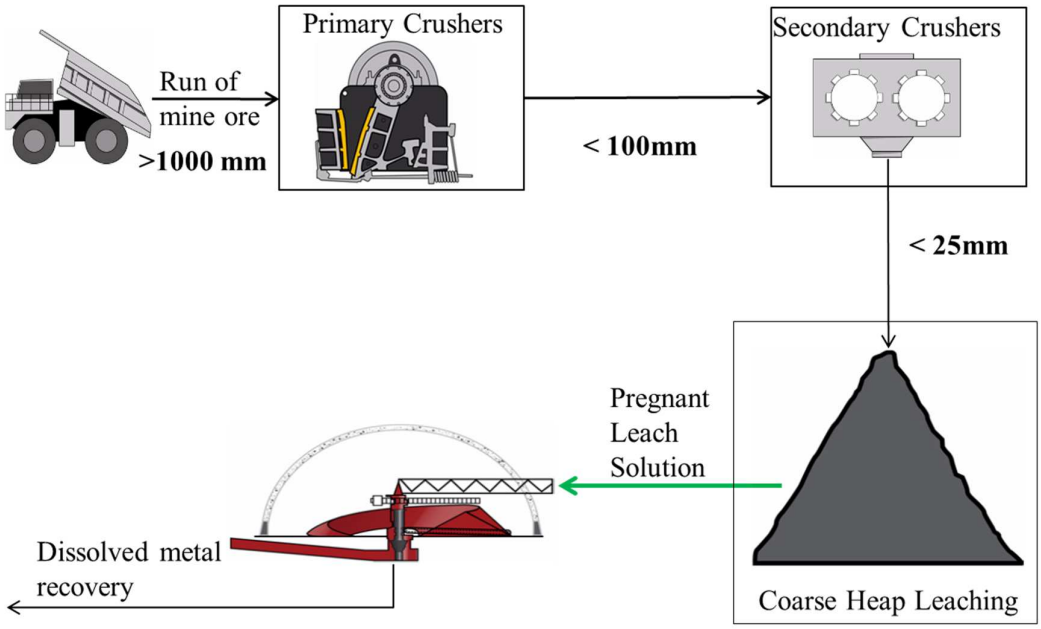

Figure 2-1: Schematics of a typical heap leaching operation

The objective of comminution operations is to liberate value mineral. Value mineral liberation is achieved by size reduction operations. Depending upon the requirement, size reduction in a crushing plant could include primary, secondary and tertiary crushing stages. Gyratory crushers, jaw crushers are common examples of primary crushing equipment used in the mining industry. Lumps of run-of-mine ore as large as 1.5m across are reduced in the primary crushers to 100 to 200 mm (Wills, 2011). Primary crusher products is further reduced in size in secondary and tertiary crushers. Secondary and tertiary crusher equipment includes cone and HPGR crushers.

Comminution is an energy intensive, inefficient process. There has been a lot of interest in designing and introducing new comminution techniques that are more energy efficient, compared to traditional comminution techniques such as gyratory, jaw and cone crushers. This drive towards developing more energy efficient comminution methods is driven by the high cost of energy required to achieve liberation. High Pressure Grinding Rolls (HPGR) is one such relatively new technique in the mining industry that has shown benefits such as, improved comminution efficiency and reduced energy consumption (20 to 50%) when compared against conventional methods (Daniel, 2007). HPGR can be considered as both a fine grinding device as well as a crushing and grinding device for fine and coarse feeds respectively (Baum and Ausburn, 2011; Dunne et al., 2004; Rule et al., 2009).

2.5.1. High Pressure Grinding Rolls (HPGRs)

The HPGR is made up of two counter rotating rolls; one rotates on a fixed axis while the other moves linearly (Daniel, 2007; Daniel and Morrell, 2004). Pressure is applied to the moving roll by means of a hydro-pneumatic spring system which forces the moveable roller up against material fed between the rollers. Material is fed through a small feed hopper installed above the feed rolls. The surfaces of the rotating rolls grip the material and pull it into and through the rolls. The material held between the rolls is subjected to high pressure, with comminution takin place by compressive as well inter-particle breakage (Morley, 2010; Morrell, 2010; Napier-Munn, 2005). Studies on HPGR breakage mechanism, have shown that the primary breakage mechanism in an HPGR is inter-particle bed breakage (Fandrich et al., 1997; Gupta and Yan, 2006).

Particle breakage during comminution can be either single or inter-particle (Liu and Schanert, 1996). Although inter-particle bed breakage in HPGR has a lower efficiency than single particle stressing, the HPGR is more energy efficient when compared with conventional crushers and tumbling mills (Daniel, 2007; Napier-Munn, 2005). This is due to the determinate and uniform loading of material in the HPGR compression zone whereas the loading in conventional comminution equipment is random and highly variable, and therefore inefficient (Morley, 2006, 2010).The amount of material in the compression zone is a characteristic of the process ore, roll diameter and roll surface characteristics (Daniel, 2007; Daniel and Morrell, 2004; Tavares, 2005).

The HPGR product is discharged in the form of a compressed flake. The competency of the flake is a function of the ore type, its moisture content and the force applied by the HPGR device. It has generally been observed that, hard, competent ores produce fragile flakes that need no special measures for deagglomeration, while softer ores can produce competent flakes that require an additional deagglomeration step before being processed in the next unit operation (Morley and Staples, 2010; Rosario et al., 2011; Saramak and Kleiv, 2013). Thus HPGR is more suited for processing hard ores.

2.5.2. Effect of mode of comminution on preferential breakage

Phase or grain boundary fracture is a form of non-random breakage which occurs when cracks propagate along phase boundary rather than across these boundaries (King and Schneider, 1998a). An indication of whether grain boundary fracture has taken place during comminution is gained by comparing the interfacial area between the different phases before and after

breakage (Fandrich et al., 1997; King, 1992). A loss of interfacial area is indicative of grain boundary fracture having occurred. It has been suggested that grain boundary can result in preferential liberation thus, it has been the focus of a number of studies on selective liberation during comminution (King, 1992; King, 1993; Meloy and Clark, 1985). Grain boundary fracture, is strongly dependant on the stress state and material properties at grain boundary. It has been suggested that each mode of fracture occurs at particular relative energy level. For example when the required energy level for grain boundary fracture is exceeded, other forms of fracture such as trans-granular fracture may occur. This suggest that a controlled supply of energy to cracks may promote grain boundary fracture (Fandrich, 1998; Garcia et al., 2006; Meloy and Clark, 1985; Veasey and Wills, 1991).

The role of grain boundary fracture in accounting for preferential liberation is still not well understood. A number of studies have shown experimental evidence of grain boundary fracture in crushed particles. Fandrich et.al. (1997) reported evidence of preferential liberation of the gangue phase during the comminution of an iron ore by slow compression breakage in a piston and die arrangement. King and Schneider (1998a) observed preferential liberation on a binary dolomite-sphalerite ore ball mill product. In both cases the observed preferential liberation was attributed to selective breakage. Theoretical studies by King (1994) using linear intercept analysis suggest that modest amounts of grain boundary fracture do not result in an increase in the degree of liberation. The investigations used a model binary ore. The results were not validated experimentally as the determination of grain boundary fracture during multiphase particle breakage is a difficult task to achieve.

Garcia et.al. (2009) conducted a rigorous investigation on the breakage of single multiphase copper ore particles (3 mm cubic particles) by slow compression breakage. The study showed that preferential grain boundary fracture occurs at low energy dissipation rates and lead to improved mineral exposure in certain ores. The significance of grain boundary fracture was observed not only to vary with ore type but also with particle size (Garcia et al., 2006). Results of this study also substantiated earlier research suggesting that for a given ore type there may be a critical size at which the breakage mechanism for multiphase particles changes from grain boundary to inter-granular fracture (Bradt et al., 1995; Fandrich, 1998). These results suggest that comminution techniques, such as HPGR, that favour slow compression breakage, are likely to produce crushed products with greater mineral exposure, as these techniques favour grain boundary fracture (Kodali et al., 2011; Tavares, 2005).

Numerous investigation examining the mode of fracture in HPGR has been carried out. These studies have reported evidence of micro cracking along the grain boundary in HPGR products has been reported (Daniel, 2007; Fandrich et al., 1997; Kodali et al., 2011). It has been generally suggested,based on this evidence, that HPGR products have more enhanced mineral liberation properties compared to those from conventional rod/ball mills (Fandrich, 1998; Kodali et al., 2011; Tavares, 2005). The benefits of improved liberation expected from the use of HPGR is likely to be ore and size specific (Chapman et al., 2011; Daniel, 2007; Palm et al., 2010; Solomon et al., 2011; Vizcarra et al., 2010). The benefits of HPGR, relating to improved mineral exposure through preferential liberation are debatable. There is a limited amount of literature relating to rigorus investigations on mineral liberation in HPGR products. There is no conclusive evidence suggesting that the mode of fracture in HPGR products is predominantly grain boundary fracture. HPGR products have been shown to have significant micro-cracks when compared against conventional comminution products (Kodali et al., 2011).

2.6.Ore characterisation techniques

There are a number of image-based techniques for determining ore characteristics such as liberation, mineral composition and association, such as Automated SEM and high resolution XCT techniques (Cnudde and Boone, 2013; Cnudde et al., 2006; Fandrich et al., 2007; Gottlieb, 2008). The ability of each of these techniques to discriminate between mineral species varies widely (Cnudde et al., 2006; Fandrich et al., 2007; Ketcham and Carlson, 2001). Automated SEM and XCT techniques make it possible to quantitatively determine the chemical composition of materials and to study the grains and cracks in the material structure (Gottlieb et al., 2000; Fandrich et al., 2007).

2.6.1. Automated SEM techniques (QEMSCAN)

Some examples of Auto-SEM systems are QEMSCAN, Mineral Liberation Analysis (MLA), Mineralogic and Tescan Integrated Mineral Analyzer (TIMA). A QEMSCAN system was used for ore characterisation in this study. QEMSCAN produces 2D images of polished sections of mounted mineral particles, utilising back scattered electron (BSE) and Energy Dispersive Spectra (EDS) X-ray-detectors. Minerals are identified based on their elemental X-ray counts (Fandrich et al., 2007; Gottlieb, 2008; Gu et al., 2014). QEMSCAN is used widely in the minerals processing industry as a tool for the acquisition of mineralogical and metallurgical data (Lotter et al., 2011; McClung and Viljoen, 2011; Pascoe et al., 2007). QEMSCAN comprises of several modes of measurements. These are bulk mineralogical analysis (BMA), particle mineral analysis (PMA), specific mineral analysis (SMA), trace mineral search (TMS) and Field Image Analysis (Gottlieb, 2008). A detailed review of these analytical mode capabilities is given in Gottlieb et al. (2000) and Pirrie et al. (2004). The size resolution limitation for QEMSCAN is about 1 μm to 2 μm. The scanning of particles less than 5 μm in size may compromise the reliability of the analysis (Goodall, 2008).

In mineral processing separation of value minerals takes place by physico-chemical processes. In these processes separation is due to differences in physical properties of the material. The term "free particles", in comminution liberation terms, generally refers to particles consisting of a single mineral phase. While "locked particles" consist of two or more mineral phases. The "degree of liberation" is the fraction of “free particles” with respect to the total amount of particles present and it defines the limits of recovery for separation processes (Garcia et al., 2006; Miller et al., 2003). In leaching operations “exposed grains” are grains exposed at the surface of the locked particle or grains that are in the neighbourhood of cracks open to the surface. These grains are accessible to reactant solution, and can potentially be

recovered. Grains referred to as "unexposed grains" on the other hand are grains enclosed within other host mineral, such as gangue. The ratio of the volume of exposed valuable grains to the total volume of both exposed and unexposed grains in the crushed particles is defined as "the degree of exposure" and is analogous to "the degree of liberation" for crushed particles as used in particle separation processes, such as flotation (Garcia et al., 2006; Ghorbani et al., 2011a).

Analysis of mineral exposure from polished sections requires stereological transformations for estimation of 3D characteristics which is accomplished by applying stereological correction models (Fandrich et al., 1998; King and Schneider, 1998b). Stereological models are not satisfactory because model parameters depend on the ore texture which is unique for each ore type (Miller and Lin 1988). Therefore SEM-based automated image analysis systems are incapable of providing accurate direct measurements of exposed grains in ore particles. Since QEMSCAN is based on the examination of polished particle sections, there are limitations to the size and shape of particles that can be analysed using the method.

2.6.2. X-ray Computed tomography (XCT)

XCT allows for the investigation of interior features within solid objects, and for obtaining digital information regarding their 3-D geometries and properties (Cnudde and Boone, 2013; Ketcham and Carlson, 2001). Using XCT it is possible to distinguish the different mineral phases in ore particles, based on the differences in attenuation coefficients between each mineral phase. XCT produces a three dimensional map of the ore particle's internal structure and is currently the only direct measurement technique available for measuring mineral grain exposure (Garcia et al., 2006; Garcia et al., 2009; Miller et al., 2003). XCT is widely used not only for quantitative analysis of multiphase systems but also for textural characterisation (Lin and Garcia, 2005; Lin et al., 2012; Miller and Lin, 2003).

Garcia et al. (2006) utilised XCT to determine the copper mineral grain size distribution and extent of value mineral grain. XCT has also been used to investigate, the extent to which preferential grain boundary fracture contributes to liberation. Garcia (2009)used XCT to calculate the interfacial area loss in particles, crushed under different breakage conditions. For the copper ore studied, it was shown that preferential grain boundary fracture occurs at low energy dissipation rates (Garcia et al., 2009; Xu et al., 2013). XCT analysis was also used to determine the fraction of mineral exposed and thus, to predict the ultimate heap leach recovery by Miller and Lin (2003).

Lin and Garcia (2005) developed algorithms for acquiring 3D irregular mineral ore particle shapes and texture using XCT. The results showed that particle shape and texture could be described using XCT (Lin and Garcia, 2005). XCT has been successfully used, for 3D determination of internal damage of ore particles crushed under different conditions The results showed that XCT, allows for investigation of the extent of damage and crack formation, to be evaluated for different crushing conditions, at a reasonable cost and time (Lau et al., 2012). Kodali et al. (2011) evaluated particle damage and value mineral grain exposure in copper ore particles crushed under different conditions using XCT. Particle damage analysis was limited to large cracks due to voxel resolution. Cracks smaller than the voxel resolution size of 40 µm were not detected. Suggesting that the accuracy of XCT measurements of particle crack damage could be improved by using higher resolution XCT machines (Kodali et al., 2011).

Ghorbani et al. (2011b; 2012) used XCT to investigate the effect of mode of comminution (cone vs HPGR) on crack formation. The progress of crack growth during leaching in coarse sphalerite ore particles produced from cone and HPGR crushing was also investigated. Using a combination of the effective atomic number and prior knowledge of the mineralogical characteristics of the ore, the cracks and different phases in the ore were segmented (Ghorbani et al., 2011b). Leaching columns were used to simulate heap leaching conditions and the experiment was run over 11 months (Ghorbani et al., 2012). The reactors were stopped from time to time to investigate the progress of crack and micro crack growth and its effect on metal extraction using XCT. The results from XCT were validated with those obtained using traditional Auto-SEM/EDS techniques (Ghorbani et al., 2013a; Ghorbani et al., 2012). The crack network in the particles produced by HPGR, increased during the leaching process accelerating reagent diffusion into the particles resulting in increased metal extraction (Ghorbani et al., 2013b; Ghorbani et al., 2012). No significant change was observed in the crack network for the particles produced using the cone crusher (Ghorbani et al., 2012). Investigation of the reacted fraction of Zn vs distance from the centre of each particle was carried using XCT images of leached particles (Ghorbani et al., 2013b). The results showed that leaching from large HPGR crushed particles occurred predominantly at the surface, with only partial conversion in the zones that are closer to the centre of particles (Ghorbani et al., 2013b). For cone crushed particles no significant sub-surface conversion was observed (Ghorbani et al., 2013b).

2.7.Heap leaching

Heap leaching has been shown to be an economically viable, energy efficient, hydrometallurgical processing, option route for extracting metals from complex low-grade ores such as copper, zinc, nickel and gold (Pradhan et al., 2008). Heap leaching involves the dissolution of metals, by reaction with a lixiviant that percolates through a heap of crushed ore or agglomerated material. In heap leaching, the ore is typically crushed to a size fraction suitable for controlled irrigation and percolation of lixiviant and deposited in heaps. The heaps are irrigated with the lixiviant that reacts with the minerals present in the ore particles. The resultant pregnant leach solution is collected for further processing to extract the valuable metals. The kinetics of heap leaching reactions are a complex function of particle size distribution, ore mineralogy, surface properties, crack size distribution and ore permeability (Ghorbani et al., 2011b; Petersen and Dixon, 2007). One major drawback of heap leaching is the low recovery as compared to recovery by milling and flotation. This is because heap leaching is generally characterised by the extraction of valuable metals from poorly liberated, relatively coarse particles. Although mineral exposure has been shown to increase with decreasing particle size (Hsih et al., 1995; King, 1979; Miller et al., 2003). Heap leaching of too finely crushed ore may result in solution percolation and air flow problems in the heap. Thus heap leaching typically involves the recovery of metals from relatively coarse particles, often greater than 1 mm (Ghorbani et al., 2011a; Pradhan et al., 2008). Valuable mineral grain exposure and accessibility to lixiviant in these coarse particles are important factors that limit the extent of metal recovery in heap leaching. Where microorganism are used to aid the oxidation of sulphide minerals the process is known as bio-heap leaching.

Bio-heap leaching involves the use of micro-organisms (of which thiobacillus ferro-oxidans and sulpho-oxidans are most common) to catalyse the re-oxidation of ferrous to ferric by dissolved oxygen. Bio-leaching is mainly a chemical process where ferric iron and protons are responsible for the leaching reactions. The role of the micro-organisms is to produce the leaching reagents and to create the space in which the leaching reactions take place (Breed and Hansford, 1999; Gericke et al., 2009). There are three possible mechanisms by which micro-organisms can potentially interact with a sulphide mineral, these are (Crundwell, 2003; Hansford, 1997; Watling, 2006);

1. Bacteria oxidize ferrous ions to ferric ions in the bulk solution, and the ferric ions oxidize the sulphide phase.

2. Bacteria attached to the mineral surface oxidize ferrous ions to ferric ions within a biofilm comprised of bacteria and exo-polymeric material, and the ferric ions generated within this layer oxidize the sulphide phase.
3. Bacteria attached to the mineral surface oxidize the sulphide phase by biological means directly, without any requirement for ferric or ferrous ions.

They are two steps to sphalerite dissolution reported in literature (Breed and Hansford, 1999; Rodríguez et al., 2003). The first step involves the rapid attachment of micro-organisms to active pyrite surfaces leading to the oxidation of the pyrite and subsequent bio-generation of ferric ions and protons. The second step involves the continued regeneration of ferric ions by planktonic bacteria and the oxidation of the elemental sulphur reaction product. The first step is key to enhanced sphalerite leaching. There is a direct relationship between the magnitude of cell attachment in the first step of the process; and the dissolution rate in the second step (Breed and Hansford, 1999; Rodríguez et al., 2003).

Numerous advantages and disadvantages of heap leaching have been reported in literature (Brierley and Brierley, 2001; Ghorbani et al., 2011a; Pradhan et al., 2008; Watling, 2006). Some of these advantages and disadvantages are listed in Table 2-3. The major disadvantage of heap leaching operations is poor metal recovery and long extraction times (Pradhan et al., 2008; Watling, 2006). This inefficiency is as a result of poor permeability of the lixiviant through and into the ore. Poor permeability causes solution flow problems and uneven distribution of the leaching solution across the heap bed. In some cases agglomeration before stacking can offer a partial solution leaching solution flow problems (Dhawan et al., 2013). Agglomeration introduces additional costs to the heap leaching process and requires fine grinding (-75 µm) of the ore prior to agglomeration.

Table 2-3: Heap leaching advantages and disadvantages

Advantages	**Disadvantages**
• Low capital and operating costs. • The ore can be upgraded to the metal at the mine site. • Air pollution by sulphur dioxide is eliminated. • Certain mineral assemblages not amenable to treatment by conventional processes may be treated successfully. • Heap leaching is typically carried out on coarse particles -20 mm. The absence of a milling step makes heap leaching ore preparation significantly less energy intensive when compared against other methods such as agitated leaching that require the ore to be fine crushed. • Solid liquid separation steps are not required for heap leaching. • Heap leaching pads can be left in place after reclamation, with no extra costs required for tailings disposal. • Heap leaching can be used to treat low-grade ores, wastes and small deposits economically. • A low tech-process that is relative simple to operate. • Environmentally acceptable.	• Lower recovery when compared to other hydro metallurgical processes such as agitated leaching and flotation. • Solution flow problems especially when treating ores with high clay content and fines. • In areas of high rainfall, solution balance problems can arise, resulting in the need to treat and discharge process water. • Long leach cycles and hold-up. • Large environmental footprint. • Sulphur by-products are not recovered. • The excess acid generated must be neutralized. • Significant water losses occur through evaporation in the heap leach.

2.8.Factors affecting large particle heap leaching kinetics

Metal leach recovery in bioleach processes is determined by a large number of factors (Ghorbani et al., 2011a; Petersen and Dixon, 2006). Some of these factors include, physical and chemical, biological and ore characteristics. The best leach process is one whose only limitations are due to parameters beyond the control of the operator such inherent dissolution kinetics. Parameters such as mineral exposure, particle size and surface area, can be controlled by the operator as they are related to the ore preparation methods applied. Table 2-4 is a list of some of the major factors influencing metal recovery along with parameters that fall under each factor.

Table 2-4 : Factors and parameters affecting heap bio-leaching and metal recovery (Brierley and Brierley, 2001; Ghorbani et al., 2011a; Pradhan et al., 2008)

Factor	Parameters affecting bio-leaching
Physical and chemical characteristics	Temperature, pH, redox potential, CO_2 and O_2 content, nutrient availability, oxygen availability, homogenous mass transfer, Fe (III) concentration, presence of inhibitors, etc.
Biological characteristics	Microbial diversity, population density, microbial activities, metal tolerance, spatial distribution of micro-organisms, attachment to ore particles, adaption abilities of micro-organisms, and inoculum
Ore characteristics	Mineral type, acid consumption, grain size, mineral dissemination, surface area, porosity, hydrophobic galvanic interactions, and formation of secondary minerals

2.8.1. Mineral exposure of particles in the heap

The ore preparation stage of heap leaching feed, involves size reduction and in some cases agglomeration prior to stacking of the crushed ores in heaps. The objective of size reduction is to increase the mineral exposure of value mineral grains to the lixiviant by generating new surface areas and micro-cracks. Recent studies have shown that mode of comminution has an influence on heap leaching recovery (Ghorbani et al., 2012; Kodali et al., 2011). For example, heap leach feed ore prepared by HPGR crushing has been shown to result in greater heap leach recovery compared to ore particles crushed by conventional means. This has been attributed to the amount of micro-cracks produced during HPGR crushing. Greater micro-cracks are likely to result in improved mineral exposure and thus, enhanced heap leaching recovery (Garcia et al., 2006; Ghorbani et al., 2012; Kodali et al., 2011). Although minerals may be liberated through the cracks, value metal will not leach if no solution is in contact with the mineral grains.

The accessibility of mineral grains to leach solutions via cracks and pores within particles determines the performance of heap leaching sub-processes. This is because leaching primarily occurs at the sub-surface regions that are available through surface cracks and pores (Ghorbani et al., 2011a; Petersen and Dixon, 2007; Pradhan et al., 2008). In heap leaching valuable mineral grains are usually embedded within larger ore particles and thus, accessible only by diffusion through a network of connected cracks (Ghorbani et al., 2013a; Miller et al., 2003). Thus there has been recent interest in identifying ore crushing methods that favour improved mineral exposure, through generating micro-cracks. Recent studies have shown that high pressure grinding rolls (HPGR) products have more cracks when compared with products of the same size class from rod/ball mills (Daniel, 2007; Tavares, 2005). Daniel (2007) qualitatively compared MLA back scattered images of HPGR crushed particles against those from conventional ball mills. The results showed that HPGR promotes micro cracking. Vizcarra (2010) carried out studies to determine the effect of comminution mechanism on particle properties such as liberation. The results of the studies showed that liberation properties were independent of comminution route and degree of size reduction (Vizcarra et al., 2010). This suggests that the properties of the ore, and not the mode of comminution, determine the amount of cracks induced in the ore during size reduction (Powell and Morrison, 2007). Ghorbani (2011b) investigated the effect of mode of comminution on crack formation on cone and HPGR crushed particles. Using a combination of 3D X-ray computed tomography (XCT) and 2D Quantitative Evaluation of Minerals by Scanning Electron Microscopy (QEMSCAN) techniques, the study showed that HPGR produced particles with a higher density of cracks and micro-cracks compared to cone crushed products of the same size. Subsequent column leach tests of the mill products showed greater metal recovery in HPGR crushed particles than cone crushed particles due to the presence of micro-cracks (Ghorbani et al., 2013b; Ghorbani et al., 2012).

2.8.2. Solid/liquid contact area

Solid/liquid contact area is an important factor in determining the kinetics of leaching reactions. To promote maximum solid/liquid contact, heaps are operated such that the leaching solution flows evenly under the action of gravity and capillary forces and without channelling (Bennett et al., 2012; Ghorbani et al., 2011a). This is achieved by constructing heaps with good hydraulic properties that promote even lixiviant flow across the heap. Hydraulic properties of heaped ores are closely connected with available pore sizes in the ore which in turn is a function of the particle size distribution (Bouffard and Dixon, 2001). Solid/liquid contact area in low-porosity

rocks is mainly a function of particle size of the material (Bouffard and West-Sells, 2009; Ghorbani et al., 2011a). A fine particle size distribution maximises surface area and therefore reactivity, but can result in low hydraulic conductivity preventing effective fluid flow through the heap (Bartlett, 1997; Lupo, 2012). The particle size distribution must also promote physical stability within the heap. Thus there is often an effective maximum particle size for any given leach system that ensures maximum solid/liquid contact and good heap permeability (Bennett et al., 2012; Bouffard and Dixon, 2001). The presence of fine particles in the crushed ore tends to decrease permeability. Low permeability heaps result in increased operation time as it takes the leach solution longer to percolate through the heap. Where the heap is uneven channelling can occur leaving parts of the heap without immediate contact with the leach solution (Ghorbani et al., 2011a; Watling, 2006). Thus permeability of the heap and individual ore particles is important for improved heap metal dissolution rates.

Comminution methods that promote micro-cracks will offer improved solid/liquid contact at economical sizes. As leach solution is able to penetrate into micro-fissures and micro-cracks of the rock mass. In addition the overall rate of reaction in heaps, is highly dependent on the diffusion of reactants and products. Reactants diffuse in through pores in the rock matrix of each ore particle chemical reaction site where metal dissolution takes place (Ghorbani et al., 2011a; Petersen, 2010). The dissolved chemical species must diffuse through the stagnant solution occupying the bed voidage in order to be recovered in the pregnant leach solution (da Silva, 2004). The extent of this inter-particle pore diffusion on extraction rate and mineral leaching depends on the length of the diffusion pathway, which may be significant for systems with poor solution distribution (Bouffard and Dixon, 2001; Petersen and Dixon, 2007). Diffusion is a function of the size of the particles. Thus large particles require longer times for reagents to penetrate and dissolved metal species to diffuse out. Thus metal recovery rates in large particles is usually very low. The presence of high density micro-cracks could potentially shorten the diffusion pathway, with the result being improvements in overall rate of reaction (Ghorbani et al., 2011a; Ghorbani et al., 2012; Kodali et al., 2011).

2.8.3. Type of ore material Mineral composition (Dissolution potential)

Minerals are typically present as small grains contained in a matrix of inert material. The effectiveness of bio-leaching process depends largely on the nature of ore material in which the metal exists. Metal dissolution during leaching is a selective process. This selective dissolution is due to galvanic interactions resulting from the differences in the rest potential values of phases present in the ore when in contact with solution (da Silva, 2004; Ghorbani et

al., 2013a). Thus galvanic interactions depend on the mineralogical association between the mineral phases in the ore. For example when galena and sphalerite are both in contact with solution, selective dissolution of galena takes place. Since galena is relatively more electronegative than sphalerite, a galvanic current would flow from galena to sphalerite, resulting in the selective oxidation of galena (Olubambi, 2009).

Heap leaching can be affected by the presence of swelling clay minerals, which can clog the natural flow channels of the lixiviant, leading to poor solution distribution and hence, low metal recovery. Mineral composition also has an influence on the acid consumption rate as gangue metals consume lixiviant along with the metals of interest (Pradhan et al., 2008). Very high acid consumption rates can have a negative impact on the economics of the heap leaching process (Watling, 2006). Not all types of ores are suitable for bio-heap leaching, as the ore needs to provide sufficient quantity of nutrients to the micro-organisms for growth. For example quartzic and garnitic ores show variable susceptibility to microbial leaching (Pradhan et al., 2008).

2.8.4. Bacterial activity

Micro-organisms play a vital role in the regeneration of the leaching agents for sulphide mineral dissolution, which may either be ferric ion or hydronium ions or both. The rate of microbial oxidation of ferrous ion and sulphur species is directly proportional to microbial abundance and activity (Bennett et al., 2012; Suzuki, 2001). Micro-organisms only limit the leach process when their activity is very low, either due to low population density or to unconducive chemical and thermal conditions. When they are present in sufficient quantities and conditions are suitable, the limits on ferrous oxidation will be controlled by the local chemistry (Bennett et al., 2012; Rawlings, 1998). Attachment of microorganism to the ore particles has been well proven (Rodríguez et al., 2003; Watling, 2006). Numerous studies have demonstrated the presence of bacteria attached to the ores and/or present in the pregnant leach solutions (PLS) in commercial operations (Porro et al., 1997; Sand et al., 1995).

The solution pH in a bioleach operation is the result of many factors, including ore mineralogy, mineral dissolution rates and amount of acid available in the irrigation feed (Plumb et al., 2008; Xingyu et al., 2009). Micro-organisms used in bio-heap leaching are normally autotrophic, they grow in low pH environments (pH 1.5 to pH 2) and obtain energy for growth from oxidizing reduced forms of iron and sulphur present in the mineral (Halinen et al., 2009; Johnson, 2001; Tupikina et al., 2011). Various studies have demonstrated that bioleach operations operate optimally at pH values less than 2 (Demergasso et al., 2005; Deveci et al.,

2004; Rawlings et al., 2003). An increase in hydrogen ion (H+) concentration in solution, provides an increased challenge for micro-organisms to reject the transport of H+ across the cell membrane. As soon as H+ is transported across the cell membrane, the pH of the cell's cytoplasm decreases which may lead to the death of the microorganism (Baker-Austin and Dopson, 2007).

2.8.5. Aeration

Aeration in heap leaching processes can be passive, with air being drawn into the heaps as a result of the flow of liquids, or active with air blown into the heap through piping installed near the bottom (du Plessis et al., 2007; Pradhan et al., 2008). Aeration has an influence on heap leaching recovery, since any changes in gas flow results in changes in the transport of oxygen through the heaps. Increasing the rate of aeration, may improve heap leach recovery (Rawlings et al., 2003). Aeration is the source of supply of both O_2 and CO_2 to the leaching system. Oxygen is required for oxidative metabolism thus, its depletion has rate limiting effect (Gericke et al., 2009; Ghorbani et al., 2011a). Micro-organisms oxidize ferrous iron and reduced sulphur species only to the extent to which oxygen is available in the system. Oxygen is therefore a key reactant in heap bio-leaching. Carbon dioxide in the air serves as a source of carbon needed for biomass generation (Pradhan et al., 2008; Watling, 2006).

2.8.6. Passivation

Precipitation of iron hydroxide and jarosite phases in the leaching system may suppress the metal dissolution by preventing contact between the leaching agent and the mineral (Ghorbani et al., 2011a; Klauber, 2008). This can have significant impact on overall metal recovery. The formation of ferric iron precipitate and jarosite is highly pH dependent and can be controlled by maintaining the pH at values, that prevent the formation of jarosites (Leahy and Schwarz, 2009; Mousavi et al., 2006). Studies have observed that the precipitation of jarosite is more pronounced within the 1.9 to 2.2 pH range. Jarosite precipitation is undesirable since it decreases the effectiveness of reagent and mineral surface interaction (Ghorbani et al., 2013a; Watling, 2006).

2.9.Critical analysis of literature

2.9.1. Quantifying microwave induced crack damage

Numerous investigations have shown the potential process benefits of microwave heating of ores, to induce thermal fracture (Al-Harahsheh and Kingman, 2004; Bradshaw et al., 2007; Haque, 1999; Kingman, 2006). Most of the work reported in literature has focused on microwave assisted comminution, where the ability of microwaves to selectively heat a multi-phase ore is exploited, to weaken ores before further grinding (Jones et al., 2005; Kingman et al., 2004b; Kingman and Rowson, 1998; Kingman et al., 2000b; Kobusheshe, 2010; Scott et al., 2008). Some of the work reported in literature was carried out at energy input levels not considered economical to favour the overall process economics (Clark and Sutton, 1996; Haque, 1999; Kingman and Rowson, 1998). The extent of microwave induced damage was measured indirectly using point load and drop weight tests (Kingman et al., 2004c; Kobusheshe, 2010). Significant reductions in strength and increases in liberation, of milled microwave treated ore feed has been reported, for some ores (Kingman, 2006; Kingman et al., 2004c; Kobusheshe, 2010). Results of these material strength tests, showed a high degree of variability and were less accurate for some ores (Kobusheshe, 2010). This suggest a need to apply direct measurement techniques such as XCT, to quantify microwave induced crack damage and to assess its potential process benefits. There is a gap in literature pertaining to information on the application of such direct measurement techniques to quantify and characterise microwave induced crack damage in ores.

There are limited studies in open literature on microwave enhanced mineral exposure in coarse particles (≥ 1 mm) Microwave enhanced liberation has been reported at coarse size fractions, from MLA carried out on milled microwave treated ores (Kingman, 2006; Kobusheshe, 2010; Scott, 2006). The milling of microwave treated ores prior to MLA introduces uncertainties in reported results (Kobusheshe, 2010; Scott et al., 2008). Additionally these reported improvements in liberation have not translated to significant improvements in recoveries in conventional ore separation processes such as flotation (Charikinya, 2011; Kobusheshe, 2010). A comprehensive study to determine directly enhanced mineral exposure of microwave treated particles will aid in the selection of flow sheets that maximise microwave induced damage.

Some studies have suggested that the best way to gain improved liberation in microwave treated ore is by subsequent crushing using slow compression breakage and producing a coarse product (Ali and Bradshaw, 2011). Modifications to the existing conventional flowsheets are

required to aid the recovery of the coarser liberated fractions in microwave treated feeds (Charikinya, 2011). This suggests a need to explore alternative ore processing methods that directly exploit microwave induced damage in ores such as heap leaching.

2.9.2. Downstream benefits of microwave treated ores

A number of experimental studies have been carried out to determine the downstream processing benefits of microwave assisted comminution of different ores. Some improvements in downstream recovery have been demonstrated experimentally, although these benefits varied with ore type and were not significant enough to justify the commercial application of the technology (Charikinya, 2011; Kobusheshe, 2010; Scott et al., 2008). Limited studies on the application of microwave treatment in the preparation of bio-heap leach feed ores has been reported in literature (Al-Harahsheh and Kingman, 2004; Olubambi, 2009; Schmuhl et al., 2011). Various studies have demonstrated the role of micro-cracks, produced during size reduction operations, in aiding recovery of metals in bio-heap leach operations (Ghorbani et al., 2012; Kodali et al., 2011; Olubambi et al., 2007; Schmuhl et al., 2011). The role of cracks induced during comminution, in aiding recovery during heap leaching has been shown to be a function of the following crack characteristics; micro crack density, mode of fracture and crack width. There is a limited understanding on the characteristics and potential role of microwave induced cracks in aiding coarse particle bio-heap leaching. Demonstrating experimentally the potential process benefits of bio-heap leaching of microwave treated ore is an important step towards commercial adaption of microwave technology to heap leaching. A comprehensive experimental investigation to determine the effects of microwave induced cracks on overall recovery, will give a clear understanding on the role of microwave induced cracks during bio-heap leaching.

2.9.3. Modelling of microwave induced damage

Previous studies quantifying microwave induced crack damage have been limited to numerical models with no corresponding physical experimental studies to validate the predicted crack damage (Ali and Bradshaw, 2009; Jones et al., 2005; Whittles et al., 2003). Results of the numerical studies reported in literature suggests that not all ores are amenable to microwave treatment and that in order to predict how certain ores will respond to microwave treatment, it is important to have prior knowledge of the mineralogy and texture of the ore (Ali and Bradshaw, 2009, 2010; Wang et al., 2008; Wang and Djordjevic, 2014). Despite textural properties (grain size, dissemination and association) playing an important role in determining

the nature of microwave induced cracks, there has been few reported physical experimental attempts to measure and quantify this influence. This has been due to the difficulties associated with directly measuring microwave induced cracks non-destructively. Thus most of the model results reported in literature have never been validated. In order to provide an understanding of the means by which microwave treatment improves downstream processing recovery, it is important to understand the microwave interaction with mineral textural properties and its corresponding effects on microwave induced crack damage. Improving on and validating numerical models for simulating microwave induced will allow for the investigation of the microwave treatment response of a wide range of ores.

2.9.4. Approach of this work

The limitations in existing literature on microwave treatment of ores, assessing downstream processing benefits of microwave technology and predicting the microwave treatment response of ore particles have been highlighted in this chapter. The mode of fracture in coarse microwave treated particles is not well understood and the models that have been developed to predict this fracture have not been validated due to lack of both quantitative and qualitative experimental data on microwave induced crack damage. Although most studies have demonstrated the potential energy savings of microwave heating ores, there are few studies that have investigated the downstream processing benefits of microwave treatment of ores.

This research study aims to contribute to existing literature on the application of microwave technology to mineral processing by determining experimentally for the first time, the extent of crack damage in microwave treated particles. It also aims to contribute towards the development of models to predict microwave induced crack damage in coarse particles. The use of non-destructive ore characterisation techniques will allow for the first time a more accurate assessment of the nature of microwave induced cracks and provide experimental data to validate microwave induced crack damage prediction models.

Potential heap leaching processing benefits of microwave treatment of ores will be elucidated. The approach to leaching experiments used in this study is similar to that used by Ghorbani et al. (2012). Ghorbani et al. (2012) investigated the long term progression of leaching in coarse sphalerite particles crushed under different breakage conditions. In this study ore particles are crushed under different breakage conditions and microwave treated prior to heap leaching.

CHAPTER 3

3. MATERIALS AND METHODS

This chapter details the materials and methods that were used in the study. It describes ore preparation methods used along with a description of the microwave treatment experimental set up. It details the microwave treatment conditions that were applied to induce microwave damage. This is followed by a description of XCT and QEMSCAN analysis techniques that were applied to characterise and quantify microwave crack induced damage. Lastly details of the column heap leach experimental set up and microbial cultures preparation is provide.

3.1.Materials and ore preparation

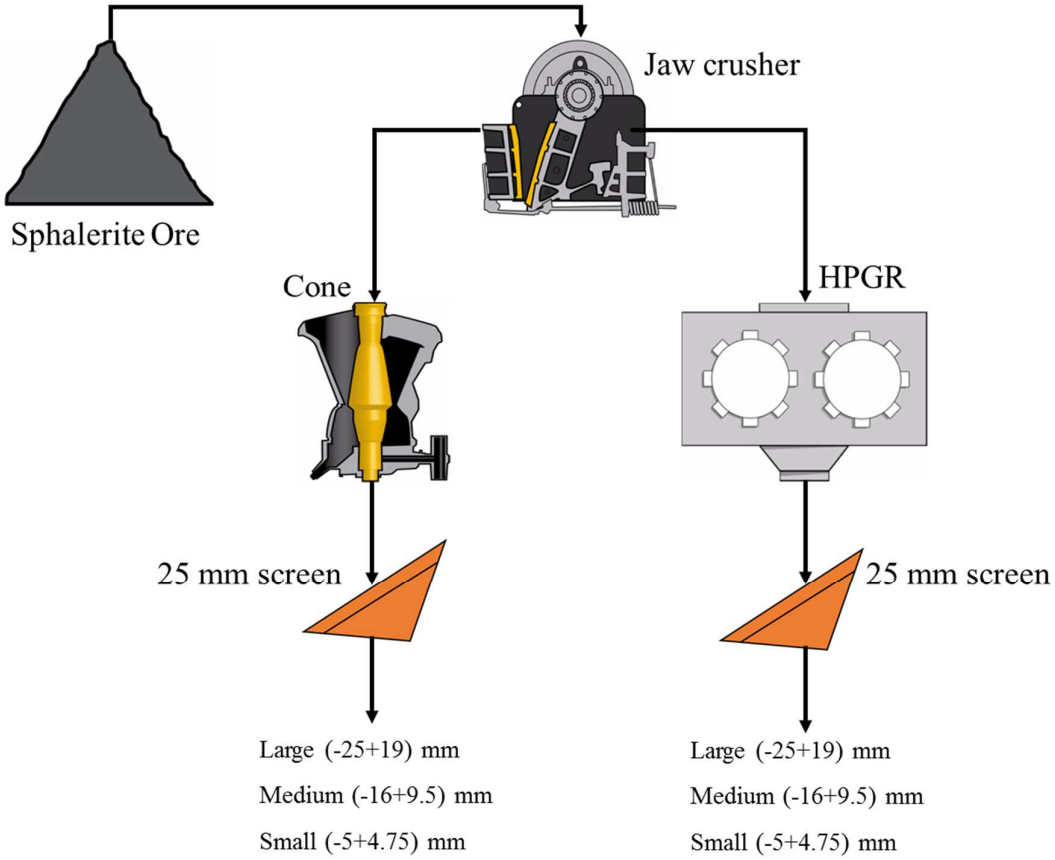

Figure 3-1: Sample preparation flow sheet

The ore was split using screens into the following size fractions (-25+19) mm, (-19+16) mm, (-16+9.5) mm, (-5+4.75) mm. Sample preparation was carried out using a primary jaw crusher. The crusher material was split into two 250 kg parts for further crushing by either HPGR or cone crusher. Figure 3-1 shows the sample preparation flowsheet. A detailed

description of the sample preparation is given in Ghorbani et al. (2011b). For this study sub-samples from Ghorbani et al. (2011b) were selected for use in the investigation representing small (-5+4.75) mm, medium (-16+9.5) mm, and large (-25+19) mm particle sizes.

3.2.Microwave treatment

A single-mode microwave heating system was used in this study to microwave treat the ore particles. A single-mode microwave cavity is one for which the dimensions support a well defined electromagnetic field pattern giving a restricted volume of high intensity electric field suitable for heating relatively small volumes of material at high dissipated power density. The microwave heating system consisted of the single-mode microwave applicator coupled to a switched mode power supply and a water cooled microwave transmission sub- system operating at 2.45 GHz. The single-mode applicator included a sliding short and stub tuners to match the impedance of the Magnetron microwave generator to the impedance of the applicator, ensuring a minimum amount of reflected power (see Figure 3-2 and Figure 3-3).

The single-mode applicator had an internal diameter of 80 mm and a height of 120 mm. The microwave cavity contained a cylindrical 75 mm diameter microwave transparent sample holder which has a capacity for 0.04 to 0.1 kg of ore particles per treatment, depending on particle size. The specific microwave heating energy absorbed by the particles ranged between 2 and 3 kWh/t (Table 3-1). This falls within the probable economic range for microwave treatment of between 1 to 3 kWh/t (Bradshaw et al., 2007). Examples of how the specific energy input was calculated is presented in Appendix B. Figure 3-4 shows the microwave treatment experimental set up that was used in this study.

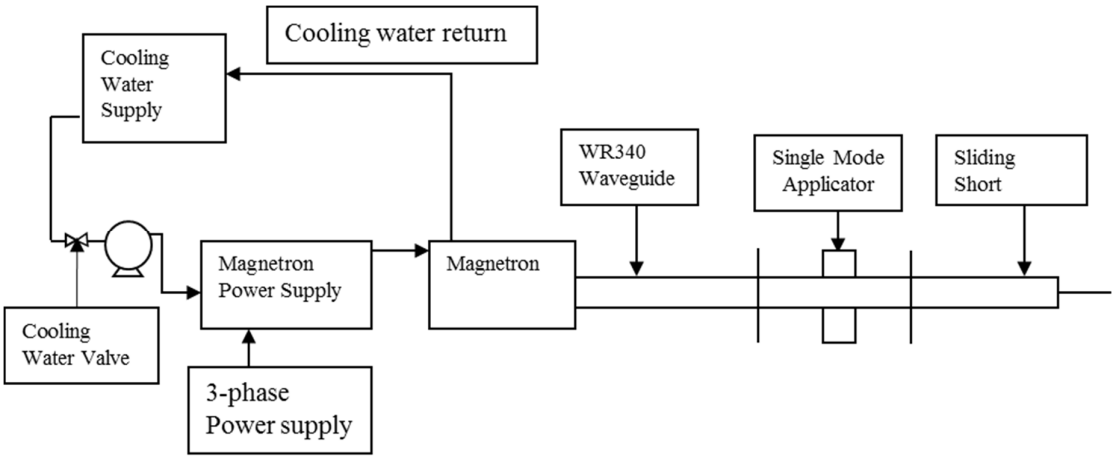

Figure 3-2: Schematic of microwave treatment experimental set up

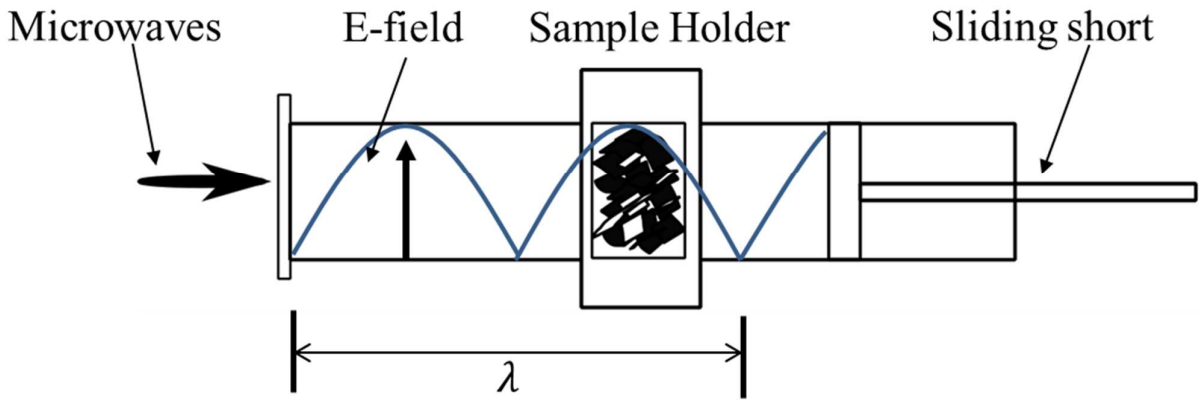

Figure 3-3: Schematic of a single-mode cavity

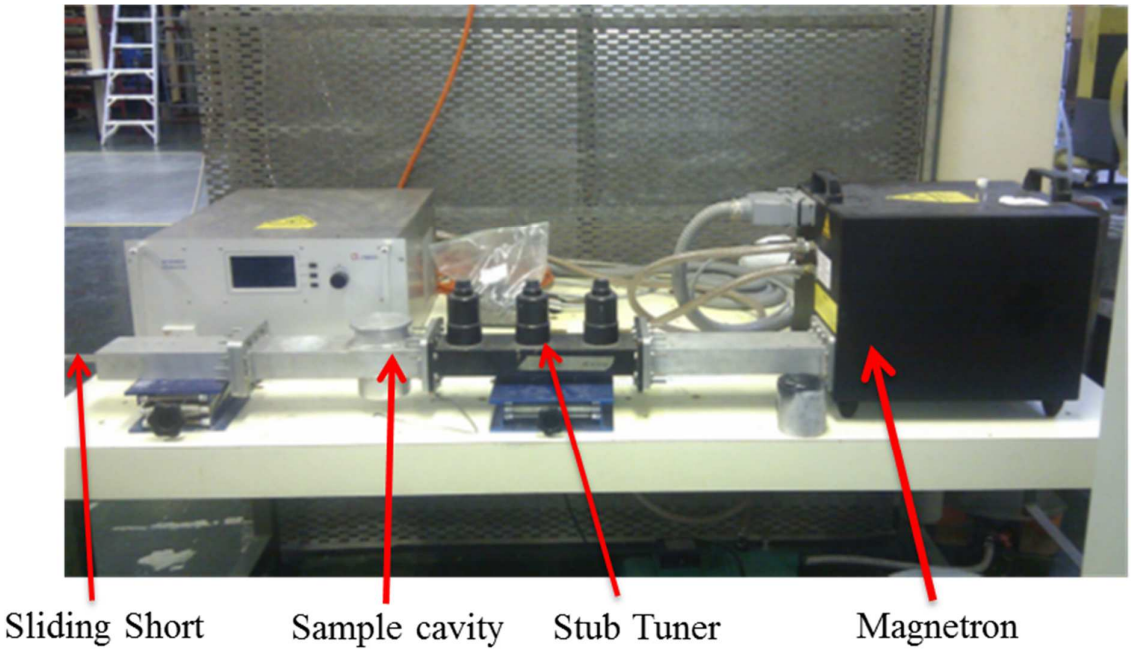

Figure 3-4: Microwave treatment experimental set up

Table 3-1: Microwave treatment conditions used in carrying out investigations

Size (mm)	Forward applied power (kW)	Reflected power (kW)	Time (sec)	Actual energy input into ore sample (kWh/t)
(-25+19)	5.92	0.93	1.00	2.11
(-16+9.5)	5.50	0.53	1.00	2.65
(-5+4.75)	5.56	0.71	1.00	2.37

3.3.X-ray computed tomography (XCT) image acquisition and quantitative analysis

The XCT analysis was conducted on the selected size fractions using a General Electric Phoenix VTomex L240 high resolution XCT at Stellenbosch University (Figure 3-6). The basic layout of the XCT system is shown in Figure 3-5. A sample is placed between the X-ray source and a detector. X-ray photons pass through the sample as it rotates about a single axis. The photons passing through the sample are partially attenuated and a projected image is collected by the detector from photons that successfully pass through the sample. A three dimensional (3D) array is reconstructed from the collected set of projection images.

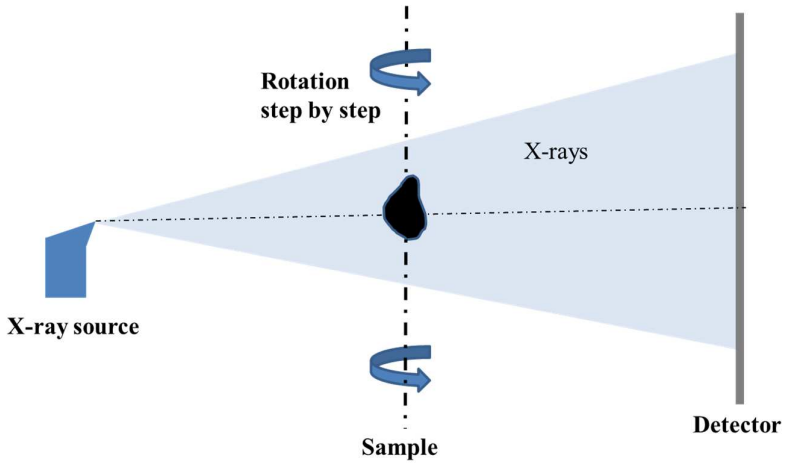

Figure 3-5: Basic layout of XCT system

Figure 3-6: General Electric Phoenix VTomex L240 with NF180 additional X-ray tube

A useful description of the XCT methodology is provided by Miller et al., (2003). Volume elements of reconstructed back-projected 3D images in XCT are the voxels which represent cubes of the material in the field of view and their size represents the extent of resolution. The value of the attenuation coefficient assigned to each voxel is a material property and represents the average value of the material occupying that cubic space. Differentiation of features within the particle is possible because the linear attenuation coefficient at each point depends directly on the electron density, the effective atomic number of the material comprising the particle, and the energy of the X-ray beam (E). This relationship is expressed by the following equation:

$$\mu_i = \rho\left(a + \frac{bZ_e^{3.8}}{E^{3.2}}\right) \qquad 3\text{-}1$$

Where ρ the density of the phase is, a is the quantity with relatively small energy dependence and b is a constant. When a mixture of atomic species is present, Z_e(the effective atomic number) is defined by

$$Z_e^{3.8} = \sum_i (f_i [Z_i]^{3.8}) \qquad 3\text{-}2$$

where f_i is the fraction of the total number of electrons contributed by element i with atomic number Z_i.

The gray scale levels of the images are based on the relative attenuation coefficient and are indicative of different mineral phases present in the sample. The separation of materials in XCT data is based on density dependent attenuation of X-rays, where XCT imagery visualises greater density as lighter and lesser density as darker. The ore particles that were analysed in this study consisted of material phases that were easily identified by their grayscale intensity in XCT acquired images such as; cracks (air voids), sulphides (sphalerite, pyrite, pyrrhotite, galena) and gangue (quartz, mica, calcite). Table 3-2 shows properties of some the major mineral phases in the ore particles. There is a clear difference in densities and effective atomic number between the gangue and the sulphide minerals in the ore.

Table 3-2: Properties of major mineral phases in the sphalerite ore used in the study

Major mineral phases in the ore	Density (g/cm^3)	Effective atomic number Z_e
Galena	7.4	78.3
Pyrite	5.01	22.1
Chalcopyrite	4.19	25
Sphalerite	4.05	27.2
Pyrrhotite	4.61	23.2
Quartz	2.62	14.4

The ore particles were scanned at a 200 kV/120 μA power setting. XCT scans were done on each individual ore particle at the best resolution and contrast settings for that particle size. This produced 2D images (3200 frames) of 5, 15 and 25 μm voxel resolution for the small, medium and large particles respectively. A summary of the experimental conditions used for XCT measurements are shown in Table 3-3. Volume reconstructions were carried out using the system-supplied Datos 2.1 reconstruction software. Analysis of the reconstructed 3D images was done using VG Studio Max 2.1 software (VGSTUDIO, 2010).

Table 3-3: Experimental conditions used for XCT measurements

X-ray system	240 kV micro focus tube
Voltage	200 kV
Current	120 μA
Integration frames	1 second per frame
Number of frames	3200

To improve the statistical significance of microwave treated particle microstructural properties measurements, XCT analysis was performed on at least 30 randomly selected particles at specific sizes i.e. small, medium, and large. For each particle, XCT scans were carried out before and after microwave treatment, with the scans prior to microwave treatment forming the baseline scans for detecting changes in the ore microstructural properties due to microwave treatment. Crack volume, defined as the volume of the cracks in a particle and reported as a percentage of the individual particle volume, was used to quantify the amount of cracks present in the particles before and after microwave treatment. Analysis of variance was done using a one-way ANOVA classification at the 0.05 level of significance to determine if changes in percentage crack volume due to microwave treatment were statistically significant.

Image thresholding techniques were used to distinguish the mineral phases and to visualise the cracks in the 3D reconstructed particle model (Figure 3-7 and Figure 3-8). Comparison between 3D images of particle cracks before and after microwave treated was carried out by using spatial image registration techniques in VG Studio Max 2.1 software to align data sets representing volumes of each particle before and after microwave treatment into the same coordinate system. Image segmentation techniques in VG Studio Max 2.1 software were applied to visualise the cracks in the treated ore samples before and after microwave treatment as well as to quantify changes in crack volume (VGSTUDIO, 2010).

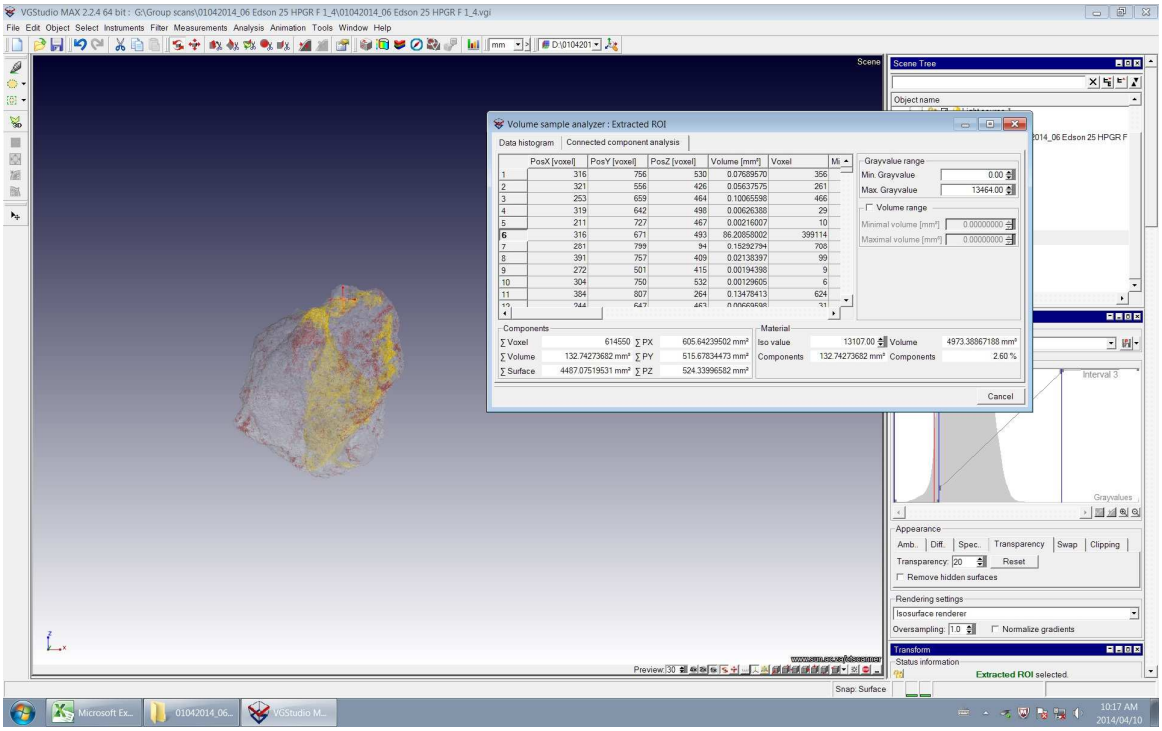

Figure 3-7 : An example crack segmentation and volume measurement using VG Studio Max 2.1 software with cracks highlighted in yellow and red

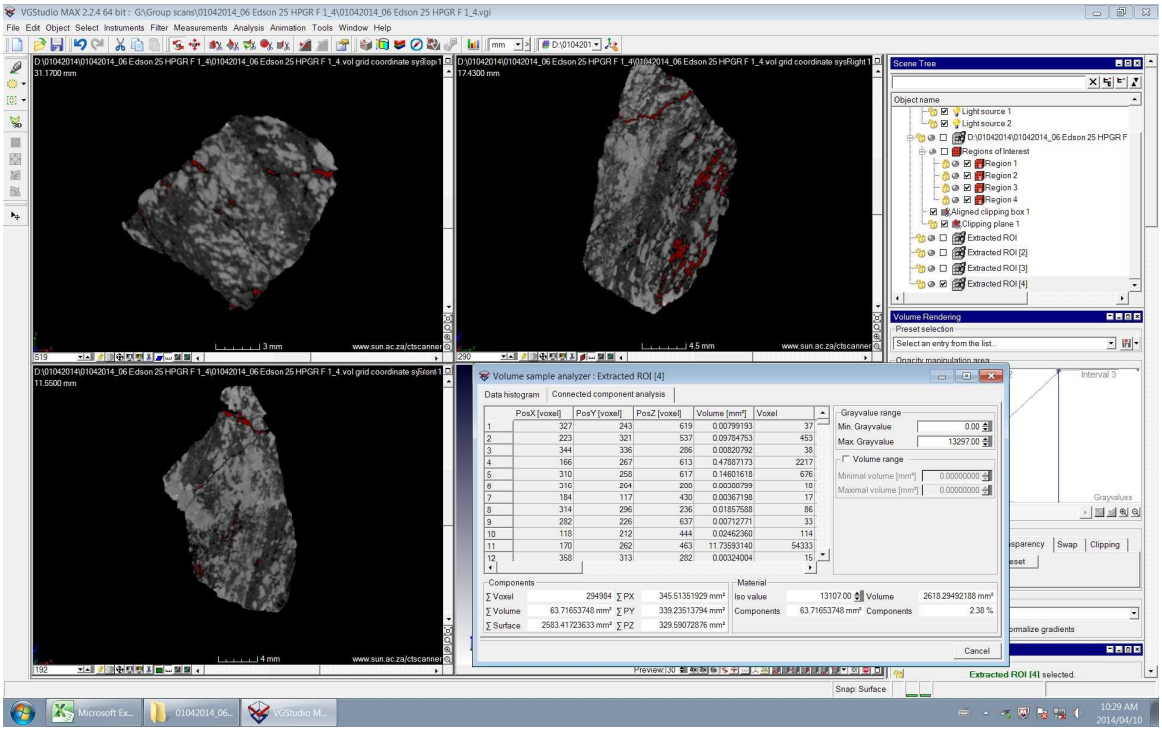

Figure 3-8: 2D slice images of segmented cracks (red) in VG Studio Max 2.1 software

3.4.Interfacial area measurement procedure

Based on the mineralogical data from QEMSCAN analysis, the ore consists of three major phases, pyrite (36.00 wt. %), sphalerite (17.04 wt. %) and gangue minerals (43.35 wt. %). To simplify phase segmentation the ore was reduced to two major phases, sulphides and gangue minerals. Figure 3-9 shows schematic representation of a two-phase A and B particulate material showing examples of internal grains, exposed grains and phase interface.

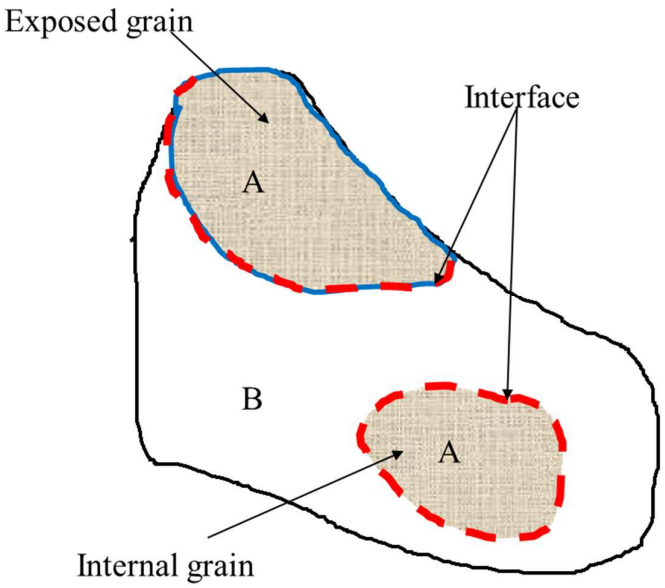

Figure 3-9: Schematic representation of two-phase A and B particulate material showing internal grain, exposed grain and interface

The phases composing the ore particles in this study (sulphide, cracks and gangue phases) can be distinguished clearly from the 3D reconstructed images (Figure 3-7 and Figure 3-8). Since the voxels that compose the reconstructed image have a value that corresponds to the attenuation coefficient of each phase at a particular point. Here it is assumed that any improvements in exposure of the total sulphide grains will result in improvements in exposure of sphalerite grains. If any grain boundary fracture occurs it will occur around the microwave absorbing sulphide grains. An equation for calculating interfacial area associated with each particle used by Garcia et al., (2009) was applied for interfacial area calculations in this study. The equation is derived as follows. The interfacial area of the internal grain is given by:

$$S_{\text{internal grains interfacial area}} = \text{Surface area of internal grain} \qquad 3\text{-}3$$

The interfacial area of the exposed grain is given as

$$S_{\text{exposed grain interfacial area}} = \frac{S_{\text{exposed grains}} + S_{\text{gangue}} - S_{\text{particle}}}{2} \quad 3\text{-}4$$

In this study exposed grains are defined as, the volume of sulphide grains exposed to the particle surface or grains neighbouring cracks open to the particle surface. Since the interface area of the exposed grain is added twice in calculating the interfacial area of the exposed grain the expression to right of Equation 3-4 is divided by 2. Thus the total interfacial area between phases A and B in the particle is given by Equation 3-5,

$$\text{Interfacial area} = S_{internal\ grains\ int\ area} + S_{exposed\ grain\ int\ area} \quad 3\text{-}5$$

$$\text{Interfacial area} = S_{\text{internal grains}} + \frac{S_{\text{exposed grains}} + S_{\text{gangue}} - S_{\text{particle}}}{2} \quad 3\text{-}6$$

where S is the surface area for each interface type.

Once the surface areas for each of the four interface types are determined, the interfacial area associated with each particle can be calculated from Equation 3-6. The surface area was measured using a particle phase separation image analysis procedure that was developed using algorithms in VG Studio Max 2.1 software.

3.4.1. Particle phase separation procedure

The image analysis procedure comprised the segmentation of sulphide grains, gangue and cracks and the measurement in 3D of the exposed sulphide grains. The gangue phases, internal and exposed grains were classified by applying the defect analysis algorithm in VG Studio Max 2.1 software. A screenshot of VG Studio Max 2.1 software showing the input parameters required to run the tool is shown in Appendix C. The defect detection procedure works by checking each voxel in the region of interest (ROI) being considered and identifying if the voxel is a defect, thereby creating groups of connected defect candidates. In the analysis cracks are represented as connected voids while sulphide grains are defined as inclusions. The grayscale values of voids (cracks) is lower than that of the surrounding material (gangue and sulphides), while the grayscale values of inclusions (sulphides) is higher.

ROIs of total voids (cracks) and inclusions (sulphides) in the ore particle being analysed were created separately using image segmentation algorithms in VG Studio Max 2.1 software. An algorithm to dilate each voxel making up inclusions (sulphides) ROI was applied to ensure maximum overlap between neighbouring voids (cracks) and inclusions (sulphides), after merging the ROIs. The defect analysis algorithm was run on the custom defect mask of the merged voids (cracks) and inclusion (sulphides) ROIs, to identify connected voxel groups consisting of voids (cracks) and inclusions (sulphides) which make up exposed grain defect

candidates. An analysis of grayscale deviation within each voxel group was carried out, with a low grayscale deviation in voxel groups indicating internal sulphide grain candidates and high deviation indicating exposed grain candidates. A threshold voxel grayscale deviation value was set indicating the point of separation between exposed and internal grain defect candidates, for each particle analysed. To obtain an exposed grain ROI, voxel groups with voxel grayscale deviation values lower than the set threshold value were removed. The internal grain ROI was obtained by removing voxel groups with grayscale deviation values higher than the threshold value. By applying this procedure individual ROI of exposed grains, internal grains, cracks and gangue phases in each particle were obtained. Figure 3-10 illustrates the steps for the determination of interfacial area. Figure 3-11 shows the grayscale value histogram of particle ROI (A) before, (B) after microwave treatment, (C) grayscale value histogram of merged cracks ROI and sulphide grains ROI, (D) Grayscale value histogram of gangue phase ROI. Figure 3-12 shows the segmentation of sulphide grains.

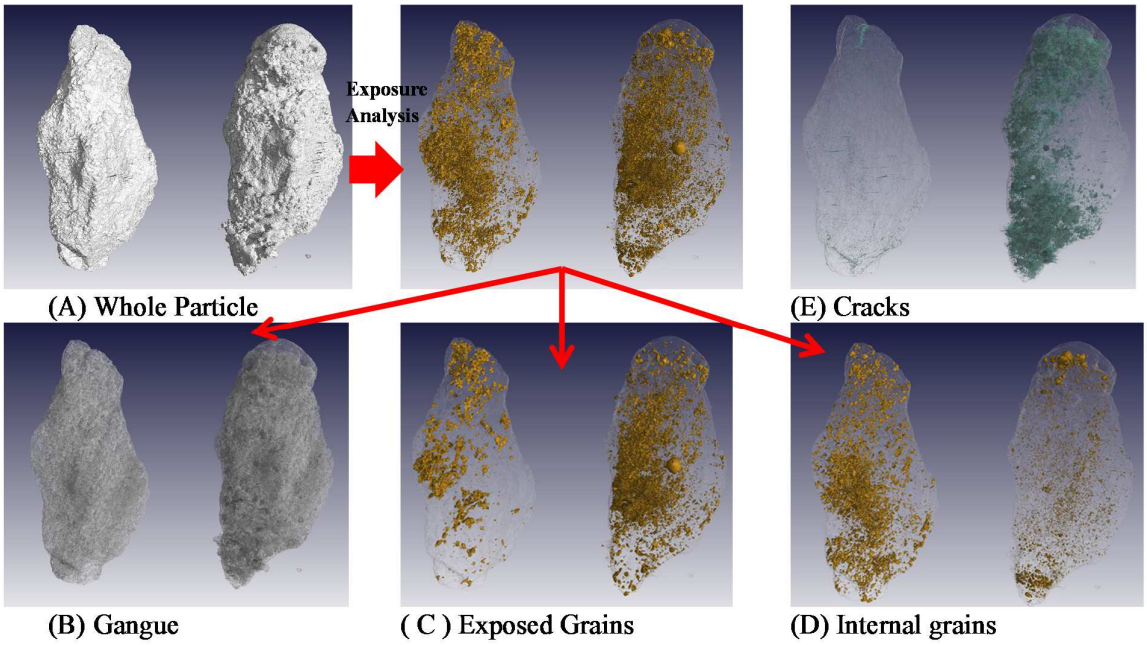

Figure 3-10: Schematic of steps for the determination of small HPGR crushed particle interfacial area

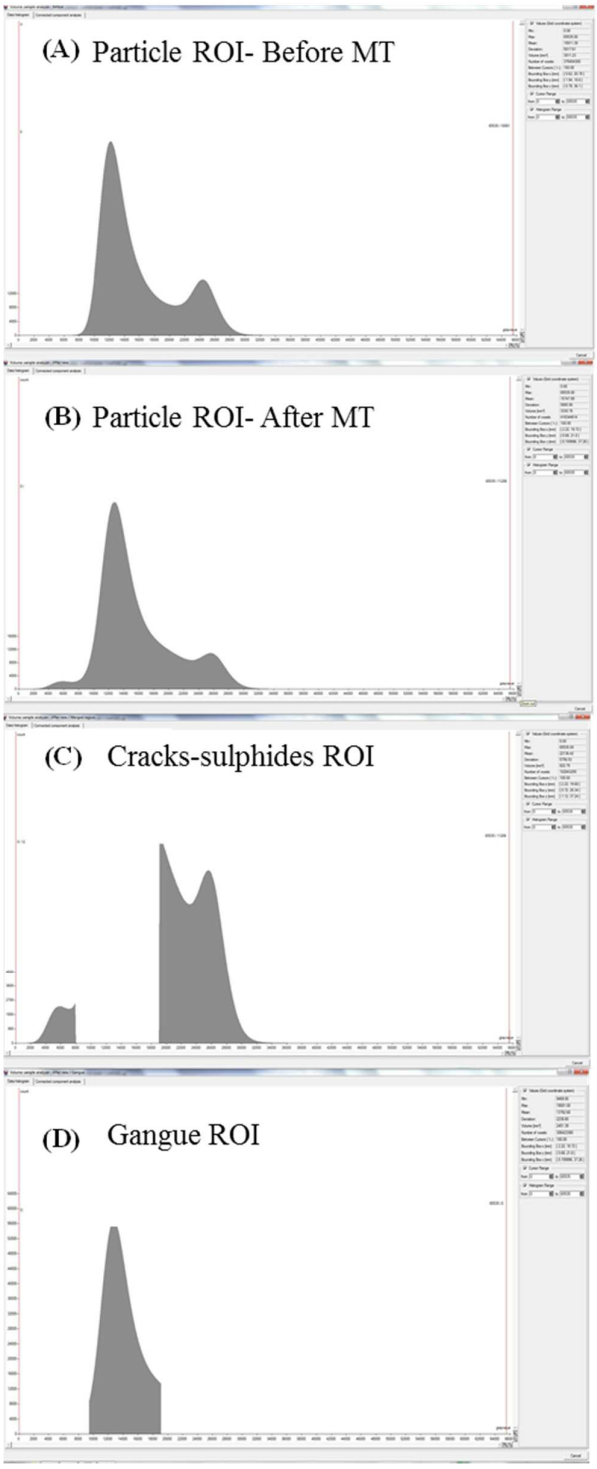

Figure 3-11: Grayscale value histogram of 16mm HPGR crushed particle (A) before, (B) after microwave treatment (C) grayscale value histogram of merged cracks and sulphide grains regions in the 16mm HPGR crushed particle, (D) Grayscale value histogram of gangue phase.

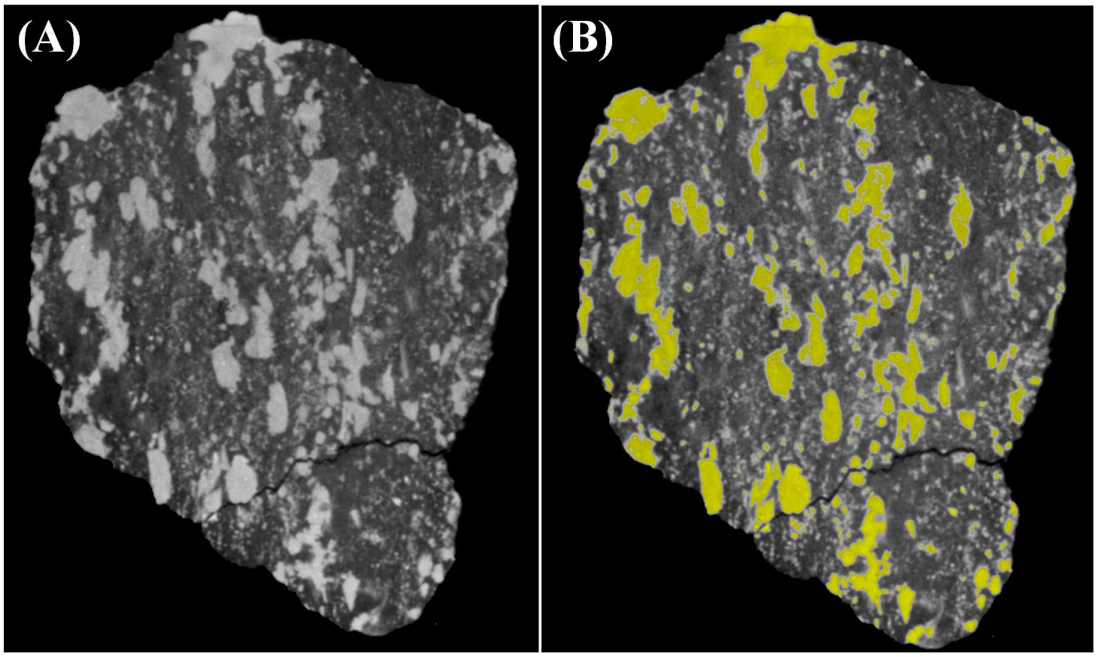

Figure 3-12: (A) 2D slice image of 16mm HPGR crushed, (B) yellow false colour image showing regions containing sulphide grains.

3.4.2. Mineral exposure analysis

The degree of exposure of the sulphide phase F_E in each particle was calculated as the ratio of mass of exposed grains to the mass of total sulphide grains in that particle (Hsih et al., 1995).

$$F_E = \frac{Volume\ of\ exposed\ sulphide\ grains}{Total\ volume\ of\ sulphide\ grains} \qquad 3\text{-}7$$

3D reconstructed images of each particle before and after microwave treatment were obtained from XCT analysis. The phase separation image analysis procedure described above was applied to determine the mineral composition of each particle in the population from the 3D XCT data. For each particle, the interfacial area was determined based on the total sulphide mineral grain types, exposed or internal, from mineral exposure analysis. Geometrical properties, such as volume and surface area of each mineral phase for each particle was determined from the XCT reconstructed images. These geometrical properties were then used to calculate the interfacial area.

Partial volume effect is (PVE) refers to the blurring effect and sampling error of the finite discrete voxels or pixels which affect image intensities of multiphase particles using XCT and SEM techniques. Specifically, significant error for surface area measurement is due to the uncertainty arising from the PVE of the surface voxels / perimeter pixels (Erlandsson et al., 2012; Ketcham, 2006). Partial volume effect (PVE) can limit quantitative analysis in some

cases due to inaccurate image classification and segmentation (Lin and Miller, 2005). In this study the cracks and sulphide grains were quantified at crack widths and grain sizes greater than 3 voxels which excludes partial volume effect. Thus no correction for PVE was performed on the mineral exposure analysis data.

3.5.Auto-SEM (QEMSCAN) analysis

QEMSCAN was used to determine the bulk mineralogy and crack characterisation in the ore sample (before and after microwave treatment). A useful description of the QEMSCAN methodology is provided by Gottlieb (2008). An FEI QEMSCAN 650F on a Field Emission Gun (FEG) SEM platform, at the University of Cape Town equipped with two Bruker 6030 SDD detectors was used in this study. The operating conditions were set at 25 kV and 5 nÅ beam current. Bulk mineralogy data was available from a previous study on the ore by Ghorbani et al. (2011b). For QEMSCAN analysis particles were analysed before and after microwave treatment per size fraction for each mode of comminution. All QEMSCAN post sample processing was done using the FEI QEMSCAN iDiscover software.

Individual ore particles (5 to 25 mm) were mounted in resin, polished and carbon coated in preparation for QEMSCAN analysis. The QEMSCAN blocks were analysed using the Field Image Analysis routine – a specialised routine developed for the analysis of particles larger than the operating field size, as defined by the appropriate magnification needed to image features of interest. Individual fields were mapped during the measurement and then adjacent fields stitched together as part of the post processing methodology. Digital false colour mineral maps for each particle were then produced from which the associated mineralogy and textural information (Figure 3-13) could be extracted: mineral association, dissemination and grain size distribution. The area occupied by cracks was determined using the “injector” functionality whereby a dummy phase was virtually injected into the particle replacing all internal particle pixels which had been classified as background. The dummy phase was then renamed as cracks (Figure 3-13), and could be characterised and quantified similarly to any other particular mineral of interest. After obtaining the processed QEMSCAN image for each particle size fraction, further analysis was carried out to determine particle texture and percentage crack volume.

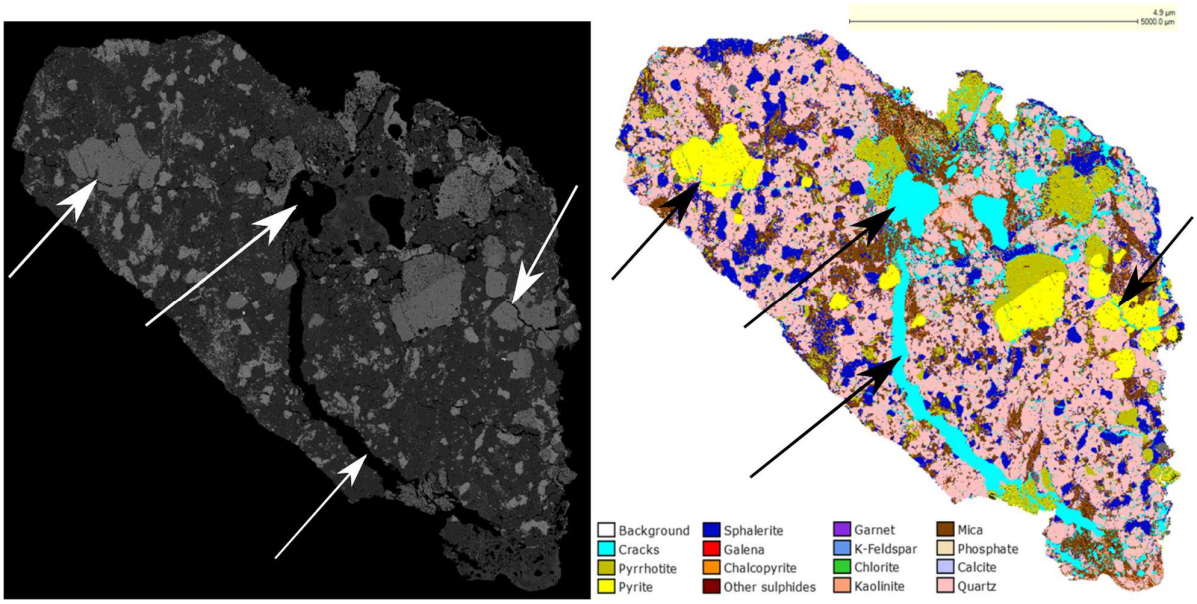

Figure 3-13: Left QEMSCAN BSE image, right QEMSCAN Digital false colour mineral map with arrows showing cracks

3.6.Column leaching experiments

The ore samples investigated consisted of small (-5+4.75) mm, medium (-16+9.5) mm, and large (-25+19) mm HPGR and cone crushed microwave treated and untreated particles. The specific microwave heating energy absorbed by the particles in each subsample ranged between 2 and 3 kWh/t. Table 3-4 is a summary of the ore samples placed in each leach reactor and microwave treatment specific energy input used to treat the samples. Since only eight reactors were available for the experiment, the leaching response of untreated cone crushed ore was not investigated in this study.

Table 3-4: Summary of the ore samples placed in each leach reactor

Reactor	Comminution method	Size	Microwave treated	Total mass (g)	Specific energy input (kWh/t)
1	HPGR	Large	No	3600	-
2	HPGR	Small	No	3600	-
3	HPGR	Medium	No	3600	-
4	Cone	Medium	Yes	3600	2.65
5	HPGR	Small	Yes	3600	2.37
6	HPGR	Medium	Yes	3600	2.23
7	Cone	Large	Yes	3600	2.38
8	HPGR	Large	Yes	3600	2.11

The ore samples were packed in reactors in which the lixiviant was continuously circulated around stacked baskets containing ore particles. The particles were fully immersed in leach solution and the reactors were operated in continuous mode for 350 days. The volume

of each cylindrical reactor was 10 L, 140 mm in diameter and 500 mm in length. The schematic and experimental set up for the column leach experiments are shown in Figure 3-14 and Figure 3-15. Internal circulation of the leach solution was achieved through a central draft tube into which air was bubbled at 1500 mL/min. This set up was designed to achieve well mixed conditions at the surface of all particles throughout the reactor.

Fresh leach solution, containing 1 g/L ferrous ion and pH adjusted to 1.50 with concentrated H_2SO_4 was pumped into the reactor from the bottom by means of a peristaltic pump at a rate of 50 mL/hr over 350 days without recycle. The columns were operated in a temperature controlled room at (30 °C). The PLS was collected from the top. The pH and oxidation reduction potential (ORP) of the pregnant leach solution (PLS) was periodically measured. The pH was measured by a pH probe (826 pH-meter Meterohm model) calibrated with a low pH buffer. The ORP was measured by a silver/silver chloride reference redox probe (Metrohm 704 voltmeter). During the bio-leaching experiments, samples of solution were taken periodically and analysed for total Fe, Zn, Mg and Al by an atomic absorption spectrophotometer (Varian 220). Concentrations of ferrous ion were determined spectrophotometrically (Helios spectrophotometer) using the 1, 10-phenanthroline method.

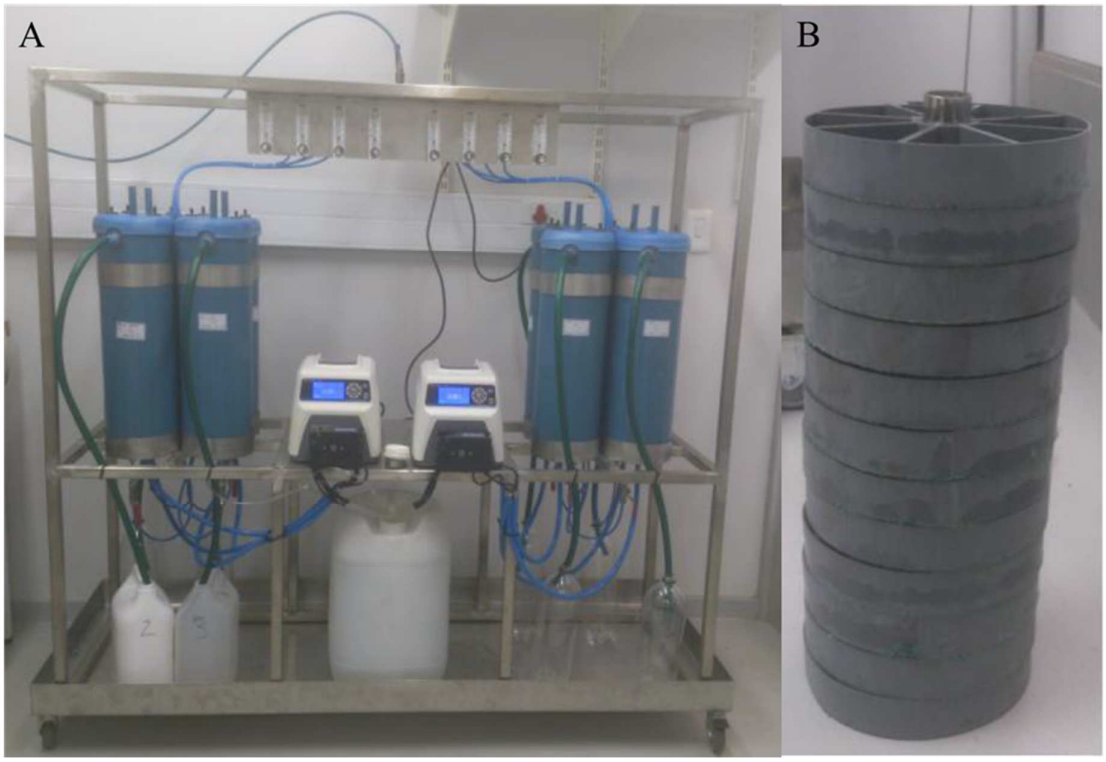

Figure 3-14: Leach columns, set up of leach reactors with stand and two 4-channel pump-head (A), designed frame inside the leach reactor loosely holding individual labelled particles (B)

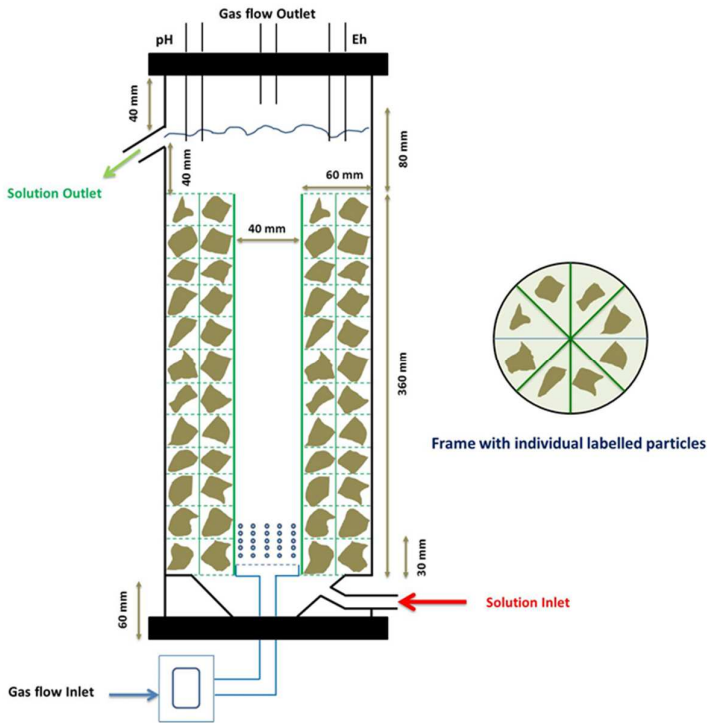

Figure 3-15: A schematic drawing of leach reactor and a frame with individual labelled particles

Zn leaching recovery was calculated as a function of time for each reactor as

$$R_{Zn} = \frac{(C_t - C_0)V_t}{Zn\ content\ in\ feed\ ore} \times 100 \qquad 3\text{-}8$$

where R_{Zn} is the percentage Zn recovery from leaching, $C_t$is the Zn concentration in PLS at time t (g/L),C_0 the Zn concentration in inlet leach solution (g/L) V_t is the volume of the PLS at time t(L).

3.6.1. Leached ore particles sample analysis

The reactors were stopped on day 40, 140, 200, 300 and 350 to determine the progress of leaching on selected tagged particles in each column over 350 days. The progression of leaching in each column was evaluated by monitoring the disappearance of pyrite, sphalerite and other grains as determined by XCT and QEMSCAN analysis in these tagged particles. The XCT scans were done before the start of the leaching experiment and on days the reactors were stopped. While QEMSCAN analysis was carried out on selected particles before leaching and on selected leach residue samples after 350 days of leaching.

3.6.2. Microbial cultures and inoculum preparation

Reactors were inoculated with a mixed culture of mesophilic acidophilic chemolithotrophs at a concentration equivalent to 1.86×10^{10} cell/kg ore. The culture had previously been adapted to a finely ground sphalerite-containing ore in a 2 L stirred batch reactor over a period of two months prior to inoculation. Previous analysis of this culture has shown that it consists predominately of L. ferriphilum ($\geq$ 98%) (2012). The role of the bacteria in bio-leaching is to catalyse the oxidation of Fe (II) to Fe (III) (see Equation 3-9 to 3-11). The Me in Equation 3-9 represents a metal (e.g., zinc, copper, lead, etc.)

$$MeS \rightarrow Me^{2+} + S^{0} + 2e^{-} \quad \text{3-9}$$

$$\frac{1}{2}O_2 + H_2O + 2e^{-} \rightarrow 2OH^{-} \quad \text{3-10}$$

$$Fe^{3+} + e^{-} \rightarrow Fe^{2+} \quad \text{3-11}$$

CHAPTER 4

4. CHARACTERISING AND QUANTIFYING MICROWAVE DAMAGE

As discussed in chapter 2 the use of non-destructive imaging techniques to characterise and quantify microwave induced crack damage, is an important step towards assessing the process benefits of utilising microwaves in mineral processing. Non-destructive imaging techniques such as XCT allow for repeated imaging of full 3D ore particle microstructure. Making it possible to image and analyse the same ore samples before and after microwave treatment. There is a gap in literature pertaining to the application of such direct measurement techniques to quantify and characterise microwave induced crack damage in ores. There are limited studies in open literature on measuring microwave enhanced mineral exposure in coarse particles (≥ 1 mm).

The aim of this chapter is to present on work carried out to characterise and quantify microwave induced particle cracks for the first time using high resolution XCT and Auto-SEM /EDS techniques. As well as to determine if microwave treatment results in enhanced value mineral exposure in coarse particles. Traditional Auto-SEM /EDS techniques offer a means of validating XCT measurements. The use of a non-destructive ore characterisation technique will allow for the first time a more accurate assessment of the nature of microwave induced cracks and provide experimental data to validate microwave induced crack damage prediction models. The chapter is structured as follows, section 4.1 presents results and discussion of the mineralogical and textural analysis of the feed ore that was carried out, to determine if the ore was suitable for microwave treatment. This is follows by section 4.2, which presents results and discussion on microwave induced crack characterisation. Lastly results of interfacial area measurements and mineral exposure analysis are presented in section 4.3 and 4.4 respectively.

4.1.Mineralogical texture characterisation

The texture and mineralogy of the ore particles was assessed using QEMSCAN analysis. Table 4-1 presents the bulk modal mineralogy of the ore and Figure 4-1 groups the minerals according to their microwave heating response. Figure 4-2 presents the classified images showing examples of the texture. The ore consists of a microwave-transparent gangue matrix predominantly of quartz and mica (Table 4-1) with microwave absorbent phases distributed as large discrete grains of sulphide (pyrite, sphalerite and pyrrhotite) and Fe oxides (Figure 4-2).

Based on the mineral association analysis, there is a low level of mutual association between the sulphides and oxides. Within the sulphide grains, there is a low level of association between pyrite and the sphalerite, whereas a high degree of association exists between pyrite and pyrrhotite.

Previous studies have reported that pure sphalerite (ZnS) is a poor microwave absorber among the common sulphide minerals (Chen et al., 1984; Walkiewicz et al., 1988). These studies have shown that the response of minerals to microwave heating depends on their composition; for example, when Fe substitutes for Zn in sphalerite, the resulting high-Fe sphalerite becomes microwave responsive (Chen et al., 1984; Hua and Liu, 1996). The sphalerite in this study contains Fe (9.72 ± 0.74 wt. %) and Mn (4.44 ± 1.10 wt. %) impurities substituting for Zn in its crystal structure and can be classified as a high-Fe sphalerite ore (Ghorbani et al., 2013a). These impurities, coupled with high microwave power densities of up to 1 $\times 10^9$ W/m^3_{abs}, in the absorbent phase used in this study, are expected to result in improved microwave treatment response of the sphalerite phase. The power densities used in the microwave treatment experiments were calculated, by considering the measured net input power (2 to 3 kWh/t), sample mass (0.04 to 0.10 kg) and mass fraction of absorbent phase (see Table 4-1). yrite, which constitutes the bulk of the absorbent phase, is expected to facilitate greater crack damage of the ore, as it is highly microwave absorbent compared to sphalerite (Chen et al., 1984; Haque, 1999).

The absorbent grains show no preferential association with either of the major gangue phases (Figure 4-2). A combination of coarse microwave absorbent grains (with some grains exceeding 5 mm) within a microwave transparent gangue presents a texture and mineralogy most suitable for generation of fractures due to microwave treatment (Ali and Bradshaw, 2009). The bulk of the absorbent phase grains in the ore had sizes ranging from an effective lower limit of 10 µm to above 1 mm, with greater than approximately 50% of the grains coarser than 1.0 mm. The effectiveness of microwave treatment will rely on the expansion of the absorbent grains, predominantly pyrite and sphalerite, against the microwave transparent gangue matrix. There is sufficient absorbent phase present in the ore (> 40% wt. %) that is locked in a gangue matrix to generate significant thermal stresses when the absorbent phase expands during microwave exposure to result in extensive micro crack damage (Figure 4-1). The bulk of the gangue is quartz (25.5 wt. %) and mica (7.9 wt. %). Previous studies have shown that phyllosilicates dehydrate when exposed to microwaves, and that this dehydration results in macro fracture (Kobusheshe, 2010). Thus based on the mineralogical and textural characterisation results, the sphalerite ore being used in this study is a good candidate for

microwave treatment (Ali and Bradshaw, 2010). Previous studies have shown that the presence of any amount coarse-grained microwave absorbent phase offers the best opportunity for generating microwave cracks (Batchelor et al., 2015; Jones et al., 2005).

Table 4-1: Bulk modal mineralogy of sphalerite ore (Ghorbani et al., 2011b) **and the susceptibility of the mineral to microwave heating according to observations made by Chen et al. (1984)**

Phase	Mineral	Abundance (wt. %)
Absorbent	Sphalerite (high-Fe; $((Zn_{0.78},Mn_{0.07}Fe_{0.15})S)$	16
	Pyrite	33.8
	Pyrrhotite	1.2
	Galena	0.2
	Chalcopyrite	< 0.1
	Fe oxides/hydroxides	1.9
	Other sulphides (mostly Molybdenite, Pentlandite, Arsenopyrite)	3.2
Transparent	Garnet	0.3
	K-Feldspar	0.4
	Chlorite	1.7
	Kaolinite	2.8
	Mica	7.9
	Phosphate	2
	Calcite	< 0.1
	Quartz	25.5
	Others	3.1

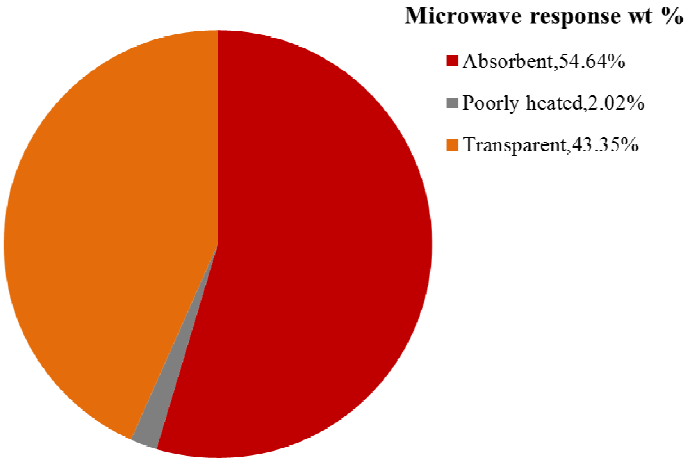

Figure 4-1: Overall Gamsberg Zinc ore susceptibility to microwave heating based on bulk mineralogy data

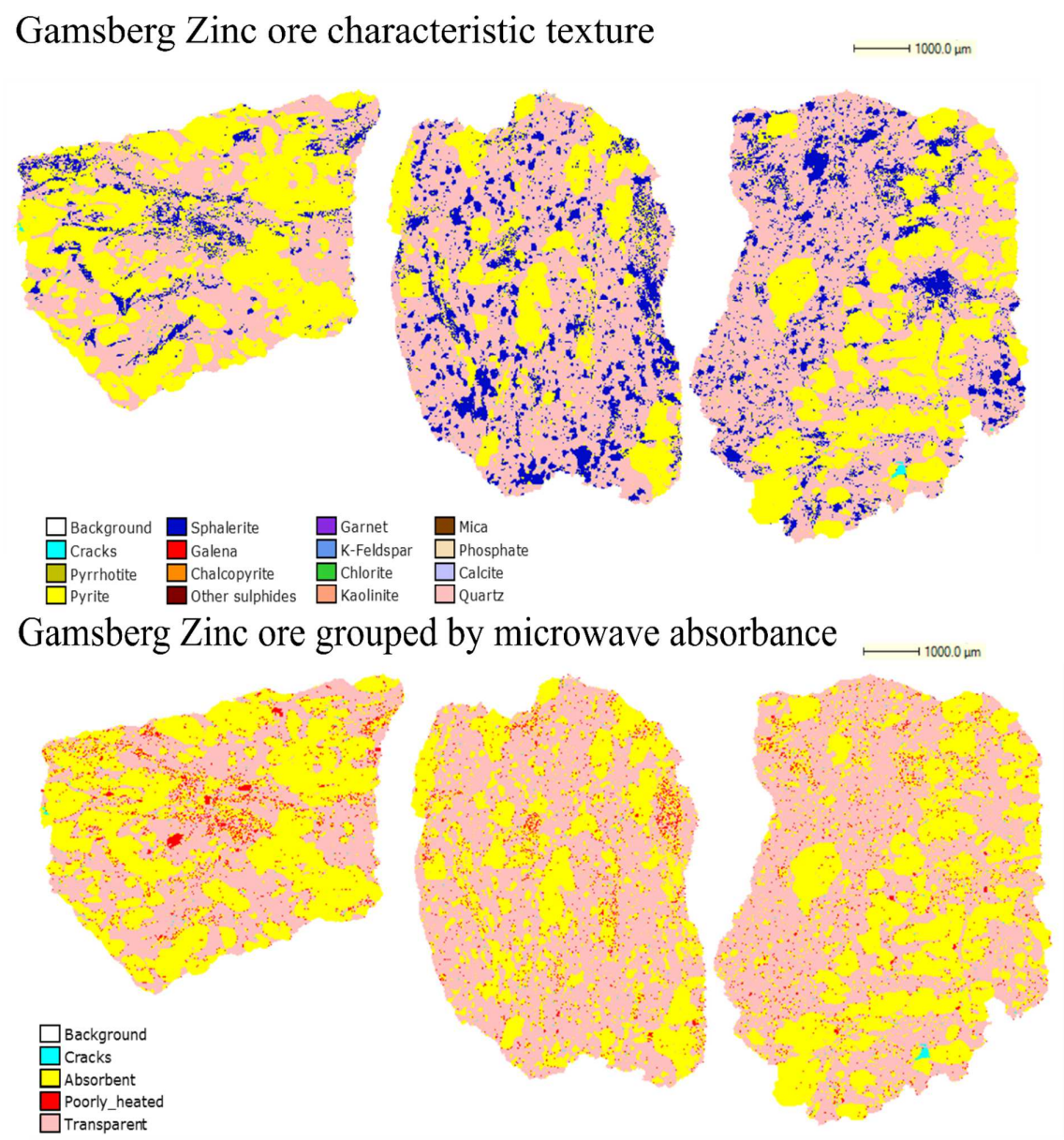

Figure 4-2: **Gamsberg Zinc Ore characteristic texture measured using QEMSCAN**

4.2.Microwave induced crack characterisation

4.2.1. Microwave induced crack pattern

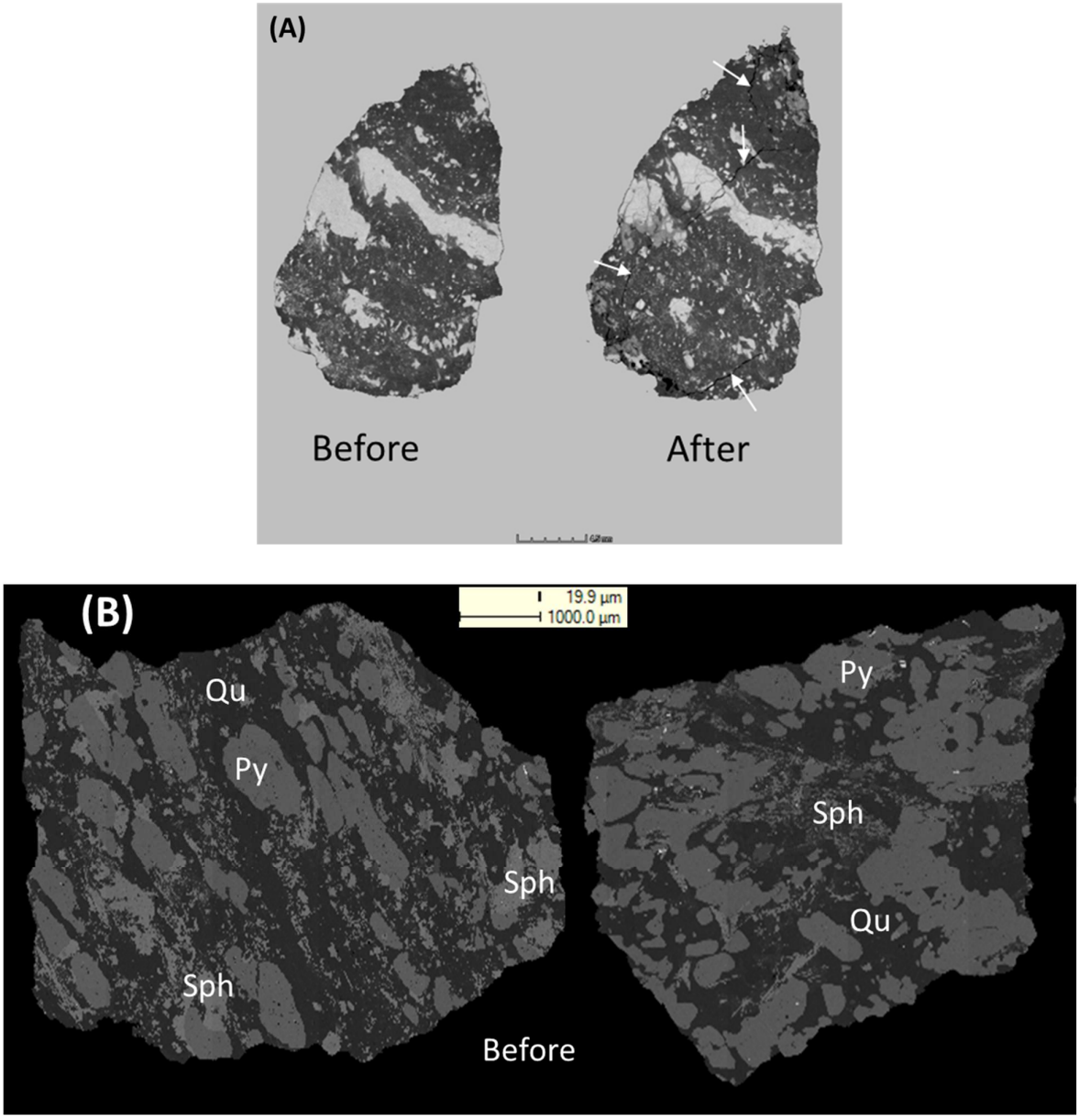

Figure 4-3: (A) 2D XCT slice image of a (16+9.5) mm cone crushed particle before and after microwave treatment with white arrows showing microwave induced cracks (B) QEMSCAN BSE images showing (16+9.5) mm HPGR crushed particle before microwave treatment.

The effect of microwave treatment on cone and HPGR crushed ore was investigated by analysing cracks in the ore particles using XCT and QEMSCAN analysis. Figure 4-3 shows an example of the XCT 2D section and QEMSCAN images of cone and HPGR crushed (-16+9.5) mm particles before microwave treatment. From the XCT analysis, more micro-cracks were present in the HPGR crushed particles compared with the cone crushed particles prior to microwave treatment. The HPGR crushed particles had an average percentage crack volume of 0.52% compared to 0.21% for cone crushed particles across all sizes. A similar result was observed from the QEMSCAN images (HPGR 0.42% and cone 0.10% average percentage crack volume). These values compared well with those obtained from previous studies on the same ore by Ghorbani et al. (2011b) (see Table 4-2). Since the XCT and QEMSCAN analysis of the individual ore particles was carried out at a voxel resolution of between 5 and 25 microns, it is possible that micro-cracks smaller than the XCT and QEMSCAN resolution were not detected.

Table 4-2: Comparison of avarage crack volume (%) across all sizes measured from XCT (3D) and QEMSCAN (2D) measurements for HPGR and cone crushed ore before microwave treatment. nd denotes not detected.

	This study		Ghorbani et al. (2011b)	
	XCT	QEMSCAN	XCT	QEMSCAN
HPGR	0.52%	0.42%	0.76%	1.07%
Cone	0.21%	0.10%	nd	nd

To determine the significance of these undetected cracks over the resolution range used in this study, QEMSCAN analysis was carried out at different pixel spacing on a HPGR crushed microwave treated ore sample block. Table 4-3 shows the variation in measured percentage crack volume of the sample at different pixel sizes. The results show no statistically significant correlation at the 0.05 level of significance, between QEMSCAN resolution and measured percentage crack volume for microwave treated ore particles. Sub-micron cracks identifiable only at lower pixel spacing (< 2µm) are volumetrically insignificant considering their width and number in relation to the larger cracks detected above the 5 µm pixel spacing. This suggests that errors in measuring percentage crack volume due to undetected cracks below the experimental resolution limit are expected to be negligible for QEMSCAN analysis. Although the Field Emission Gun (FEG) QEMSCAN system used in this study had the capability of producing higher resolution scans, with a theoretical minimum pixel spacing of 0.5 µm, this was not considered practical due to the extended measurement times required for the analysis (from hours to days).

Evidence of microwave induced cracks in both cone and HPGR crushed particles at all sizes was found from both the XCT and QEMSCAN images. Figure 4-4 shows SEM images of two different HPGR crushed medium particles, one microwave untreated and treated one. Figure 4-5 to Figure 4-10 shows the XCT scan results of cone and HPGR crushed small, medium and large particles before and after microwave treatment along with corresponding 3D crack visualisation images. There are visible thermally induced cracks in the small, medium and large cone and HPGR particles after microwave treatment (Figure 4-5 to Figure 4-10). These cracks consist of both surface and internal cracks.

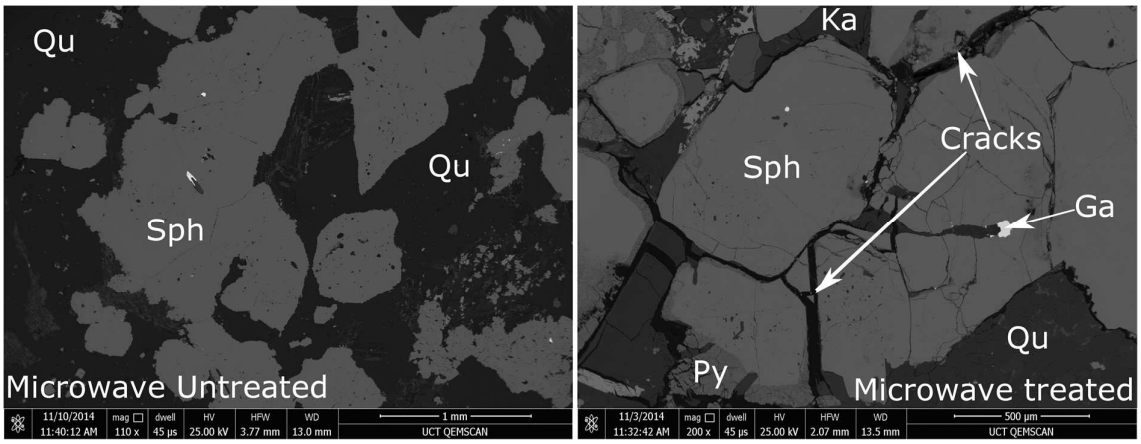

Figure 4-4: SEM images showing microwave untreated and treated (16+9.5) mm HPGR crushed particles. Qu-Quartz, Sph-Sphalerite, Py-Pyrite, Ka-Kaolinite, Ga-Galena.

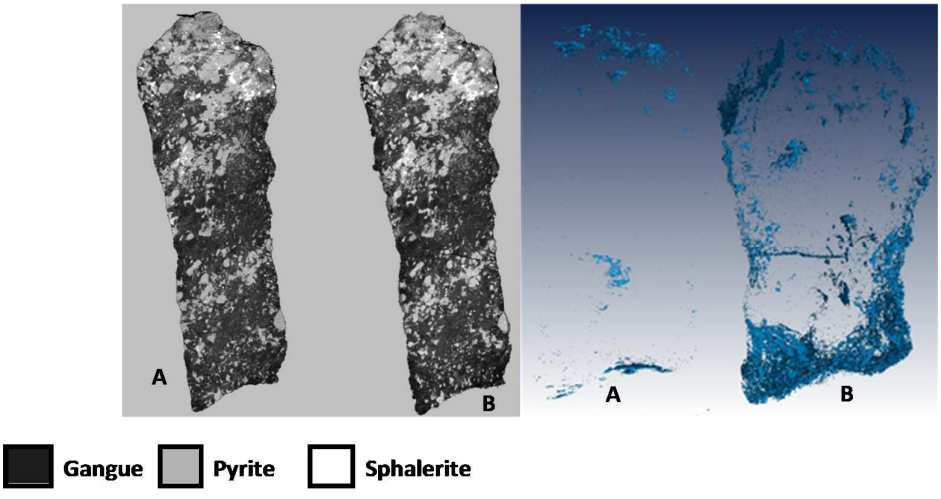

Figure 4-5: Left 2D XCT slice image of a (-25+19) mm HPGR crushed particle before (A) and after(B) microwave treatment, right 3D XCT projection of cracks (blue) in the particle before (A) and after (B) microwave treatment.

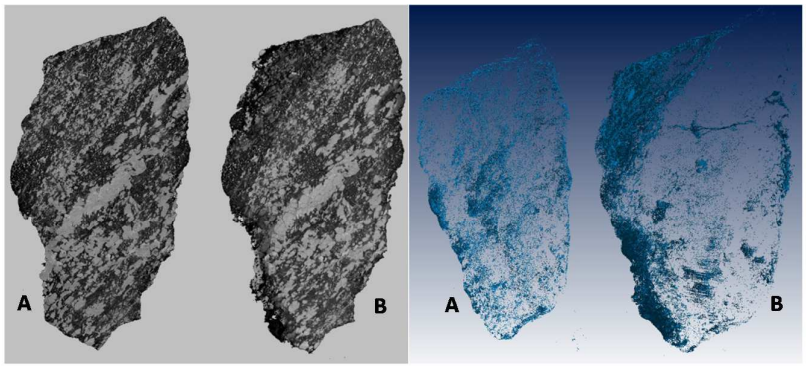

Gangue Pyrite Sphalerite

Figure 4-6: Left 2D XCT slice image of a (-25+19) mm cone crushed particle before (A) and after(B) microwave treatment, right 3D XCT projection of cracks (blue) in the particle before (A) and after (B) microwave treatment.

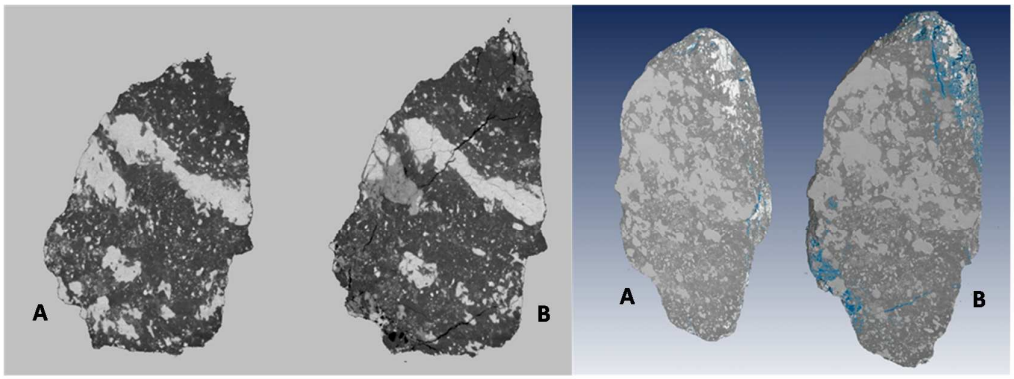

Gangue Pyrite Sphalerite

Figure 4-7: Left 2D XCT slice image of a (-16+9.5) mm cone crushed particle before (A) and after(B) microwave treatment, right 3D XCT projection of cracks (blue) in the particle before (A) and after (B) microwave treatment.

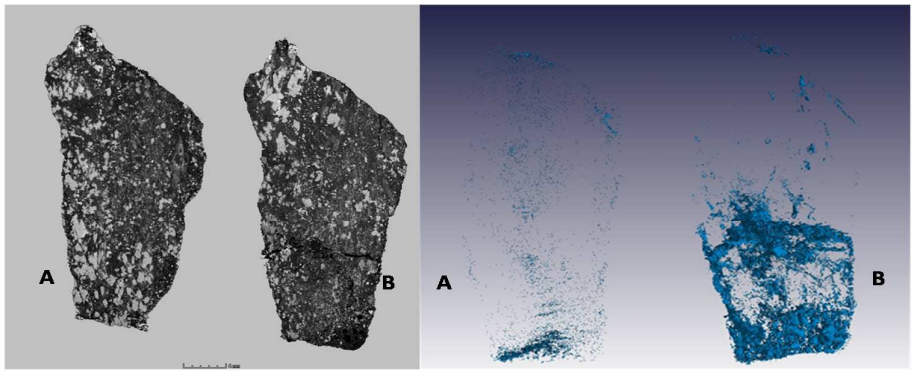

Gangue Pyrite Sphalerite

Figure 4-8: Left 2D XCT slice image of a (-16+9.5) mm HPGR crushed particle before (A) and after(B) microwave treatment, right 3D XCT projection of cracks (blue) in the particle before (A) and after (B) microwave treatment.

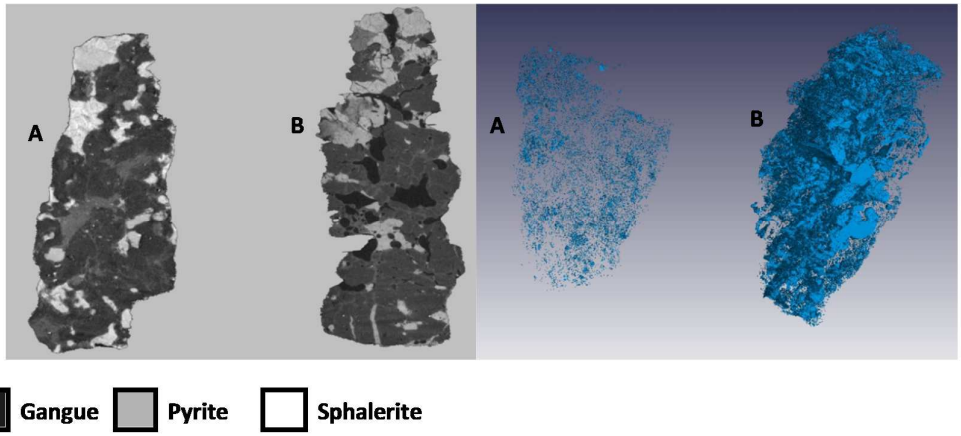

Figure 4-9:Left 2D XCT slice image of a (-5+4.75) mm cone crushed particle before (A) and after(B) microwave treatment, right 3D XCT projection of cracks (blue) in the particle before (A) and after (B) microwave treatment.

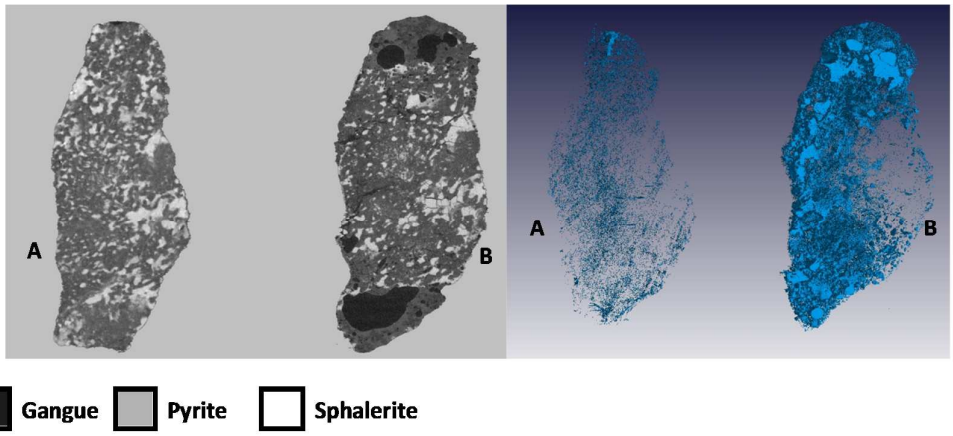

Figure 4-10:2D XCT slice image of a (-5+4.75) mm HPGR crushed particle before (A) and after(B) microwave treatment, right 3D XCT projection of cracks (blue) in the particle before (A) and after (B) microwave treatment.

Further analysis of the nature of the microwave induced crack pattern shows fracture along grain boundaries, interphase trans-granular fractures across grains (Figure 4-11). The trans-granular cracks are a result of interphase cracks propagating across the grains of different phase material. The boundary cracks appear along the absorbent phase grains (Figure 4-11). Further qualitative analysis of the XCT and QEMSCAN images shows that the boundary cracks are fewer compared to the interphase cracks across all particle sizes. The QEMSCAN mineral association results illustrated in Figure 4-12 show that the microwave induced cracks in all the particle size classes show the strongest association to gangue mineral phases, followed by pyrite and sphalerite. It can be concluded from these results that microwave treatment has effectively induced visible micro-cracks in the ore. While previous theoretical studies suggested that microwave treatment would result predominantly in grain boundary fracture (Ali and Bradshaw, 2010), the results here show that the cracks consist of both interphase trans-granular and grain boundary cracks.

Table 4-3: QEMSCAN variation of measured crack volume with field spacing resolution for small HPGR crushed microwave treated ore sample block

Pixel size	Crack volume %
5 µm	5.49
10 µm	5.26
20 µm	4.64

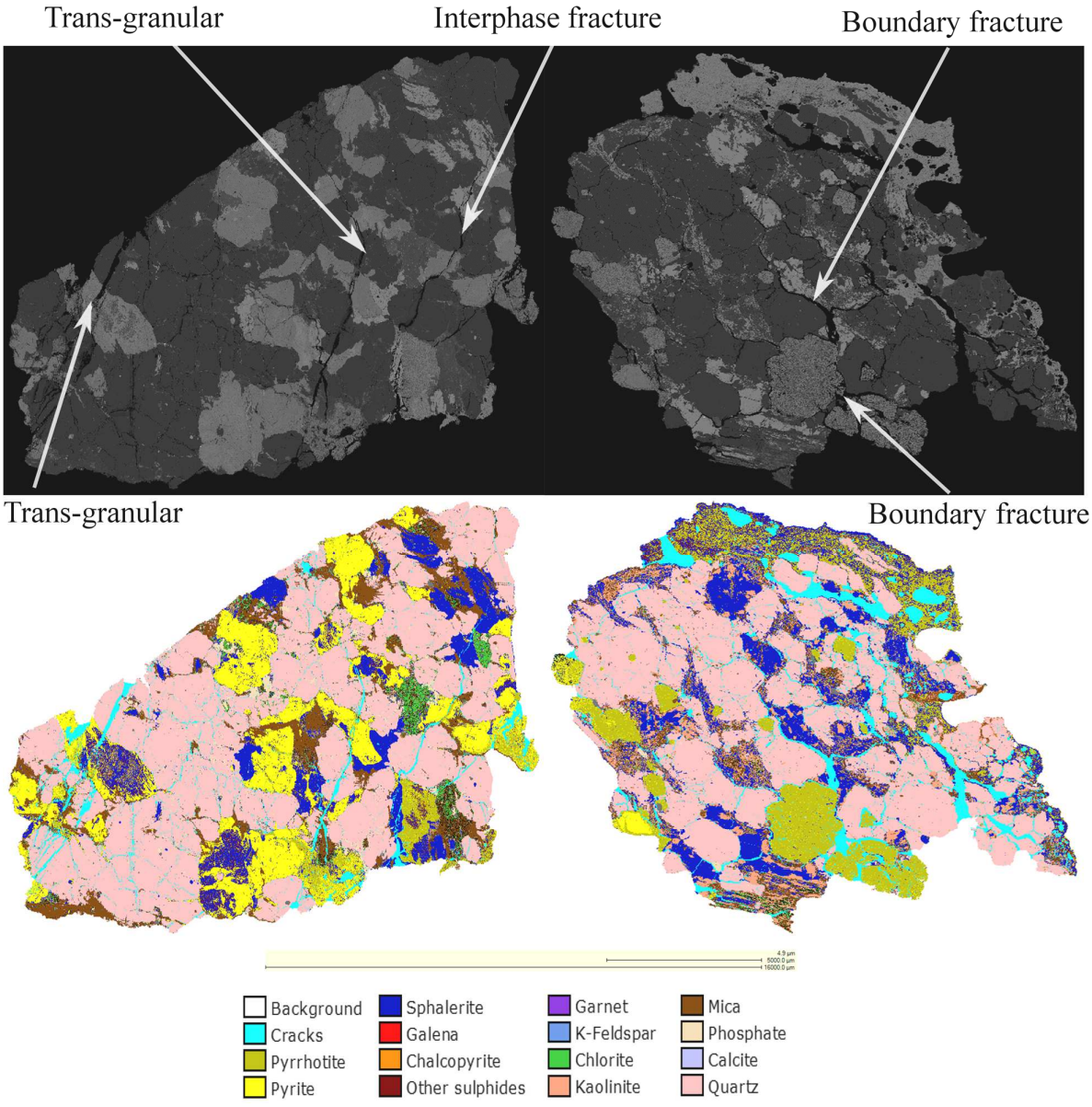

Figure 4-11: QEMSCAN BSE images showing microwave induced interphase trans-granular, and boundary fracture with corresponding QEMSCAN false colour image.

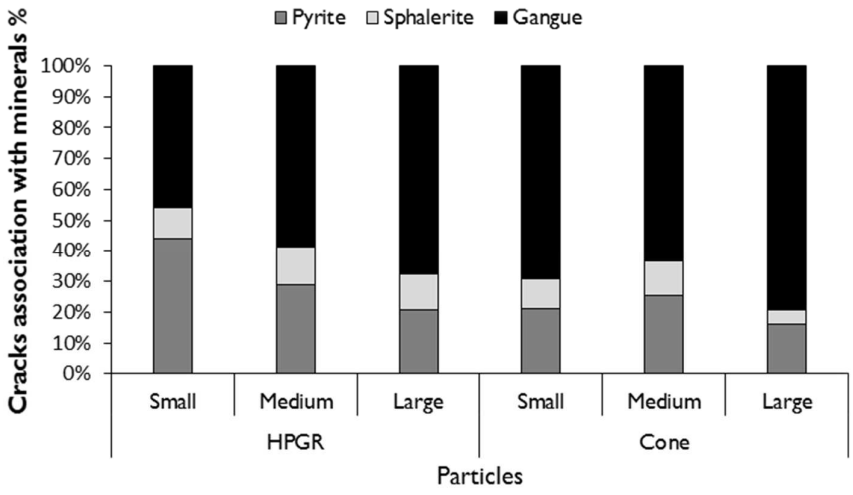

Figure 4-12*: QEMSCAN microwave induced cracks association with the major mineral phases in the ore* (pyrite, sphalerite and gangue) across all sizes.

4.2.2. Quantification of crack volume

XCT and QEMSCAN analyses were used to calculate the particle percentage crack volume in order to quantify microwave induced damage in cone and HPGR crushed particle. An analysis of variance was done at the 0.05 level of significance to determine if changes in XCT and QEMSCAN measured percentage crack volume after microwave treatment were statistically significant. For both modes of prior comminution, the increase in percentage crack volume after microwave treatment was statistically significant, but there was no statistically significant difference in percentage crack volume between modes of prior comminution. Analysis of the XCT and QEMSCAN results shows no significant difference in percentage crack volume between the cone and HPGR crushed particles either before or after microwave treatment for all sizes (see Figure 4-13).

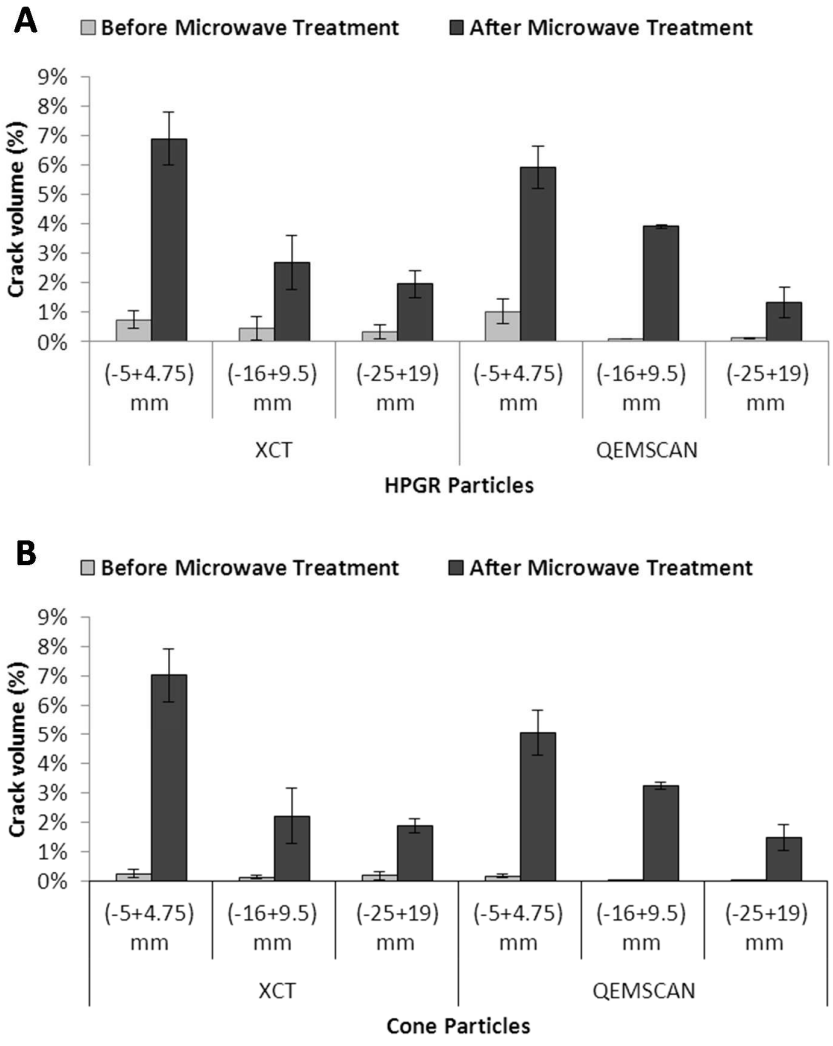

Figure 4-13: XCT and QEMSCAN measured crack volumes with error bars representing standard deviation for HPGR crushed (A) and cone crushed (B) particles before and after microwave treatment.

Table 4-4: Comparison of XCT measured crack volume against QEMSCAN measured crack volume before and after microwave treatment

Crushing method	Size	XCT (3D)		QEMSCAN (2D)	
		Before	After	Before	After
HPGR	(-5+4.75) mm	0.75%	6.90%	1.03%	5.93%
	(-16+9.5) mm	0.45%	2.69%	0.10%	3.91%
	(-25+19) mm	0.35%	1.96%	0.12%	1.35%
CONE	(-5+4.75) mm	0.28%	7.04%	0.19%	5.06%
	(-16+9.5) mm	0.15%	2.23%	0.05%	3.25%
	(-25+19) mm	0.20%	1.89%	0.04%	1.49%

The increase in percentage crack volume of the small particles is at least 2 times greater than that which was measured for the medium and large particles for both XCT and QEMSCAN measured percentage crack volume. This suggests greater particle damage due to microwave treatment for the small particles compared to larger cone and HPGR crushed particles (Figure 4-13). This is probably because the small particles were more closely packed in the microwave applicator sample holder compared to the larger particles. This more uniform packing is likely to have led to an electromagnetic field distribution closer to that envisaged during the design of the microwave cavity. The design process optimised the field distribution so that sufficiently high electric field intensity could be achieved over a significant volume of the sample. To do this, the design simulations assume that the sample holder is filled with a solid, homogeneous sample of appropriate dielectric properties. For the case of the large particles, the packing is highly irregular in the sample holder, which will result in an electric field distribution significantly perturbed from the design ideal, with the likelihood of isolated regions of high electric field intensity in specific locations in individual particles. Note that this effect is directly related to the operating frequency (2.45 GHz), single-mode cavity type, and particle size. Were a lower frequency to be used in an industrial application (896 or 915 MHz), the applicator would be significantly larger and the large particles would pack more uniformly into it.

Comparison of the percentage crack volume determined by XCT showed good agreement with the QEMSCAN results (Table 4-4). Differences in the XCT and QEMSCAN percentage crack volume results can be attributed to the fact that the particles analysed were not identical, as well as possible stereological effects from 2D QEMSCAN measurements (King and Schneider, 1998b; Lätti and Adair, 2001). It is possible that stereological effects could result in an over estimation of the QEMSCAN measured percentage crack volume as the sectioned particles on the polished sections might appear to have a higher crack surface area than actual. This is because QEMSCAN crack volume network characterisation is based on the examination of 2D polished particle sections. Application of QEMSCAN analysis alone as a crack volume network measurement method provides a characterisation of crack networks in 2D, with conclusions about the 3D crack volume network based on 2D measurements. The percentage crack volume measured using QEMSCAN is calculated based upon the assumption that area equates to volume. In contrast XCT offers direct 3D crack volume measurements based on analysis of the total volume of the particle.

Using XCT it was possible to measure and compare the individual particle bulk volume of each particle before and after microwave treatment. Here bulk volume is defined as the sum

of the material and crack volume. The XCT measured particle bulk volume increases after microwave treatment for all sizes (Figure 4-14). For the small crushed particles the bulk volume occupied by the particle increased by 18%, while for the medium and large particles a volume increase of 7.2% and 5.1% was observed. This increase in bulk volume is due to an increase in crack volume within the particle caused by microwave treatment (Figure 4-14). Despite undergoing considerable microwave induced damage, the microwave treated particles in all size fractions remained intact as the microwave induced crack damage did not result in particle fragmentation. This is particularly important in heap leaching where the particle size has an influence on fluid flow dynamics. Microwave induced fragmentation when preparing heap leach feed can result in fines generation, which could lead to fluid flow problems during heap leaching

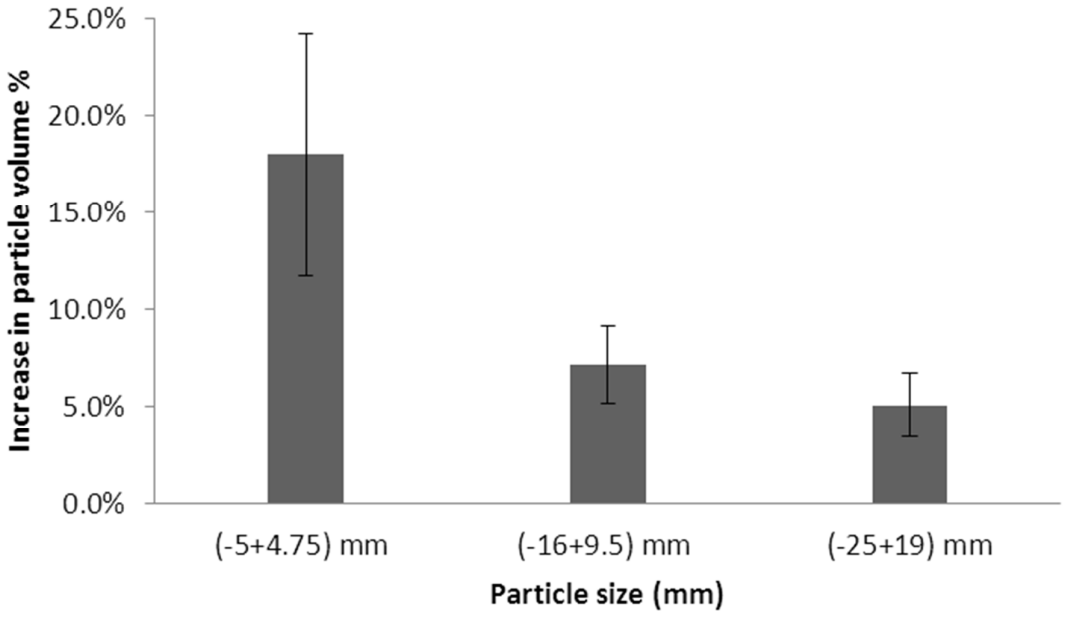

Figure 4-14: XCT measured average percentage increase in particle crack volume before and after microwave treatment calculated for each size fraction with error bars representing standard deviation.

4.2.3. Crack width distribution

The crack width distribution of the microwave induced cracks was measured and is shown in Figure 4-15 for both QEMSCAN and XCT measured cracks. Crack width in this study is defined as the diameter of a sphere with a volume equivalent to that of the measured cracks. Based on the respective pixel (QEMSCAN) and voxel (XCT) sizes used in this study, the finest cracks detected were 10, 20 and 20 microns, and 25, 45 and 75 microns for the small, medium and large particle size classes respectively. There is no significant difference in crack width distribution according to mode of comminution (cone vs HPGR) prior to and after microwave treatment (Figure 4-15). This further shows that mode of prior comminution had no effect on microwave induced damage. QEMSCAN results show a finer crack width distribution than XCT. This is a function of the image resolution (minimum crack width detectable) as well as the application of the connected component algorithm in VG Studio Max 2.1. The connected component analysis detects the individual connected components of the crack voxels in the selected 3D virtual segmented crack ROI and measures these connected components as an individual crack voxel grouping. A similar connected component algorithm was not available in the iDiscover software that was used to analyse the QEMSCAN data.

Figure 4-16 is a 3D view of the microwave induced cracks, showing the connected network of microwave induced cracks in ore particles of different sizes. The largest cracks in the ore particles are shown in yellow while the red highlights other smaller connected cracks within the ore matrix. Previous studies have reported on the difficulties associated with identifying cracks formed during comminution from low resolution (> 20 μm) XCT images (Lin et al., 2012). These challenges are due to the physical size of cracks produced as a result of particle crushing, of which at times these cracks can measure in the sub-micron range (< 1 μm). In contrast microwave induced cracks are fairly wider and of higher density (Figure 4-13). Thus even at relatively low resolution (> 20 μm), microwave induced cracks are large enough to still be identifiable in XCT scans.

Overall results of the crack characteristics suggest that microwave treatment is likely to result in improved mineral exposure in coarse particles. This is expected to have significant implications in heap leaching operations, since improvements in heap leaching recovery depend on the accessibility of valuable minerals to the lixiviant (Wen et al., 1996).

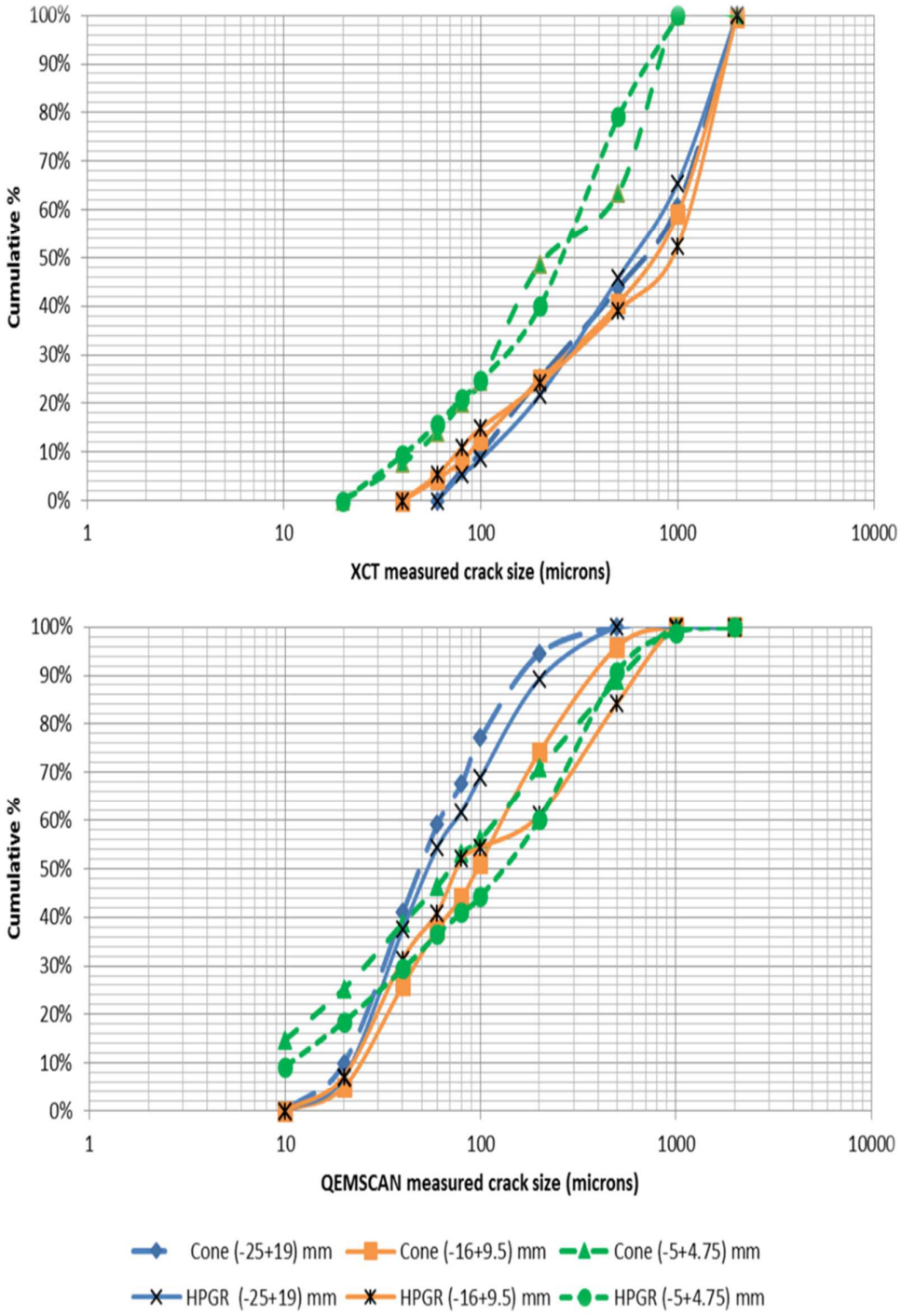

Figure 4-15: QEMSCAN and XCT calculated crack width distributions of microwave treated sphalerite ore obtained from cone and HPGR crushed particles for small, medium and large size particles.

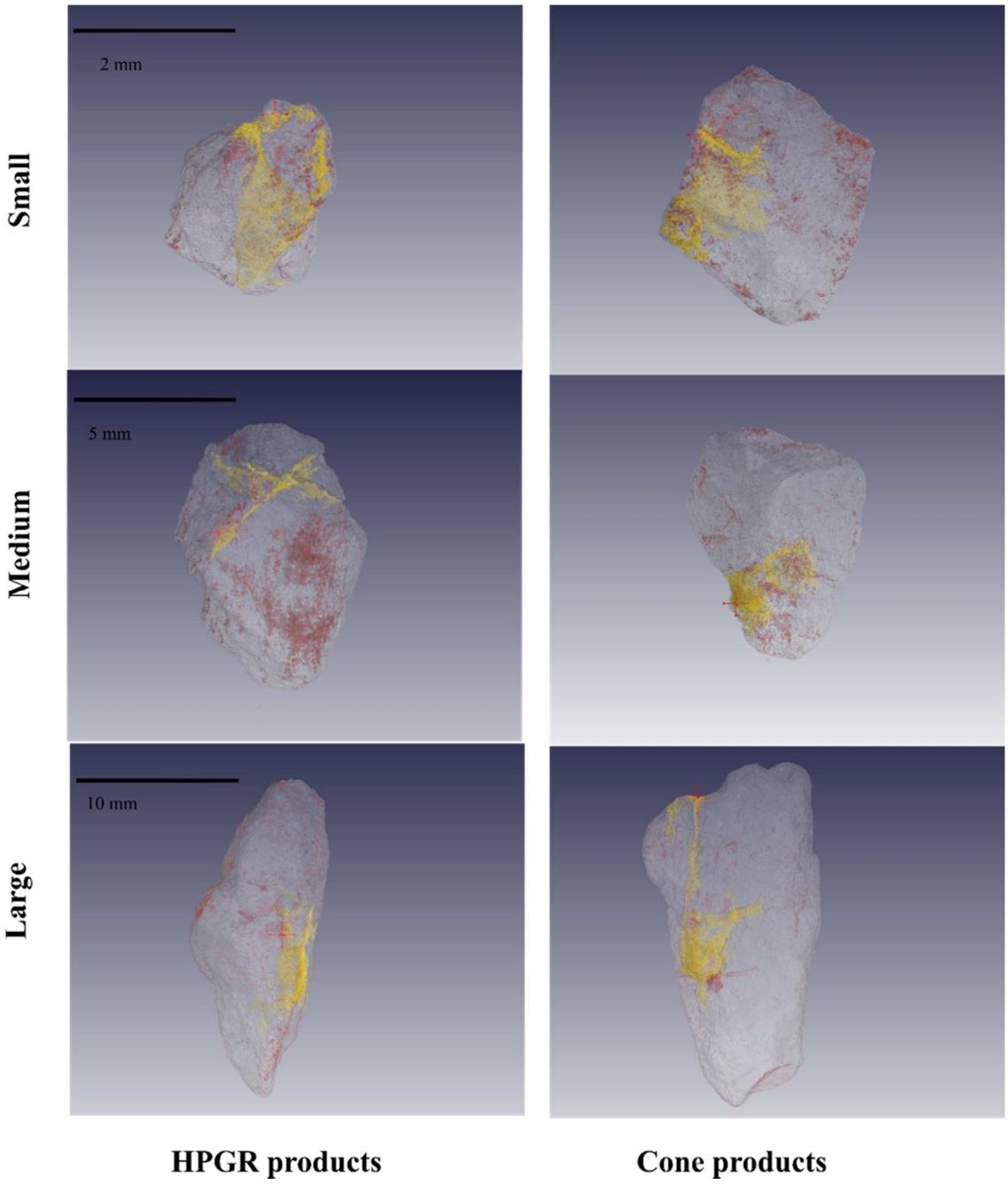

Figure 4-16: XCT 3D image projections of HPGR and cone crushed particles, showing connected cracks in red and yellow, yellow shows the biggest size connected cracks in the particle.

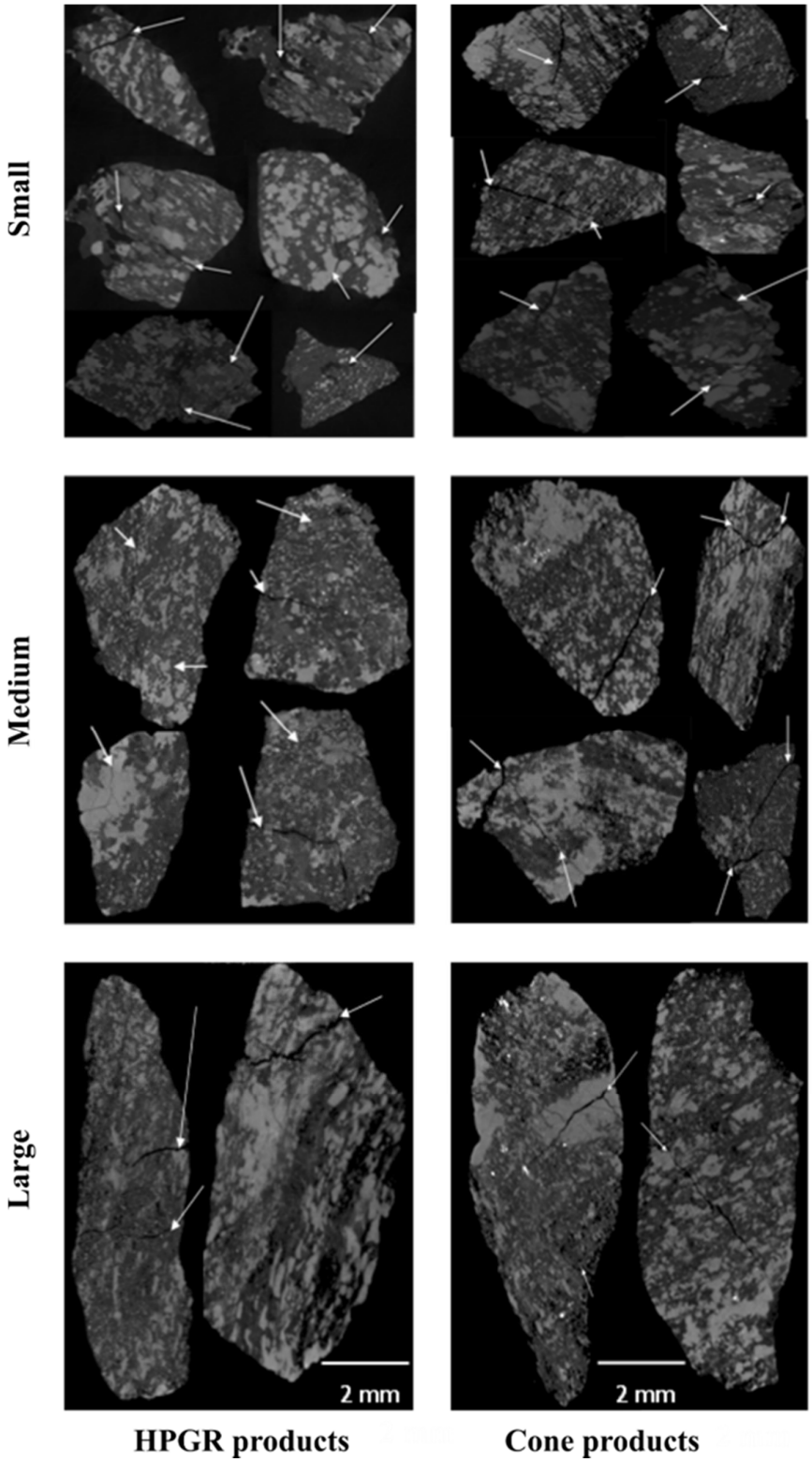

Figure 4-17: 2D XCT slice images for microwave treated sphalerite ore particles white arrows showing microwave induced cracks.

4.3.Interfacial area measurement results

The ratio of specific interfacial area after microwave treatment to specific interfacial area before microwave treatment, in an individual particle, is an indicator of the degree of grain boundary fracture. When the mode of fracture is grain boundary there is a loss in interfacial area. A ratio close to 1.00 suggests conservation of interfacial area during microwave induced crack propagation and thus, no grain boundary fracture. On the other hand as the ratio gets smaller, the degree of grain boundary fracture that is the amount of specific interfacial area lost, increases. The measurement and calculation of specific interfacial area ratios (after microwave treatment/before microwave treatment) obtained for small, medium and large particles are summarized in Table 4-5, Table 4-6 and Table 4-7 respectively. The average specific interfacial area values for HPGR particles before and after microwave treatment are summarized in Figure 4-18. The results show a general decrease in specific interfacial area after microwave treatment. This suggests some degree of preferential breakage taking place.

The average specific interfacial area ratio shows an increase in the specific interfacial area ratio with size (Figure 4-19). The small, medium and large particles have an average specific interfacial ratio of 0.69, 0.77 and 0.84 respectively. This indicates an average decrease in interfacial area after microwave treatment of 31%, 23% and 16% for small, medium and large particles. The result suggests a greater degree of preferential breakage taking place in the small sized particles compared to the large particles. It can be concluded from this result that for large particles little interfacial area is lost and microwave induced breakage occurs primarily by random fracture for this particular ore. Previous studies have suggested that microwave treatment of ores predominantly results in preferential grain boundary fracture. Results from this study suggests that the mode of fracture consists of both trans-granular (random) and preferential grain boundary fracture (Figure 4-19). With the extent of preferential grain boundary fracture varying with particle size. As indicated by Vorster et al.,(2001b), microwave treatment results in some degree of preferential fracture and weakening of treated particles when compared against microwave untreated particles from conventional crushing equipment.

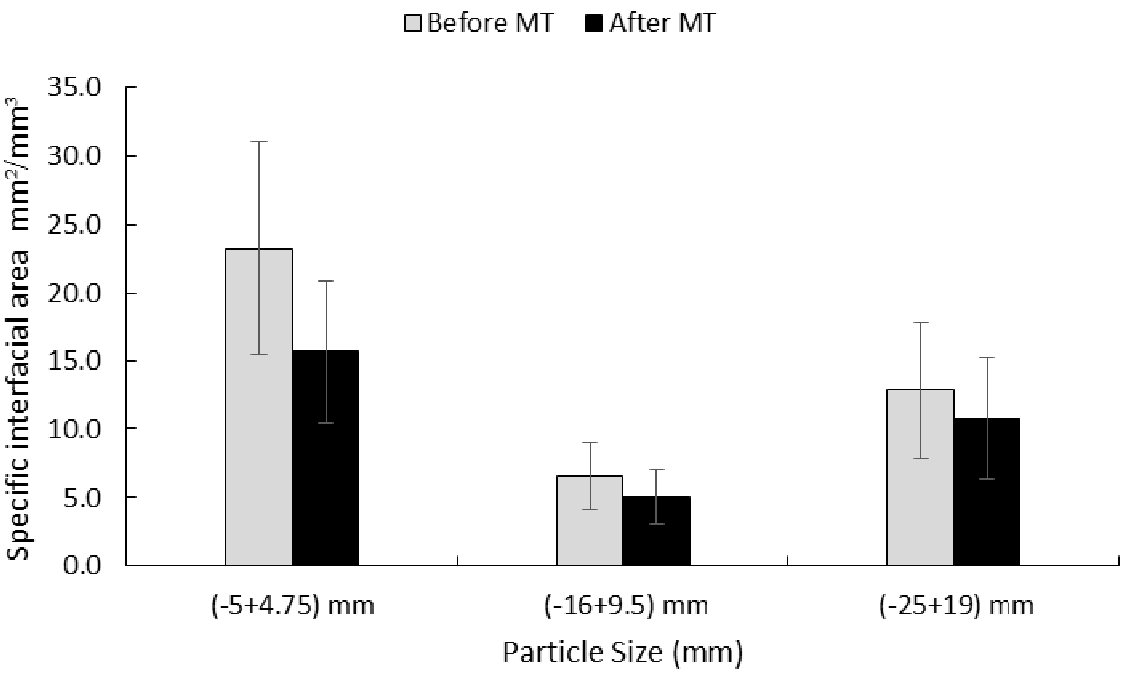

Figure 4-18: Average specific interfacial before and after microwave treatment for HPGR crushed particles. Error bars represent standard deviation

Table 4-5: Specific interfacial area before and after microwave treatment of HPGR crushed small particles and corresponding specific interfacial area ratios, MT-Microwave Treatment (voxel resolution = 5 micron)

Particle number	Specific interfacial area (mm^2/mm^3)		Specific interfacial area ratio after MT/before MT
	Before MT	After MT	
1	37.07	25.09	0.68
2	28.25	21.97	0.78
3	20.75	11.81	0.57
4	16.79	12.70	0.76
5	31.12	17.62	0.57
6	31.95	18.39	0.58
7	12.76	11.13	0.87
8	16.13	15.56	0.96
9	29.83	24.30	0.81
10	25.15	16.30	0.65
11	14.51	7.62	0.53
12	18.31	13.77	0.75
13	16.74	12.31	0.74
14	31.11	17.57	0.56
15	17.73	9.22	0.52

Table 4-6: Specific interfacial area before and after microwave treatment of HPGR crushed medium particles and corresponding specific interfacial area ratios, MT-Microwave Treatment (voxel resolution = 15 micron)

Particle number	Specific interfacial area (mm^2/mm^3)		Specific interfacial area ratio after MT/before MT
	Before MT	After MT	
1	9.58	8.39	0.88
2	5.10	4.02	0.79
3	4.14	3.12	0.76
4	7.07	4.12	0.58
5	6.68	6.25	0.94
6	6.30	4.53	0.72
7	6.32	4.71	0.75
8	5.64	3.80	0.67
9	8.06	4.34	0.54
10	6.15	4.90	0.80
11	13.38	10.19	0.76
12	6.86	5.47	0.80
13	5.56	5.03	0.90
14	4.08	3.30	0.81
15	3.94	3.34	0.85

Table 4-7: Specific interfacial area before and after microwave treatment of HPGR crushed large particles and corresponding specific interfacial area ratios, MT-Microwave Treatment (voxel resolution = 25 micron)

Particle number	Specific interfacial area (mm^2/mm^3)		Specific interfacial area ratio after MT/before MT
	Before MT	After MT	
1	9.19	8.06	0.88
2	11.82	10.36	0.88
3	20.63	12.82	0.62
4	7.61	4.56	0.60
5	5.56	5.08	0.91
6	5.27	4.89	0.93
7	12.94	12.03	0.93
8	13.40	12.77	0.95
9	20.41	19.80	0.97
10	16.42	12.65	0.77
11	18.51	16.27	0.88
12	17.97	15.89	0.88
13	9.85	9.43	0.96
14	12.05	8.61	0.71
15	11.35	8.43	0.74

4.4.Mineral exposure analysis results

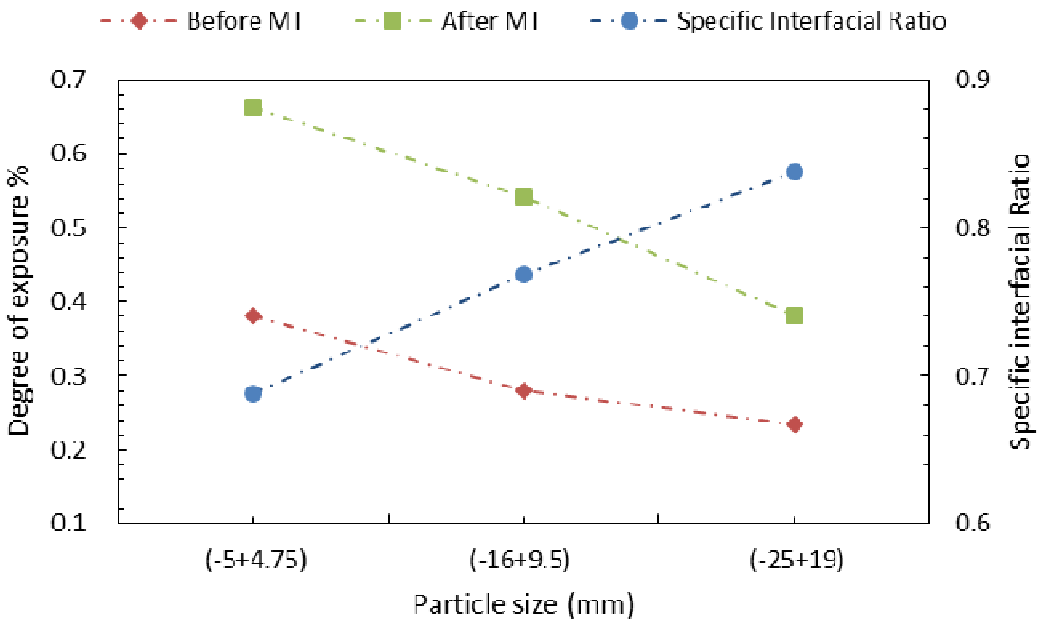

Figure 4-19 : Comparison of the measured degree of exposure for HPGR particles before and after microwave treatment and the average specific interfacial ratio

Figure 4-19 shows the calculated average degree of exposure using Equation 3-7, for small (-5+4.75 mm), medium (-16+9.5 mm), and large (-25+19) mm HPGR particles before and after microwave treatment along with the average specific interfacial area ratio. As expected there is a general increase in degree of exposure with particle size after microwave treatment (see Figure 4-19). Previous studies have shown that the degree of mineral exposure increases with decreasing particle size (Barbery, 1984; King, 1979; King, 1993). The results show a general increase in degree of exposure in the individual particles after microwave treatment. The exposure analysis shows an average increase in the degree of sulphide grain exposure by 28%, 26% and 15% for small, medium and large particles after microwave treatment. Improvement in mineral exposure is achieved by microwave crack networks running through the microwave treated particles (see Figure 4-20 and Figure 4-21.) These cracks provide an additional surface front for chemical attack of grains deep within the particle by leaching solution (Hsih et al., 1995; Miller et al., 2003). It is therefore expected that microwave treatment will result in value mineral recovery during based on enhanced mineral grain exposure.

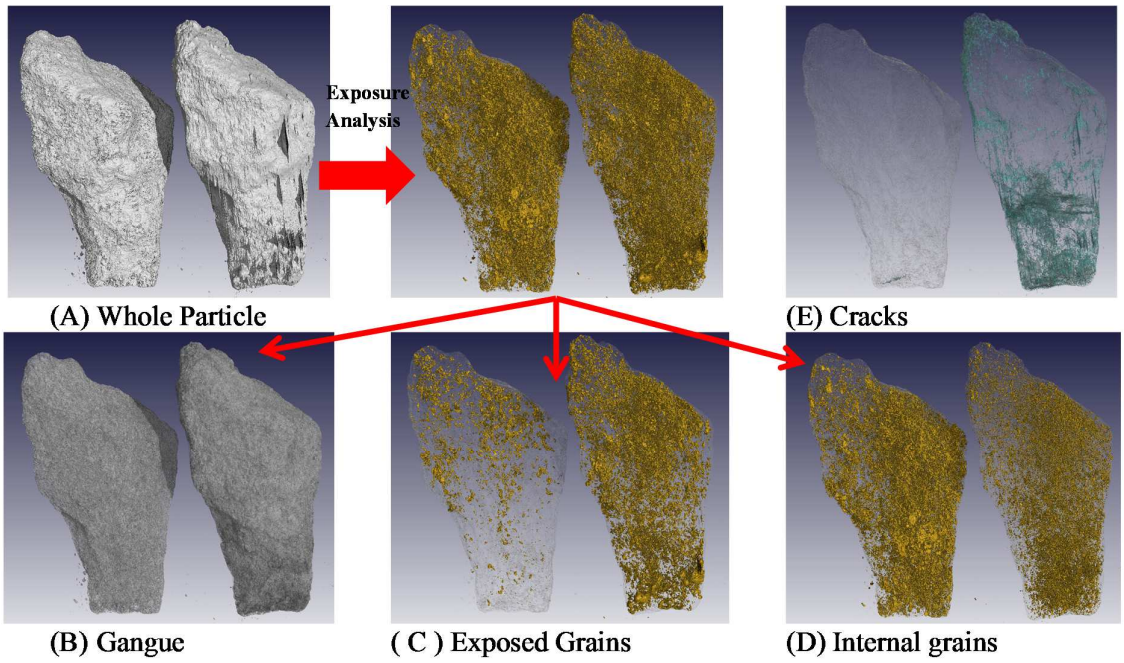

Figure 4-20: Schematic of steps for the determination of medium (16+9.5 mm) HPGR crushed particle interfacial area

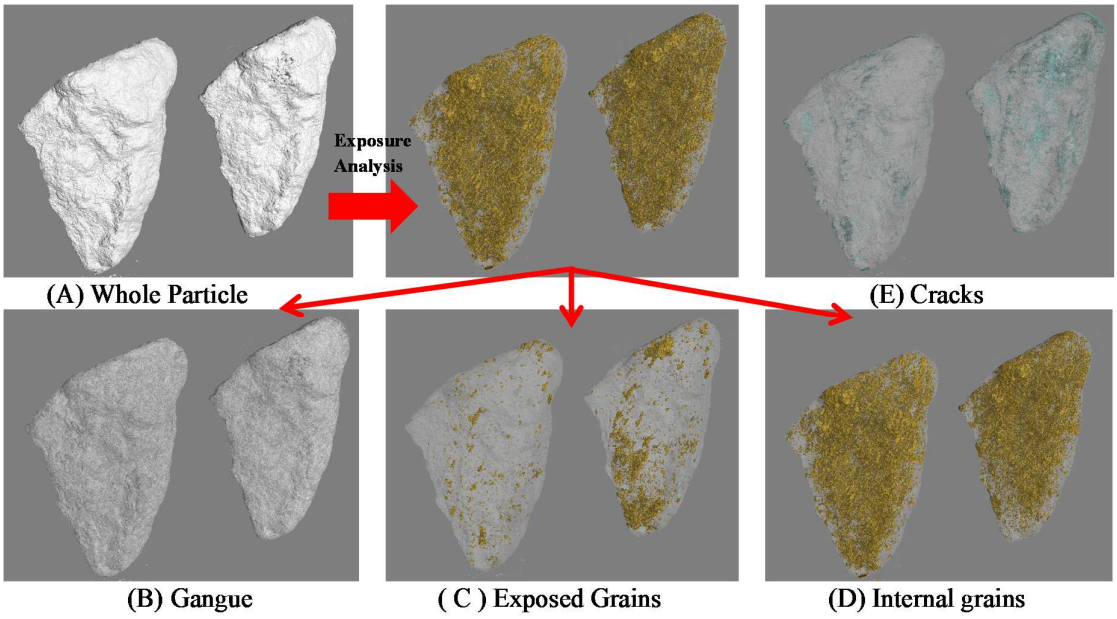

Figure 4-21: Schematic of steps for the determination of large (25+19) mm HPGR crushed particle interfacial area

4.5.Chapter summary

Results presented in this chapter have shown that coarse-grained (≥ 5 mm) massive sulphide ores are amenable to microwave treatment. Previous studies have suggested that microwave treatment results predominantly in grain boundary fracture however, the results show that the cracks consist of both interphase trans-granular and grain boundary cracks. This suggests that more benefit would be obtained from microwave technology by applying downstream processing methods that directly utilise microwave induced cracks in recovering valuable metals such as heap leaching. Both XCT and QEMSCAN analysis results showed that microwave treatment resulted in a significant increase in percentage crack volume for both modes of prior comminution at all particle sizes. For both modes of prior comminution, the increase in percentage crack volume after microwave treatment was statistically significant, but there was no statistically significant difference in percentage crack volume between modes of prior comminution.

The extent of particle damage in microwave treated ores was also evaluated for the first time using XCT and mineral grain exposure analysis. XCT measured particle geometrical properties were used to calculate the interfacial areas of mineral grains in microwave treated particles and mineral exposure before and after microwave treatment. The ratio of specific interfacial area after microwave treatment to specific interfacial area before microwave treatment was used as an indicator of the degree of preferential grain boundary fracture. Results presented in this chapter show that significant grain boundary fracture is achieved by microwave treatment at higher power density and short exposure time for all particle sizes. The degree of grain boundary fracture was observed to increase with decreasing particle size. For example, for small sized particle about 31% of the interfacial area was lost compared to 23% and 16% for medium and large particles. The exposure analysis shows an average increase in the degree of sulphide grain exposure by 28%, 26% and 15% for small (-5+4.75 mm), medium (-16+9.5 mm), and large (-25+19) mm particles after microwave treatment.

Results presented in this chapter indicate that microwave pre-treatment of crushed ore for heap leaching is a viable processing route that has the potential to improve mineral exposure to lixiviant and hence heap leaching recovery. This work has shown how XCT and QEMSCAN crack characterisation techniques complement each other in the study of cracks in multiphase materials. By applying XCT and QEMSCAN techniques this study provides quantitative and qualitative data on microwave induced crack damage.

CHAPTER 5

5. HEAP LEACHING OF MICROWAVE TREATED ORE

The aim of this part of the study was to determine the effects of microwave induced crack damage reported in chapter 4, on the dissolution kinetics of (bio) heap leaching processes of a typical massive sulphide ore. In this chapter, results of column leaching experiments carried out in the eight reactors are presented and discussed (see Table 5-1). The results are related to the different feed size fractions small (-5+4.75 mm), medium (-16+9.5 mm), and large (-25+19) mm) and different ore preparation procedures (cone, HPGR, microwave treatment). The effects of microwave induced cracks on leaching recovery is discussed. Mineral dissolution in microwave treated and untreated single ore particle is investigated using XCT and QEMSCAN analysis. Lastly conclusions are drawn on the influence of microwave induced crack networks on metal recovery.

Table 5-1: Summary of reactor conditions, (T) refers to microwave treated ore, (UT) refers to microwave untreated ore.

Reactor	Ore samples	Total mass (g)
1	(-25+19) HPGR UT	3600
2	(-5+4.75) HPGR UT	3600
3	(-16+9.5) HPGR UT	3600
4	(-16+9.5) Cone T	3600
5	(-5+4.75) HPGR T	3600
6	(-16+9.5) HPGR T	3600
7	(-25+19) Cone T	3600
8	(-25+19) HPGR T	3600

5.1.Column leaching results

5.1.1. Reactor ORP and pH

Bio-leaching of sphalerite ore includes acid consuming and acid producing reactions. The main acid consuming reactions are the dissolution of Fe oxides/hydroxides, pyrrhotite and gangue minerals as well as the bacterial oxidation of Fe^{2+} to Fe^{3+}, while acid producing reactions consist of the bacterial oxidation of sulphur, the dissolution of pyrite and the hydrolysis of ferric ion to form jarosite (Ahmadi et al., 2011; Mousavi et al., 2008). Given the fact that iron oxidizing micro-organisms transform ferrous to ferric ions, activity of bacteria in bio-leaching can be determined by oxidation reduction potential (ORP) of leaching environment (Lotfalian et al., 2012). In this research, no attempt was made to count bacterial cells in the leaching

environment (solid surface and solution), but the ORP of the solution was used to indicate bacterial activity (see Figure 5-1).

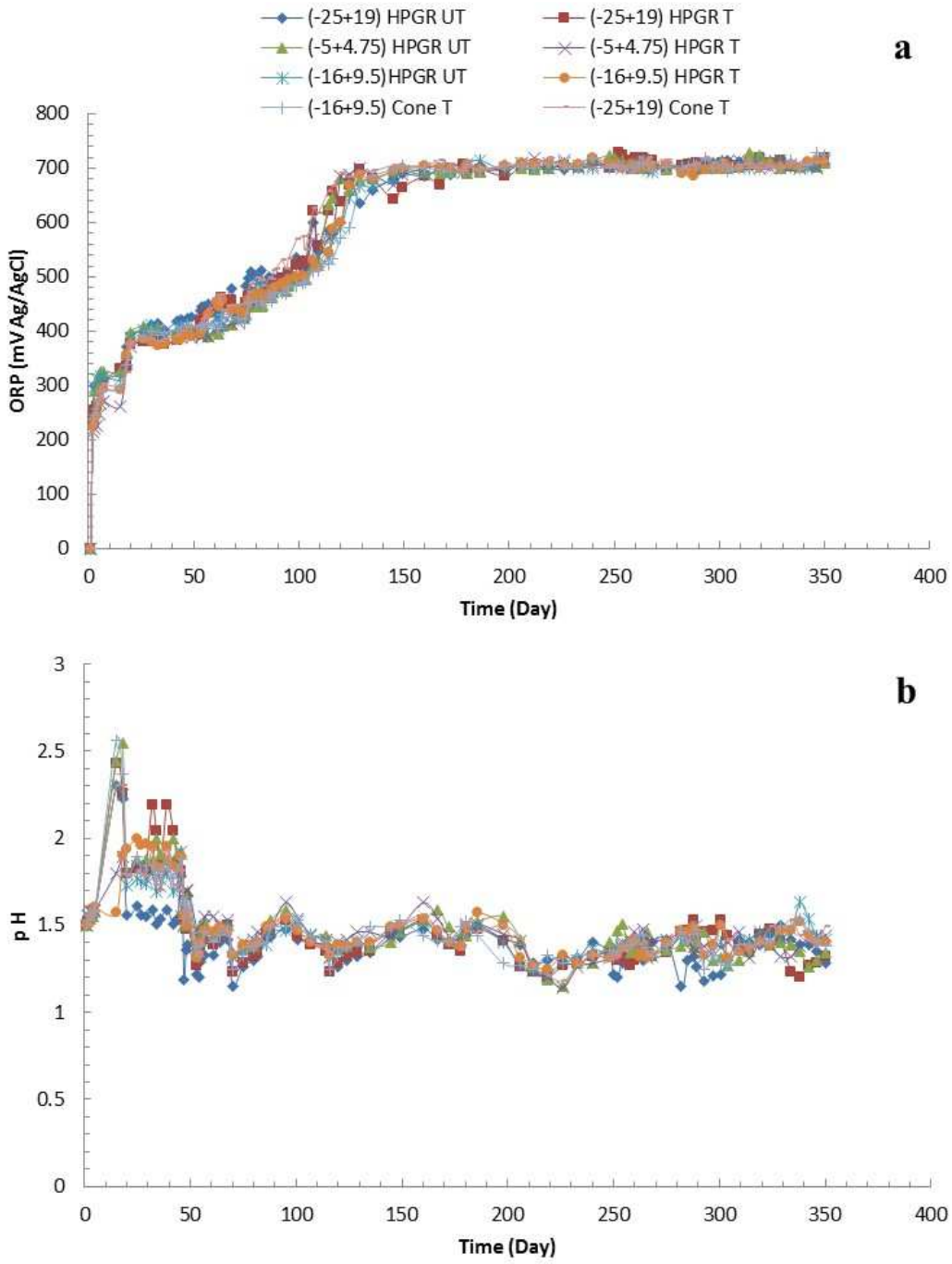

Figure 5-1: Changes of the redox potential profile (a) and pH profile (b) versus time (days) for all reactors

The dissolution of gangue minerals lead to an initial increase in the solution pH within the first 40 days, and possibly lead to a decrease in bacterial activity needed for the oxidation of Fe^{2+} to Fe^{3+}. This corresponded with the patterns of pH and redox potential in Figure 5-1. In the beginning of the bio-leaching experiments, the only source of acid was the feed solution and consequently the pH of the medium increases due to acid consuming reactions. Beyond the first 40 days of bio-leaching, the dissolution reaction had entered an acid producing phase, accelerated by pyrite dissolution thus the pH decreased and stabilised around the feed value. This phase is favourable to microbial activity and the subsequent oxidation of Fe^{2+} to Fe^{3+}, which concurrently increases the solution potential in Figure 5-1 (Lotfalian et al., 2012; Watling, 2006). The initial low solution potential was due to ferrous ions not being oxidized soon after inoculation. The dominance of Fe^{3+} was taken as an indication of good bio-leaching activity throughout the run such that mineral leaching was the limiting rate step.

There was no substantial increase in redox after initial inoculation on day 1 in the first 30 days suggesting limited bacterial activity. A cell count after two weeks showed a low density of bacteria in the columns. The columns were re-inoculated on day 30, after which there was a steady rise in redox potential in all columns. The redox potential reaching 700 mV after 100 days and remaining stable thereafter. Similar trends in pH and Eh were observed for all eight leach reactors (Figure 5-1). Suggesting bacterial activity was the same in all leach reactors, thus any differences in metal recovery observed in each reactor is dependent on the particle property (size, crack density) and mineral association within the particles and not the reactor conditions.

5.1.2. Cumulative zinc extraction trends

Figure 5-2 shows zinc metal extraction over time in all eight reactors (see Table 5-1). The cumulative zinc recovery was calculated using Equation 3-8. The Zn content in the feed ore to the reactors was obtained from a chemical assay of the combined bulk sample of leach reactor feed using QEMSCAN. Table 5-2 below is a summary of the chemical assay results, showing average values of the elements in the feed ore.

Table 5-2: Elemental analysis results for bulk sample of combined leach reactor feed using QEMSCAN

Element	Al	Ca	Cu	Fe	Mg	Mn	Pb	S	Si	Ti	Zn
Chemical assay %	2.43	0.21	0.16	20.07	0.73	0.24	0.19	25.3	14.52	0.18	10.15

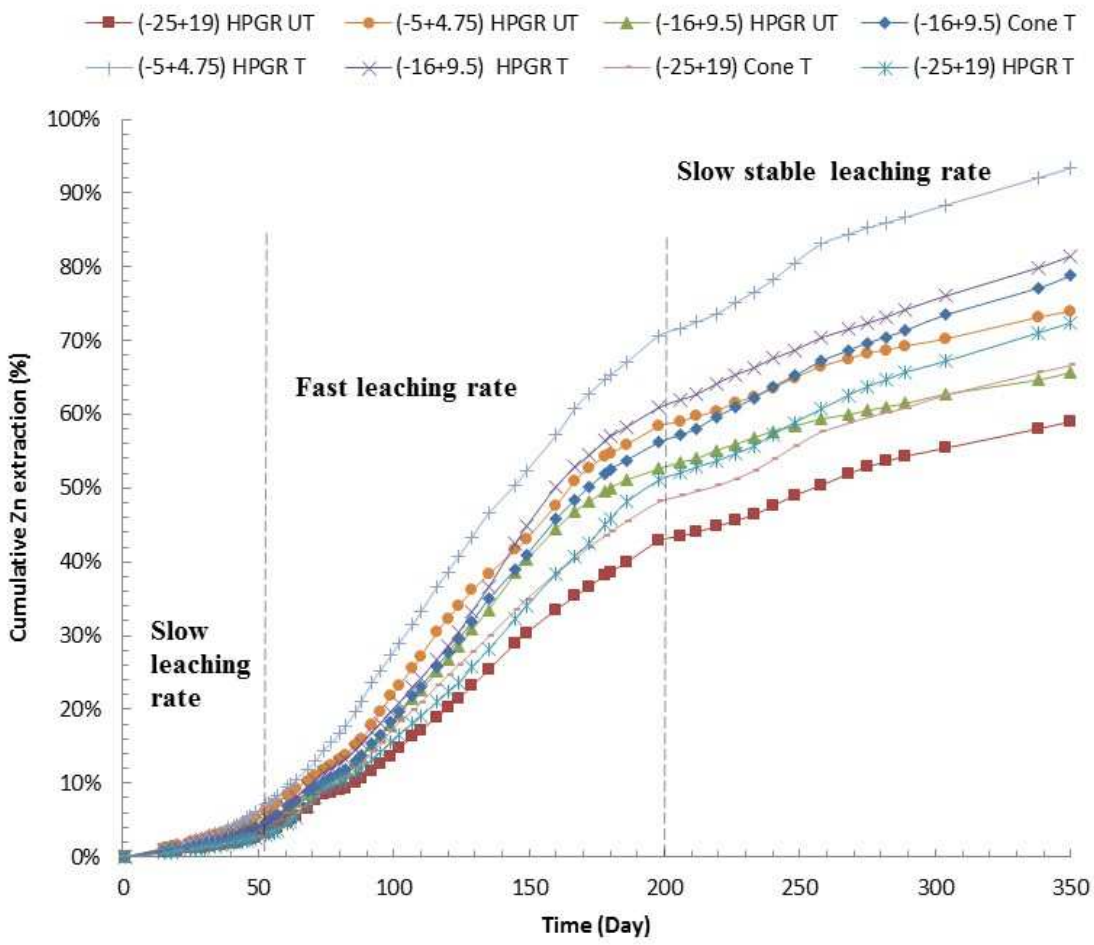

Figure 5-2: Cumulative zinc extraction trends over time in all eight reactors. Reactor 1 (HPGR (-25+19) UT), Reactor 2 (HPGR (-5+4.75) UT), Reactor 3 (HPGR (-16+9.5) UT), Reactor 4 (Cone (-16+9.5) T), Reactor 5 (HPGR (-5+4.75) T), Reactor 6 (HPGR (-16+9.5) T), Reactor 7 (Cone (-25+19) T), Reactor 8 (HPGR (-25+19)). Where UT (microwave untreated), T (microwave treated)

Metal extraction rates in the reactors characteristically showed an initially slow leaching rate in the first 40 days of leaching, followed by a fast leaching rate, reaching up to 40–65% extraction between 50 to 200 days, this was followed lastly by a slower stable rate period, reaching up to 50–90% copper extraction over the following 200 to 350 days. This trend is in agreement with other studies (Ghorbani et al., 2012; Watling, 2006). Slow leaching of value metal occurs in all size classes initially, this is due to the bacteria adapting to the reactor conditions after inoculation. The initial low solution potential indicates that ferrous ions are not oxidized at the initial period of bio-leaching. Since the role of the micro-organisms is to transform ferrous to ferric ions, low solution potential indicates low bacteria activity initially, thus, resulting low value metal extraction rates. As bacteria activity increases as observed by increasing potential rapid leaching occurs in all size classes, leading to near complete recovery in the smaller sizes, but only fractional conversion in the larger sizes. After this initially rapid

phase, leaching slows down considerably as there is a depletion of easy-to-leach surface value mineral, at this stage value mineral accessible through crack networks offer a path for the lixiviant to migrate deeper into the particles.

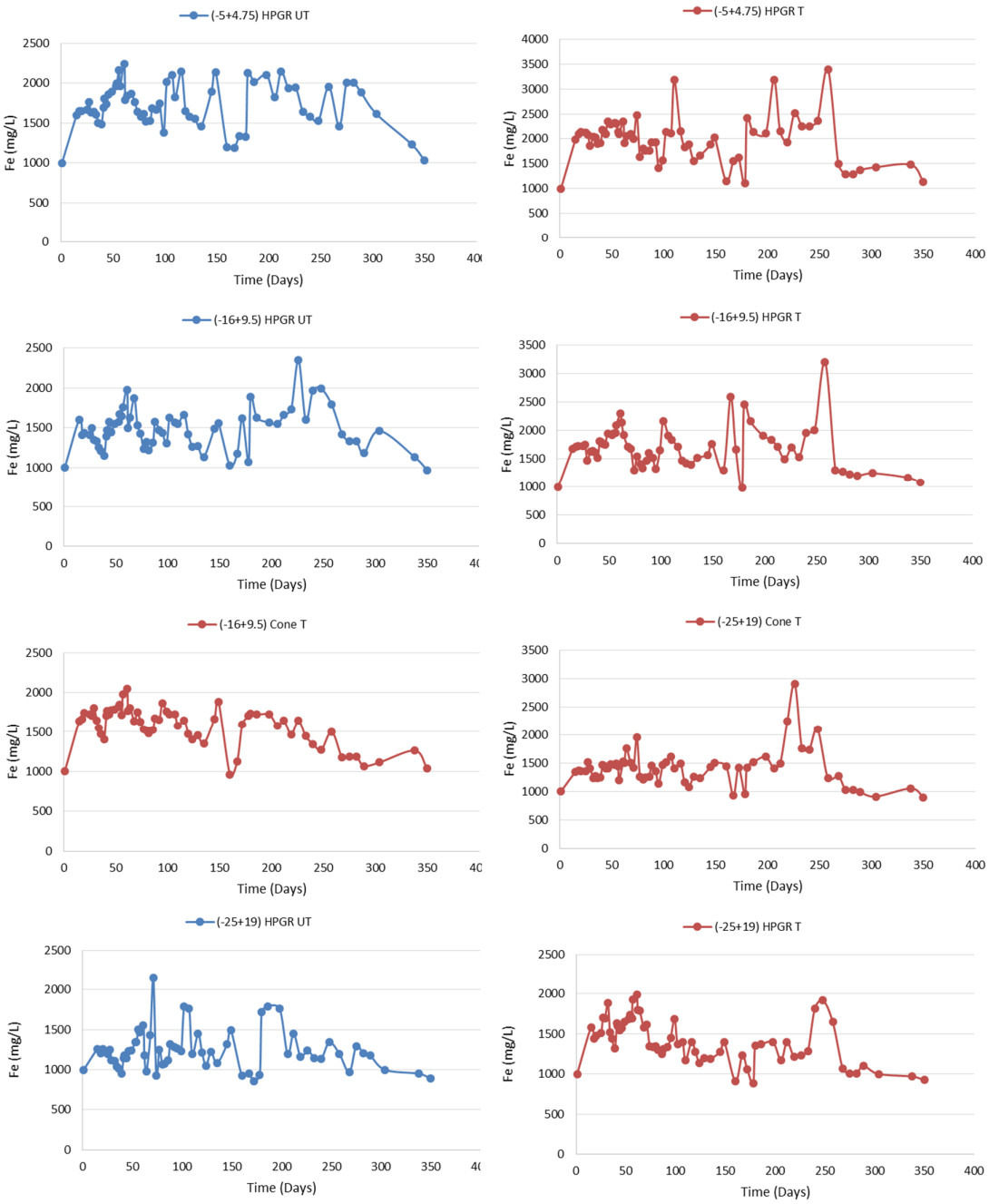

Figure 5-3: Comparison of the amount of total Iron in the PLS in all the reactors

Figure 5-3 shows the concentrations of total iron (Fe) in the PLS from the reactors. In addition to the ferrous ions present in the feed (1000 mg/L) the total Fe in the PLS includes Fe generated from the bio-oxidation of iron bearing minerals such as pyrite. It has been shown in previous studies that, provided an appropriate pH is chosen, the presence of Fe in solution has a positive impact on the sphalerite dissolution rate (Crundwell, 1987; Pina et al., 2005; Sokić et al., 2012). Excess Fe coupled with a pH greater than two can cause a reduction in the leaching rate due to formation of jarosite. Jarosite formation has a negative effect on bacteria growth and sphalerite dissolution. The total Fe concentration is all leaching reactors was well below 5000 mg/L and the pH was maintained between a values of 1.5 to 2. There was no notable evidence of jarosite formation in all reactors during the leaching period. The total Fe concentration trend in solutions from microwave treated ore is similar to the trend observed in solutions from untreated ore of the same size, suggesting that microwave treatment of ores does not affect the bio-oxidation of Fe bearing minerals. It has been suggested that, there is a level of oxidation or phase change on the surface of pyrite minerals, that takes place when pyrite is microwave treated (Uslu et al., 2003; Waters et al., 2007; Znamenáčková et al., 2005). The total Fe concentration results do not suggests any differences in surface properties of microwave treated and untreated ore.

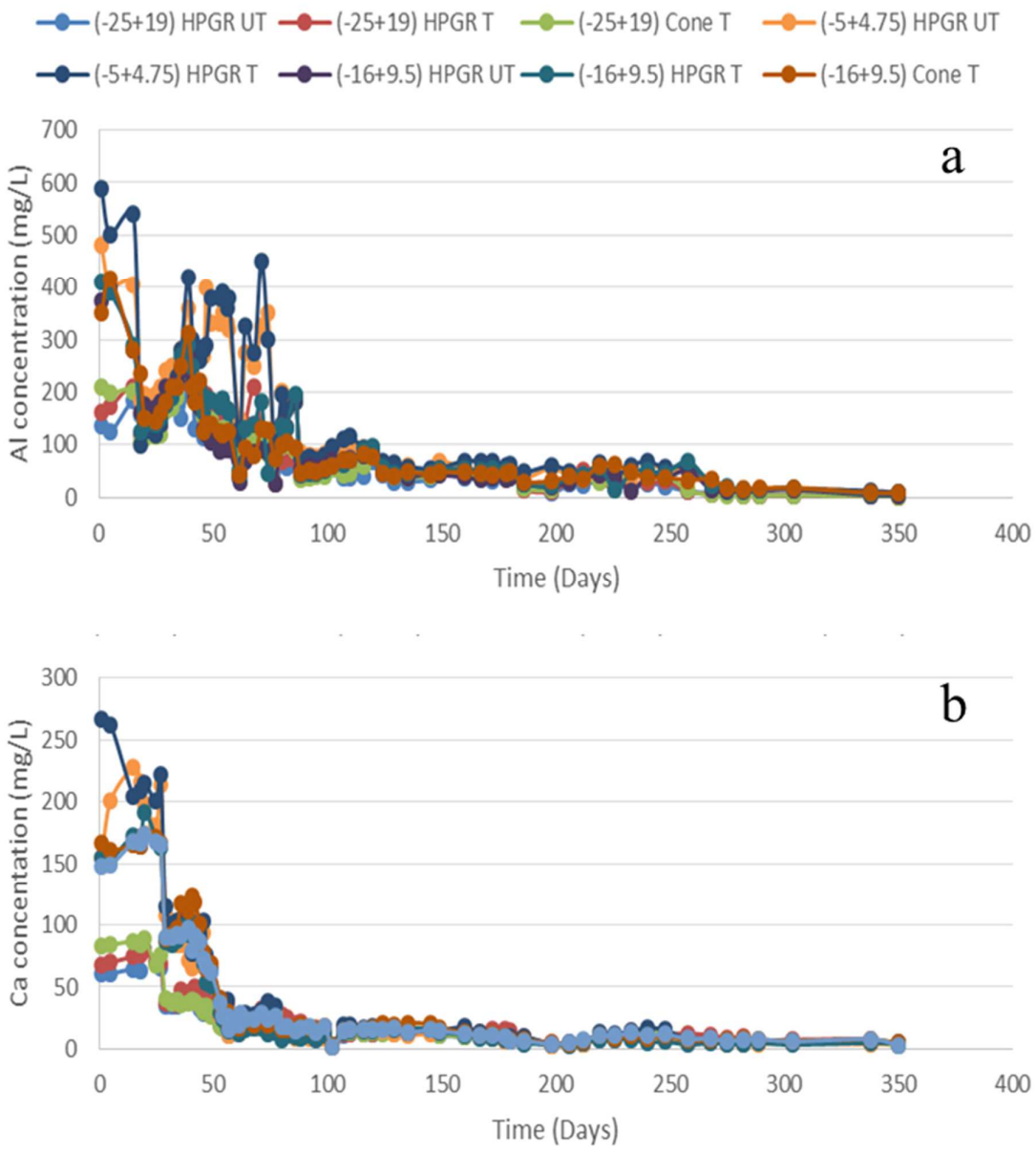

Figure 5-4: Solution concentrations of the metals from gangue minerals, a. Aluminium, b. Calcium, in the PLS from all reactors

The aluminium and calcium concentration in solution is high during the initial contact with acidic solution initially (Figure 5-4). The solution concentrations were higher in small sized fractions compared to coarser fractions. No significant aluminium and calcium was leached into solution after 50 days, suggesting no further leaching of gangue minerals. Solution concentrations of the other metals (Mn and Mg) from gangue minerals is presented in Appendix D.

5.1.3. Effect of microwave treatment on zinc extraction

To determine the effect of microwave treatment on zinc extraction, an investigation of zinc leach behaviour of microwave treated small, medium and large HPGR crushed ore against untreated ore of the same size was carried out (see Figure 5-5). The results show an overall trend of enhanced cumulative value metal recovery in microwave treated HPGR crushed ore compared to untreated ore of a similar size over 350 days.

A detailed analysis of the trend in cumulative zinc recovery of the small HPGR crushed ore shows an initial slow leaching rate in the first 50 days of leaching for both microwave treated and untreated ore. This was followed by a fast leaching rate, reaching up to 58% extraction between 50 to 200 days, followed lastly by a slower stable rate period, reaching up to 74% zinc extraction over day 200 to 350 for the untreated ore. A similar trend in cumulative zinc recovery was observed for the microwave treated ore however, the leaching rate was higher than that of the untreated ore. The fast leaching rate period was observed for slightly longer for microwave treated ore compared to untreated ore. The leaching rate for small microwave treated ore slowed down after 200 days reaching up to 93% over 350 days. Previous results have shown that leaching conditions, mode of comminution and particle size are important factors that influence leaching recovery in columns. Since the leaching conditions, mode of comminution and particle sizes of the ore in the two columns (HPGR (-5+4.75) UT), (HPGR (-5+4.75) T) are the same it can be concluded that the differences in zinc recovery observed between the columns is due to microwave treatment. For the medium and large HPGR crushed particles the microwave treated ore yielded higher cumulative zinc extraction rates than the untreated ore (Figure 5-5).

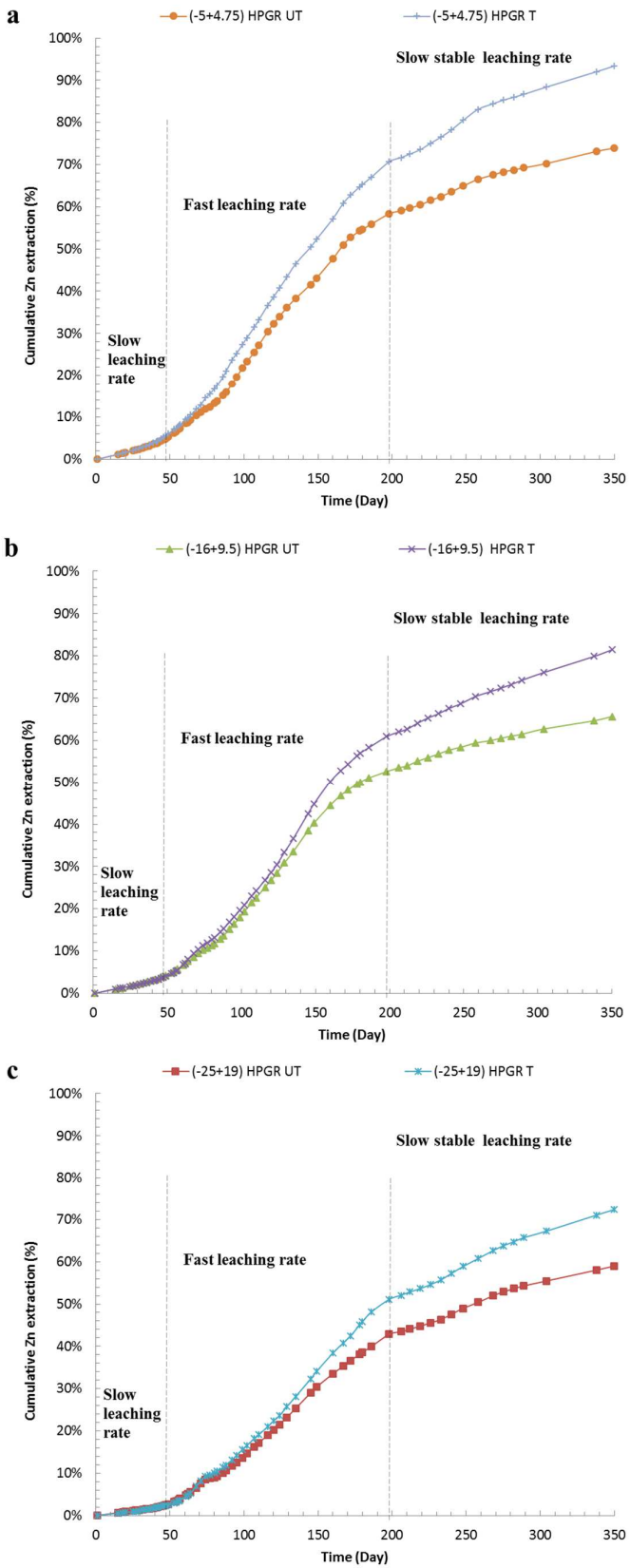

Figure 5-5: The influence of microwave pre-treatment on cumulative zinc extraction during column leaching of, (a) small, (b) medium and (c) large HPGR crushed ore particles

The enhancement in zinc yield as a result of microwave treatment for small, medium and large crushed HPGR ore is presented in Figure 5-6. For the small sized ore a positive improvement in zinc yield is observed from the onset of the leaching experiment. There is a steady increase in the degree of enhancement in zinc recovery in the first 50 days after which a slow decrease in the degree of enhancement can be seen, stabilising at around 26 % over a period of 350 days. For the coarser fractions (medium (-16+9.5) mm, and large (-25+19) mm), there is no significant increase in the degree of enhancement initially over the first 50 days. After 50 days there is a steady increase in the degree of enhancement in zinc recovery yield which reaches a value of 24% and 23% for medium and large HPGR crushed ore respectively. This trend is possibly due to the particle size effects on heap leaching recovery. Studies have shown that the overall rate of value metal recovery, when leaching from large particles is dependent on diffusion. This is because reactants must diffuse in through pores or cracks in the rock matrix of each ore particle, to reach the chemical reaction site where metal dissolution takes place (Ghorbani et al., 2011a; Petersen, 2010). After dissolution the dissolved chemical species must diffuse through the stagnant solution occupying the bed voidage in order to be recovered in the PLS (da Silva, 2004).Thus for the coarser size fractions (medium (-16+9.5) mm, and large (-25+19) mm), the benefits of microwave induced cracks are not immediately observed in the first 50 days, as large particles require longer times for reagents to penetrate and dissolved metal species to diffuse out.

The observed general trend in increased value metal recovery in microwave treated ore during column leaching is due to the presence of microwave induced cracks in the particles that result in increased surface area and enhanced value mineral exposure. The influence of microwave treatment on value metal recovery is more pronounced for the small sized particles compared to the coarser fractions. This is explained by the fact that microwave treatment was observed to result in a greater increase in crack volume for the smaller size fractions compared to the coarser medium and large fractions. However, the size effects of microwave treatment response of ores, observed in this study was a result of the microwave delivery system that was used to microwave treat ores in this study, which favoured the treatment of smaller particles, as previously mentioned in chapter 4. Mineral exposure and crack volume analysis results presented in this study show greater improvements in mineral exposure and crack volume for small (-5+4.75) mm sized fractions compared to the coarser fractions, due to greater crack damage occurring during microwave treatment. An increase in the degree of sulphide grain exposure of 28%, 26% and 15% for small, medium and large HPGR crushed ore after microwave treatment was observed (Table 5-3). Similarly an increase in crack volume of

microwave treated particles of 40% to 90% for small, medium and large particles. Modelling studies have shown that during leaching of microwave untreated ores, all minerals near the surface are depleted first before the leach front can migrate further into the particle (Ogbonna et al., 2006). Due to the presence of microwave treated crack networks, microwave treated ore has a greater exposed mineral surface compared to untreated ore, hence the improvement in the degree of value mineral recovery.

Table 5-3: Percent zinc recovery after 350 days leaching and percent sulphide grain exposure of HPGR crushed treated and untreated, sphalerite ore particles

	Particle size (mm)	Untreated	Treated
% Zn recovery	(-5+4.75)	74%	93%
	(-16+9.5)	66%	81%
	(-25+19)	59%	72%
% Mineral exposure	(-5+4.75)	38%	66%
	(-16+9.5)	28%	54%
	(-25+19)	23%	38%
% Crack volume	(-5+4.75)	0.75%	6.90%
	(-16+9.5)	0.45%	2.69%
	(-25+19)	0.35%	1.96%

The trend in enhanced zinc recovery with size for microwave treated ore suggest that the influence of microwave treatment is immediate for the small sized ore compared to the coarser sized fractions (medium and large) in the first 50 days of leaching. During the initial 50 days of leaching no significant improvements is observed in zinc leach recovery for medium and large ore compared to the small sized ore. This could be due to the rate of value mineral dissolution during column leaching being controlled either by molecular diffusion of lixiviant through a boundary layer extending into the fluid or by reaction at the particle surface. If the particle contains cracks which are open to the fluid, lixiviant diffuses into the interior of the particle and reacts there. The extent of mineral depletion in such a case is controlled by the diffusion of lixiviant in and out of the particles. The size and length of the cracks determines the diffusion distance. Thus the diffusion distance is shorter for small sized particles compared to coarser sized fractions. This would account for the observed greater degree in enhanced zinc recovery in the initial 50 days for small sized fractions compared to the coarser fractions.

A study conducted by Ghorbani et al. (2012) showed that the presence of cracks in particles, apart from providing an additional surface front of target mineral grains attack by the leaching solution, they also offer higher potential attachment sites for micro-organisms. The attached micro-organisms are responsible for regeneration of ferrous to ferric ion as leach reagent closer to the mineral surface and increase metal recovery during bio-leaching. Investigations carried out to characterise cracks in microwave treated and untreated particles suggest the presence of high density microwave induced cracks in HPGR particles with greater grain boundary fracture present in the small HPGR particles compared to coarser particles. Thus microwave treated ore has greater potential sites for microorganism attachment compared to the untreated ore. This explains the observed results which show increased zinc recovery for microwave treated ore compared to untreated.

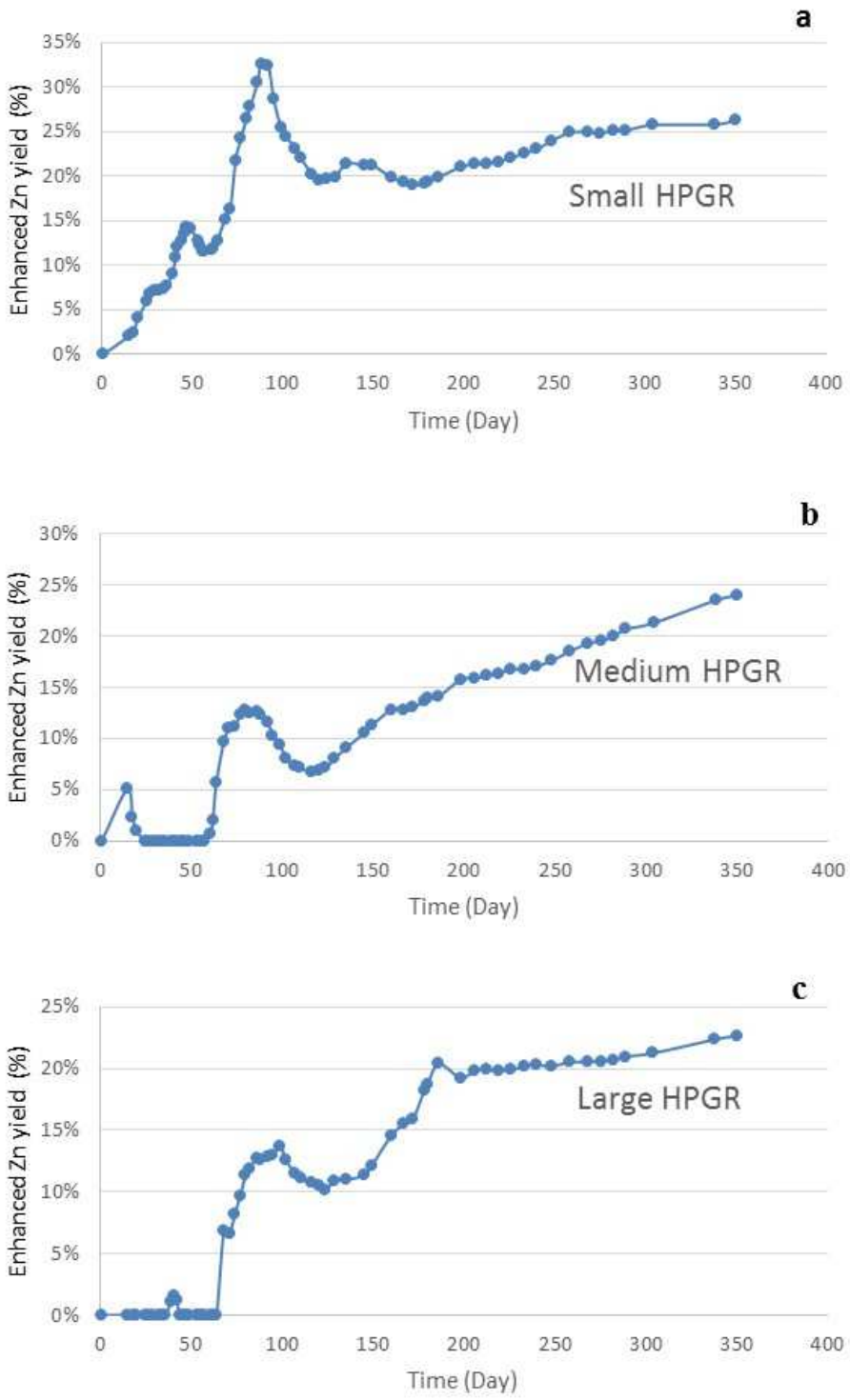

Figure 5-6: The enhancement of the zinc yield due to microwave pre-treatment over untreated ore particles is shown for a) small, (b) medium and (c) large HPGR crushed ore particles

The observed trend in overall zinc column leach recovery results are in correspondence with crack volume and mineral exposure analysis results (Table 5-3). Table 5-3 shows a comparison of zinc recovery with mineral exposure and crack volume of HPGR crushed ore in the leaching reactors. Previous studies have shown that as particle size decreases the amount of surface area exposed for value mineral recovery increases (Kodali et al., 2011; Lottering et al., 2008; Lundgren and Silver, 1980). The process of size reduction leads to micro-cracks in the ore particles. This study has shown that microwave treatment has the potential to increase the extent of crack damage in ore particles. Mineral exposure analysis of the microwave treated particles also shows that the amount of exposed mineral grains increases correlates with decreasing particle size (Table 5-3). The degree of improved mineral exposure correlates with measured increase in crack volume after microwave treatment. These results demonstrate that microwave induced cracks result in sphalerite mineral grains becoming more accessible to the leach solution and leads to an increase in leaching kinetics.

Leaching results of microwave treated ore suggest that higher metal recovery is achievable at coarser sizes compared to microwave untreated ore. For example the overall zinc leach yield for large HPGR microwave treated particle was 72% and that of small HPGR untreated particle was 74%. Thus comparable metal recovery to small HPGR crushed ore was achieved by microwave treating large particles. The zinc leaching extraction yield results of medium sized HPGR microwave treated ore is higher than that of small sized HPGR untreated ore. The increase in the zinc recovery at coarser sizes observed in this study has significant implications on the economics of heap leaching operations, which are normally characterised by low recoveries at coarse particle sizes.

5.1.4. Comparison of recovery in microwave treated HPGR and cone crushed particles

A comparison of zinc recovery in leach solution of microwave treated ore as a function of particle size and mode of comminution was carried out (Figure 5-7). Figure 5-7 compares the zinc extraction rates over 350 days of leaching from microwave treated medium and large ore crushed by HPGR and cone crushers. The results show that zinc recovery increases with reducing size for all modes of comminution, this is due to an increase in mineral exposure and surface area with decreasing size. These results follows the expected trend in particle size relationship with metal recovery from literature. For example the overall zinc recovery of medium and large microwave treated cone crushed products was 78.8 % and 66.6% respectively.

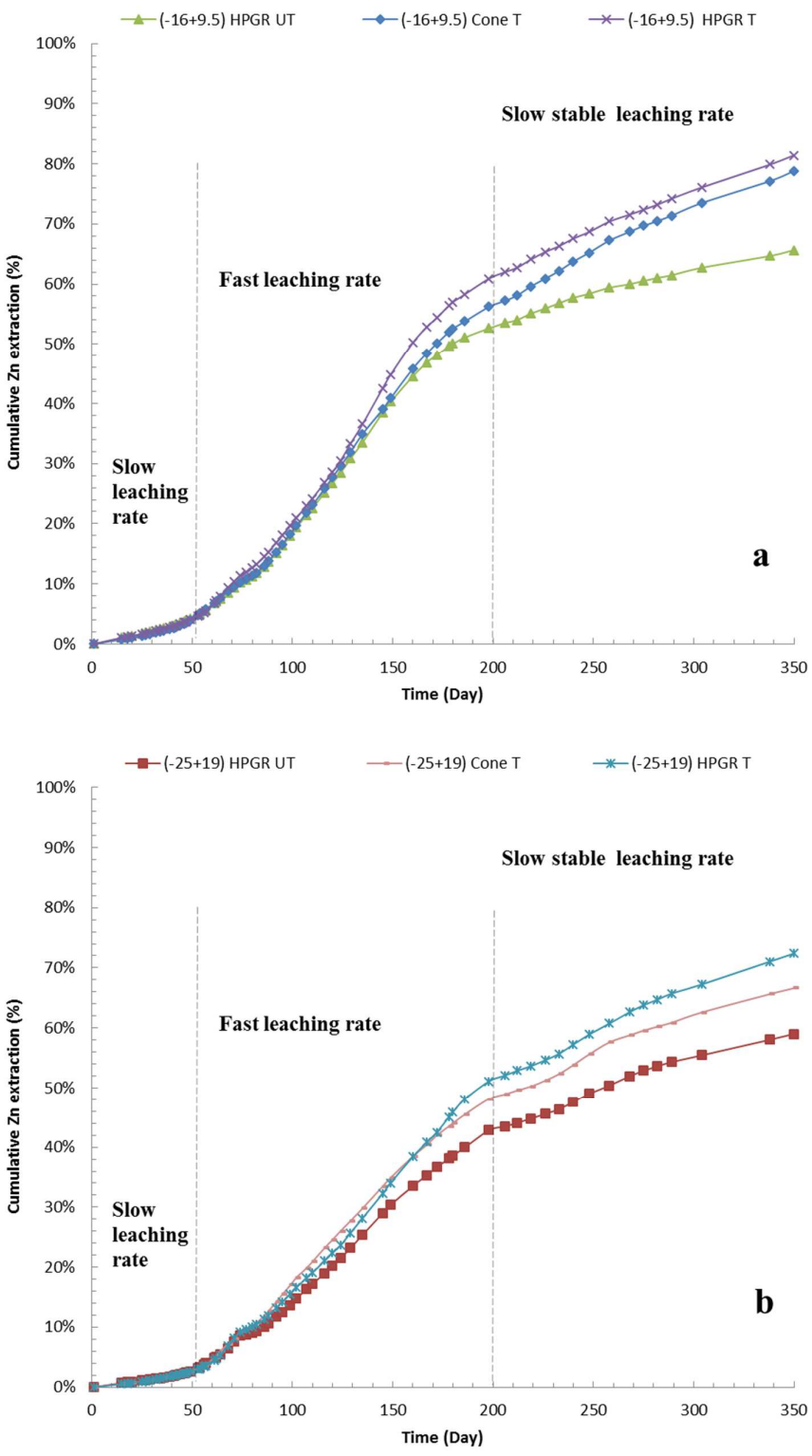

Figure 5-7: Comparison of the influence of microwave pre-treatment on cumulative zinc extraction during column leaching of, (a) medium and (b) large HPGR and cone crushed ore particles

Results from the column experiments show that metal recovery of microwave treated HPGR crushed products is higher than recovery from cone crushed products at all sizes (see Figure 5-7 and Figure 5-8). For example there was a difference of 2.2% and 5.4 % between the overall zinc recovery of medium and large cone crushed microwave treated products and microwave treated HPGR products (Table 5-4). When recovery from microwave treated cone crushed products is compared against that of untreated HPGR crushed products, the microwave treated cone crushed product had a higher metal recovery (Figure 5-8 and Table 5-4). Previous studies have shown that the leachability of products prepared using HPGR is higher when compared to those prepared using conventional crushers (Ghorbani et al., 2012; Kodali et al., 2011). A previous study by Ghorbani et.al (2012) investigating the effects of mode of comminution on leaching recovery of the ore used in this study observed that, metal recovery from cone crushed ore was lower, when compared against recoveries from HPGR crushed ore particles of the same size (see Table 5-4). Results of this study show a variation in this trend after microwave treatment, with microwave treated cone crushed ore having recoveries that are greater than microwave untreated HPGR ore of the same size. This suggest that the presence of microwave induced cracks in cone crushed ore has the effect of increasing metal recovery in cone crushed particles to values higher than those obtained for untreated HPGR crushed particles. For example there was a difference of 13.1 % and 7.6 % between overall zinc recovery of medium and large cone crushed microwave treated products and untreated HPGR medium and large products (see Table 5-4).

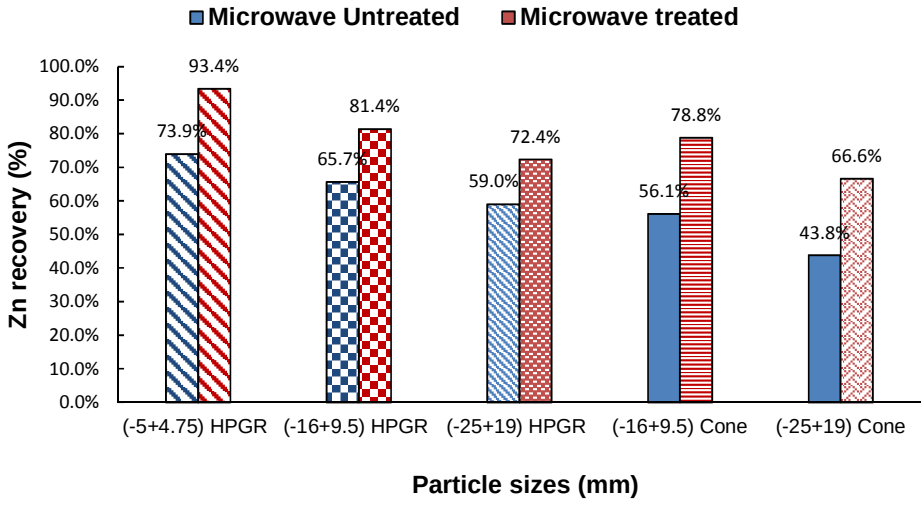

Figure 5-8: Overall zinc recovery from microwave treated and untreated sphalerite ore samples for different HPGR and cone crushed particles. Zinc recovery values for microwave untreated cone crushed medium and large particles adapted from Ghorbani et al. (2012) are shown in solid bars.

Table 5-4: Comparison of overall zinc recovery from microwave treated and untreated sphalerite ore samples for different HPGR and cone crushed particles obtained in this study with, zinc recovery values for microwave untreated particles obtained from a study by Ghorbani et al. (2012).

Particle size (mm)	Microwave untreated	Microwave treated	Ghorbani et al. (2012)
(-5+4.75) mm HPGR	74.0%	93.0%	79.4%
(-16+9.5) mm HPGR	66.0%	81.0%	68.7%
(-25+19) mm HPGR	59.0%	72.0%	59.1%
(-16+9.5) mm Cone	nm	78.8%	56.1%
(-25+19) mm Cone	nm	66.6%	43.8%

Since only eight reactors were available for the experiment, the leaching response of untreated cone crushed ore was not investigated in this study. In order to quantify the enhancement in zinc extraction due to microwave treatment of cone crushed ore, column leaching results of untreated cone crushed medium and large ore from a previous study carried out on the same ore over 11 months of leaching under the same conditions as those applied in this study, was used as a comparison (see Table 5-4) (Ghorbani et al., 2012). As expected, the overall zinc recovery of microwave treated product was higher than that of the untreated cone crushed ore. It is possible that the observed difference in recovery might be due to differences in experimental conditions however, comparison of microwave treated cone crushed ore against HPGR untreated ore offers definitive evidence of enhanced zinc recovery in microwave treated cone crushed products.

The observed increase in zinc recovery of cone crushed products after microwave treatment when compared against untreated HPGR crushed product is due to greater crack density in treated ore compared to untreated. Microwave induced cracks increase the surface area of exposed value mineral grains per unit mass of ore particles exposed to lixiviant and this results in improved mass transfer and enhanced hence leaching recovery. The amount of cracks induced is a function of particle size ore texture and mineralogy and is independent of the mode of comminution of the treated particles as has been shown is this study.

5.2.Leach progression in single ore particles

This section presents results on investigations carried out on individual particles to understand the progression of leaching in microwave treated particles using XCT and QEMSCAN analysis techniques.

5.2.1. Dissolution of sulphide grains during leaching

XCT analysis was used to quantify the effect of microwave induced cracks on high density sulphide phase dissolution in individual HPGR crushed particles. From time to time the column leaching experiments were stopped to carry out XCT analysis on selected tagged particles from each column. Table 5-5 is a summary of the tagged particles that were monitored during the column leaching experiments. These tagged particles were monitored to allow for the investigation of high density phase dissolution kinetics in individual microwave treated and untreated particles. XCT scans of individual tagged samples were carried out on days 1, 40, 140, 200, 300 and 350. The volume of the sulphide grains and cracks in each individual particle was quantified using a combination of threshholding, segmentation and connected component analysis techniques. Due to the limited number of particles that were analysed in each column, the trends in high density phase dissolution measured for each individual ore particle may not be statistically representative of the overall column leaching recovery trends presented in Figure 5-5 and Figure 5-7.

Table 5-5: Tagged particles monitored during leaching using XCT analysis

Reactor	Crusher condition	Number of tagged particles
Reactor 2	(-5+4.75) HPGR Untreated	4
Reactor 5	(-5+4.75) HPGR Treated	4
Reactor 3	(-16+9.5) HPGR Untreated	3
Reactor 6	(-16+9.5) HPGR Treated	3
Reactor 1	(-25+19) HPGR Untreated	2
Reactor 8	(-25+19) HPGR Treated	2

To characterise the effect of microwave induced cracks on high density sulphide phase dissolution in microwave treated and untreated HPGR crushed particles, high density mineral grains were classified and their dissolution tracked during the leaching period. Dissolved grains were identified by comparing XCT images of high density grains at leaching periods of 1, 40, 140, 200, 300 and 350 days respectively. Image registration techniques were applied to align the images in 3D of the leached particles during the different leaching periods. The sulphide grains and the cracks in the particles were segmented from the low density gangue phase. Figure 5-9 shows the measured high density phase dissolution against time for individual tagged HPGR microwave treated and untreated particles. The 3D views of the particle, high density phase and cracks within the particle during different leaching periods for small medium

and large microwave treated particles are shown in Figure 5-10, Figure 5-11 and Figure 5-12. Different mineral phases inside the particles are clearly distinguishable in the 2D image slices.

The XCT measured average sulphide phase dissolution in single individual ore particles shows evidence of sulphide grain dissolution over 350 days of leaching (Figure 5-9). XCT images of the sulphide grains suggest that as time proceeds, exposed grains have a higher percent of volume reduction, compared to locked grains (Figure 5-10, Figure 5-11 and Figure 5-12). These exposed grains consist of grains at the surface of the particle and grains that lay along the microwave induced cracks. The sulphide grain dissolution results show improved dissolution rate in microwave treated particles compared to the untreated particles at all sizes (Figure 5-9). The rate of dissolution of the high density sulphide grains for small, medium and large microwave treated HPGR crushed particles after 350 days of leaching was about 74%, 57% and 52% respectively (Figure 5-9). For the microwave untreated HPGR crushed particles the dissolution rate of high density sulphide grains was 54%, 48% and 38% respectively over 350 days (Figure 5-9).

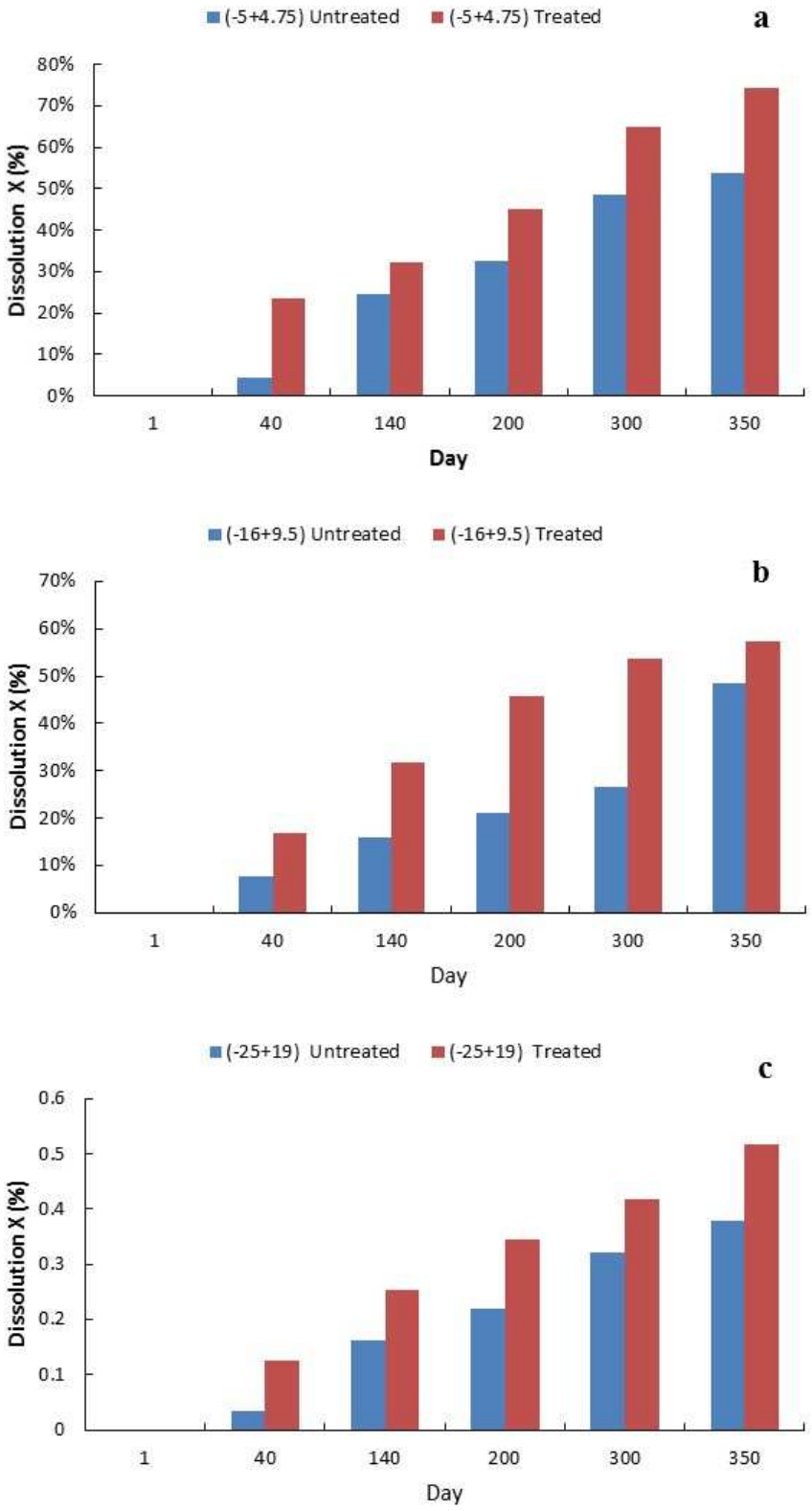

Figure 5-9: XCT measure average sulphide dissolution in single individual microwave treated and untreated ore particles over 350 days of leaching (a) small, (b) medium and (c) large particle

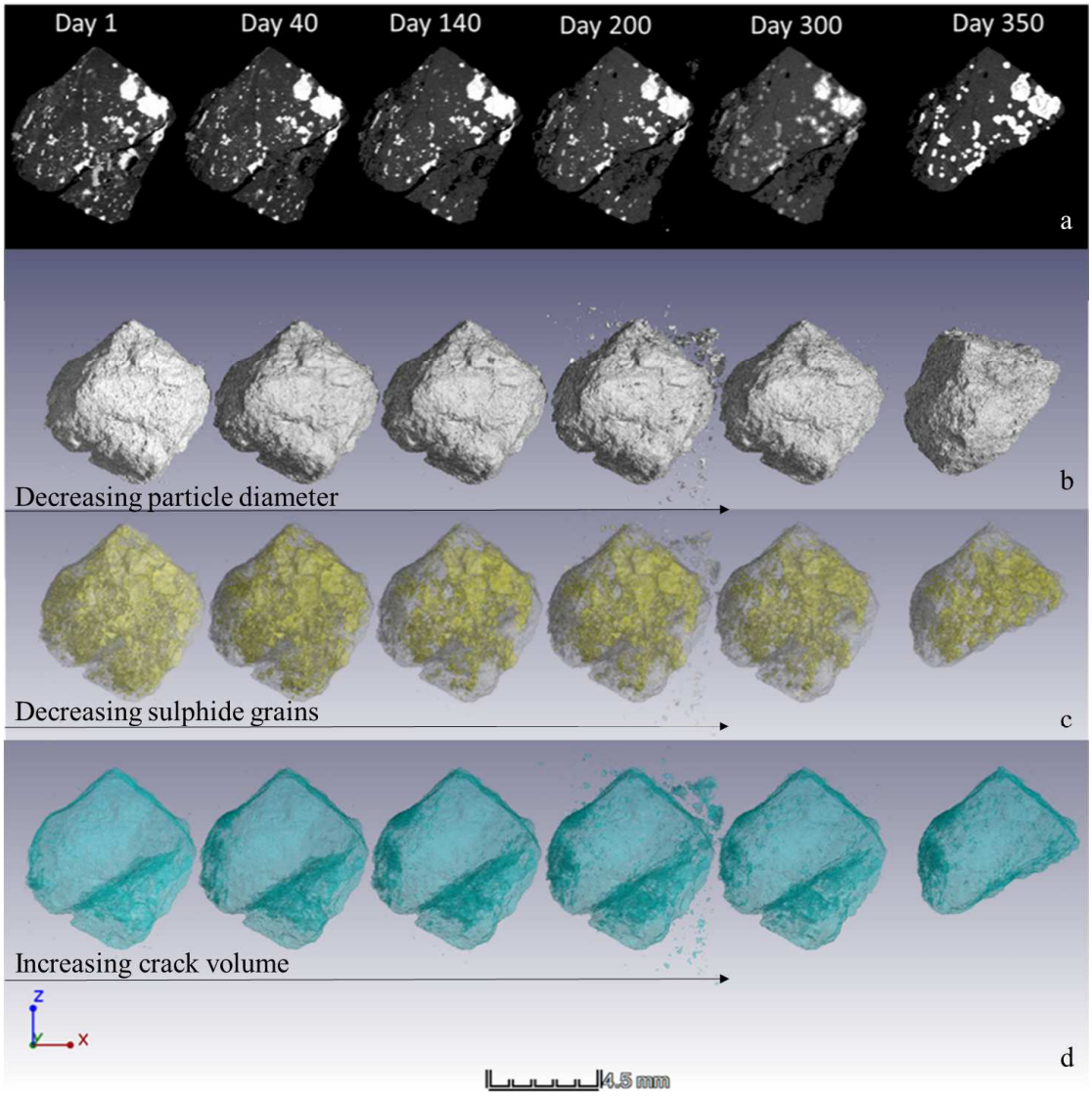

Figure 5-10: XCT generated story body of a HPGR crushed microwave treated small sized particle showing the variation in particle volume, sulphide grains and cracks in an individual particle over the course of bio-leaching. (a) XCT 2D slice image of the particle, (b) 3D projection of particle, (c) 3D projection of sulphide phase (shown yellow) in the particle, (d) 3D projection of cracks in the particle (shown in blue)

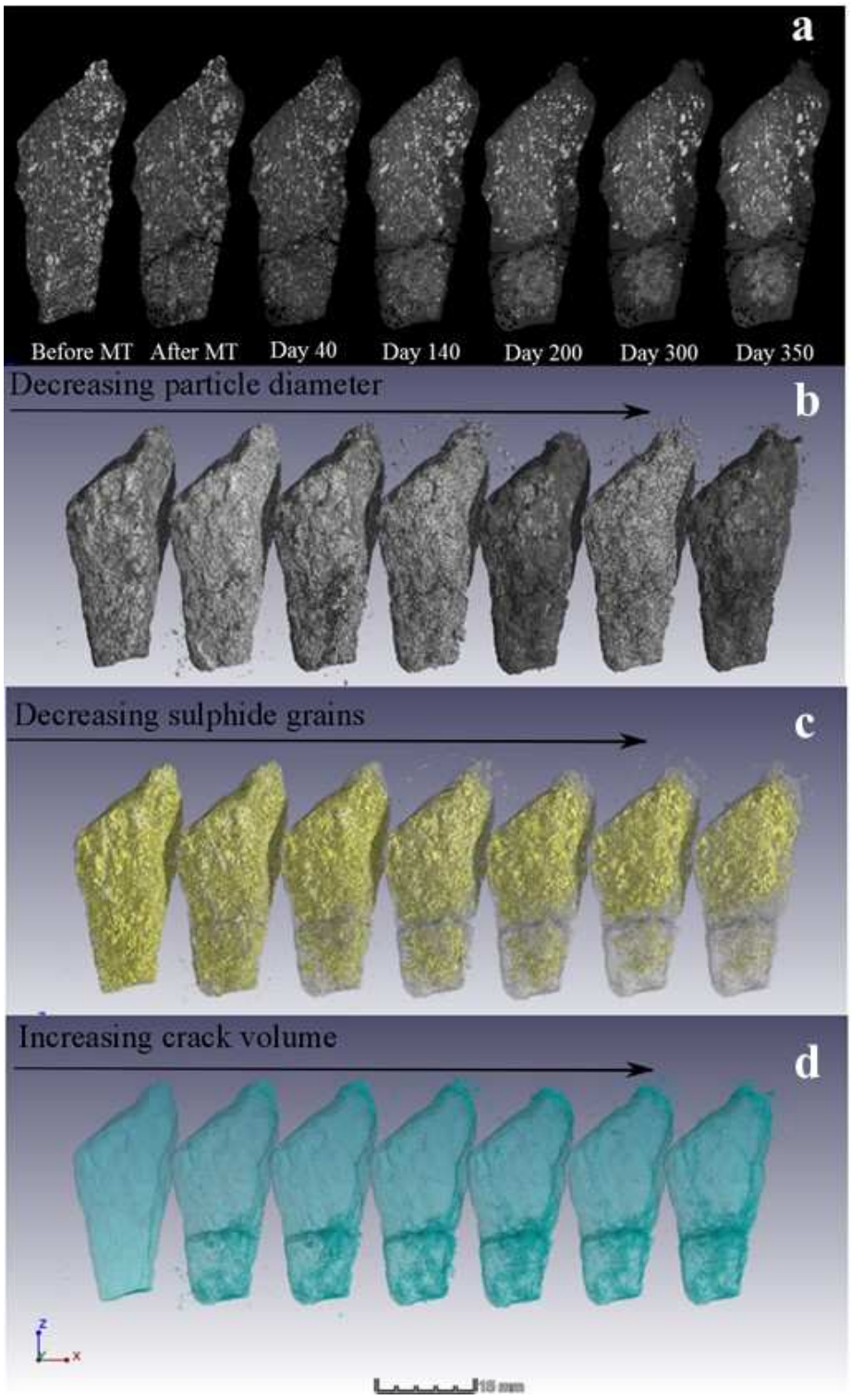

Figure 5-11: XCT generated story body of a HPGR crushed microwave treated medium sized particle showing the variation in particle volume, sulphide grains and cracks in an individual particle over the course of bio-leaching (a) XCT 2D slice image of the particle, (b) 3D projection of particle, (c) 3D projection of sulphide phase (shown yellow) in the particle, (d) 3D projection of cracks in the particle (shown in blue).

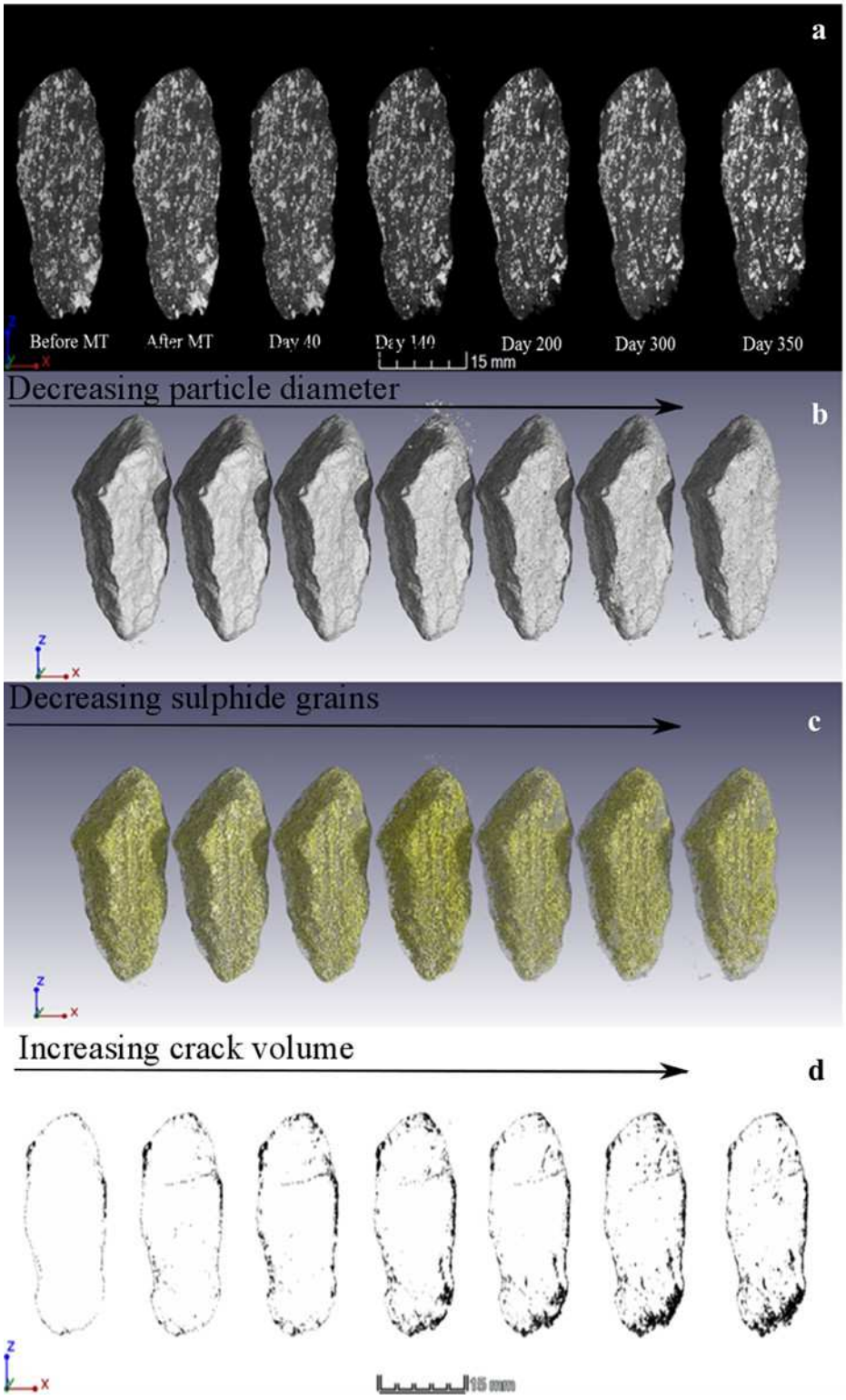

Figure 5-12: XCT generated story body of a HPGR crushed microwave treated large sized particle showing the variation in particle volume, sulphide grains and cracks in an individual particle over the course of bio-leaching. (a) XCT 2D slice image of the particle, (b) 3D projection of particle, (c) 3D projection of sulphide phase (shown yellow) in the particle, (d) 3D projection of cracks in the particle (shown in blue).

Figure 5-13 shows XCT measured changes in particle crack volume in individual particles over 350 days of leaching. Figure 5-14 presents the QEMSCAN measured changes in crack volume of particle before and after leaching, because QEMSCAN analysis is carried out on polished sections, the residue samples analysed after leaching are not the same as those analysed before leaching. Microwave treatment has the effect of increasing the volume of micro-cracks in individual particles before leaching, this has a positive effect on the rate of dissolution of value mineral as shown in Figure 5-13 and Figure 5-14. Microwave induced cracks increase the solid/liquid contact area which is a major factor in determining the kinetics of value mineral dissolution. Value minerals are typically present as small grains contained in a matrix of gangue material. During leaching the process of transporting reactants and reaction products to and from reaction sites within the particle is important. This process is diffusion governed, and is limited by the size of the particle and the density of micro-cracks in the ore particle, the diffusion gradient, and the diffusivity of the species (Bartlett, 1992; Petersen, 2010).

There is a readily leachable fraction of Zn in each individual ore particle, which is accessible through the crack network and a poorly leachable fraction, which is locked within zones that are not cracked. The fraction of locked grains is greater for larger particles compared to small particles. The first stage of leaching, involves leaching of grains at the surface of the ore particles followed by a second stage, which is leaching of the grains located in the subsurface within the thickness of the penetration depth. Microwave induced cracks result in an increase in penetration depth and hence recovery. Microwave treated particles in all size fractions have a higher specific surface area (per unit mass of particles) and relatively greater penetration depth, resulting in the dissolution of a larger number of grains during the first stage of leaching.

Internal grains beneath the particle surface can be dissolved only when these grains are directly exposed to the action of the leaching solution at the particle surface. Thus cracks offer a pathway for leaching solution to access internal cracks. Individual particle dissolution kinetics consistently show that microwave treated particles have a greater crack network compared to untreated particles. This supports the previous findings that showed greater value mineral recovery in microwave treated particles compare to untreated. There is an increase in crack volume with time at all particle sizes (small (-5+4.75) mm, medium (-16+9.5) mm, and large (-25+19) mm) for both microwave treated and untreated particles (Figure 5-13). This supports results from previous studies that reported an increase in the crack network of individual HPGR crushed ore particles during the leaching process (Ghorbani et.al, 2013).

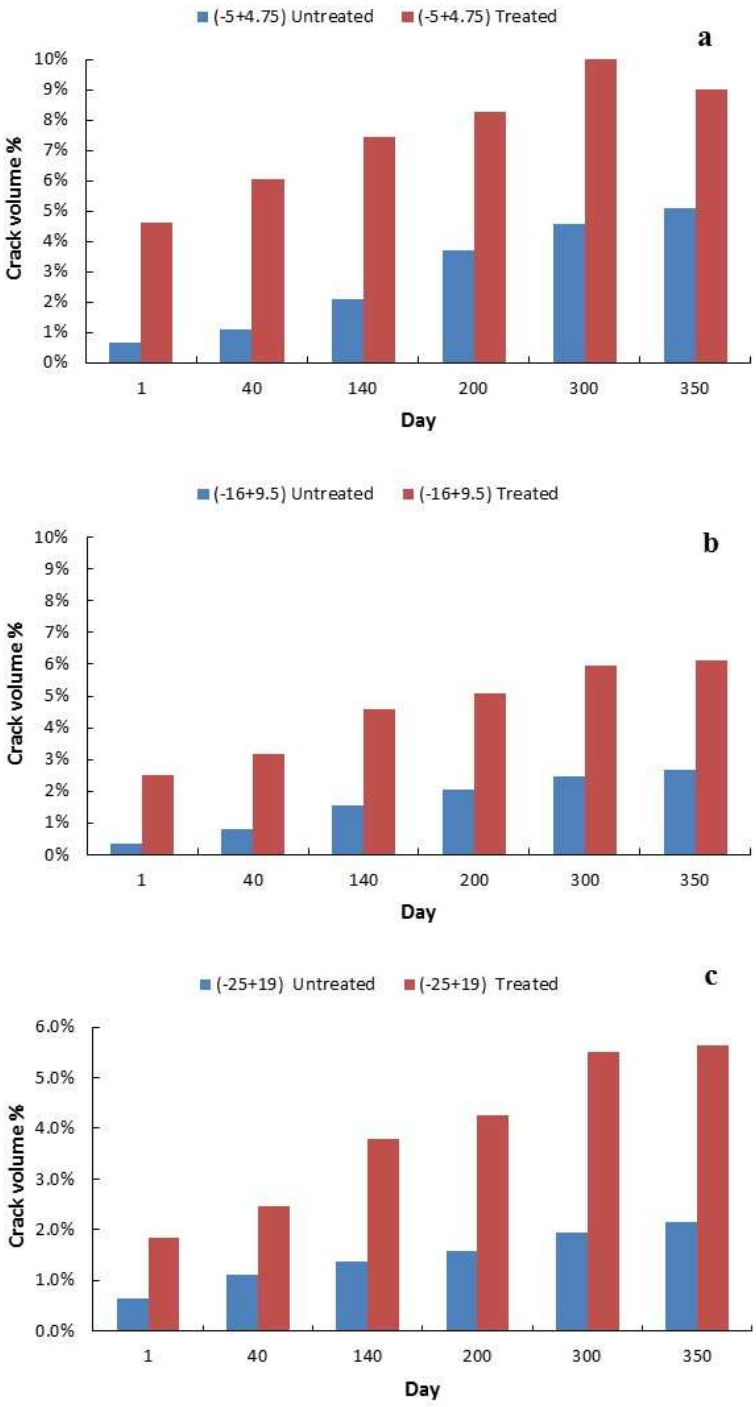

Figure 5-13: XCT measure average crack volume variation in single individual HPGR crushed microwave treated and untreated ore particles over 350 days of leaching (a) small, (b) medium and (c) large particle

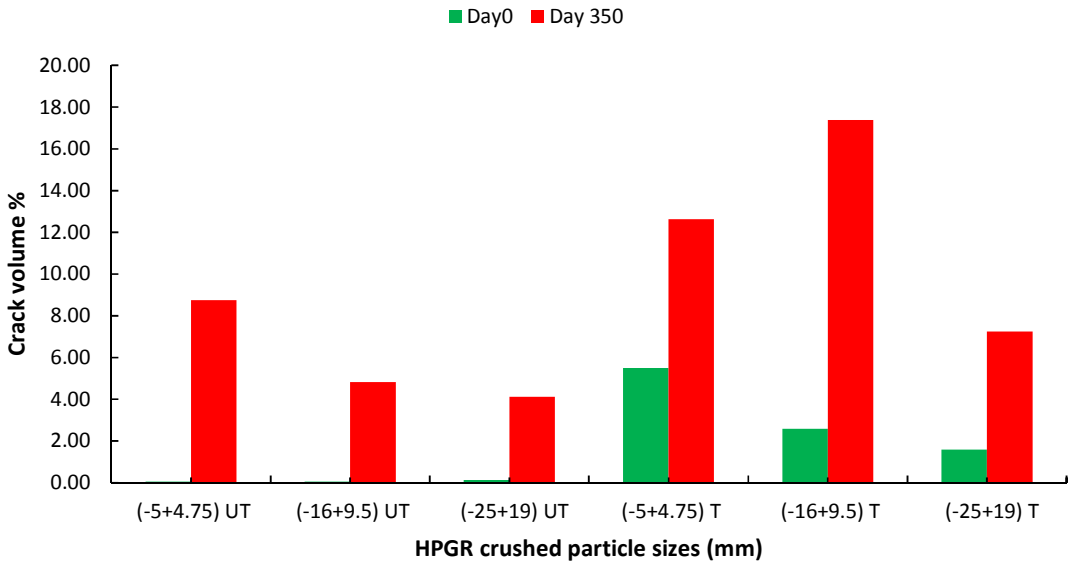

Figure 5-14: QEMSCAN measured crack volume in microwave treated (T) and untreated (UT) HPGR crushed particles measured for samples before and (after 350 days of leaching

5.2.2. Characterising leaching reaction front in single particles

The comparison tool in VGStudio Max image analysis software for determining changes in object structure over time was used to compare the voxel data sets of the particle before leaching with voxel data sets of the particle at different leaching periods (day 40, 140, 200, 300 and 350). This was done in order to investigate the loss of surface area during leaching at an individual particle level and to identify the role of microwave induced cracks in this process. The voxel data set of the particle before leaching was used as the reference data set. Thus voxel data sets of the particle at different leaching periods were examined against the reference data. The differences between the reference voxel data set and data sets at particular leaching periods were highlighted by a false colour image map indicating variance. Where the surface of the reference data set was below the surface of the data set under examination the variance between the two surfaces was positive. A negative variance indicated that the surface of the reference object was above the surface of the data set under examination. Where both surfaces matched the variance was zero. Each data set of the particle at a particular leaching period was analysed against the reference data set and colour coded according to its deviation from the reference data set. 3D images of the critical areas that were generated for different particles sizes are shown in Figure 5-15, Figure 5-16 and Figure 5-17.

Analysis of the 3D colour coded variation maps of microwave treated and untreated particles during the leaching period shows surfaces changes in the individual particle structure. This variation is due to the depletion of minerals in the particle during leaching. Most of the reaction during leaching occurs on the surface where the value mineral grains are exposed to lixiviant. Thus there is a progressive loss of material at the surface of the particle as leaching progresses as shown by the decrease in particle volume over the 350 days of leaching. This is highlighted by the negative variation observed in the 3D images on the surface of the particle. The results suggest that the minerals near the surface are depleted first before the leach front can migrate further into the particle.

Since the rate of reaction of a particle during leaching is controlled either by molecular diffusion through a boundary layer extending into the fluid or by the reaction at the surface. Cracks play an important role in aiding the diffusion of lixiviant deep into the interior of the particle. The microwave treated particles in this study, have high density crack networks which play a role in value mineral dissolution by allowing lixiviant flow to penetrate internal grains resulting in mineral depletion deep within the particle. As indicated by the negative variance in the 3D colour images of the leaching story body of microwave treated particles shown in Figure 5-15, Figure 5-16 and Figure 5-17. As the leaching progresses there are some changes to the shape of the particle due to mineral depletion and fragmentation. Thus some points of positive variance are observed as the shape of the particle begins to transform over the leaching period resulting in the surface of the reference data set being below the surface of the data set under examination.

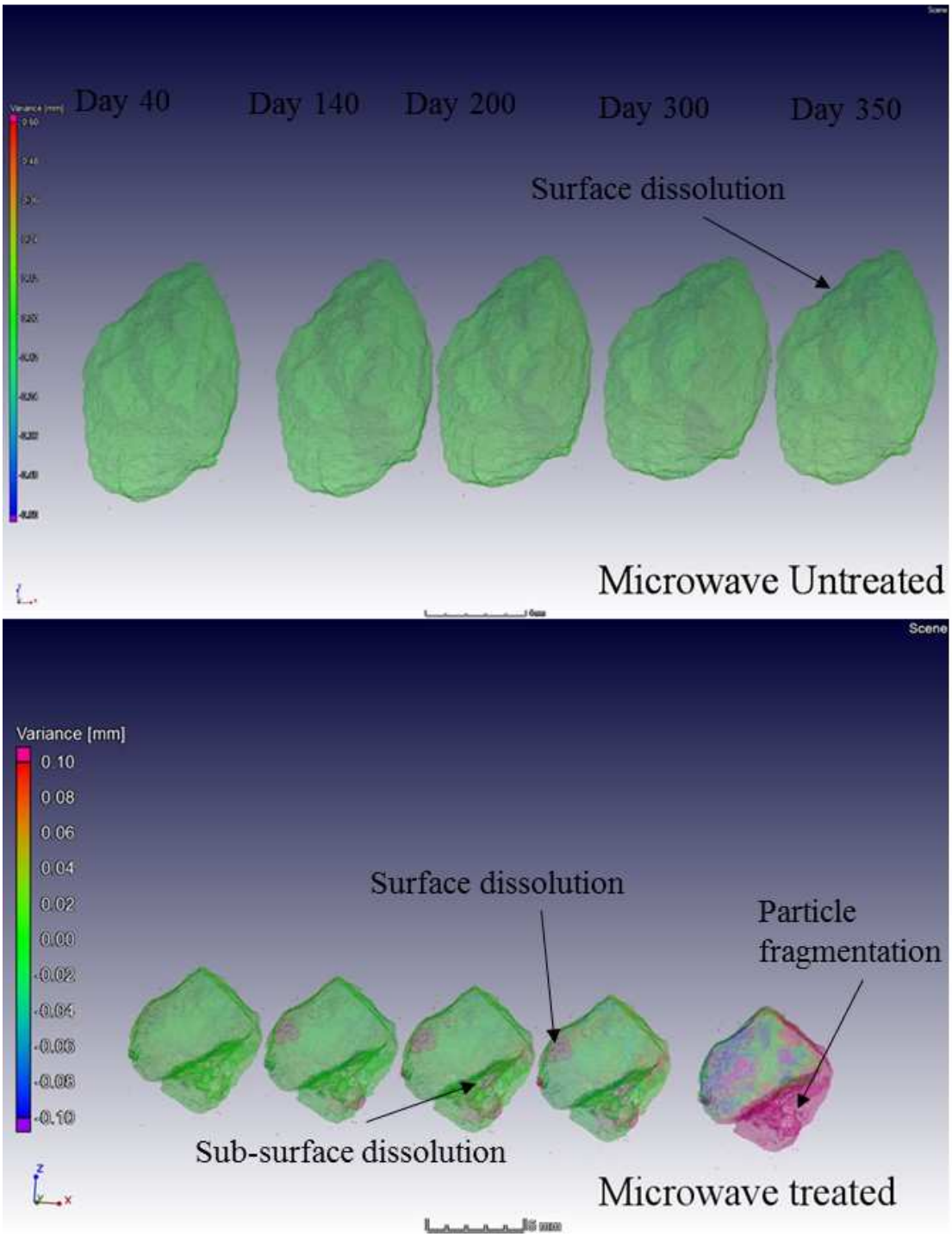

Figure 5-15: 3D colour coded variation maps of microwave treated and untreated small HPGR crushed particle over 350 days of leaching

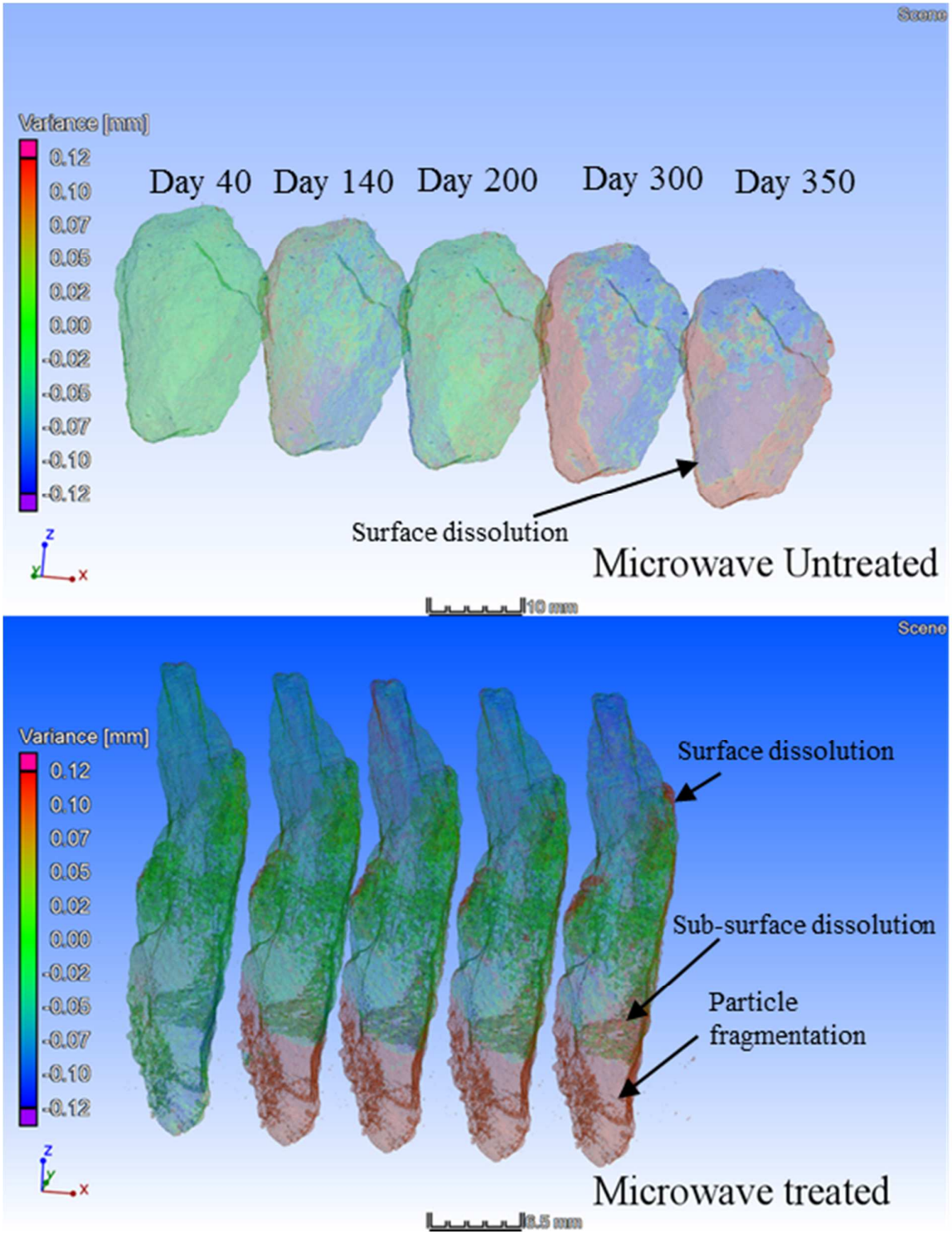

Figure 5-16: 3D colour coded variation maps of microwave treated and untreated medium HPGR crushed particle over 350 days of leaching showing areas of mineral dissolution over 350 days of leaching

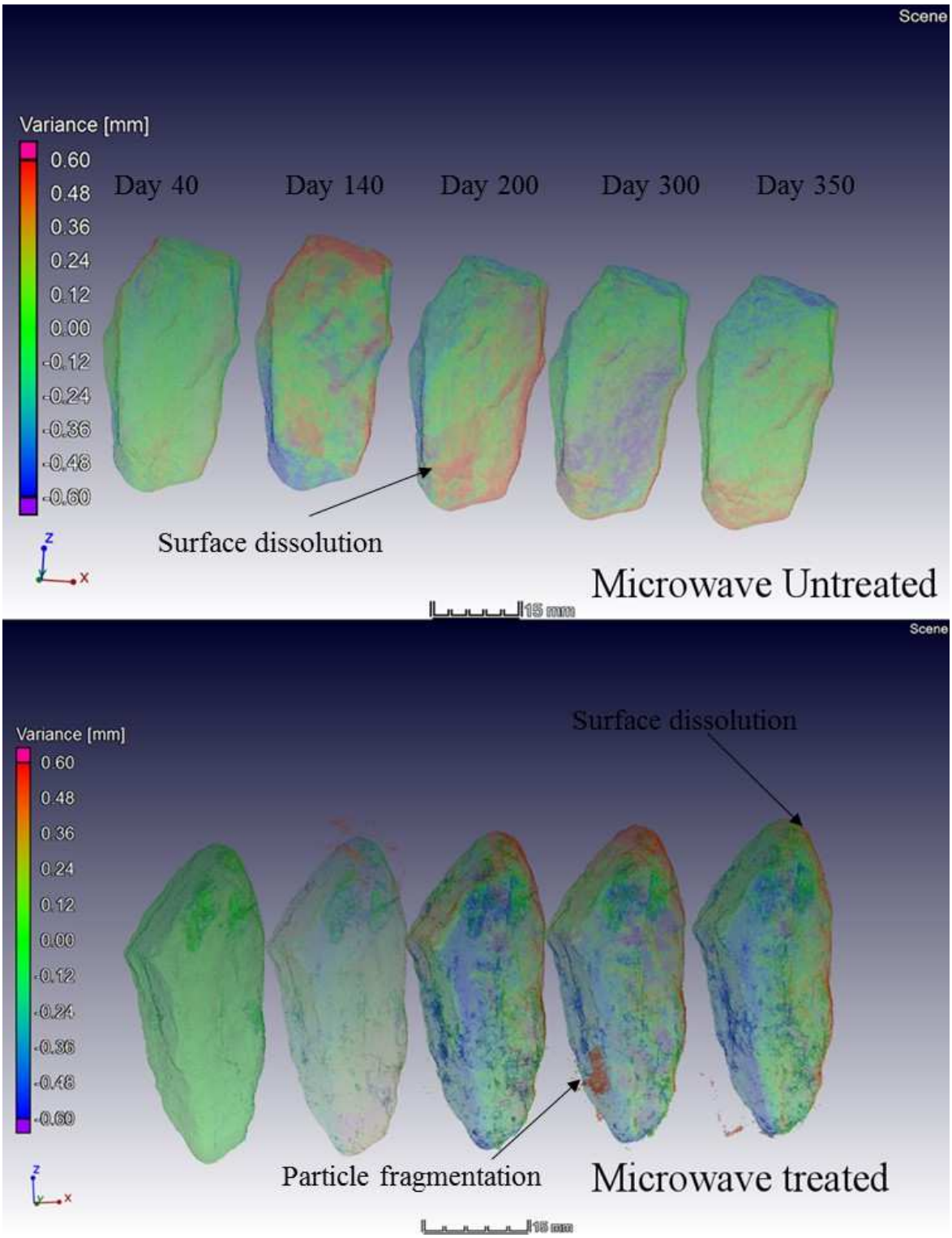

Figure 5-17: 3D colour coded variation maps of microwave treated and untreated large HPGR crushed particle over 350 days of leaching

5.2.3. Characterisation of leach reactor residue

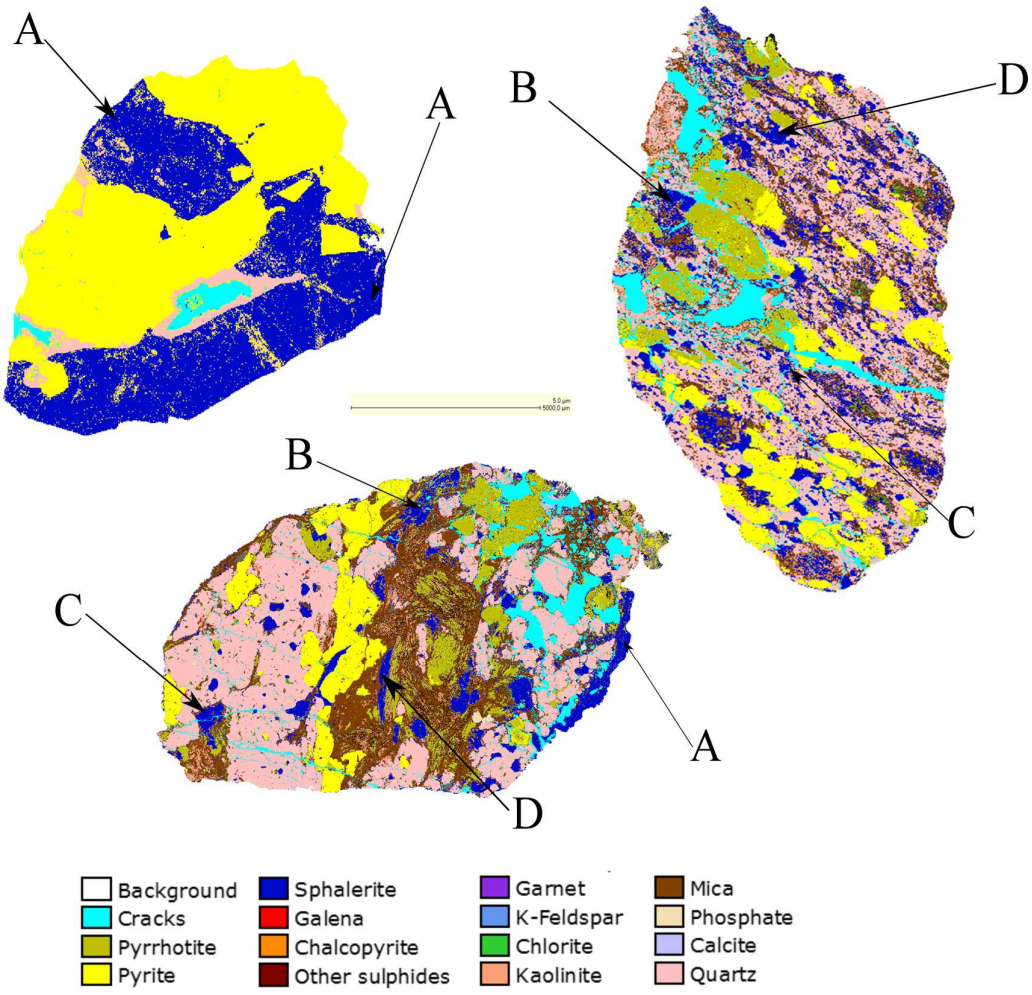

Figure 5-18: QEMSCAN images of three ore particles illustrating four main classes of sphalerite grain distribution in relation to possible exposure to lixiviant, labels A,B,C,D show different types of grain location in the ore particles in relation to exposure to lixiviant.

QEMSCAN analysis of selected samples of ore residue from the reactors was carried out to determine mineral associations as well as to identify regions containing unreacted sphalerite after leaching for both microwave treated and untreated ore. The location of sphalerite grains in the particles in relation to exposure to lixiviant can be classified under the following four main categories (Figure 5-18);

a. Grains located at the surface of the particles and exposed to the leach solution (e.g. grain marked A)
b. Grains located close to the surface of particles which become exposed to the leach solution after surface grains have been depleted (e.g. grain marked B)

c. Internal grains exposed to the surface by the cracks and hence lixiviant (e.g. grain marked C)
d. Internal grains not exposed to the surface of the particle (e.g. grain marked D)

Based on the above grain classification it is expected that most sphalerite grains in regions exposed to lixiviant will react and undergo dissolution after 350 days of leaching. An analysis of the QEMSCAN images of microwave treated and untreated ore residue shows the depletion of readily accessible grains on the particle surface compared to inaccessible grains within the particles (Figure 5-19 and Figure 5-20). Additional QEMSCAN and SEM images of leached residue are presented in Appendix E. QEMSCAN mineral association analysis shows a decrease in the association of sphalerite with cracks in Figure 5-21 and a decrease in sphalerite grains associated with the background in Figure 5-22 (surface exposed grains) during the course of the leaching experiment. This further shows that minerals near the surface are readily depleted followed by sphalerite grains that are exposed to lixiviant by cracks. Although some regions exposed to lixiviant through cracks remained unreacted. A previous study by Ghorbani et al. (2012) showed that accessibility of grains to lixiviant is not the only important factor that influence metal recovery rates.

Other factors such as target mineral composition precipitation and diffusion path are also important rate limiting factors. The formation of passivating layers on the sphalerite surface by substances such as elemental sulphur and iron hydroxide precipitates, particularly jarosites or intermediate polysulphides has been shown to limit the extraction of value minerals during bio-leaching (Ahmadi et al., 2010; Watling, 2006). In particular the precipitation of iron hydroxide and jarosite phases in bio-leaching may suppress value metal solubilisation by preventing contact between the leaching agent and the mineral. The formation of ferric hydroxide during bio-leaching depends on pH and solution redox potential (Li et al., 2013). For example at neutral pH in the presence of oxygen, ferric ions form highly insoluble precipitates (e.g., jarosite), causing a decrease in ferric ion concentration. SEM images of selected samples were taken to investigate the surface morphology of the particles and to identify formation of precipitates on the surface of the particles. Analysis of the images showed that jarosite precipitation was minor and insufficient to prevent the dissolution of the sphalerite in this study. This was due to the relatively low pH that was maintained over the 350 days of leaching. The main role of maintaining low pH was to prevent hydrolysis of ferric ions.

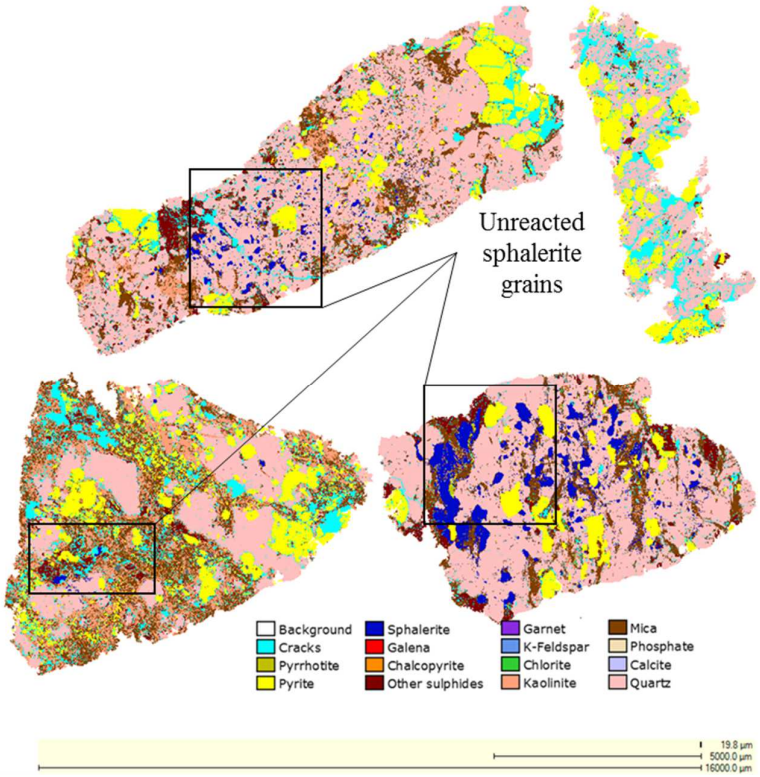

Figure 5-19: Unreacted sphalerite grains in microwave untreated small HPGR leach residue after 350 days of leaching

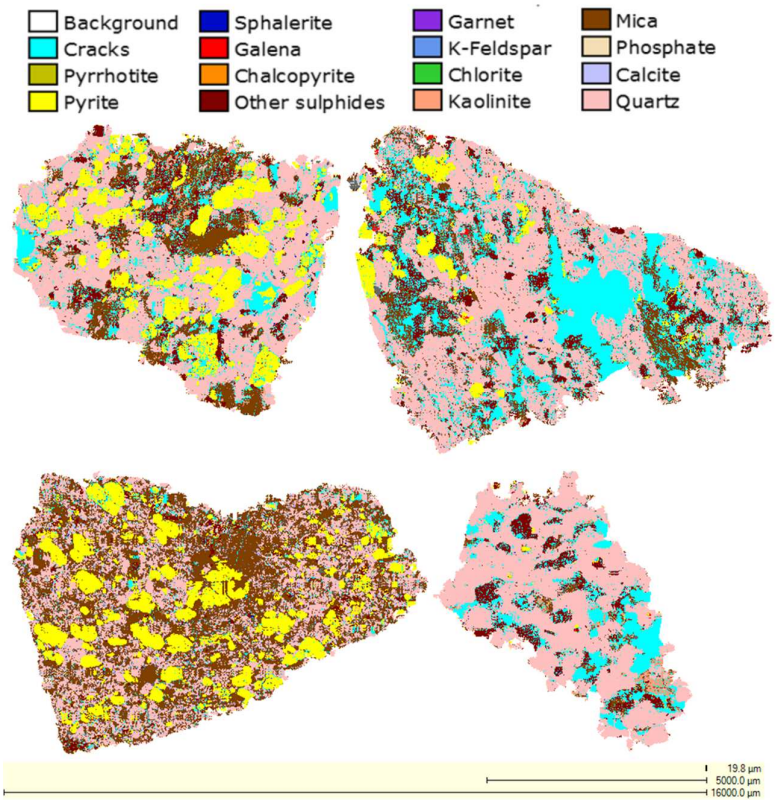

Figure 5-20: Leach residue of microwave treated small HPGR crushed particles, showing almost complete sphalerite depletion

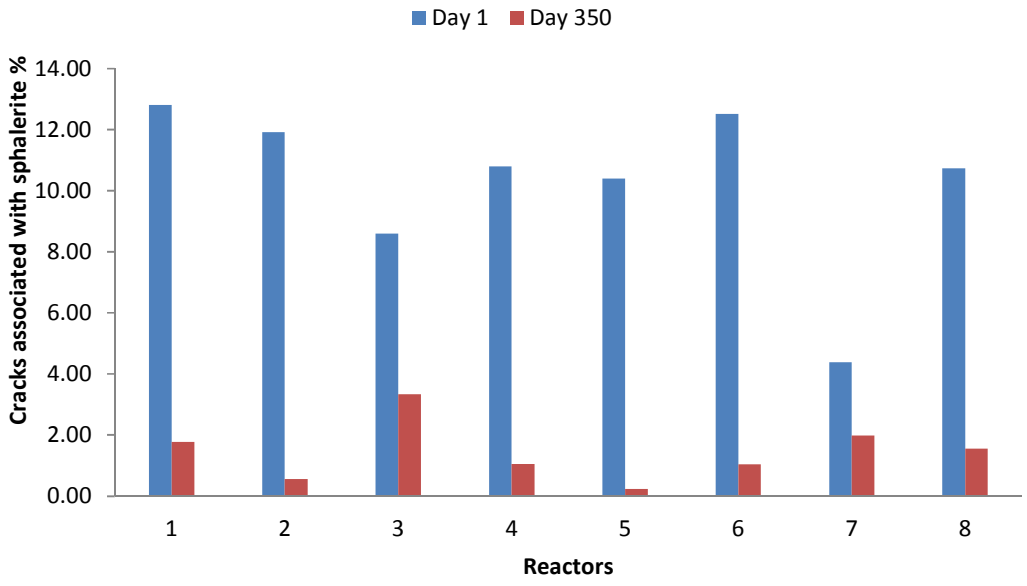

Figure 5-21: QEMSCAN analysis results for the trend of the cracks association with sphalerite before and after leaching. Reactor 1 (HPGR (-25+19) UT), Reactor 2 (HPGR (-5+4.75) UT), Reactor 3 (HPGR (-16+9.5) UT), Reactor 4 (Cone (-16+9.5) T), Reactor 5 (HPGR (-5+4.75) T), Reactor 6 (HPGR (-16+9.5) T), Reactor 7 (Cone (-25+19) T), Reactor 8 (HPGR (-25+19)). Where UT (microwave untreated), T (microwave treated)

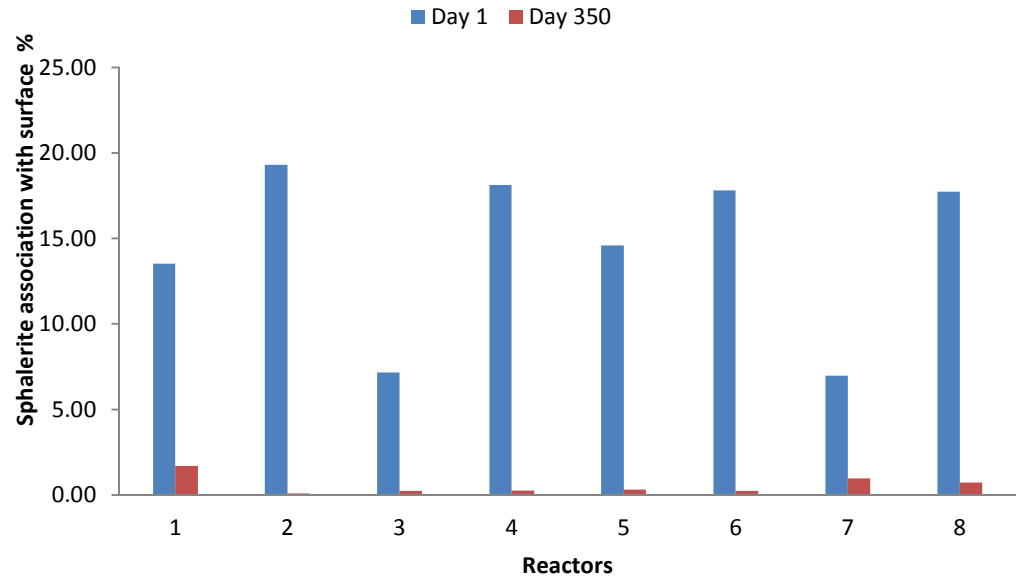

Figure 5-22: QEMSCAN analysis results for the trend of the sphalerite association with the particle surface before and after leaching. Reactor 1 (HPGR (-25+19) UT), Reactor 2 (HPGR (-5+4.75) UT), Reactor 3 (HPGR (-16+9.5) UT), Reactor 4 (Cone (-16+9.5) T), Reactor 5 (HPGR (-5+4.75) T), Reactor 6 (HPGR (-16+9.5) T), Reactor 7 (Cone (-25+19) T), Reactor 8 (HPGR (-25+19)). Where UT (microwave untreated), T (microwave treated)

5.3.Chapter summary

Leaching results of microwave treated ore presented in this chapter suggest that higher metal recovery is achievable at coarser sizes compared to microwave untreated ore. For example the overall zinc leach yield for large (-25+19) mm HPGR microwave treated particle was 72% and that of small (-5+4.75) mm HPGR untreated particle was 74%. Thus comparable metal recovery to small (-5+4.75) mm HPGR crushed ore was achieved by microwave treating large (-25+19) mm particles. This has implications on energy savings during comminution. As the amount of energy used during size reduction increases with decreasing product particle size. The increase in the zinc recovery at coarser sizes due to microwave treatment observed in this study has significant implications on the economics of heap leaching operations, which are normally characterised by low recoveries at coarse sizes. Results from the column experiments show that the value metal recovery of microwave treated HPGR crushed products is slightly higher than recovery from cone crushed products at all sizes. It can be concluded from this result that after microwave treatment the effect of mode of comminution on leaching recovery is reduced. Previous studies have shown that the leachability of products prepared using the HPGR is higher when compared to those from a cone crusher. In conclusion this study shows that microwave treatment of ore at economical microwave treating rates prior to leaching results in improved leaching recoveries at coarse sizes.

CHAPTER 6

6. MODELLING OF MICROWAVE INDUCED CRACKS

Determining the microwave treatment conditions (exposure time and power density) and process system designs required to obtain optimal formation of cracks during microwave treatment of ores is an important step towards scaling up the process. Process scaling needs model development, simulation and understanding of the effect of microwave treatment on the downstream processing of microwave treated ores (Bradshaw et al., 2007). To date, there are no validated models for understanding the behaviour of microwave treated ores and there exist no predictive tools to forecast expected damage in an ore for a given microwave treatment condition. Physical experiments alone are not sufficient in determining processing limits associated with the application of microwave technology as they do not offer the possibility of investigating a large number of case studies at a reasonable cost and in a reasonable time period. Bonded particle modelling offers a partial solution to these challenges due to the fact that a wide range of scenarios can be investigated rapidly and at relatively low cost.

Bonded “particle” models (BPM) represent solids through an assembly of micro-scale “particles” bonded together at contact points. In BPM thermal and heat generation models can be coupled to mechanical models (Itasca, 2008; Potyondy and Cundall, 2004). BPM techniques thus, allow the possibility of simulating the microwave treatment of ores under different microwave exposure conditions. BPM has been successfully used to simulate thermally induced stresses and micro crack patterns caused by volumetric heating of microwave absorbing phases in binary ores (Ali and Bradshaw, 2010; Wanne and Young, 2008). Ali and Bradshaw (2009, 2010) carried out numerical simulation investigations into the mechanism of microwave induced micro fracture using bonded particle modelling. The models were not validated. XCT allows microwave induced crack formation inside particles to be observed allowing possibility of qualitative and quantitative validation. Validation of these models is a necessary step towards gaining a fundamental understanding of the optimal microwave treatment conditions for different ore types and mineralogy. The main aim of this part of the work was to use the XCT and QEMSCAN experimental results presented in chapter 4, to validate and to improve on the models.

Section 6-1 serves as an introduction to BPM techniques used in this thesis. In section 6-2, the methodology used for modelling the macroscopic properties of the model materials is provided. Section 6-3 discusses the model development and investigations into the effect of

model resolution on predicted crack damage that was carried out. This is followed by section 6-4 where the developed model is used to investigate the effect of absorbent phase on crack damage. The influence of absorbent phase content on crack propagation under different microwave treatment conditions is elucidated in this section.

6.1.Numerical modelling methodology

6.1.1. Bonded particle modelling using PFC

Bonded particle modelling represents solid rock material as an assembly of particles that are joined together by breakable parallel bonds. The mechanical behaviour of the system is described by the movement of each particle and the force and moment acting at each contact. Newton's second law is used to determine the translational and rotational motion of each particle arising from the contact, applied and body forces acting upon it, while the force–displacement law is used to update the contact forces arising from the relative motion at each contact. A parallel bond approximates the mechanical behaviour of brittle elastic cement joining bonded particles. Parallel bonds establish an elastic interaction between these particles that acts in parallel with the grain based portion of the force displacement behaviour (Itasca Consulting Group, 2008). The parallel bond is defined by: normal and shear stiffness per unit area, $\bar{k}_n$ and $\bar{k}_s$; tensile and shear strengths, $\bar{\sigma}_c$ and $\bar{\tau}_c$; and bond radius multiplier,$\bar{\lambda}$, such that parallel bond radius

$$\bar{R} = \bar{\lambda}\min(R^A, R^B) \qquad 6\text{-}1$$

with R^A and R^B being the particle radii. The total force and moment acting at each cemented contact is comprised of a force,F_i, arising from particle-particle overlap (grain based portion of the force displacement behaviour) and a force, moment, $\bar{F}_i$ and $\bar{M}_i$, carried by the parallel bond (cement based portion of the force displacement behaviour) (Potyondy and Cundall, 2004). The quantities contribute to the resultant force and moment acting on the two contacting particles. The grain based portion is defined by: the normal and shear stiffness, k_n and k_s, and the friction coefficient, μ_f, of the two contacting particles, which are assumed to be disks of unit thickness. The force–displacement relation relating contact normal force F^n,contact overlap U^n,increment of shear force ΔF^s and shear displacements ΔU^s, between two particles is given by

$$\begin{cases} F^n = k_n U^n \\ \Delta F^s = -k_s \Delta U^s \end{cases} \qquad 6\text{-}2$$

where k^n and k^s are the contact normal and shear stiffness respectively. The increments of elastic force and moment are given by

$$\Delta\bar{F}^n = \bar{k}_n A\, \Delta U^n \quad 6\text{-}3$$

$$\Delta\bar{F}^s = \bar{k}_s A\, \Delta U^s \quad 6\text{-}4$$

$$\Delta\bar{M}^n = -\bar{k}_s J \Delta\theta^n \quad 6\text{-}5$$

$$\Delta\bar{M}^n = -\bar{k}_n I \Delta\theta^s \quad 6\text{-}6$$

where A, I, and J are the area, moment of inertia and polar moment of inertia of the parallel bond cross section, respectively. $\Delta\theta^n$ and $\Delta\theta^s$ is normal and shear directed rotation increments. ΔU^s and $\Delta U^n$is the shear and normal displacement increments. The maximum tensile and shear stresses acting on the parallel bond periphery given by

$$\bar{\sigma}^{max} = \frac{-\bar{F}^n}{A} + \frac{|\bar{M}^s|\bar{R}}{I} < \bar{\sigma}_c \quad 6\text{-}7$$

$$\bar{\tau}^{max} = \frac{|\bar{F}^s|}{A} + \frac{|\bar{M}^n|\bar{R}}{J} < \bar{\tau}_c \quad 6\text{-}8$$

where $\bar{R}$ is the radius of the parallel bond, $\bar{\sigma}_c$ and $\bar{\tau}_c$ are the tensile and shear strength of the cemented contact, respectively. The values can be calculated as:

$$A = \pi\bar{R}^2 \quad 6\text{-}9$$

$$J = \frac{1}{2}\pi\bar{R}^4 \quad 6\text{-}10$$

$$I = \frac{1}{4}\pi\bar{R}^4 \quad 6\text{-}11$$

Young's moduli for particle contacts, E_c and particle bondage $\bar{E}_c$ are defined to relate the contact and bond stiffness as follows:

$$E_c = \frac{k_n}{2t} \ (t = 1\ in\ 2D) \quad 6\text{-}12$$

$$\bar{E}_c = \bar{k}_n(R^A + R^B) \quad 6\text{-}13$$

If the maximum and tensile stress exceeds the tensile strength or the maximum shear stress exceeds the shear strength, then the parallel bond breaks, resulting in the formation of cracks. Thus crack damage occurs by bond breakages. The micro crack initiation and propagation can be expressed as a progressive breakage of contact bonds. BPM does not impose theoretical assumptions and limitations on macroscopic material behaviour, as do continuum models. In a BPM, micro-cracks are able to form, interact and coalesce into macroscopic fractures. A useful description of the basic theory of BPM is given in Potyondy and Cundall (2004).

6.1.2. Mechanical model

Simulated material characterisation in BPM requires the following microscopic properties:

1. Particle radius
2. Stiffness of the particle contacts
3. Friction coefficient between particles
4. Normal and shear strength of particle bonds

These microscopic properties are chosen to represent a real intact material (with the required macroscopic properties) and cannot be measured directly from laboratory experiments. This is done by carrying out numerical calibration to back calculate microscopic properties required to simulate a solid such as a real intact rock. A number of simulated material strength test are carried out using assumed microscopic properties to match the simulated rock properties (intact rock UCS, Young's modulus and Poisson's ratio) with laboratory measured material properties following the procedures outlined by Potyondy and Cundall (2004). Figure 6-1 shows the material calibration algorithm used in this study. Numerical strength tests are performed using assumed initial micro properties and the results are compared against the desired response of the real intact material. When a match has been found, the corresponding set of micro properties is used in the full simulation. Table 6-1 shows the complete set of micro-parameters required to characterise a parallel bond material.

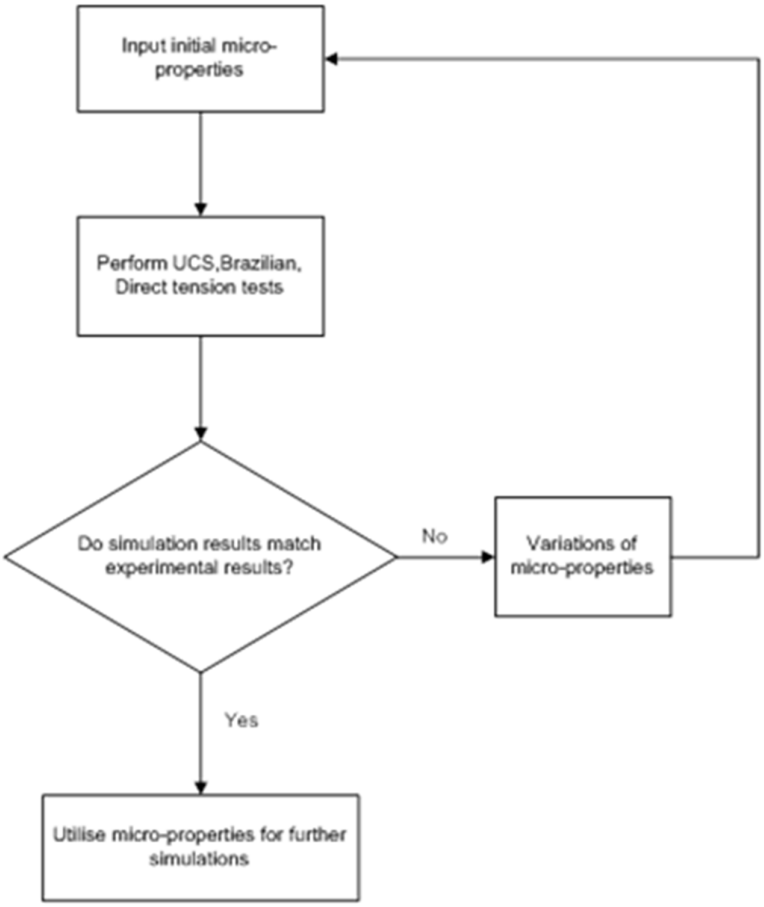

Figure 6-1: Model material properties calibration algorithm in BPM

Table 6-1: Complete set of micro-parameters that characterise a parallel-bonded material

Description	Symbol
Ball properties	
Density	ρ_b
Young modulus	E_c
Stiffness ratio	k_n/k_s
Friction	μ
Minimum radius of ball	R_{min}
Ratio of maximum and minimum ball radius	R_{max}/R_{min}
Cement properties	
Radius multiplier	$\bar{\lambda}$
Young modulus	$\overline{E_c}$
Stiffness ratio	$(\overline{k_n}/\overline{k_s})$
Normal strength mean (mean $\pm$ std.dev)	$\overline{\sigma_c}$
Shear strength mean (mean $\pm$ std.dev)	$\overline{\tau_c}$

The density of the ball $\boldsymbol{\rho_b}$is calculated from

$$\rho_b = \frac{\rho}{(1-n)} \quad 6\text{-}14$$

where ρ is the density of the solid and n is the average porosity of the modelled material. For densely packed and model specimen assemblies, the value of (n) is fixed by the initial microstructure and is approximately 0.16 (Itasca Consulting Group, 2008).The first step in the calibration process is to specify a specimen geometry. This includes specimen dimensions width and height (*Wlx* and *Wly*), ball minimum size (R_{min}) and the radius ratio (R_{max}/R_{min}) of the balls. The minimum ball size influences the model resolution. In this study model resolution is defined as:

$$\psi = min(Wlx, Wly)\ /2R_{min} \quad 6\text{-}15$$

where $R_{min}$is the mean particle radius. Potyondy and Cundall (2004) have shown that ball size has an influence on tensile strength and packing density and thus it cannot be regarded as a free parameter that only controls model resolution. The particle diameters satisfy a uniform particle size distribution bounded by R_{min} and R_{max} and a dense packing is obtained by applying a material genesis procedure to generate random packing of particles. The material genesis procedure applied in creating the ore specimen is described by Potyondy and Cundall (2004).

6.1.3. Thermal model

Heat flow

Thermal algorithms in BPM allow the simulation of heat conduction and the development of thermally induced displacement and forces. In these algorithms, thermal material is presented as a network of heat reservoirs (particles) and thermal pipes (contacts between particles). Heat flow occurs via conduction in the pipes connecting the reservoirs. This approach allows the evolution of the heat network during the modelling. Once the thermal micro properties are specified, subsequent crack damage will modify the number of active pipes, and thereby change the ability of the material to conduct heat. The thermal input parameters for a thermal PFC model are the specific heat(C_p), the linear thermal expansion coefficient(α), and the thermal conductivity(K). In BPM, the conductivity tensor is estimated for a given material; then, the thermal resistance computed from the conductivity is assigned to all pipes (Itasca Consulting Group, 2008).

Microwave heating

The heat conduction equation for quasi-static mechanical problems for solids is given by

$$-\frac{\partial q_i}{\partial x_i} + q_v = \rho C_p \frac{\partial T}{\partial t} \quad 6\text{-}16$$

Where q_i is the heat flux vector which is governed by the Fourier's law in (W/m^2), q_v is the volumetric heat intensity in (W/m^3), ρ is the density of the material (kg/m^3) and C_p is the specific heat capacity (J/kgK).

The amount of thermal energy deposited into a material due to microwave heating (power density) is dependent on the internal electric field strength within the mineral, frequency of the applied microwave radiation, and the dielectric constant and loss factor of the material. If the electric field strength is known the power absorption density per unit volume of the mineral is given by:

$$P_d = 2\pi f \varepsilon_0 \varepsilon_r'' E_0^2 \quad 6\text{-}17$$

where P_d is the power density (W/m^3), f is the frequency of the microwave radiation (Hz), ε_0 is the permittivity of free space (8.854x10^{-12} F/m), ε_r'' is the dielectric loss factor of the mineral, E_0 is the magnitude of the electric field of microwave energy inside the material (V/m).

Combining Equation 6-16 and 6-17 gives

$$-\frac{\partial q_i}{\partial x_i} + P_d = \rho C_p \frac{\partial T}{\partial t} \quad 6\text{-}18$$

A solution to Equation 6-18 provides information on the temperature rise in material for a given microwave treatment condition (power density and exposure time)

Thermal-mechanical coupling

Thermal strains as a result of heating BPM simulated material are generated by accounting for the thermal expansion of the particles and bonding material that joins them.

$$\Delta R = \alpha R \Delta T \quad 6\text{-}19$$

where α is the coefficient of linear thermal expansion associated with the particle (1/°C). It is assumed that only the normal component of the force vector carried by the bond $\Delta\bar{F}^n$ will be affected by the temperature change. Thus the normal component of the bond force is given by

$$\Delta\bar{F}^n = -\bar{k}_n A \Delta U^n = -\bar{k}_n A (\bar{\alpha} \bar{L} \Delta T) \quad 6\text{-}20$$

Where $\bar{k}_n$ is the bond normal strength, A is the area of the bond cross section. $\bar{\alpha}$ is the expansion coefficient of the bond material (1/°C), (taken to be equal to the average temperature change of the two particles at the ends of the pipe associated with the bond). $\bar{L}$ is bond length (mm).

6.2. Macro-mechanical and thermal properties data

In this study BPM was carried out using PFC3D/ PFC2D modelling software (Itasca Consulting Group, 2008) .A three phase mineral model of a sulphide ore was generated in PFC, the model consisted of sphalerite and pyrite grains locked in a quartz matrix. These mineral phases were chosen to represent the simulated ore as they were identified to be the major mineral phases in the Gamsberg ore used in the experimental investigations presented in chapter 4. The laboratory measured macro-mechanical and thermal properties used to calibrate the modelled minerals are presented in Table 6-2 to Table 6-5. The elastic properties of the minerals were obtained from Bass (1995) and the tensile strength vales were typical values quoted for the minerals in Lama and Vutukuri (1978a). The thermal conductivities of the minerals were obtained from Diment and Pratt (1988) while the expansion coefficients were obtained from Clark (1966). Each thermal property was expressed as a function of temperature and incorporated into the thermal constitutive models in PFC^{3D}/ PFC^{2D}. Previous studies have shown that calibrating PFC^{3D}/ PFC^{2D} material to the UCS strength results in very low triaxial strength values (Potyondy and Cundall, 2004). Thus in this study the material strength was calibrated using the Brazilian tensile strength as it was not possible to match both UCS and tensile strength using the same microscopic parameters (Ali and Bradshaw, 2010).

Table 6-2: Physical and macro-mechanical properties of pyrite and quartz (Bass, 1995; Lama and Vutukuri, 1978b)

	Experimental		
	Pyrite	Quartz	Sphalerite
Young modulus stress (GPa)	291.	95.6	83.2
Tensile strength (MPa)	10.5	8.5	10.72
Density (kg/m^3)	5016	2648	4044

Table 6-3: Thermal conductivity as a function of temperature (Diment and Pratt, 1988)

Mineral	Thermal conductivity ($W/m.K$)		
	298K	500K	1000K
Quartz	6.15	2.92	1.87
Pyrite	23.2	9.48	5.85
Sphalerite	26.61	-	-

Table 6-4: Thermal expansion coefficient as a function of temperature (Clark, 1966)

Mineral	Thermal expansion coefficient α_v ($10^{-6}K^{-1}$)			
	373K	473K	673K	873K
Quartz	45.5	43.3	49.7	77.9
Pyrite	27.3	29.3	33.9	-
Sphalerite	19.5	24.4	23.6	24.8

Table 6-5: Ball density used in the modelling

Mineral	Density ρ (kg/m^3)	Ball density ρ_b (kg/m^3)
Pyrite	5016	5971.4
Sphalerite	4088	4866.7
Quartz	2650	3154.8

6.3.Effect of model resolution on crack damage

6.3.1. Introduction

Previous studies have investigated model resolution (ψ) effects (Equation 6-15), on BPM specimen mechanical properties (Potyondy and Cundall, 2004). These studies have shown that elastic properties such as Young modulus and Poisson ratio are independent of particle size. The Brazilian strength and the crack initiation stress were observed to show a clear dependence on particle size, with tensile strength decreasing with particle size (Koyama and Jing, 2007; Potyondy and Cundall, 2004; Wong and Zhang, 2013). Previous studies investigating microwave induced crack propagation using BPM method assumed model resolution (ψ) to be a free parameter which had no influence on predicted microwave induced crack damage and observed crack patterns (Ali and Bradshaw, 2010). The aim was to investigate model particle size scale effects on the thermal cracking patterns produced using BPM. This would allow for assessment of the feasibility of the application of BPM to reproduce microwave induced crack pattern in real ores.

6.3.2. Methodology

To investigate the effect of model resolution (ψ) on crack damage a numerical routine was developed to generate a PFC^{2D} binary ore specimen consisting of randomly disseminated pyrite grains making up 10% by area of the total particle in a transparent quartz phase (constituting the remaining 90%). The approximate diameters of the grains ranged from 0.056 to 0.83 mm. The created specimen measured 15mm by 20mm. Binary ore specimens were created representing six different model resolutions (see Table 6-6). During model specimen generation and calibration, a model resolution of 268 (R_{min} value = 0.028 mm) was observed to be the maximum possible resolution for generating model ore specimen in this study. For each model resolution, ten different samples were produced with different packing arrangements through varying the seed for the random number generator in the material genesis procedure (Potyondy and Cundall, 2004). Table 6-6 shows the material properties of the model

specimen at different resolution. At higher model resolutions there is an increase in the number of discs and hence the number of active contacts. In PFC^{3D}/ PFC^{2D} the packing fabric or connectivity of the bonded assembly, is controlled by the ratio (R_{max}/R_{min}); for a fixed ratio, varying R_{min} changes the absolute packing size but does not affect the packing fabric. Therefore the ratio (R_{max}/R_{min}) was fixed in this study at a value of 1.66 and only R_{min} was varied (specimen resolution (ψ)).

Table 6-6: Model resolution (ψ) considered in this study

R_{min} (mm)	Model resolution (ψ)	Average size (mm)	Number of discs	Number of active contacts	Number of parallel bonds
0.25	30	0.329	794	2037	1497
0.1	75	0.132	4966	10001	9764
0.075	100	0.099	9580	24713	19051
0.056	134	0.074	15837	40761	31557
0.035	214	0.046	40543	104636	81289
0.028	268	0.037	63349	163825	127464

Material calibration was carried out for each model resolution to match the macro-mechanical properties to their corresponding experimental determined values. Simulated biaxial and Brazilian tests were used to calibrate the model specimen by matching the model specimen Young modulus and tensile strength to laboratory determined values from literature for each material considered (Table 6-7). Laboratory macro-mechanical properties were successfully matched to the model specimen for model resolutions 30 up to 214. BPM ore specimen macro property values at a resolution of 268, were a poor match to literature values. At a model resolution of 268, the generated model ore specimen required greater computational time and increased iterations to match model macro properties with laboratory values.

Table 6-7: Laboratory determined Young modulus and tensile strength values from literature (Bass, 1995; Lama and Vutukuri, 1978b), compared against BPM ore specimen values for different minerals at different model resolution

Mineral		Laboratory	BPM Macro properties					
	Model resolution (ψ)		30	75	100	134	214	268
Quartz	Young Modulus Stress (GPa)	95.60	95.80	95.31	95.50	95.76	95.44	96.74
	Tensile strength (MPa)	8.50	8.70	8.60	8.20	8.84	8.90	7.15
Pyrite	Young Modulus Stress (GPa)	291.00	290.00	291.50	291.70	291.30	291.20	292.30
	Tensile strength (MPa)	10.50	10.24	10.27	10.40	10.70	10.50	8.10
Sphalerite	Young Modulus Stress (GPa)	83.20	83.28	82.98	83.26	83.92	83.74	84.10
	Tensile strength (MPa)	10.72	10.91	10.87	10.75	13.46	13.00	6.48

In this study it was important to quantify microwave induced crack damage. BPM crack damage is defined differently to crack damage measured experimentally. In chapter 4 a relative increase in crack volume after microwave treatment, was considered to be a measure of the degree of microwave induced damage. In BPM cracks form in PFC models due to bond breakage events, the distance between bonded particles after bond breakage remains constant. Additionally BPM model ore specimen lack existing cracks thus, the experimental definition of crack damage is not appropriate for measuring crack damage in BPM. Crack damage was thus, defined as the number of bonds broken due to microwave treatment divided by the total number of bonds present in the material specimen before microwave treatment.

$$Crack\ damage\ = \frac{Number\ of\ parallel\ bonds\ broken}{Total\ number\ of\ parallel\ bonds} \qquad 6\text{-}21$$

6.3.3. Results and discussion

COMPARISON BETWEEN THERMAL MODELLING IN PFC^{2D} AND PFC^{3D}

Two PFC model specimens, a two dimensional 15mm by 20mm rectangular specimen (with PFC^{2D}) and a three dimensional parallelepiped specimen 15mm by 15 mm by 20mm (with PFC^{3D}), were generated with about 794 and 67541 particles, respectively Table 6-8. The specimen consisted of pyrite grains (10%) in a transparent quartz phase (90%). Simulations were undertaken using a power density of 1 x 10^{10} W/m$^3_{abs}$, and an exposure time varying from 0.01 to 4 seconds. This power density was chosen to represent the power density in the 6 kW source, 2.45GHz single-mode applicator used in the physical experimental investigation in this study.

Table 6-8: Comparison of the number of bonds in 2D model against those in 3D.

PFC	2D	3D
Number of balls/discs	794	67541
Number of contacts	7979	320890
Number of active contacts	5654	194043
Number of pbonds	5499	194044

The variation in crack damage with increasing exposure time of the PFC^{3D} and PFC^{2D} simulations results were similar as can be seen in Figure 6-2. PFC^{2D} model ore specimen had a higher disc to parallel bond ratio compared to the PFC^{3D} model ore specimen (see Table 6-8). This could be due to PFC^{2D} having a more compact packing after specimen generation (porosity n = 0.16) compared to PFC^{3D} (porosity n = 0.35) (Potyondy and Cundall, 2004).

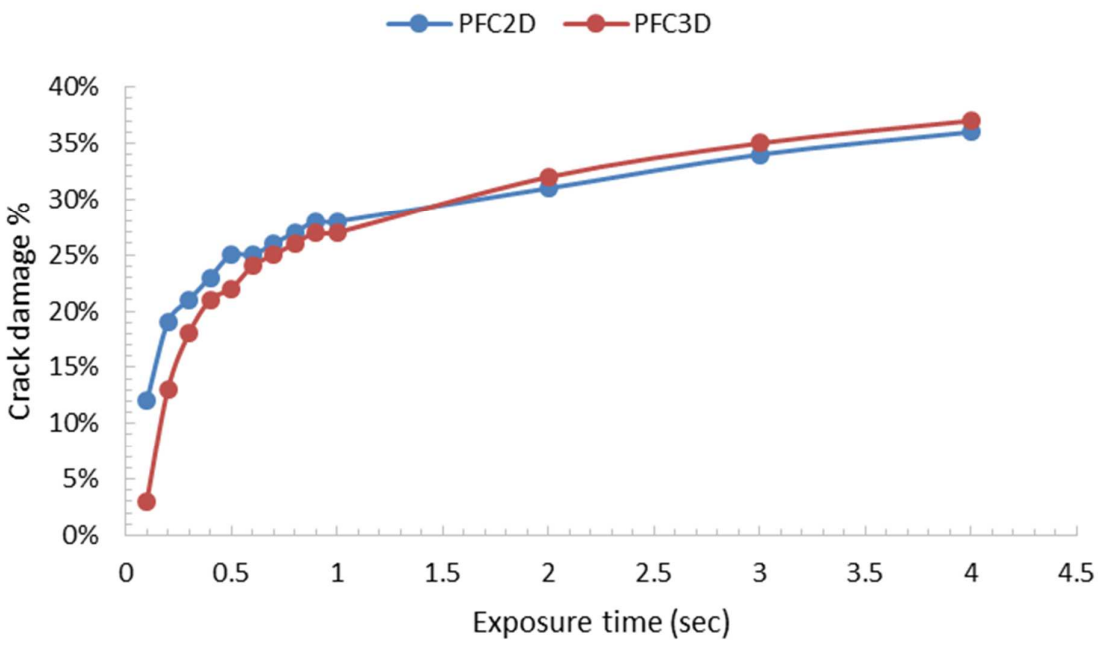

Figure 6-2: Comparison of thermal simulations carried out in PFC2D against those in PFC3D (power density of 10^{10} W/m^3_{abs})

Figure 6-2 and Figure 6-3 show that as exposure time increases microwave induced crack damage reaches a maximum value. For example comparing the number of parallel bonds in the PFC2D material (see Table 6-8) against the number of microwave induced cracks at exposure times over 5 seconds (see Figure 6-3), shows that over 50% of parallel bonds holding the material together would have broken resulting in complete failure of the material. Visualising the cracks in PFC^{3D} and PFC^{2D} shows that the dominant mode of bond breakage is tensile failure (see Figure 6-3 and Figure 6-4).

One main advantage of modelling in PFC^{2D} is that the maximum model resolution possible (lowest R_{min} value) in PFC^{2D} is higher compared to that possible in PFC^{3D}. High resolution simulations in PFC3D require longer computational time compared to simulations in PFC^{2D}. Since there is no difference in predicted thermal crack damage with increasing exposure time, all further simulations carried out in this study were done using PFC^{2D}.

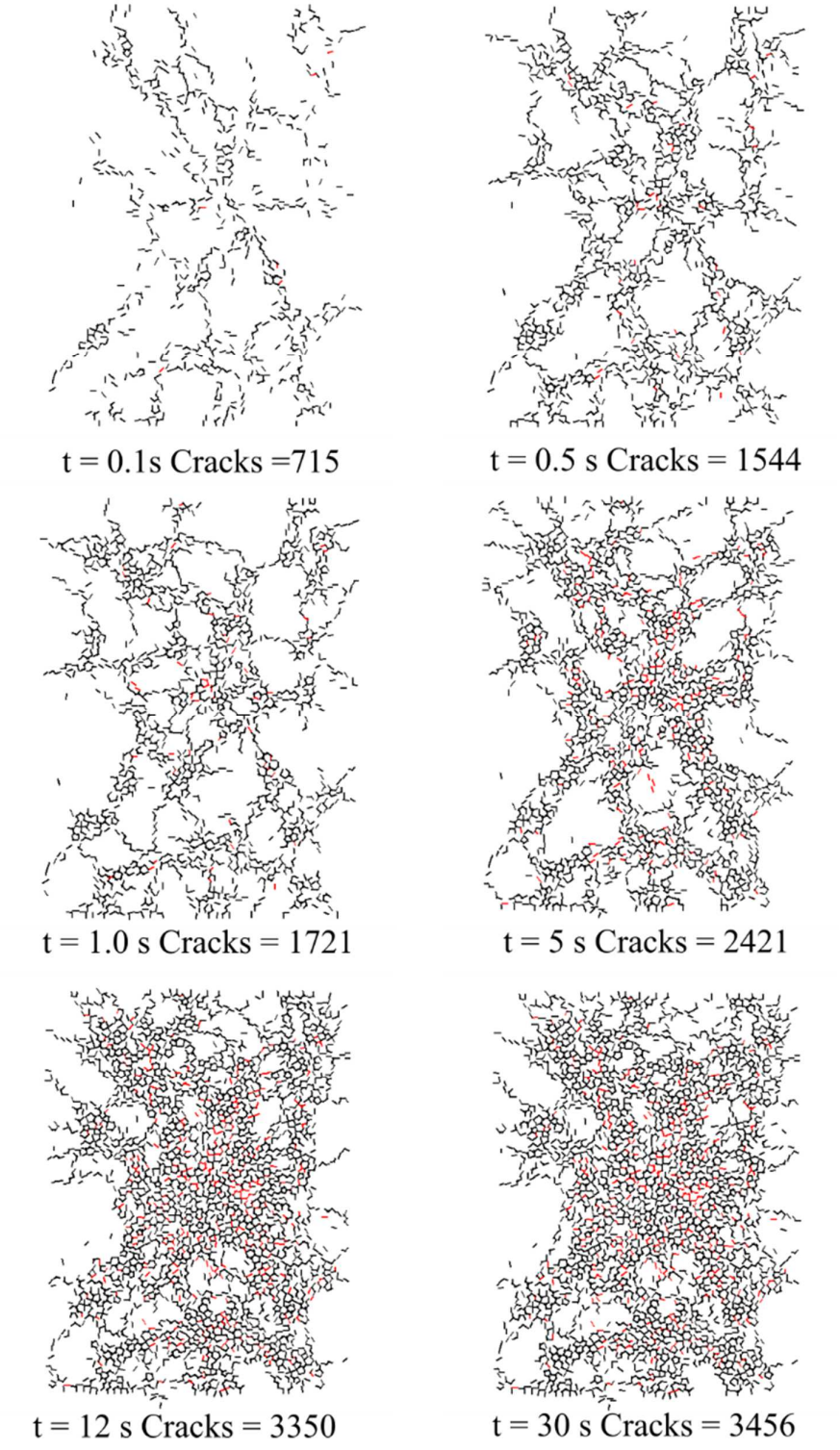

Figure 6-3: PFC^{2D} microwave damage crack visualisation at different exposure times black/red=normal/shear failure

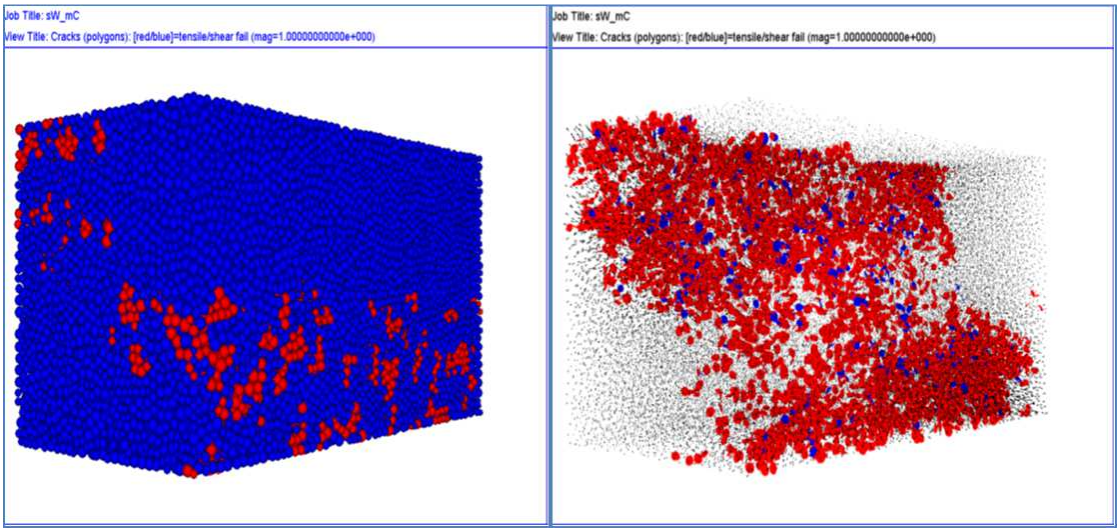

Figure 6-4: Right Parallel piped 3D pyrite quartz binary specimen, Left 3D crack visualisation (power density of 1 x 10^{10} W/m^3_{abs}, exposure time 1.00)

EFFECTS OF MODEL RESOLUTION ON CRACK PATTERNS

The effect of model resolution on microwave induced crack patterns in PFC^{2D} was investigated by carrying out simulations at fixed power density of 1 x 10^{10} W/m^3_{abs}, and varying exposure time from 0.01 to 1 second for each model specimen resolution considered in this study. Figure 6-5 shows the values of the simulated crack damage with increasing exposure time obtained from the PFC^{2D} simulations at different model resolutions. These results suggest that model resolution has an effect on the magnitude of simulated crack damage due to microwave treatment in PFC^{2D}. Despite the fact that in PFC thermal expansion is independent of particle size (Equation 6-19), model resolution appears has an effect on the crack damage observed due to the macroscopic thermal expansion of the microwave absorbent phase during the simulations (see Figure 6-5). The results show increasing crack damage with increasing exposure time for all model resolutions. There is a significant difference in simulated crack damage between the low 30 and high (greater than 75) model resolution. There is no significant difference in the magnitude of the crack damage between the 75 and 268 model resolution specimens. The trend in the increase in percentage crack damage with increasing exposure time for the 268 model resolution specimen is different to the trend observed for most of the high resolution models ($\geq$ 100). This could be due to, the previously mentioned difficulties encountered in calibrating the model specimen at a resolution of 268, the model specimen macro properties at this resolution were a poor match to laboratory measured values (see Table 6-7).

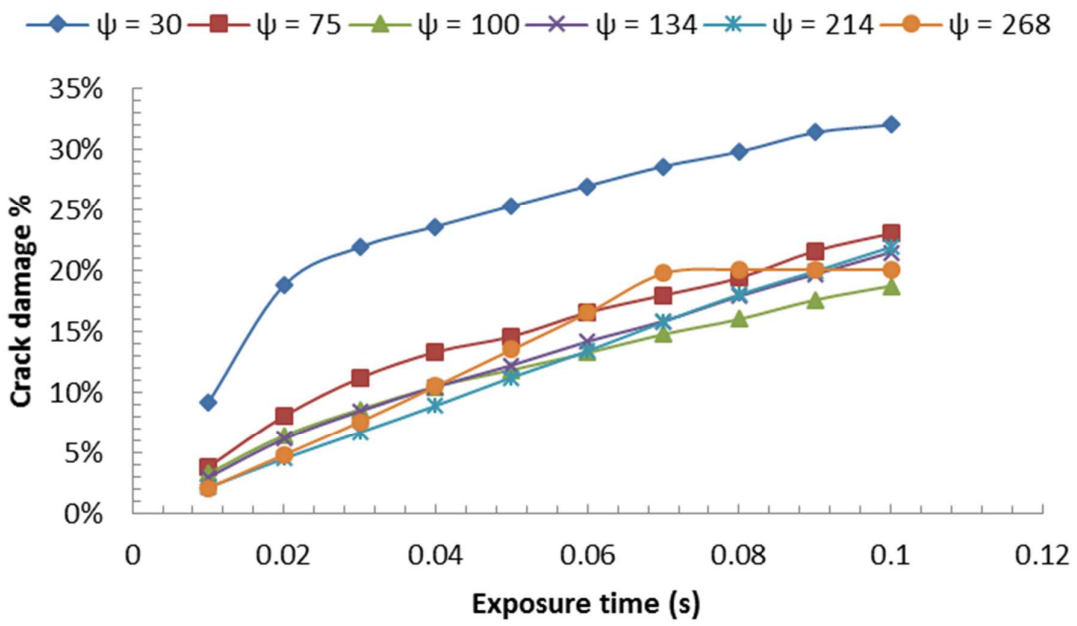

Figure 6-5: Crack damage against time at different model resolution (ψ) (power density of 1 x 10^{10} W/m^3_{abs})

Analysis of the crack damage at 0.01 second (see Figure 6-6) shows a decrease in crack damage with increasing model resolution. A similar trend is observed at 0.1 second (see Figure 6-6). The majority of the cracks observed are tensile cracks with very few shear cracks. From Equation 6-19, thermal expansion is represented as a relative change of the ball size due to a temperature increase; the resulting tensile stress due to the thermal expansion results in bond breakage when the tensile stress exceeds the bond tensile strength. By definition, micro-cracks form in PFC models due to the bond breakages. Therefore, shearing of already-cracked surfaces does not produce any observed events. Hence the amount cracks recorded due to shear failure are very insignificant (see Figure 6-7 and Figure 6-8).

The driving force for crack damage is the tensile stresses that are generated at the grain boundary of the absorbent phase. These thermal stresses are as a result of the thermal expansion of the microwave absorbent phase stretching the transparent matrix creating high tensile stresses around the grain boundaries. Where these stresses are greater than the bond strength between two contacts, bond breakage occurs. Bond failure leads to a force distribution around the breakage that can lead to further breakage thus, resulting in crack propagation. Crack propagation follows regions in which the bond strength is lower. Thus increased exposure time results in increased crack damage as shown in Figure 6-5 for all model resolutions.

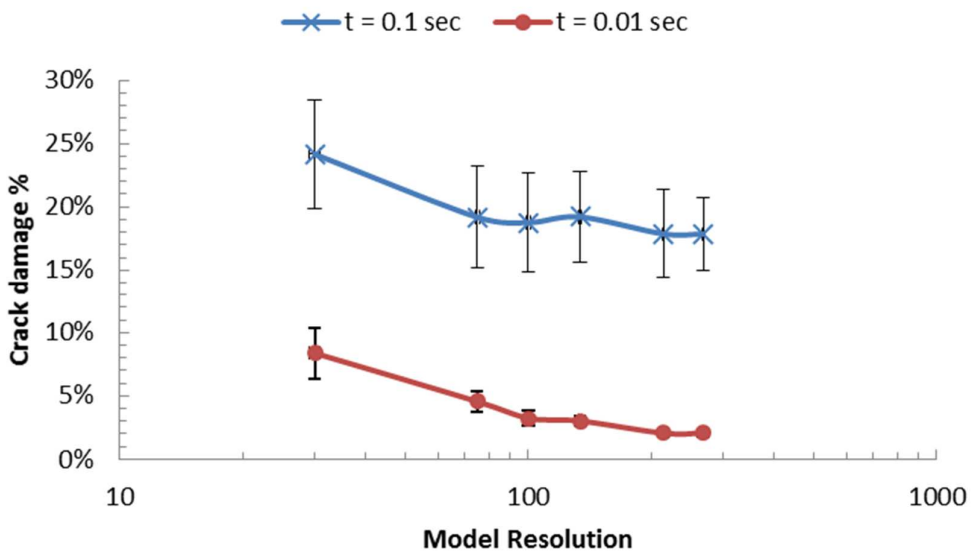

Figure 6-6: Crack damage at different model resolution (ψ) at an exposure time of 0.01 and 0.1 seconds (power density of 1 x 10^{10} W/m^3_{abs})

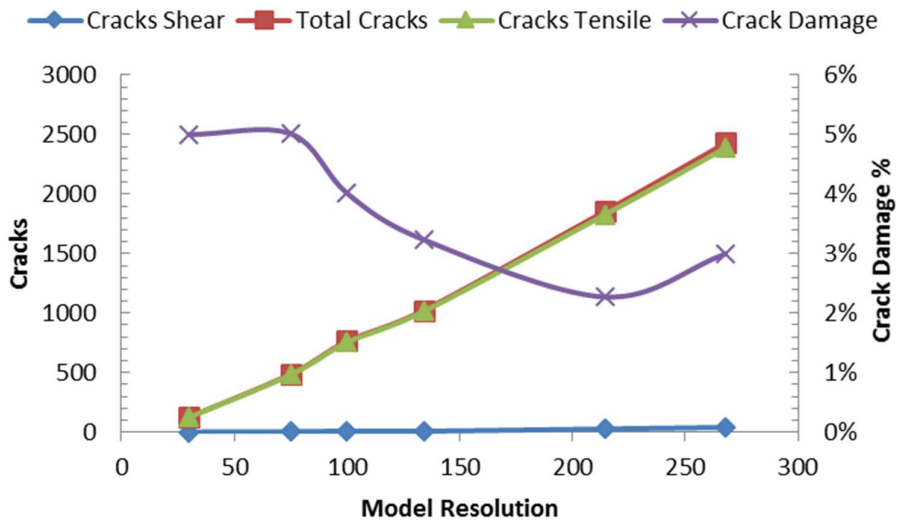

Figure 6-7: Number and types of cracks at different model resolutionv(ψ) at an exposure time of 0.01 seconds (power density of 1 x 10^{10} W/m^3_{abs})

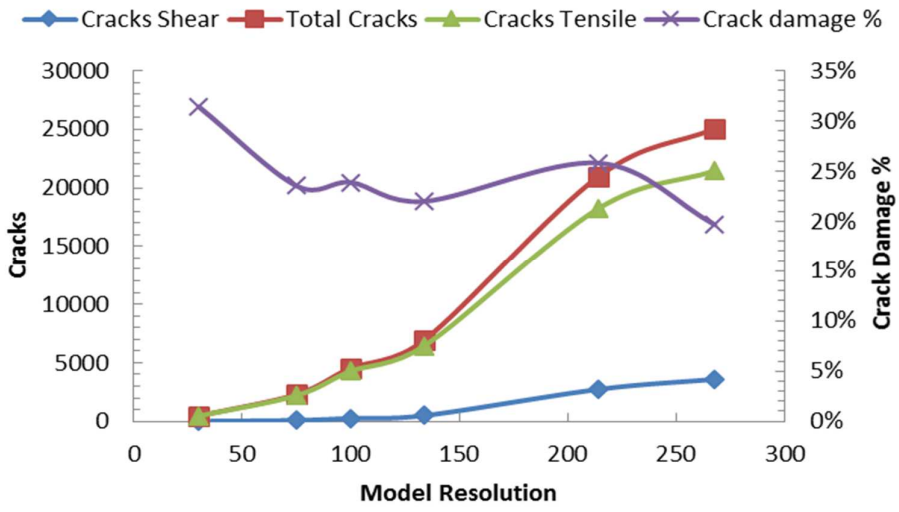

Figure 6-8: Number and types of crack at different model resolution (ψ) at an exposure time of 0.1 seconds (power density of 1 x 10^{10} W/m^3_{abs})

Crack image results of the simulated crack patterns due to microwave treatment for all model resolutions considered in this study at an exposure time of 0.01 seconds at fixed power density of 1 x 10^{10} W/m^3_{abs} are shown in Figure 6-9. The microwave induced crack damage patterns shown Figure 6-9 were predicted for a microwave energy input value of 1 x 10^8 J/m^3_{abs}.The crack patterns shown in Figure 6-9 correspond to the calculated crack damage shown in Figure 6-6. There is no notable difference in crack pattern distribution of model ore specimen with model resolution 75 and above. Cracks appear to propagate from the absorbing phase into the transparent quartz matrix. At short microwave treatment exposure times (0.01 seconds) the crack pattern distribution is narrow and continuous for high model resolutions and wide and discontinuous for the low model resolution. A marginal difference in crack patterns between the 134 and 268 specimen resolution was observed. The results show that cracks in low resolution ore model specimen ($\psi \leq 30$) propagate in a different pattern despite having macro-mechanical properties that are similar to higher resolution models ($\psi \leq 75$). A qualitative analysis of the effects of model resolution on predicted microwave induced crack patterns suggest that, there is a difference in predicted microwave crack propagation between low resolution models ($\psi \leq 30$) and high resolution models ($\psi \leq 30$). This is in contract with quantitative results where the predicted calculated crack damage varies with increasing resolution for model resolutions between 30 and 134.

Images of the simulated crack patterns due to microwave treatment for all model resolutions at exposure time of 0.1 seconds and fixed power density of 1 x 10^{10} W/m^3_{abs} are shown in Figure 6-10. The microwave induced crack damage patterns shown in Figure 6-10

were predicted for a microwave energy input value of 1 x 10^9 J/m^3_{abs}. Crack patterns shown in Figure 6-10 correspond with the model calculated crack damage shown in Figure 6 6. At higher exposure times (0.10 s) there is no notable difference in crack pattern distribution of model ore specimen with model resolution 75 and above. Significant grain boundary and trans-granular fracture is observed for model ore specimens with model resolutions 75 and above. For model ore specimen with a model resolution of 30 the crack pattern is not well defined (see Figure 6-10). Despite the model ore specimen at different model resolution having the same mechanical and thermal properties there is at least a 20% difference in predicted crack damage values for model resolution less than 75, for a microwave energy input value of 1 x 10^8 J/m^3_{abs} (see Figure 6-7). At a higher energy input (1 x 10^9 J/m^3_{abs}) the difference is at least 12% (see Figure 6-8). When qualitatively analysing the nature of the predicted crack damage patterns, notable differences are observed between low (ψ = 30) and high resolution models, for all energy input values (1 x 10^8 J/m^3_{abs} and 1 x 10^9 J/m^3_{abs}) (see Figure 6-9 and Figure 6-10). At model specimen resolutions 134 or higher, changes in model resolution have no notable effect on both predicted percentage crack damage and microwave crack induced patterns (see Figure 6-7 and Figure 6-8). These results suggests that model specimen resolution cannot be chosen arbitrary when simulating thermal damage. Methods of model calibration using the usual simulated UCS and Brazilian tests alone are not adequate to produce models that can give a reasonable prediction of the expected microwave thermal damage from real ores.

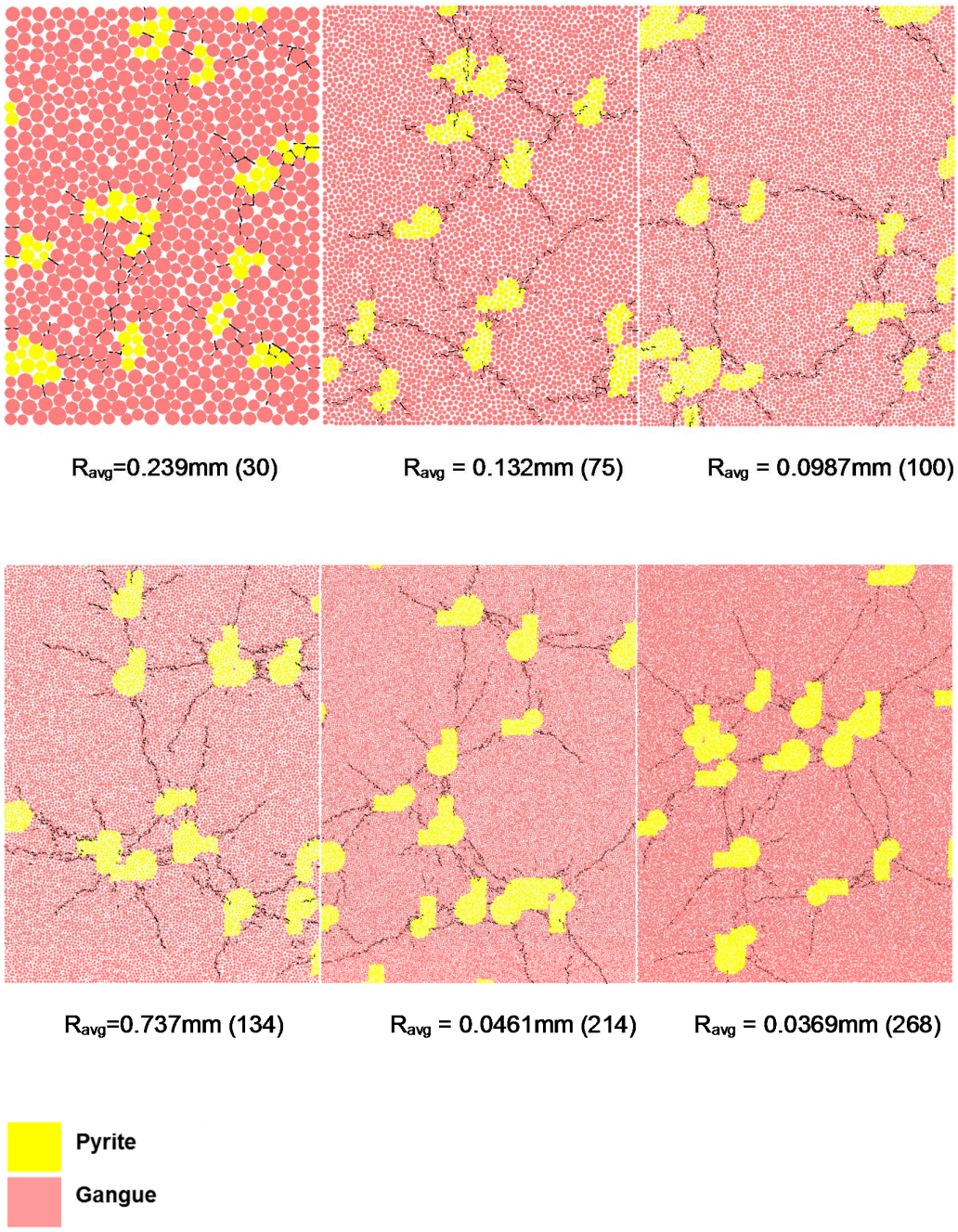

Figure 6-9: Crack patterns at different model average particle size (resolution) in Pyrite Quartz specimen at an exposure time of 0.01 seconds (power density of 1 x 10^{10} W/m^3_{abs})

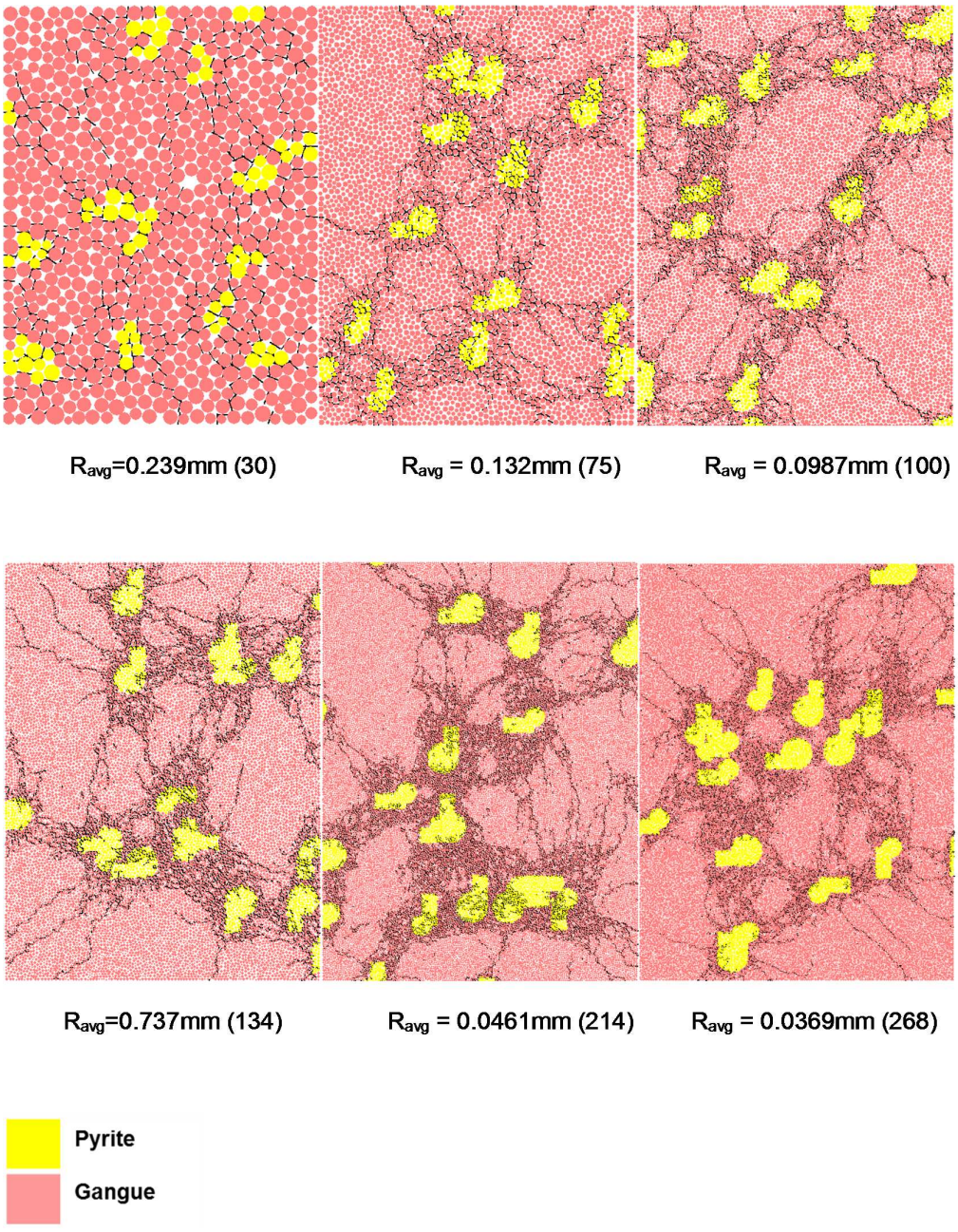

Figure 6-10:Crack patterns at different model average particle size (resolution) in Pyrite Quartz specimen at an exposure time of 0.1 seconds (power density of 1 x 10^{10} W/m^3_{abs})

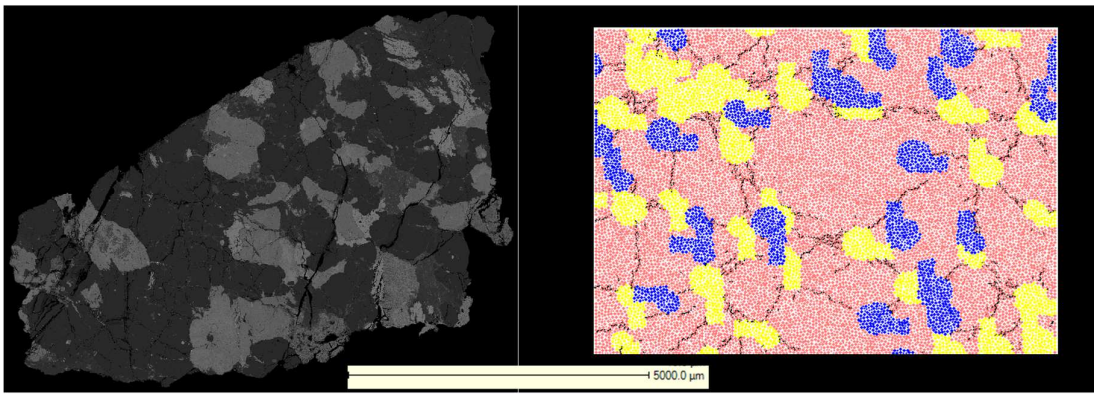

Figure 6-11: Left 2D XCT image of a microwave treated 16 mm sphalerite particle, right 15 by 20 mm pyrite quartz specimen (ψ = 214)

The simulated crack damage at different model resolutions were compared against those observed from the physical experiments measured using XCT carried out in this study, at similar energy input values (1 x 10^9 J/m^3_{abs}). It can be concluded based on the comparison that high resolution models ($\psi \geq 134$) give a better prediction of microwave induced crack patterns compared to lower model resolution (see Figure 6-11). At very low model resolution the predicted crack pattern distribution does not appear similar to crack patterns observed in physical particles. It is therefore suggested that a model resolution should be selected that gives a simulated crack pattern distribution that is similar to cracks observed in microwave treated real ores when simulating microwave induced damage. A priori model specification is difficult, as there is limited experimental data of microwave induced crack patterns. This challenge could be overcome by choosing a model resolution that lies in the range of model resolution values where variation in resolution does not affect predicted crack damage, because in this region predicted crack patterns match those observed in real ores.

Results of this study suggest that model resolution in PFC has a significant effect on simulated microwave induced damage and crack pattern distribution. The quantitative prediction of microwave induced crack damage in ores, under different microwave treatment conditions is important, as it allows for the design of better microwave treating applicators and for the assessment of potential process benefits of microwave heating different ores. The use of modelling to predict the nature of microwave induced crack patterns is also equally important as it allows for BPM to be used in predicting the degree of enhanced mineral exposure and liberation for different ores. It is therefore important that both the qualitative and quantitative predictions of microwave treatment response of ores using modelling techniques be as accurate as possible.

6.3.4. Conclusion

This study has shown that simulated rock model specimen resolution has an influence on the predicted microwave treatment response of ores under different microwave treatment conditions. The most notable effect of model resolution is on the prediction of the percentage crack damage. A comparison of the predicted crack damage for different model resolution shows that in PFC^{2D} low model resolution ($\psi \leq 75$) percentage crack damage predictions are at least 20% and 12 % higher than those predicted by higher resolution models ($\psi \geq 75$) at microwave energy input values of 1 x 10^8 J/m^3_{abs}.and 1 x 10^9 J/m^3_{abs} respectively. These results show that high resolution models ($\psi \geq 134$) give a better prediction of microwave induced crack patterns compared to low model resolution. Notable differences were observed between low ($\psi = 30$) and high resolution models, predicted crack patterns. It can be concluded based on these results that model resolution has an effect on BPM system behaviour and care should be taken in selecting minimum model particle sizes. When predicting the microwave treatment response of materials, model specimen resolution cannot be chosen arbitrarily. It is suggested that the choice of model resolution should be made after determining a range of model resolution values between which there are no notable variations in predicted crack damage, because in this region predicted crack patterns match those observed in real ores.

6.4.Effects of absorbent phase on crack damage

6.4.1. Introduction

Ore particles during microwave treatment are expected to have varying absorbent phase content. The influence of absorbent phase content variation on the extent of microwave induced damage is not well understood. Previous studies have shown that grain texture has a significant influence on the extent of microwave damage (Ali and Bradshaw, 2010). These studies investigating microwave induced damage were carried out on simulated binary ore with a fixed absorbent phase content at low model resolution values (ψ = 30) (where ψ calculated from Equation 6-15). Results from the previous section have shown how model resolution influences predicted microwave treatment response of materials, such as predicted percentage crack damage and microwave induced crack patterns. High resolution models ($\psi \geq 134$) gave a better prediction of microwave induced crack damage and crack patterns.

This section presents results of simulations carried out using a high resolution model (ψ = 214) ternary sulphide ore having textures and mineralogy similar to the ore used in the experimental study presented in chapter 4. The simulated ore was exposed to microwaves at different microwave treatment conditions. The aim was to investigate in detail the effect of power density, exposure time and absorbent phase content on the extent of microwave induced damage and fracture pattern in the sulphide ore used in the physical experiments. Damage maps which show percentage of micro-fractures as a function of power density and exposure time for different microwave absorbent phase content values in the ore were constructed. This was done so as to provide guidelines concerning the microwave treatment operating conditions for microwave applicators and to determine how these design parameters are affected by absorbent phase content variation. The intention of this part of the work was to provide design target and operating conditions for current and future industrial microwave applicators.

6.4.2. Methodology

In total, five different ternary ore models were investigated with different absorbing phase material. The model materials were produced by using the material genesis procedure in *PFC* as discussed in section 6-1. Different irregular shaped absorbent phase (sphalerite/pyrite) grains were randomly disseminated in a transparent matrix (quartz). The six ore models were assigned different absorbent mineral composition of 9%, 19%, 33%, 47% and 55% with the remainder being microwave transparent phase by volume. The ore models contained pyrite,

sphalerite and quartz with the proportion of sphalerite/pyrite absorbing phase in each ore model being similar to that in Table 6-9.

Table 6-10 is a summary of the bulk mineralogy of the ore used in the experimental investigation in this study. The total particle size was 15×20 mm. Each ternary ore, had coarse absorbent grains (grain size = 1 - 2.5 mm)**.** Each ore was then exposed to microwaves at different power densities ranging from $1 \times 10^9 W/m^3$ to $1 \times 10^{11} W/m^3$. The construction of the damage maps was made as follows. First, each ore model was treated at different power densities ranging from 1×10^9 W/m^3_{abs} to 1×10^{11} W/m^3_{abs} and range of exposure time between 10^{-3} to 10^0 s, giving energy inputs between 1×10^8 J/m^3_{abs} and 1×10^9 J/m^3_{abs}. These power density values were chosen to represent the power density in the 6 kW source, 2.45GHz single-mode applicator used in the physical experiments presented in this study. The number of micro-cracks at each treatment condition was then quantified. Crack damage was calculated as percentage of bonds broken due to microwaves treatment (Equation 6-21).

Table 6-9: Summary of the bulk mineralogy of the ore used in the experimental investigation in this study

Mineral	Weight %	Microwave treatment response
Pyrite	39%	Heats readily classified as absorbing phase
Sphalerite	16%	Difficult to heat classified as absorbing phase
Quartz	46%	Does not heat classified as transparent phase
Total	100%	

Table 6-10: Mineralogy of the five models used in the investigation

Mineral	Weight %				
Ore model	1	2	3	4	5
Pyrite	6%	13%	23%	33%	39%
Sphalerite	3%	6%	10%	14%	16%
Quartz	91%	81%	67%	53%	45%
Total	100%	100%	100%	100%	100%

6.4.3. Results and discussion

Statistical analysis was carried out to determine if the absorbent phase content in ore model had a significant effect on crack damage. Each ore model was microwave treated at different power densities and exposure times and the crack damage value were calculated for each treatment condition. This was repeated for all ore models, a total of 100 different microwave treatment conditions were considered. Crack damage was considered the dependant variable in the analysis. A repeated measures ANOVA statistical analysis was used to test the hypothesis

that there are no differences between the mean crack damage values of the different ore models, at a significance level of 0.05. Detailed statistical analysis results are presented in Appendix F. Based on the statistical analysis results it was concluded that there is a statistically significant difference in crack damage with changes in absorbent phase. Figure 6-12 shows an increasing trend in the crack damage with increasing absorbent phase (power density of $1 \times 10^{10} W/m^3_{abs}$.). To further determine if there was a significant variation between the individual mean values for each ore model the Benferroni test was applied. The results of the test shows that there is no significant difference in mean crack damage values between the ore models with absorbent phase values of 47% and 55%.

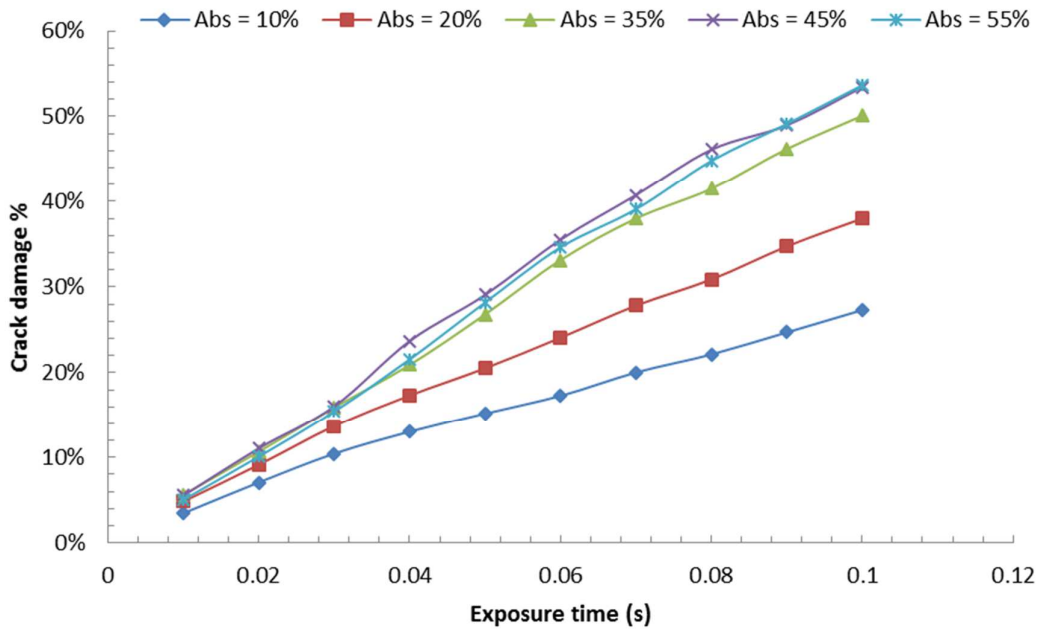

Figure 6-12: Crack damage as a function of exposure time for the different ore models with varying absorbent phase content (Abs %)(power density of 1 x 10^{10} W/m^3_{abs})

Since the only difference between the ore models is the amount of microwave absorbent phase content, the variation in crack damage observed between the different ore models is due to differences in microwave absorbent phases (Figure 6-12). Since the driving force for bond breakage is the strong tensile stresses at the grain boundary of the absorbent phase. Increasing the absorbent phase content leads to an increase in the grain boundary specific surface area. Since microwave induced cracks initiate at the grain boundaries where tensile stresses are generated due thermal expansion of the microwave absorbing phase (Ali and Bradshaw, 2010; Wang and Djordjevic, 2014). An increase in boundary area will lead to an increase in crack

initiation sites and therefore crack damage. As the surface area of the absorbent phase grain increases to above 47% the rate of increase in crack damage with absorbent phase decreases (Figure 6-12). This is due to limited number of parallel bonds available for breakage at higher absorbent phase content. Since crack propagation follows regions in which the bond strength is lower.

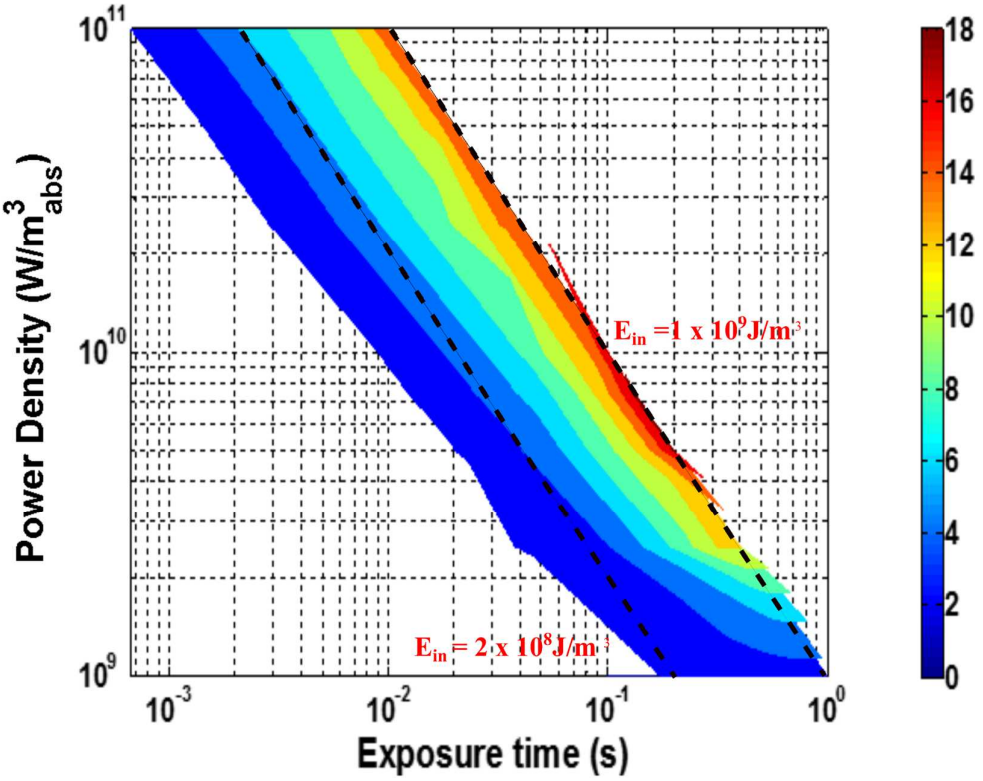

Figure 6-13: Damage map in terms of percentage crack damage for coarse-grained sulphide ore with 9% microwave absorbent phase content

Figure 6-13 shows the damage map for coarse-grained sulphide ore with 9% microwave absorbent phase content. Contours of constant microwave energy input are highlighted on the plot, at values of 2 $\times 10^8$ J/m$^3_{abs}$ and 1 $\times 10^9$ J/m$^3_{abs}$. Analysing the trend in percentage crack damage, over the two highlighted energy input contours, shows that the damage contours are parallel to the microwave energy input contours (Figure 6-13). This trend changes at the bottom of the damage plot, in the region between power densities 1 $\times 10^9$ W/m$^3_{abs}$ to 4 $\times 10^9$ W/m$^3_{abs}$. In this region the damage contours cut across the energy input contours. When microwave treating ores under conditions where the damage contours are parallel to the energy input contour (e.g. shorter exposure, high power densities), increasing the power density at constant energy input, will not result in an increase in crack damage (Figure 6-13). For conditions falling the region where the damage contour cuts across the energy input contours, increasing the

power density at constant energy input, will result in increased crack damage. For example, at a constant microwave energy input of 1 $\times 10^9$ J/m$^3_{abs}$ in Figure 6-13, it is possible to increase the crack damage from around 2% to 18% by increasing power density from 1 $\times 10^9$ W/m$^3_{abs}$ to 1 $\times 10^{10}$ W/m$^3_{abs}$ and lowering the exposure time to 0.1 s. Further increasing the power density beyond 1 $\times 10^{10}$ W/m$^3_{abs}$ does not improve the percentage crack damage. At a lower microwave energy input of 2 $\times 10^8$ J/m$^3_{abs}$ increasing the power density above 1$\times 10^9$ W/m$^3_{abs}$, results in an increase in crack damage from around 2% to a maximum of 6% (Figure 6-13). Further increases in power density, do not yield any additional improvements in percentage crack damage.

Analysis of the number of microwave induced cracks in the model ore specimen, at energy inputs 2 $\times 10^8$ J/m$^3_{abs}$ and 1 $\times 10^9$ J/m$^3_{abs}$, further highlights the observed trend in percentage crack damage with varying power density along the constant energy contours. Figure 6-14 shows that at an energy input of 2 $\times 10^8$ J/m$^3_{abs}$, increasing power density from 1$\times 10^9$ W/m$^3_{abs}$ to 1 $\times 10^{10}$ W/m$^3_{abs}$ results in over a 100% increase in the number of cracks. Increasing the power density further from 1 $\times 10^{10}$ W/m$^3_{abs}$ to 1 $\times 10^{11}$ W/m$^3_{abs}$ increases the number of cracks by 34%. At energy input 1 $\times 10^9$J/m$^3_{abs}$ increasing power density from 1 $\times 10^9$ W/m$^3_{abs}$ to 1 $\times 10^{10}$ W/m$^3_{abs}$ results in over a 400% increase in the number of cracks (Figure 6-15). However, increasing the power density further from 1 $\times 10^{10}$ W/m$^3_{abs}$ to 1 $\times 10^{11}$ W/m$^3_{abs}$ does not result in any increase in the number of cracks. The number of cracks observed at a power density of 1 $\times 10^{11}$ W/m$^3_{abs}$ (4757 cracks), 13% lower than the number of cracks observed at a power density of 1 $\times 10^{10}$ W/m$^3_{abs}$ (5445 cracks) for the same energy input. This suggest that the optimal conditions for microwave treating the modelled sulphide ore (9% absorbent phase), at energy input of 1 $\times 10^9$J/m$^3_{abs}$ lies at a power density closer to 1 $\times 10^{10}$ W/m$^3_{abs}$ and exposure time of 0.01 as shown on the damage plot (Figure 6-13). Beyond this power density no further increases in microwave induced cracks would be obtained.

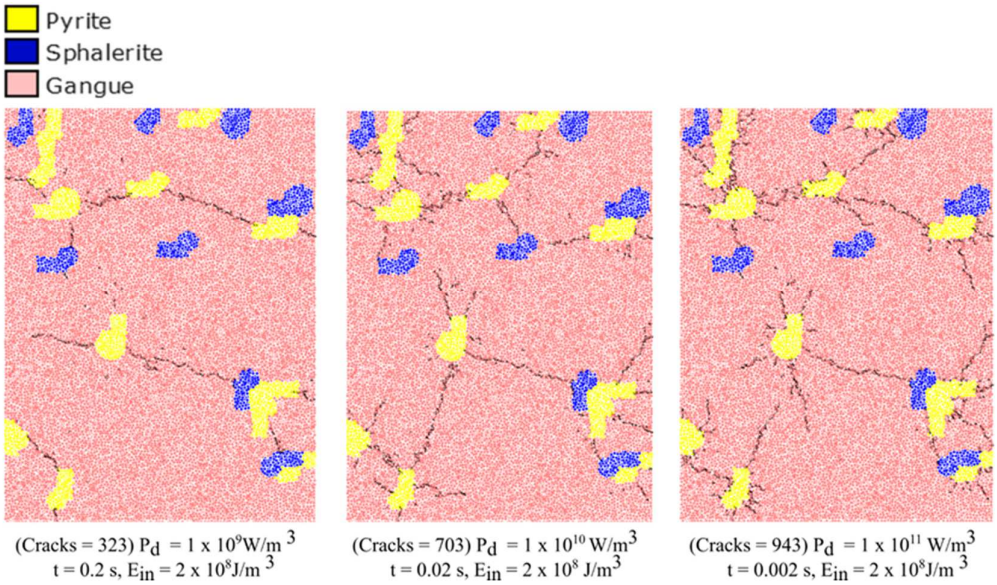

Figure 6-14: Microwave induced crack damage in coarse-grained sulphide ore with 9% microwave absorbent phase content (energy input 2 ×10^8 J/m^3_{abs})

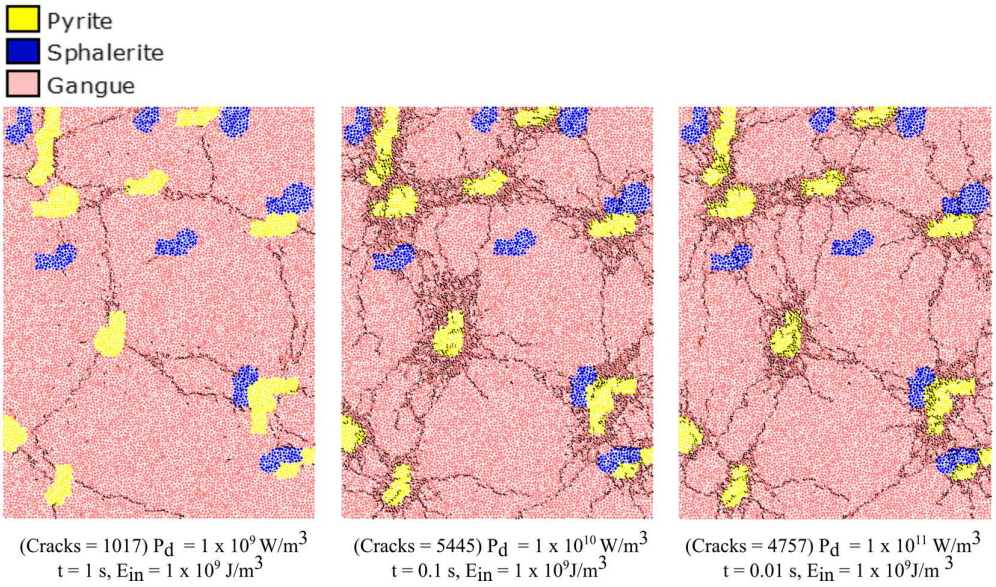

Figure 6-15: Microwave induced crack damage in coarse-grained sulphide ore with 9% microwave absorbent phase content (energy input 1 ×10^9 J/m^3_{abs})

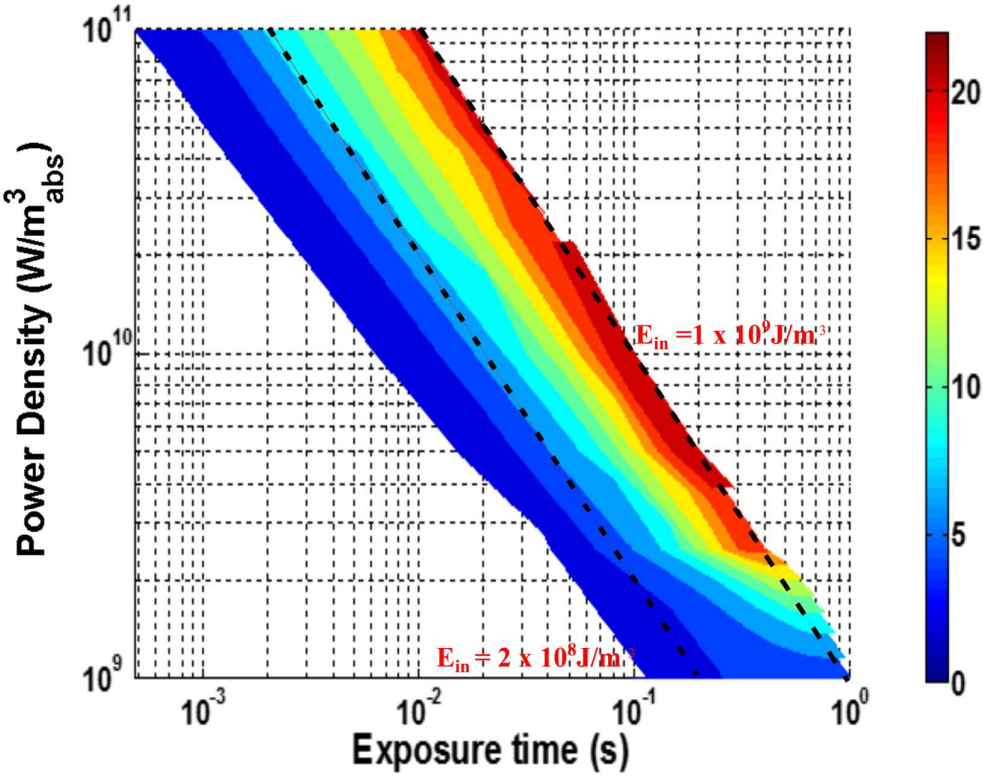

Figure 6-16: Damage map in terms of percentage crack damage for coarse-grained sulphide ore with 19% microwave absorbent phase content

Figure 6-16 shows the damage plot for coarse-grained sulphide ore with 19% microwave absorbent phase content. For a microwave energy input of 2×10^8 J/m$^3_{abs}$, at a power density of 1×10^9 W/m$^3_{abs}$, around 3% crack damage is observed. However, increasing the power density from 1×10^9 W/m$^3_{abs}$ to 3×10^9 W/m$^3_{abs}$, there is an increase in crack damage from around 3% around 7% (for the same energy input), further increasing the power density at this energy input, results in an increase in crack damage from 7% to around 9%. The improvement in crack damage from increasing power density is small. However, at a higher energy input 1×10^9 J/m$^3_{abs}$, at a power density of 1×10^9 W/m$^3_{abs}$, around 5% crack damage is observed (Figure 6-16). It can be seen that increasing the power density up to 1×10^{10} W/m$^3_{abs}$ results in an increase in crack damage from 5% to over 20%. Above 1×10^{10} W/m$^3_{abs}$, increasing the power density, does not yield any additional improvements in crack damage.

Comparing damage plots for ore models with absorbent phase 9% and 19%, (see Figure 6-13 and Figure-6-16), shows that microwave treating ores with high absorbent phase content, produces greater crack damage for the same energy input (2×10^8 J/m$^3_{abs}$ and 1×10^9 J/m$^3_{abs}$). For example, analysing the amount of microwave induced cracks, for the ore model with 19%

absorbent phase content, at energy input 2 ×10^8 J/m^3_{abs}, shows that at a power density of 1 ×10^9 W/m^3_{abs} and exposure time of 0.2 s produces 564 cracks (see Figure 6-17). Increasing power density from 1 ×10^9 W/m^3_{abs} to 1 ×10^{10} W/m^3_{abs} results in an increase in number of microwave induced cracks from 564 to 998 cracks. Increasing the power density further from 1 ×10^{10} W/m^3_{abs} to 1 ×10^{11} W/m^3_{abs} increases the number of cracks by 30% only. The amount of cracks produced at energy input (2 ×10^8 J/m^3_{abs} and 1 ×10^9 J/m^3_{abs}) are higher when compared to those produced for the ore model with 9% absorbent phase content (see Figure 6-14 and Figure 6-15). At an energy input 1 ×10^9 J/m^3_{abs} and a power density of 1 ×10^9 W/m^3_{abs}, 1414 cracks are formed, increasing power density from 1 ×10^9 W/m^3_{abs} to 1 ×10^{10} W/m^3_{abs} results in an increase crack damage from 1414 cracks to 8014 cracks (see Figure 6-18).. The extent of microwave crack damage at a power density of 1 ×10^{10} W/m^3_{abs} (8014 cracks) is greater than that obtained at a higher power density of 1 ×10^{11} W/m^3_{abs} (6735 cracks) for the same energy input (see Figure 6-18). This suggests that power densities close to 1 ×10^{10} W/m^3_{abs} (energy input of 1 ×10^9 J/m^3_{abs}), offer the most optimum conditions for inducing cracks in sulphide ores with absorbent phase content similar to the modelled ore (19% absorbent phase content).

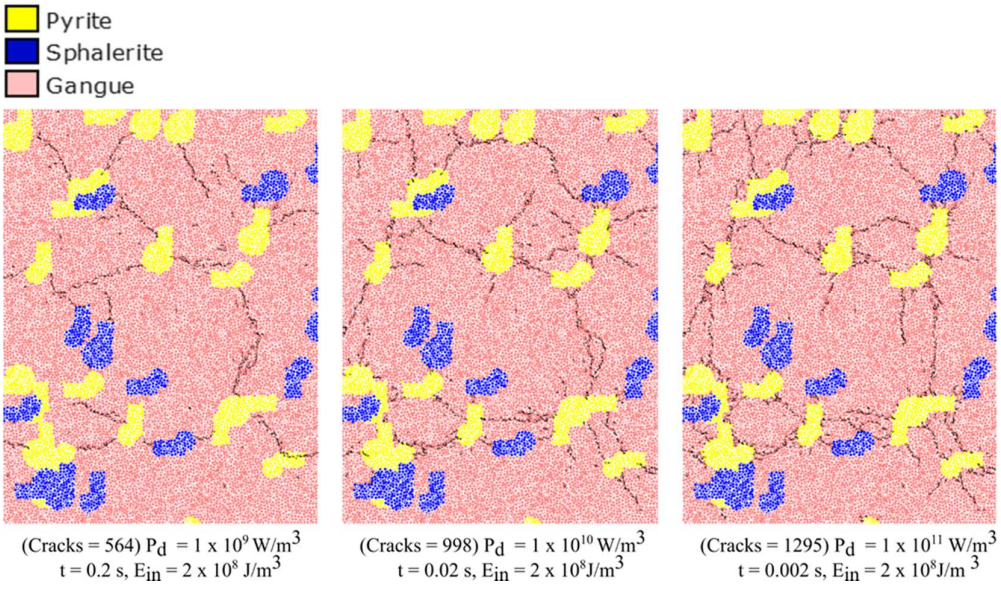

Figure 6-17: Microwave induced crack damage in coarse-grained sulphide ore with 19% microwave absorbent phase content (energy input 2 ×10^8J/m^3_{abs})

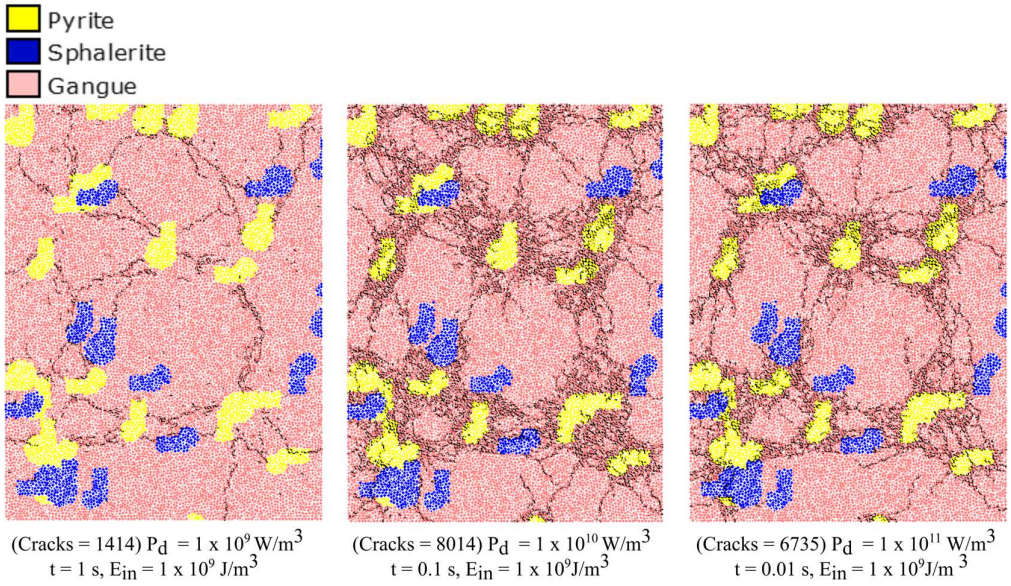

Figure 6-18: Microwave induced crack damage in coarse-grained sulphide ore with 19% microwave absorbent phase content (energy input 1×10^9J/m^3_{abs})

Figure 6-19 shows the damage map for coarse-grained sulphide ore with 33% microwave absorbent phase content. For a microwave energy input of 2×10^8 J/m^3_{abs}, at a power density of 1×10^9 W/m^3_{abs}, no crack damage is observed. However, at higher energy input 1×10^{10} J/m^3_{abs}, at a power density of 1×10^9 W/m^3_{abs}, about 5% crack damage is observed. Increasing the power density from 1×10^9 W/m^3_{abs} to 1×10^{10} W/m^3_{abs} at energy input 1×10^9 J/m^3_{abs} results in crack damage increasing from around 5% to 30%.

Comparing the damage plot for ore models with 9%, 19% and 33% absorbent phase content suggests that the minimum power density required to induce crack damage, at low energy input (2×10^8 J/m^3_{abs}) is greater for higher absorbent phase ores. For example analysing the amount of microwave induced cracks, at energy input 2×10^8 J/m^3_{abs}, for ore model with 33% absorbent phase, shows that at a power density of 1×10^9 W/m^3_{abs} and exposure time of 0.2 s no cracks are formed (see Figure 6-19). In contrast for ore models with 9% and 19% absorbent phase, crack damage is observed at the same energy (2×10^8 J/m^3_{abs}) input and power density (1×10^9 W/m^3_{abs}). This suggests microwave treating ores with high absorbent phase at low energy inputs requires, high power microwaves ($\geq1\times10^9$ W/m^3_{abs}) to observed microwave induced crack damage.

Analysing the amount of microwave induced cracks, at energy input 2×10^8 J/m^3_{abs}, shows that as power density increases from 1×10^9 W/m^3_{abs} to 1×10^{11} W/m^3_{abs}, the amount of cracks induced increases from zero to 1672 (see Figure 6-20). At a higher energy input 1×10^{10} J/m^3_{abs}, increasing power density above 1×10^{10} W/m^3_{abs} does not result in improved crack

damage (see Figure 6-21). At a power density of 1 $\times 10^{11}$ W/m$^3_{abs}$, lesser crack damage is observed compared to a power density of 1 $\times 10^{10}$ J/m$^3_{abs}$, at energy input 1 $\times 10^{10}$ J/m$^3_{ab}$ (see Figure 6-21).

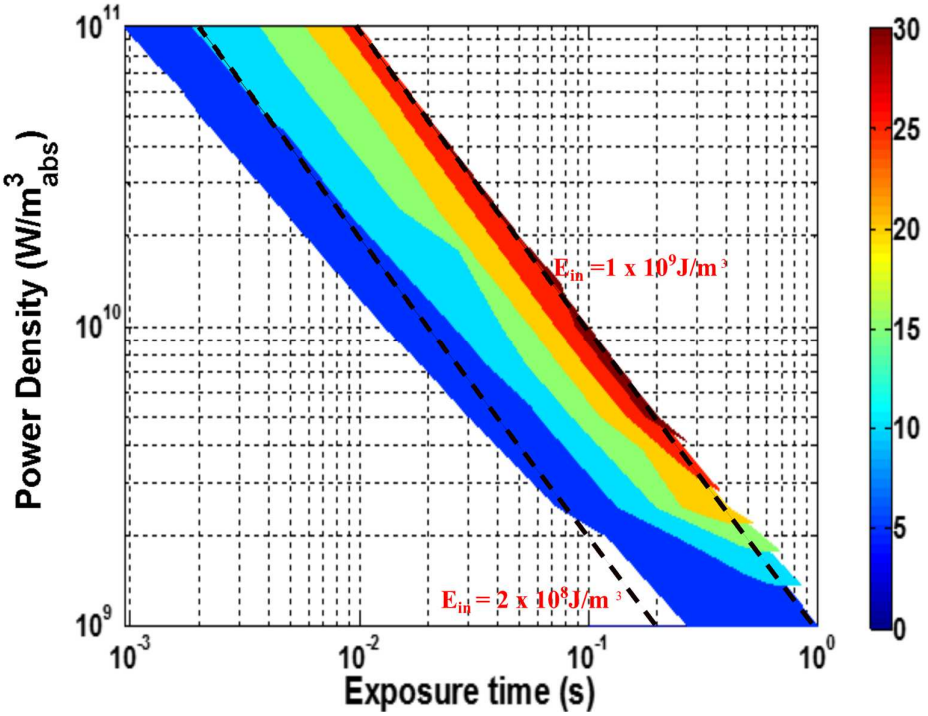

Figure 6-19: Damage map in terms of percentage crack damage for coarse-grained sulphide ore with 33% microwave absorbent phase content

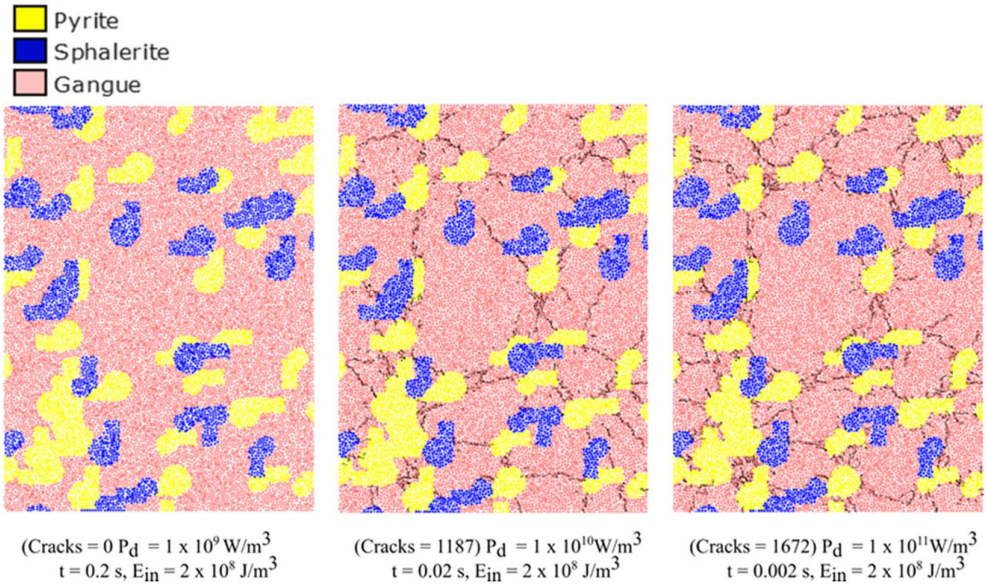

Figure 6-20: Microwave induced crack damage in coarse-grained sulphide ore with 33% microwave absorbent phase content (energy input 2 $\times 10^8$J/m$^3_{abs}$)

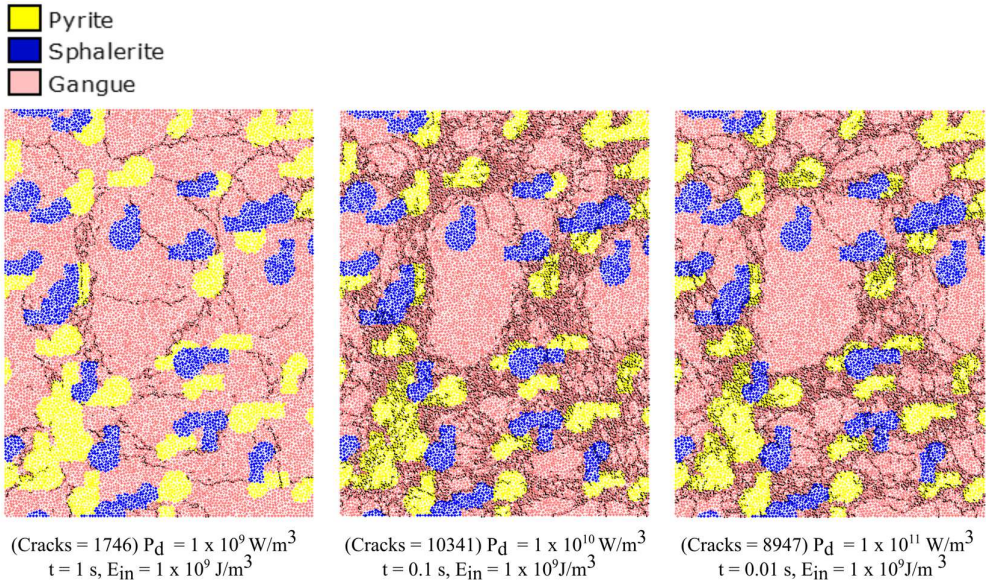

Figure 6-21: Microwave induced crack damage in coarse-grained sulphide ore with 33% microwave absorbent phase content (energy input 1 ×10^9 J/m^3_{abs})

Figure 6-22 shows the damage map for coarse-grained sulphide ore with 47% microwave absorbent phase. For a microwave energy input of 2 ×10^8 J/m^3_{abs}, at a power density of 1 ×10^9 W/m^3_{abs}, no crack damage is observed. However, increasing the power density from 1 ×10^9 W/m^3_{abs} to above 2 ×10^9 W/m^3_{abs} results in crack damage of around 7% (for the same energy input). Further increasing the power density (from 1 ×10^{10} W/m^3_{abs} to 1 ×10^{11} W/m^3_{abs}) at this energy input, does not results in increased percentage crack damage from 7% to around 13% (see Figure 6-22).

At higher energy input 1 ×10^{10} J/m^3_{abs}, at a power density of 1 ×10^9 W/m^3_{abs}, 5% crack damage is observed. It can be seen that increasing the power density up to 1 ×10^{10} W/m^3_{abs} results in an increase in percentage crack damage, from 5 % to a maximum of 40% crack damage. However, at power densities above 1 ×10^{10} W/$m^3_{abs,}$ increasing the power density, does not yield additional improvements in crack damage (see Figure 6-22). This general trend is similar to that observed for ores with percentage absorbent phase content 9%, 19% and 33% at the same energy input (see Figure 6-16 and Figure 6-19).

Analysis of the number of microwave induced cracks in the model ore specimen, at energy input 2 ×10^8 J/m^3_{abs} and 1 ×10^9 J/m^3_{abs} further highlights the observed trend in percentage crack damage with varying power density, along the constant energy contours. For low energy input 2 ×10^8 J/m^3_{abs} the number of cracks increases with increasing power density (see Figure 6-23). At higher energy input 1 ×10^9 J/m^3_{abs} increasing the power density, results

in more cracks up to a power density of 1 ×10^{10} W/m^3_{abs}, further increasing power density does not yield any benefits in crack damage (see Figure 6-24).

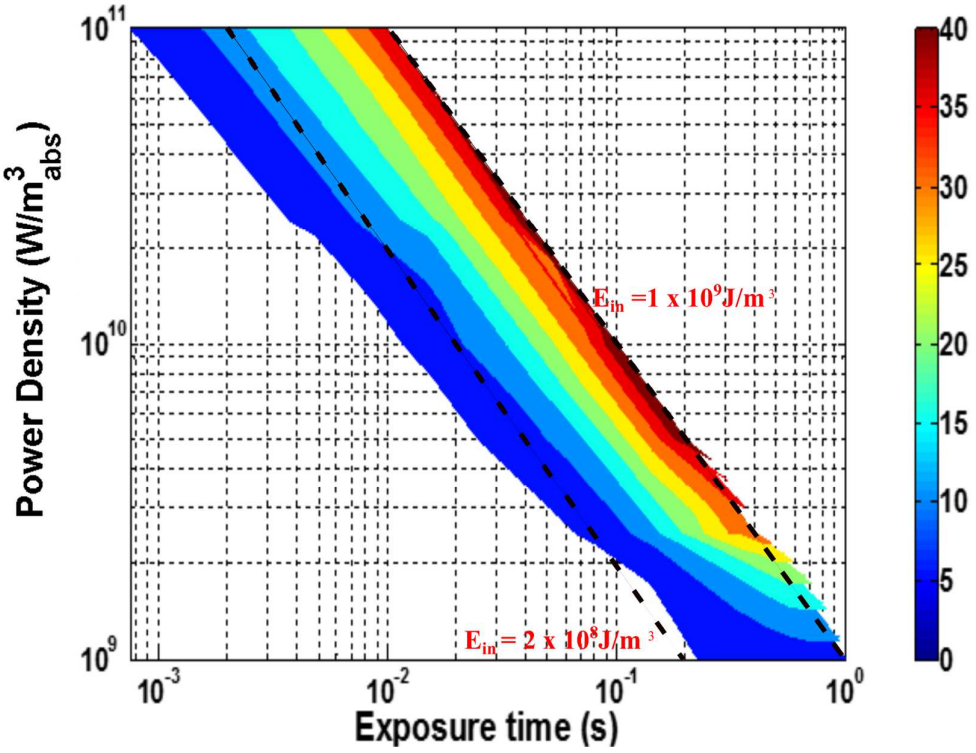

Figure 6-22: Damage map in terms of percentage crack damage for coarse-grained sulphide ore with 47% microwave absorbent phase content

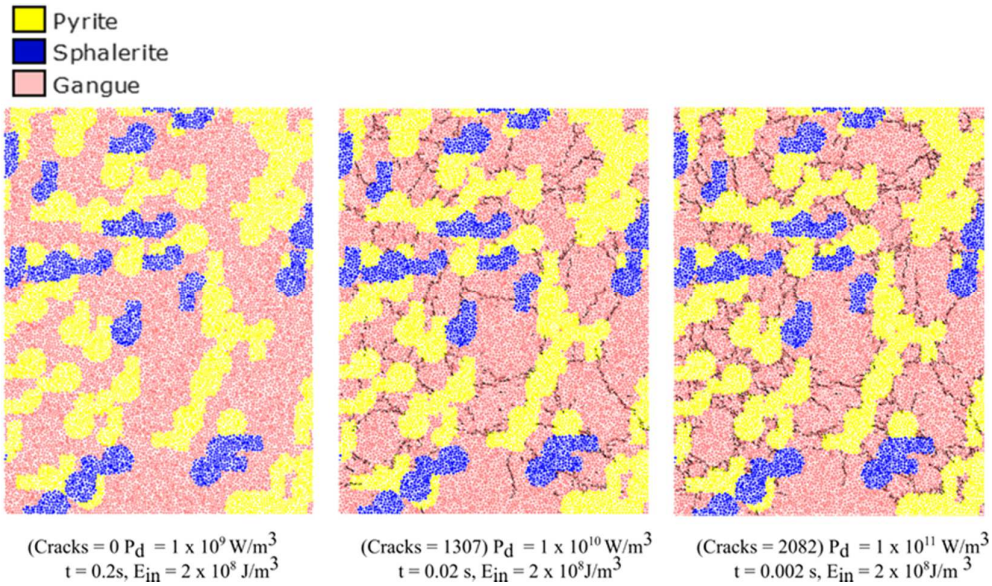

Figure 6-23: Microwave induced crack damage in coarse-grained sulphide ore with 47 % microwave absorbent phase content (energy input 2 ×10^8 J/m^3_{abs})

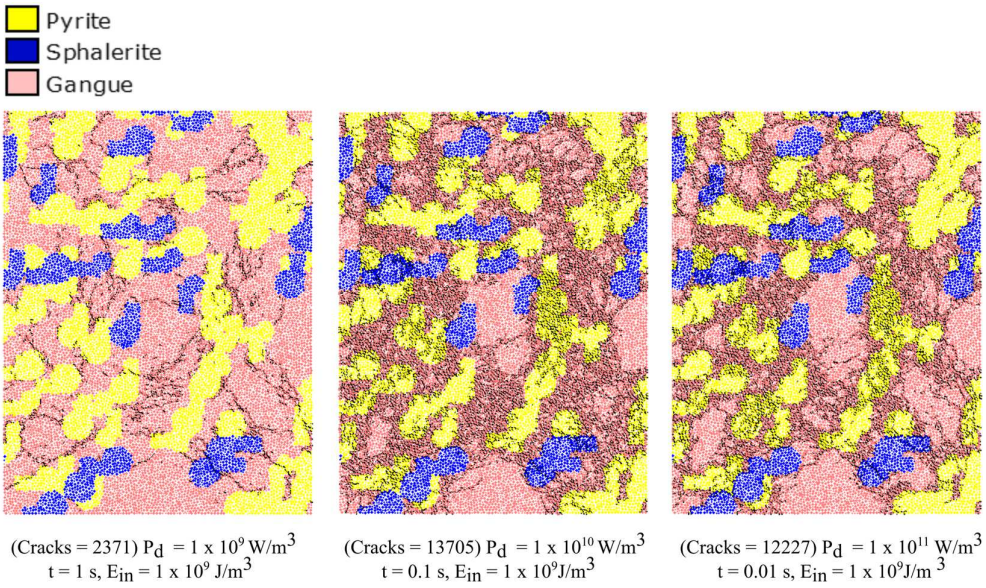

Figure 6-24: Microwave induced crack damage in coarse-grained sulphide ore with 47% microwave absorbent phase content (energy input 1 ×10^9J/m^3_{abs})

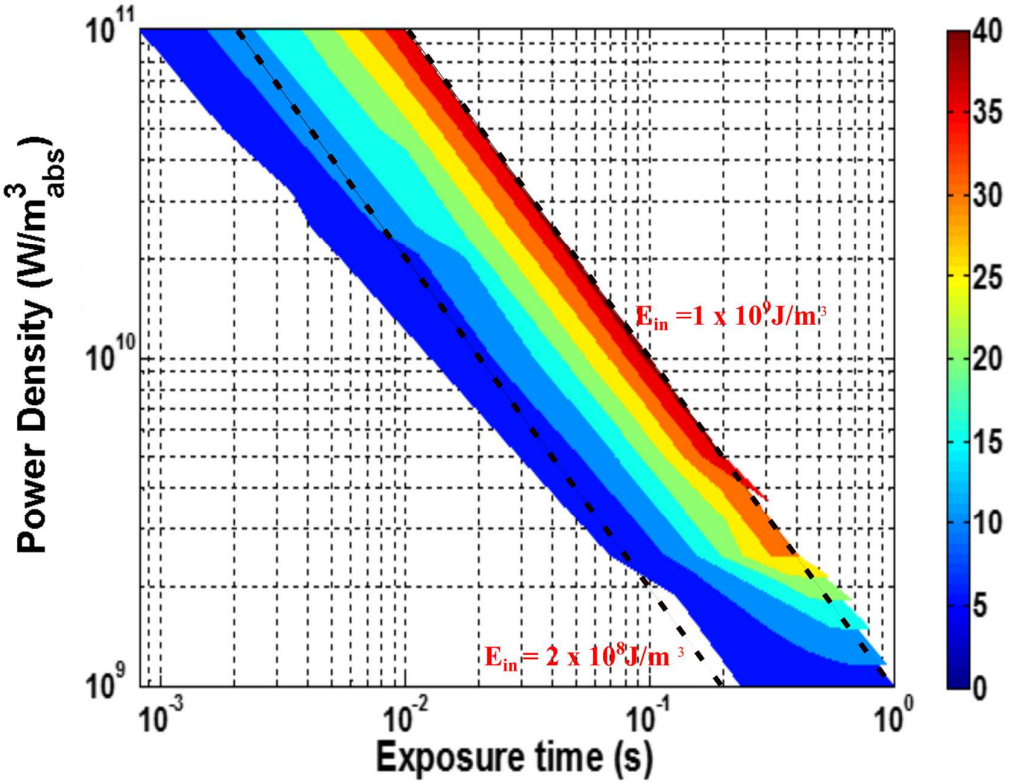

Figure 6-25: Damage map in terms of percentage crack damage for coarse-grained sulphide ore with 55% microwave absorbent phase content

Figure 6-25 shows the damage map for coarse-grained sulphide ore with 55 % microwave absorbent phase content. For a microwave energy input of 2 $\times 10^8$ J/m$^3_{abs}$, at a power density of 1 $\times 10^9$ W/m$^3_{abs}$ no crack damage is observed. However, increasing the power density from 1 $\times 10^9$ W/m$^3_{abs}$ to above 2 $\times 10^9$ W/m$^3_{abs}$ results in crack damage of around 7% (for the same energy input). Further increasing the power density (from 1 $\times 10^{10}$ W/m$^3_{abs}$ to 1 $\times 10^{11}$ W/m$^3_{abs}$) results in an increase in crack damage from 7% to 15% (see Figure 6-25). At higher energy input 1 $\times 10^{10}$ J/m$^3_{abs}$, at a power density of 1 $\times 10^9$ W/m$^3_{abs}$, a 5% crack damage is observed. Increasing the power density up to 1 $\times 10^{10}$ W/m$^3_{abs}$ results in an increase in percentage crack damage from 5 % to a maximum of 40%. However, at power densities above 1 $\times 10^{10}$ W/m$^3_{abs}$, increasing the power density, does not yield additional improvements in crack damage. The damage plot shows a similar trend to that obtained for the 47 % absorbent phase model, at the same energy inputs.

Analysis of the number of microwave induced cracks in the model ore specimen with 55% absorbent phase, at energy input 2 $\times 10^8$ J/m$^3_{abs}$ and 1 $\times 10^9$ J/m$^3_{abs}$ further highlights the observed trend in percentage crack damage with varying power density, along the constant energy contours. For low energy input 2 $\times 10^8$ J/m$^3_{abs}$ the number of cracks increases with increasing power density (see Figure 6-26). At higher energy input 1 $\times 10^9$ J/m$^3_{abs}$ increasing the power density, results in more cracks up to a power density of 1 $\times 10^{10}$ W/m$^3_{abs}$, further increasing power density does not yield any benefits in crack damage (see Figure 6-26). These results suggest that above a certain limit increasing power density does not yield in significant increases in microwave induced cracks. The observed trend crack damage variation at energy inputs 2 $\times 10^8$ J/m$^3_{abs}$ and 1 $\times 10^9$ J/m$^3_{abs}$ is similar to that observed for ore with 33% and 47% absorbent phase content (see Figure 6-19 and Figure 6-22). For example Figure 6-29 shows that at a power density of 1 $\times 10^9$ W/m$^3_{abs}$ and energy input of 2 $\times 10^8$ J/m$^3_{abs}$ 2350 cracks were induced increasing the power density to 1 $\times 10^{10}$ W/m$^3_{abs}$ at the same input results in a substantial increase in cracks up to 13262. Further increases in power density yields lower amount of cracks (12628).Analysis of the amount of microwave induced cracks in the ore model, at energy inputs of 2 $\times 10^8$ J/m$^3_{abs}$ and 1 $\times 10^9$ J/m$^3_{abs,}$ shows that for low energy input 2 $\times 10^8$ J/m$^3_{abs}$ the number of cracks increase (0 to 1941 cracks) with increasing power density (see Figure 6-26).

Figure 6-26 shows a comparison in crack pattern between modelled crack damage and experimentally QEMSCAN measured crack damage (1 $\times 10^9$ J/m$^3_{abs}$, exposure time 1.0 s), of the sulphide ore used in the study. The model ore shows greater preferential phase breakage compared to the experimental results. However, comparing the experimental results against a

model ore treated at similar conditions shows that model compares well with the experimentally observed crack pattern (see Figure 6-27). Crack patterns at power densities above 1 $\times 10^{10}$ W/m$^3_{abs}$ at energy input 1 $\times 10^9$ J/m$^3_{abs}$, show more trans-granular cracks however, the crack patterns are not well defined.

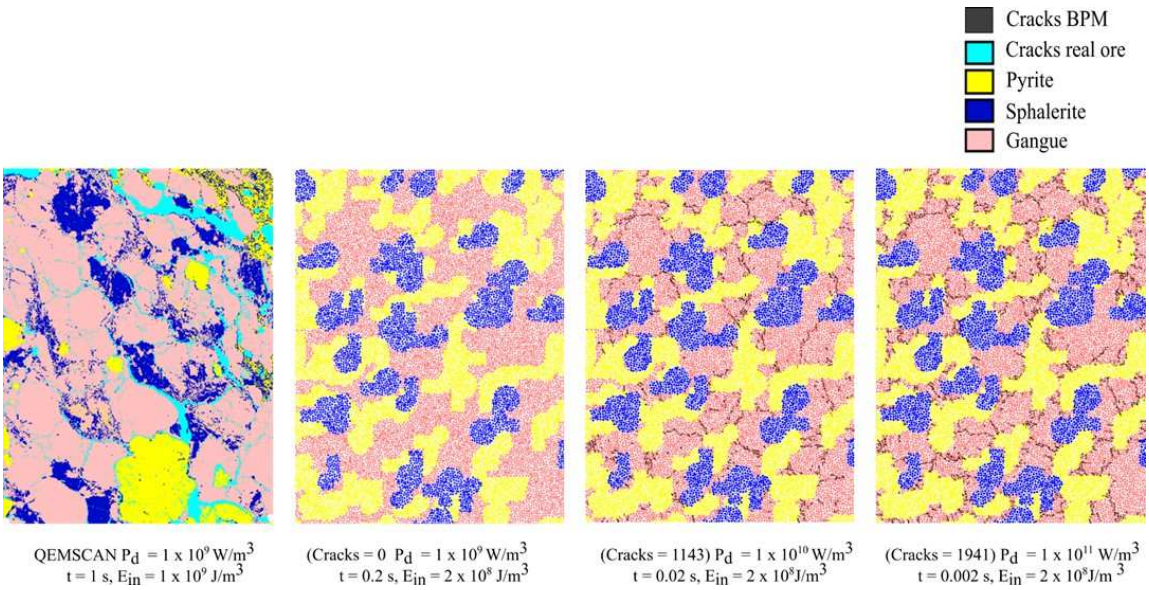

Figure 6-26: Microwave induced crack damage in coarse-grained sulphide ore with 55% microwave absorbent phase content (energy input 1 $\times 10^8$J/m$^3_{abs}$)

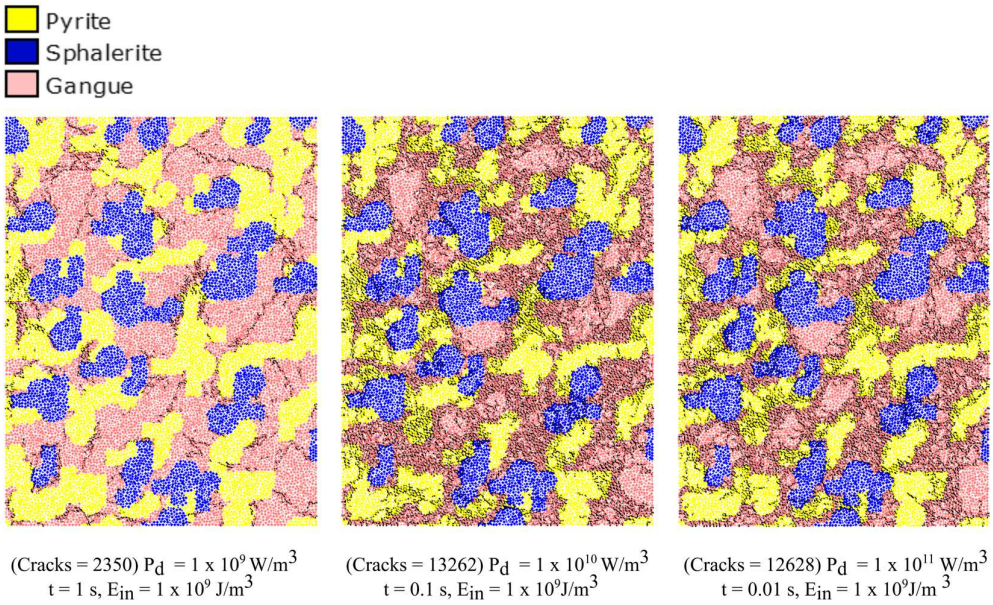

Figure 6-27: Microwave induced crack damage in coarse-grained sulphide ore with 55% microwave absorbent phase content (energy input 1 $\times 10^9$J/m$^3_{abs}$)

Table 6-11: Summary of the trend in crack damage at different power densities and energy input (2×10^8 J/m$^3_{abs}$ and 1×10^{10} J/m$^3_{abs}$), for all the models investigated

Model ore Abs %	Number of cracks at energy input 2×10^8 J/m$^3_{abs}$			Number of cracks at energy input 1×10^9 J/m$^3_{abs}$		
	10^9 W/m$^3_{abs}$	10^{10} W/m$^3_{abs}$	10^{11} W/m$^3_{abs}$	10^9 W/m$^3_{abs}$	10^{10} W/m$^3_{abs}$	10^{11} W/m$^3_{abs}$
9%	323	703	943	1017	5445	4757
19%	564	998	1295	1414	8014	6735
33%	0	1187	1672	1746	10341	8947
47%	0	1307	2082	2371	13705	12227
55%	0	1143	1941	2350	13262	12628

Table 6-11 is a summary of the observed trend in crack damage with increasing absorbent phase at two energy input values, 2×10^8 J/m$^3_{abs}$ and 1×10^9 J/m$^3_{abs}$. The results show that the amount of crack damage, at all energy inputs increases with increasing absorbent phase up to a limit (47%), except at energy input 2×10^8 J/m$^3_{abs}$ and power density 1×10^9 J/m$^3_{abs}$ where no cracks are induced above phase content of 19%. This trend can be explained by analysing the crack patterns at condition of low (2×10^8 J/m$^3_{abs}$) and high (1×10^9 J/m$^3_{abs}$) energy input. Analysis of the fracture pattern at energy input 2×10^8 J/m$^3_{abs}$ for all models shows that the crack patterns at power density 1×10^{10} W/m$^3_{abs}$ and 1×10^{11} W/m$^3_{abs}$ are similar (Figure 6-14, Figure 6-17, Figure 6-20 and Figure 6-23). Cracks appear at a power density of 1×10^9 W/m$^3_{abs}$ only for the model with 9% and 19% absorbent phase content. The cracks do not propagate across the phase boundaries at conditions of low energy input, with boundaries acting as barriers for crack propagation. The cracks observed propagate preferentially in the non-absorbing phase and appear to originate from the absorbent phase grains. The cracks extend radially away from the absorbent phase grains.

The results show that increasing the power density (volumetric heating rate) results in more trans-granular and inter-granular breakage. This is because an increase in power densities results in rapid stress generation, which causes more crack fracture events to take place (Jones et al., 2005; Whittles et al., 2003). As the absorbent phase mineral grain content increases no cracks are induced at low volumetric heating rates (power density, 1×10^9 W/m$^3_{abs}$). This suggests that, minimum power density required to induce cracks at particular energy input, is affected by the amount of absorbent phase present in the ore.

At higher energy input the (1×10^9 J/m$^3_{abs}$) the fracture pattern at power density 1×10^{10} W/m$^3_{abs}$ and 1×10^{11} W/m$^3_{abs}$, are similar. The cracks consist of both grain boundary and trans-granular cracks. While cracks at lower density 1×10^9 W/m$^3_{abs}$ show more evidence of preferential phase breakage with the absorbent grain phase remaining intact. Thus greater trans-granular crack fracture occurs at high power densities. This suggests that at high power

densities microwave treated cracks move at high speeds ignoring obstacles in their path, even though there may be paths of lower resistance resulting in greater formation of trans-granular cracks. A crack moving slowly in a rock (stable propagation) would be expected to exploit grain boundary weaknesses as paths of least resistance, particularly as cracks propagate along grain boundaries at low velocities (Middlemiss, 2007; Wills and Atkinson, 1993).

Cracks observed at power density of 1×10^9 W/m$^3_{abs}$ at an energy input of 1×10^9 J/m$^3_{abs}$ are similar in pattern and relative number to cracks observed at a lower energy input 2×10^8 J/m$^3_{abs}$ and power density 1×10^{11} W/$_{m3abs}$. This confirms previous findings that have shown microwave equipment should be operated at high power densities and short exposure time in order to achieve significant crack damage (Kingman et al., 2004c).

Comparison of the simulated crack patterns for model ore with 33%, 47% and 55% absorbent phase content, at similar treatment conditions used in the experiment, against QEMSCAN images from the physical experimental studies shows similar crack patterns at similar energy input values and exposure times (1×10^9 W/m$^3_{abs}$, 1.0 s) (see Figure 6-28). Both grain boundary and trans-granular granular cracks are visible in the QEMSCAN images of the ores, although the absorbent phase grains appear intact compared to the BPM images. These differences are possibly due the assumptions that are made in developing the BPM model. In developing the model it is assumed that the absorbing phase is evenly heated by the incoming microwave and the power density is zero in the transparent phase. This is a simplistic approach; in reality the absorbent phase contains microwave absorbing impurities. This can have significant influence on crack propagation patterns. In BPM models the absorbent phase grains appear to act as inhibitors to crack propagation for example the crack patterns in Figure 6-28 do not extend into the absorbent grain phase. On the other hand the QEMSCAN images suggest that the propagation of microwave induced cracks is not inhibited by absorbent phase grains with significant trans-granular cracking occurring (Figure 6-28).

Another key assumption that explains some of the small difference in modelled crack patterns against experimentally measured patterns is the assumption of no existing flaws in BPM. Real rocks contain flaws and existing cracks; microwave induced thermal stresses besides generating new cracks can lead to either growth or closure of the aperture of existing cracks. Despite these differences it is evident that BPM ore models are able to simulate major characteristics of microwave induced damage.

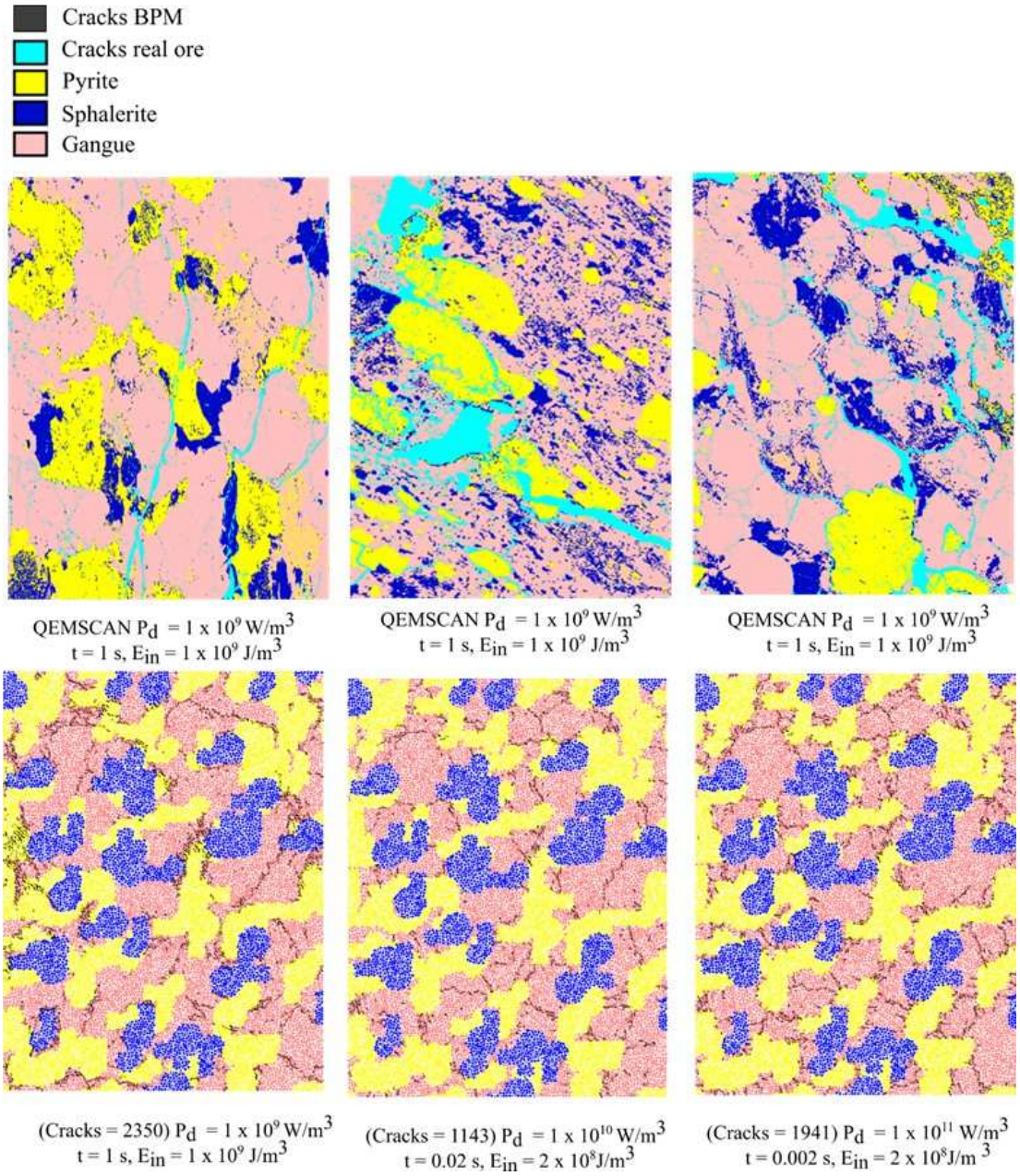

Figure 6-28: Crack damage patterns of QEMSCAN measured microwave treated sphalerite ore particles (top row) and BPM modelled microwave crack patterns at energy input 1 ×10^9J/m^3_{abs}.

The practical implications of results presented in this study is that application of microwave technology in treating coarse-grained sphalerite ore requires the use of microwave treatment equipment with the capacity to produce high power density microwaves (1 ×10^{10} W/m^3_{abs}).This is because very high power densities are required to generate significant crack damage at economic energy inputs. Results of this stud suggest that the application of microwave technology is likely to yield significant crack damage in ores that have a significant portion of absorbent phase mineral grains. The amount of microwave induced cracks and also

the mode of fracture in an ore particle depends, not only the microwave treatment condition but also on the mineralogical characteristics of the ore. Using BPM it is possible to investigate the microwave treatment response of a wide range ores with different mineralogical attributes. Despite the fact that it is difficult to validate quantitatively, model predicted microwave induced crack damage due to difference in defining crack damage in BPM and physical experiments. Qualitative comparison of predicted crack patterns against experimentally measure patterns offers some means of validating BPM models, as has been demonstrated in this study.

6.4.4. Conclusion

Damage maps which show the percentage of crack damage as a function of power density and exposure time for different sulphide ores with varying absorbent phase content were constructed. Comparison of the simulated crack patterns for model ore with 33%, 47% and 55% absorbent phase content, at similar treatment conditions used in the experiment, against QEMSCAN images from the physical experimental studies showed similar microwave induced crack patterns at similar energy input values and exposure times (1×10^9 W/m$^3_{abs}$, 1.0 s). At higher energy input the (1×10^9 J/m$^3_{abs}$) the fracture pattern at power density 1×10^{10} W/m$^3_{abs}$ and 1×10^{11} W/m$^3_{abs}$, were similar, with the cracks consisting of both grain boundary and trans-granular cracks. While cracks at lower density 1×10^9 W/m$^3_{abs}$ showed more evidence of preferential phase breakage with the absorbent grain phase remaining intact. The results showed that the amount of crack damage, at all energy inputs increases with increasing absorbent phase up to a limit (47%) and power density. As the absorbent phase mineral grain content increases no cracks are induced at low volumetric heating rates (power density, 1×10^9 W/m$^3_{abs}$). This suggests the existence of critical power density below which no microwave induced crack damage occurs. This critical power density depends the energy input and the absorbent mineral phase content in the ore particles. It can be concluded based on results from this study that, the extent of microwave induced crack damage and also the mode of fracture in an ore particle depends not only the microwave treatment condition but also on the mineralogical characteristics of the ore.

6.5.Chapter summary

The main aim of this chapter was to present work on developing and validating a BPM for predicting microwave induced damage under different treatment conditions. The investigation was divided into two parts. The first part of the work involved model development, the effects of model resolution (Equation 6) on predicted crack damage were determined. It was shown that model specimen resolution has an influence on the predicted microwave treatment response of ores. The most notable effect of model resolution was on the prediction of the percentage crack damage and crack patterns. It was observed that cracks in different model resolution specimens propagate in a different pattern despite having the same macro-mechanical properties. It was also shown that low model resolution ($\psi \leq 75$) over predicted percentage crack damage at least 20% when compared against high resolution models ($\psi \geq 134$) at microwave energy input 1 x 10^8 J/m^3_{abs}. Crack patterns obtained for high model resolution specimen ($\psi \geq 134$) were observed to compare well with crack patterns observed from physical microwave treatment experiments. It can be concluded that model calibration using the usual simulated UCS and Brazilian tests alone is not adequate to fix the model resolution for simulations of thermal induced cracks. These results show that model specimen resolution has a significant effect on observed micro crack damage and that the minimum base material "particle" size is not a free parameter. When using BPM to predict microwave treatment response of materials, model specimen resolution cannot be chosen arbitrary. It is suggested that model resolution values be chosen after carrying out a sensitivity analysis, on the effects of model resolution variation on the predicted model response.

The goal of the second part of the modelling work carried out was to use BPM to determine the effect of absorbent phase content on the sulphide ore used in the physical experiments presented in chapter 4. Damage maps which show the percentage of crack damage as a function of power density and exposure time for sulphide ores absorbent phase content were constructed. This study showed that for the same energy input and power density, the fraction of microwave induced crack damage depends on absorbent phase grain content. This study also showed that absorbent phase content had an effect on the minimum power density required to induce cracks. The optimal conditions for microwave treating sulphide ores at energy inputs between 1 x 10^9 J/m^3_{abs} 1 x 10^9 J/m^3_{abs}, considered in this study, was predicted to be at a power density of 1 ×10^{10} W/m^3_{abs} and energy input 1 x 10^9 J/m^3_{abs}. For ore model with absorbent phase content similar to that of the ore used in the study (47%), increasing the power density up to 1 ×10^{10} W/m^3_{abs} resulted in an increase in percentage crack damage from

5 % to a maximum of 40% for the same energy input 1 x 10^9 J/m^3_{abs}.However, at power densities above 1 ×10^{10} W/m^3_{abs}, increasing the power density, did not yield additional improvements in crack damage. Comparison of the simulated crack patterns for model ore with 55% absorbent phase content, against QEMSCAN images of microwave treated sphalerite ore from the physical experimental studies shows similar crack patterns at similar energy input values and exposure times (1 ×10^9 W/m^3_{abs}, 1.0 s). It can be concluded based on results from this study that, the extent of microwave induced crack damage and also the mode of fracture in an ore particle depends not only the microwave treatment condition but also on the mineralogical characteristics of the ore.

CHAPTER 7

7. CONCLUSION AND FUTURE WORK

7.1.Conclusion

The aim of this work was to determine if microwave treatment of ore particles prior to bio-leaching would induce micro-cracks and enhance value mineral exposure and to subsequently model the microwave treatment of these ore particles. Despite advances that have been made in understanding the interaction between microwaves and mineral ores, prior to this work, there has been limited investigations on the characteristics of microwave induced cracks. In order to narrow down the window of opportunity for utilising microwave technology, an understanding of the response of different minerals to microwave treatment is required, along with an assessment of the downstream processing benefits of adapting the technology. The aims of this study have been addressed by satisfying the research objectives highlighted in chapter 1 and presented again in this section.

Objective 1: "Characterise and quantify microwave induced particle cracks through the use of high resolution X-ray computed tomography (XCT) and Auto-SEM /EDS techniques."

Using XCT and QEMSCAN analysis this study was able to show experimentally for the first time that microwave treatment (at high power density (1×10^9 W/m^3_{abs}) and short exposure time (1.00 s)) of coarse crushed ores (> 5mm), results in a significant increase in percentage crack volume for HPGR and cone crushed particles. This shows that coarse textured high-Fe sphalerite ores are amenable to microwave treatment. Increases in crack volume of over 100% after microwave treatment were observed for small (-5+4.75) mm, medium (-16+9.5) mm, and large (-25+19) mm HPGR and cone crushed particles. For both these modes of prior comminution, the increase in percentage crack volume after microwave treatment was statistically significant, but there was no statistically significant difference in percentage crack volume between modes of prior comminution. This suggests that microwave treatment of ores could be applied to either cone or HPGR crushed products with no relative difference in observed crack damage after treatment.

Analysis of crack width size distributions, measured using XCT and QEMSCAN analysis, showed similar crack width size distributions of microwave induced cracks in cone and HPGR crushed particles of the same size. The microwave induced cracks were observed to be wider in size, with the crack networks penetrating deeper inside the particles, when

compared against cracks induced during cone or HPGR breakage. These observed characteristics of microwave induced cracks, are especially desirable in bio-heap leaching operations, where accessibility of grains to lixiviant has an effect on value mineral recovery. Over 50% of the measured cracks, at all particle sizes, had a width greater than greater than 10 µm. Therefore microwave induced cracks are larger than typical the size of bacteria used in bio-leaching. Thus microwave induced cracks will provide bacteria attachment sites. XCT analysis of ore particles before and after microwave treatment showed that microwave induced cracks did not result in particle fragmentation. This is particularly important in heap leaching where the particle size has an influence on fluid flow dynamics. Microwave induced fragmentation when preparing heap leach feed can result fines generation, which could lead to fluid flow problems during heap leaching. XCT measured geometric data showed an increase in the volume space occupied by particles after microwave treatment. For the small crushed particles the volume space occupied by the particle increased by 18%, while for the medium and large particles a volume increase of 7.2% and 5.1% was observed respectively. This increase in occupied particle volume space is due to an increase in particle void space caused by microwave induced cracks in the ore particles.

The amount of microwave induced cracks were observed to increase with decreasing particle size. This was due to the design of the single-mode microwave applicator used in the study. The electric field distribution during microwave treatment was highly sensitive to ore particle packing in the sample holder. Smaller particle sizes had a more uniform packing compared to larger ones. This created a more uniform electric field distribution over the closely packed small particles, ensuring a more uniform region of high electric field intensity. For the case of the large particles, the packing was highly irregular in the sample holder, this resulted in an electric field distribution significantly perturbed from the design ideal, with the likelihood of isolated regions of high electric field intensity in specific locations in individual particles. This effect is directly related to the operating frequency (2.45 GHz), the single-mode cavity type, and particle size used in the study. Were a lower frequency to be used in an industrial application (896 or 915 MHz), the applicator would be significantly larger and the large particles would pack more uniformly into it.

Objective 2: "Determine if microwave treatment results in enhanced value mineral exposure in coarse particles and to determine the mode of fracture during microwave treatment."

For the first time enhanced mineral exposure due to microwave treatment of coarse particles (> 5mm),at high power density (1×10^{9} W/m^{3}_{abs}) and short exposure time (1.00 s), has been

demonstrated in this study. 3D XCT grain exposure analysis of small (-5+4.75) mm, medium (-16+9.5) mm, and large (-25+19) mm particles before and after microwave treatment showed an increase in the degree of sulphide grain exposure of 28%, 26% and 15% respectively. These results suggest that greater process benefits could be obtained from the application of microwaves, by applying downstream processing methods that directly utilise microwave enhanced exposure without the need to further grind the microwave treated ore.

Prior to this work, there were claims that microwave pre-treatment results predominantly in grain boundary cracks. This study has qualitatively and quantitatively shown that microwave induced cracks consist of both interphase trans-granular and grain boundary cracks. Analysis of XCT and QEMSCAN images showed the presence of cracks propagating across different mineral phases and along the grain boundaries.

The ratio of specific interfacial area after microwave treatment to specific interfacial area before microwave treatment, in an individual particle, is an indicator of the degree of grain boundary fracture. When the mode of fracture is grain boundary, there is a loss in interfacial area. A ratio close to 1.00 suggest a conservation of interfacial area during crack propagation and thus, no grain boundary fracture. Measurements of the specific interfacial areas of particles before and after microwave treatment using XCT showed average losses in interfacial area of 31%, 23% and 16% for small (-5+4.75) mm, medium (-16+9.5) mm, and large (-25+19) mm particles suggesting some degree of grain boundary fracture. The amount of interfacial area loss and hence the degree of grain boundary fracture measured was observed to increase with decreasing particle size. This was due to smaller particles having a higher percentage crack volume and thus, a higher probability of interfacial area loss.

Objective 3: "Determine the effect of microwave induced cracks on the dissolution kinetics of (bio) heap leaching processes of a typical massive sulphide ore."

The results from the column leaching experiments over 350 days, demonstrate that microwave pre-treatment of crushed ore for bio-leaching, will lead to improved leaching recovery. Improvements in overall Zn metal recoveries of 26%, 24% and 23% were observed for small (-5+4.75) mm, medium (-16+9.5) mm, and large (-25+19) mm microwave treated particles during column bio-leaching, over 350 days. The enhanced metal recovery seen for microwave treated material correlates well with the internal crack volume measurements and mineral exposure results. Since the only difference between microwave treated and untreated particles was the presence of microwave induced cracks, the enhanced metal extraction is due to microwave treatment. The column bio-leaching results showed that medium (-16+9.5) mm

sized microwave treated particles had a 10.1% higher metal recovery compared to small (-5+4.75) mm untreated particles. This suggests that higher metal recovery is achievable at larger sizes (-16+9.5) mm for microwave pre-treated ore particles compared to recovery in smaller (-5+4.75) mm untreated ore particles. Thus there is a potential for energy savings during ore preparation of heap leaching feed, when microwave pre-treatment is applied. Since it will be possible to recover value metals at coarser sizes than is currently achievable using conventional ore preparation methods. The increase in the Zn recovery at coarser sizes due to microwave treatment demonstrated in this study could significantly improve heap leaching recovery, which is normally characterised by low recoveries at coarse sizes and poor solution flow at finer more liberated sizes.

Prior to this work it has been suggested that mode of comminution has an influence on heap leaching recovery with, HPGR crushed particles giving higher metal recoveries compared to cone crushed ore (Ghorbani et al., 2013a; Ghorbani et al., 2012). This study has demonstrated that microwave treatment improves heap leaching recovery in cone and HPGR crushed ore, with similar recoveries being observed for HPGR and cone crushed microwave treated products. This suggest that the presence of microwave induced cracks in cone crushed ore has the effect of increasing metal recovery in cone crushed particles to values comparable to recoveries obtained for HPGR microwave treated ore.

Analysis of the progression of leaching in individual microwave treated particles showed a growth in microwave induced crack networks over 350 days of leaching. The growth in the crack networks was due to mineral dissolution along the microwave induced crack paths and the action of the reactant. However, the growth in the crack networks in microwave untreated HPGR particles was relatively small, when compared to that observed for the microwave treated HPGR particles. This suggest that microwave induced cracks accelerates reagent diffusion into the particles resulting in increased metal extraction, during bio-leaching. Over time it was observed that, the growth of these crack networks results in particle fragmentation, which can lead to the generation of fines in heaps. This can have potentially negative impacts on the fluid flow dynamics in heaps.

This study has also shown that sub-surface conversion of minerals is more prevalent in microwave treated particles compared to untreated particles. An investigation of the dissolution of sulphide grains in selected particles, using XCT 3D image analysis techniques over the course of 350 days of leaching showed greater sub-surface conversion of minerals in microwave treated particles compared to untreated. Sub-surface conversion was more pronounced in smaller microwave treated particles as they had a higher percentage crack

volume. In general sub-surface leaching in microwave treated particles was promoted by microwave induced cracks that improved the accessibility of sub-surface grains to the lixiviant. For untreated particles sub-surface conversion was relatively less pronounced.

Objective 4 : "Use XCT and QEMSCAN experimental data to improve on and to validate numerical models for predicting microwave induced damage."

A BPM numerical model was developed to simulate a multiphase massive sulphide ore approximating the ore used in the physical experimental investigations. The developed ore model consisted of pyrite, sphalerite and quartz phases which were identified as the major phases in the ore used in the experiment. The created model ore specimen measured 15 by 20 mm. using the developed ore model. The effects of model resolution (Equation 6-15) on predicted microwave induced crack damage was investigated for the first time. Six ore model specimens were generated at the following model resolutions; 30, 75, 100, 134, 214 and 268. Microwave treatment of the ore models was simulated at a power density of 10^{10} W/m$^3_{abs}$ and exposure times ranging between 0.01 to 0.10 sec. These microwave treatment conditions were considered to be within range of the microwave energy input applied in the physical experiments (power density 1×10^9 W/m$^3_{abs}$, exposure time 1.00 s). This was especially important so as to allow for the validation of the model results with results from the physical experiments. The amount of microwave induced crack damage was calculated for each model specimen resolution. The resulting microwave induced crack patterns for different model resolution were compared against those obtained from physical experiments. The results showed that model specimen resolution has a significant effect on observed microwave induced crack damage and patterns. It was observed that cracks in different model resolution specimens propagate in a different pattern despite having the same macro-mechanical properties. Crack patterns obtained for higher model resolution specimen were observed to compare well with crack patterns observed from physical microwave treatment experiments. It can be concluded that model calibration using the usual simulated UCS and Brazilian tests alone is not adequate to fix the model resolution for simulations of thermal induced cracks. These results show that model specimen resolution has a significant effect on observed micro crack damage and that the minimum base material "particle" size is not a free parameter.

The effect of absorbent phase content on microwave induced damage was investigated for the first time using a high resolution model. Damage maps which show the percentage of micro-cracks as a function of power density and exposure time for different ternary ores and

absorbent phase content were constructed using bonded particle model. It has been shown that for the same power density and energy input, the fraction of micro-fractures induced by microwave treatment considerably depends on absorbent phase grain content. These results also confirm previous studies that have shown that significant energy saving can be achieved by reducing treatment time and increasing power density. The application of microwave technology is expected to yield significant crack damage in ores that have a significant absorbent phase content. The bonded particle models developed in this study will offer a partial solution to design challenges surrounding the application of microwave technology at a commercial scale due to the fact that a wide range of scenarios can be investigated rapidly and at relatively low cost.

7.2.Future work

The design of continuous process microwave applicator that delivers high power microwaves is an important step towards experimentally evaluating the downstream processing benefits of microwave treated ore. The microwave pre-treatment of heap leach feed presented in this study was carried out in a batch applicator capable of treating a maximum of 100 grams of ore per treatment. This presents a challenge when investigating downstream continuous processes that require a large amount of ore feed.

Future work should investigate the fluid flow pattern in heaps consisting of microwave treated particles. This could be achieved by using unsaturated irrigated heap experimental set up. Leaching column although they are useful tools in providing leaching kinetics information, they are a poor representation of actual heap leach operation as particles in a heap leach are unlikely to be saturated in lixiviant. Therefore an understanding of how microwave treatment affects ore permeability and the fluid flow pattern in heap leaching is of importance.

Industrial commercialisation of microwave technology will benefit from developing an integrated process model of the minerals beneficiation chain that incorporates all the unit operations. The developed model framework should be capable of evaluating the technical, economic, environmental and social implications of introducing microwave technology up and downstream of the intervention.

Future work should also investigate microwave induced crack damage in other ore types with different mineralogical attributes. Of particular interest is the effect of intrinsic flaws and cracks on microwave induced crack propagation. The bulk of the gangue phase in the ore used in this study consisted of quartz which has no cleavage. There were no significant pre-existing cracks identified in the untreated material.

Future work should investigate modifying and using XCT data directly in developing material models for numerical simulations. This will make it possible to validate numerical models with experimental data since the modelled ore would have the same textural properties as the physical ore under investigation.

An extensive evaluation of the economic benefits of applying microwave technology to heap leaching operations should be carried out. This study should include an estimation of the costs of all units in the flowsheet including the cost of industrial microwave equipment. This will demonstrate the economic feasibility of adapting microwave technology.

REFERENCES

Ahmadi, A., Schaffie, M., Manafi, Z., Ranjbar, M., Electrochemical bioleaching of high grade chalcopyrite flotation concentrates in a stirred bioreactor. Hydrometallurgy, 2010, 104(1), 99-105.

Ahmadi, A., Schaffie, M., Petersen, J., Schippers, A., Ranjbar, M., Conventional and electrochemical bioleaching of chalcopyrite concentrates by moderately thermophilic bacteria at high pulp density. Hydrometallurgy, 2011, 106(1), 84-92.

Al-Harahsheh, M., Kingman, S., The influence of microwaves on the leaching of sphalerite in ferric chloride. Chemical Engineering and Processing: Process Intensification, 2007, 46(10), 883-888.

Al-Harahsheh, M., Kingman, S., Hankins, N., Somerfield, C., Bradshaw, S., Louw, W., The influence of microwaves on the leaching kinetics of chalcopyrite. Minerals Engineering, 2005, 18(13–14), 1259-1268.

Al-Harahsheh, M., Kingman, S.W., Microwave-assisted leaching—a review. Hydrometallurgy, 2004, 73(3–4), 189-203.

Ali, A.Y., Bradshaw, S.M., Quantifying damage around grain boundaries in microwave treated ores. Chemical Engineering and Processing: Process Intensification, 2009, 48(11-12), 1566-1573.

Ali, A.Y., Bradshaw, S.M., Bonded-particle modelling of microwave-induced damage in ore particles. Minerals Engineering, 2010, 23(10), 780-790.

Ali, A.Y., Bradshaw, S.M., Confined particle bed breakage of microwave treated and untreated ores. Minerals Engineering, 2011, 24(14), 1625-1630.

Bailey, C., Lane, G., Morrell, S., Staples, P., 2009. What can go wrong in comminution circuit design, In *Proceedings of the 10th Mill Operatirs' Conference, Adelaide, SA.*

Baker-Austin, C., Dopson, M., Life in acid: pH homeostasis in acidophiles. Trends in microbiology, 2007, 15(4), 165-171.

Barbery, G., Prediction of Mineral Liberation Size by Modeling. Cim Bulletin, 1984, 77(866), 60-60.

Bartlett, R.W., Simulation of ore heap leaching using deterministic models. Hydrometallurgy, 1992, 29(1), 231-260.

Bartlett, R.W., Metal extraction from ores by heap leaching. Metallurgical and Materials Transactions B, 1997, 28(4), 529-545.

Bass, J.D., Elasticity of minerals, glasses, and melts. Mineral physics and crystallography: A handbook of physical constants, 1995, 2, 45-63.

Batchelor, A., Jones, D., Plint, S., Kingman, S., Deriving the ideal ore texture for microwave treatment of metalliferous ores. Minerals Engineering, 2015, 84, 116-129.

Baum, W., Ausburn, K., HPGR comminution for optimization of copper leaching. Minerals & Metallurgical Processing, 2011, 28(2), 77-81.

Bennett, C., McBride, D., Cross, M., Gebhardt, J., A comprehensive model for copper sulphide heap leaching: Part 1 basic formulation and validation through column test simulation. Hydrometallurgy, 2012, 127, 150-161.

Böttcher, C.J.F., van Belle, O.C., Bordewijk, P., Rip, A., *Theory of electric polarization.* 1978, Elsevier Science Ltd.

Bouffard, S.C., Dixon, D.G., Investigative study into the hydrodynamics of heap leaching processes. Metallurgical and Materials Transactions B, 2001, 32(5), 763-776.

Bouffard, S.C., West-Sells, P.G., Hydrodynamic behavior of heap leach piles: Influence of testing scale and material properties. Hydrometallurgy, 2009, 98(1–2), 136-142.

Bradshaw, S., Van Wyk, E., De Swardt, J., Microwave heating principles and the application to the regeneration of granular activated carbon. Journal of the South African Institute of Mining and Metallurgy(South Africa), 1998, 98(4), 201-210.

Bradshaw, S.M., Louw, W., van der Merwe, C., Reader, R., Kingman, S., Celuch, M., Kijewska, W., Techno-Economic considerations in the commercial microwave processing of mineral ores. Journal of Microwave Power and Electromagnetic Energy 2007, 40(4), 228-240.

Bradt, R., Lin, C., Miller, J., Chi, G., Interfacial fracture of multiphase particles and its influence on liberation phenomena. Minerals Engineering, 1995, 8(4), 359-366.

Breed, A., Hansford, G., Studies on the mechanism and kinetics of bioleaching. Minerals Engineering, 1999, 12(4), 383-392.

Brierley, J., Brierley, C., Present and future commercial applications of biohydrometallurgy. Hydrometallurgy, 2001, 59(2), 233-239.

Chapman, N.A., Shackleton, N.J., Malysiak, V., O'Connor, C.T., The effect of using different comminution procedures on the flotation of Platinum-Group Minerals. Minerals Engineering, 2011, 24(8), 731-736.

Charikinya, E., 2011. A modelling framework to determine the value proposition of microwave treatment of mineral ores, In *Process Engineering*. University of Stellenbosch, Stellenbosch

Chen, T., Dutrizac, J., Haque, K., Wyslouzil, W., Kashyap, S., The relative transparency of minerals to microwave radiation. Canadian Metallurgical Quarterly, 1984, 23(3), 349-351.

Chunpeng, L., Yousheng, X., Yixin, H., Application of microwave radiation to extractive metallurgy. Chin. J. Met. Sci. Technol, 1990, 6(2), 121-124.

Clark, D.E., Sutton, W.H., Microwave processing of materials. Annual Review of Materials Science, 1996, 26(1), 299-331.

Clark, S.P., *Handbook of physical constants*. 1966, Geological Society of America.

Cnudde, V., Boone, M.N., High-resolution X-ray computed tomography in geosciences: A review of the current technology and applications. Earth-Science Reviews, 2013, 123, 1-17.

Cnudde, V., Masschaele, B., Dierick, M., Vlassenbroeck, J., Hoorebeke, L.V., Jacobs, P., Recent progress in X-ray CT as a geosciences tool. Applied Geochemistry, 2006, 21(5), 826-832.

Courtney, W.E., Analysis and evaluation of a method of measuring the complex permittivity and permeability microwave insulators. Microwave Theory and Techniques, IEEE Transactions on, 1970, 18(8), 476-485.

Crundwell, F., Kinetics and mechanism of the oxidative dissolution of a zinc sulphide concentrate in ferric sulphate solutions. Hydrometallurgy, 1987, 19(2), 227-242.

Crundwell, F., How do bacteria interact with minerals? Hydrometallurgy, 2003, 71(1), 75-81.

Cumbane, A., 2003. Microwave processing of Minerals, In *Department of Chemical and Environmental Engineering*. University of Nottingham, Nottingham, UK.

Cumbane, A., Miles, N., Lester, E., Kingman, S., Bradshaw, S., Dielectric properties of sulphide minerals. Processing Microwave Technologies, 2008.

da Silva, G., Relative importance of diffusion and reaction control during the bacterial and ferric sulphate leaching of zinc sulphide. Hydrometallurgy, 2004, 73(3), 313-324.

Daniel, M.J., 2007. Energy efficient mineral liberation using HPGR technology, In *Department of Mining, Materials and Minerals Engineering*. University of Queensland, Quessnsland.

Daniel, M.J., Morrell, S., HPGR model verification and scale-up. Minerals Engineering, 2004, 17(11-12), 1149-1161.

Demergasso, C.S., Castillo, D., Casamayor, E.O., Molecular characterization of microbial populations in a low-grade copper ore bioleaching test heap. Hydrometallurgy, 2005, 80(4), 241-253.

Desmond, T., Mineral comminution: Energy efficiency considerations. Minerals Engineering, 2008, 21(8), 613-620.

Deveci, H., Akcil, A., Alp, I., Bioleaching of complex zinc sulphides using mesophilic and thermophilic bacteria: comparative importance of pH and iron. Hydrometallurgy, 2004, 73(3), 293-303.

Dhawan, N., Safarzadeh, M.S., Miller, J.D., Moats, M.S., Rajamani, R.K., Crushed ore agglomeration and its control for heap leach operations. Minerals Engineering, 2013, 41(0), 53-70.

Diment, W.H., Pratt, H.R., 1988. Thermal conductivity of some rock-forming minerals: A tabulation. US Geological Survey.

du Plessis, C.A., Batty, J.D., Dew, D.W., 2007. Commercial applications of thermophile bioleaching, In *Biomining*. Springer, pp. 57-80.

Dunne, R., Maxton, D., Morrell, S., Lane, G., HPGR - The Australian experience. Improving and Optimizing Operations: Things That Actually Work!, 2004, 153-162.

Erlandsson, K., Buvat, I., Pretorius, P.H., Thomas, B.A., Hutton, B.F., A review of partial volume correction techniques for emission tomography and their applications in neurology, cardiology and oncology. Physics in medicine and biology, 2012, 57(21), R119.

Fandrich, R., Gu, Y., Burrows, D., Moeller, K., Modem SEM-based mineral liberation analysis. International Journal of Mineral Processing, 2007, 84(1-4), 310-320.

Fandrich, R.G., 1998. Mineral liberation through confined particle bed breakage, In *Department of Mining , Minerals and Materials Engineering*. University of Queensland, Queensland.

Fandrich, R.G., Bearman, R.A., Boland, J., Lim, W., Mineral liberation by particle bed breakage. Minerals Engineering, 1997, 10(2), 175-187.

Fandrich, R.G., Schneider, C.L., Gay, S.L., Two stereological correction methods: Allocation method and kernel transformation method. Minerals Engineering, 1998, 11(8), 707-715.

Ford, J., Pei, D., HIGH TEMPERATURE CHEMICAL PROCESSING* VIA MICROWAVE ABSORPTION. Red, 1967, 6, 1000.

Fuerstenau, D.W., Abouzeid, A.Z.M., The energy efficiency of ball milling in comminution. International Journal of Mineral Processing, 2002, 67(1–4), 161-185.

Garcia, D., Lin, C., Miller, J., Experimental evaluation of a mineral exposure model for crushed copper ores. Advances in Comminution, 2006, 261-268.

Garcia, D., Lin, C.L., Miller, J.D., Quantitative analysis of grain boundary fracture in the breakage of single multiphase particles using X-ray microtomography procedures. Minerals Engineering, 2009, 22(3), 236-243.

Gericke, M., Neale, J., Van Staden, P., A Mintek perspective of the past 25 years in minerals bioleaching. Journal of the Southern African Institute of Mining and Metallurgy, 2009, 109(10), 567-585.

Ghorbani, Y., Becker, M., Mainza, A., Franzidis, J.-P., Petersen, J., Large particle effects in chemical/biochemical heap leach processes – A review. Minerals Engineering, 2011a, 24(11), 1172-1184.

Ghorbani, Y., Becker, M., Petersen, J., Mainza, A.N., Franzidis, J.-P., Investigation of the effect of mineralogy as rate-limiting factors in large particle leaching. Minerals Engineering, 2013a, 52(1), 38-51.

Ghorbani, Y., Becker, M., Petersen, J., Morar, S.H., Mainza, A., Franzidis, J.P., Use of X-ray computed tomography to investigate crack distribution and mineral dissemination in sphalerite ore particles. Minerals Engineering, 2011b, 24(12), 1249-1257.

Ghorbani, Y., Petersen, J., Becker, M., Mainza, A.N., Franzidis, J.-P., Investigation and modelling of the progression of zinc leaching from large sphalerite ore particles. Hydrometallurgy, 2013b, 131–132(1), 8-23.

Ghorbani, Y., Petersen, J., Harrison, S.T.L., Tupikina, O.V., Becker, M., Mainza, A.N., Franzidis, J.-P., An experimental study of the long-term bioleaching of large sphalerite ore particles in a circulating fluid fixed-bed reactor. Hydrometallurgy, 2012, 129–130(0), 161-171.

Goodall, W.R., Characterisation of mineralogy and gold deportment for complex tailings deposits using QEMSCAN®. Minerals Engineering, 2008, 21(6), 518-523.

Gottlieb, P., 2008. The revolutionary impact of automated mineralogy on mining and mineral processing, In *XXIV IMPC*. Science Press, Beijing, pp. pp. 165–174.

Gottlieb, P., Wilkie, G., Sutherland, D., Ho-Tun, E., Suthers, S., Perera, K., Jenkins, B., Spencer, S., Butcher, A., Rayner, J., Using quantitative electron microscopy for process mineralogy applications. JoM, 2000, 52(4), 24-25.

Gu, Y., Schouwstra, R.P., Rule, C., The value of automated mineralogy. Minerals Engineering, 2014, 58, 100-103.

Guo, S.-H., Guo, C., Peng, J.-H., Jin, C., Li, D.-B., Liu, L.-J., Microwave assisted grinding of ilmenite ore. Transactions of Nonferrous Metals Society of China, 2011, 21(9), 2122-2126.

Gupta, A., Yan, D.S., 2006. Chapter 6 - Roll Crushers, In *Mineral Processing Design and Operation*. Elsevier Science, Amsterdam, pp. 142-160.

Halinen, A.-K., Rahunen, N., Kaksonen, A.H., Puhakka, J.A., Heap bioleaching of a complex sulfide ore: Part I: Effect of pH on metal extraction and microbial composition in pH controlled columns. Hydrometallurgy, 2009, 98(1), 92-100.

Hansford, G.S., 1997. Recent developments in modeling the kinetics of bioleaching, In *Biomining*. Springer, pp. 153-175.

Haque, K.E., Microwave energy for mineral treatment processes--a brief review. International Journal of Mineral Processing, 1999, 57(1), 1-24.

Harrison, P.C., 1997. A fundamental study of the heating effect of 2.45 GHz microwave radiation on minerals. University of Birmingham.

Henckens, M., Driessen, P., Worrell, E., Metal scarcity and sustainability, analyzing the necessity to reduce the extraction of scarce metals. Resources, conservation and recycling, 2014, 93, 1-8.

Henda, R., Hermas, A., Gedye, R., Islam, M., Microwave enhanced recovery of nickel-copper ore: communition and floatability aspects. Journal of Microwave Power and Electromagnetic Energy, 2005, 40(1), 7-16.

Holderfield, S.P., Salsman, J., 1992. Observed trends in the dielectric properties of minerals at elevated temperatures, In *MRS Proceedings*. Cambridge Univ Press, p. 589.

Hsih, C.S., Wen, S.B., Kuan, C.C., An exposure model for valuable components in comminuted particles. International Journal of Mineral Processing, 1995, 43(3–4), 145-165.

Hua, Y., Lin, Z., Yan, Z., Application of microwave irradiation to quick leach of zinc silicate ore. Minerals Engineering, 2002, 15(6), 451-456.

Hua, Y., Liu, C., Heating rate of minerals and compounds in microwave field. Transactions of Nonferrous Metals Society of China (English Edition), 1996, 6(1), 35-40.

Hwang, J.-Y., Shi, S., Xu, Z., Huang, X., Oxygenated leaching of copper sulfide mineral under microwave-hydrothermal conditions. Journal of Minerals & Materials Characterization & Engineering, 2002, 1, 111-119.

Irannajad, M., Mehdilo, A., Nuri, O.S., Influence of microwave irradiation on ilmenite flotation behavior in the presence of different gangue minerals. Separation and Purification Technology, 2014, 132, 401-412.

Itasca, 2008. Particle Flow Code in 2 Dimensions Version 4.0, In *Particle Flow Code*, Version 4.0 ed. Itasca Consulting Group Inc, Minneapolis.

Itasca Consulting Group, I., 2008. Particle Flow Code in 2 Dimensions Version 4.0, In *Particle Flow Code*, Version 4.0 ed. Itasca Consulting Group Inc, Minneapolis.

Jameson, G.J., The effect of surface liberation and particle size on flotation rate constants. Minerals Engineering, 2012, 36–38(0), 132-137.

Johnson, D., Importance of microbial ecology in the development of new mineral technologies. Hydrometallurgy, 2001, 59(2), 147-157.

Jones, D.A., 2005. Understanding microwave treatment of ores, In *Department of Chemical and Environmental Engineering*. The University of Nottingham, Nottingham.

Jones, D.A., Kingman, S.W., Whittles, D.N., Lowndes, I.S., Understanding microwave assisted breakage. Minerals Engineering, 2005, 18(7), 659-669.

Jones, D.A., Kingman, S.W., Whittles, D.N., Lowndes, I.S., The influence of microwave energy delivery method on strength reduction in ore samples. Chemical Engineering and Processing, 2007, 46(4), 291-299.

Ketcham, R.A., Accurate three-dimensional measurements of features in geological materials from X-ray computed tomography data. Advances in X-ray Tomography for Geomaterials. ISTE, London. Accurate three-dimensional measurements of features in geological materials from X-ray computed tomography data, 2006, 143-148.

Ketcham, R.A., Carlson, W.D., Acquisition, optimization and interpretation of X-ray computed tomographic imagery: applications to the geosciences. Computers & Geosciences, 2001, 27(4), 381-400.

King, R., 1992. Techniques for estimating the amount of grain-boundary fracture during comminution of mineralogical materials, In *Comminution—Theory and Practice Symposium*, pp. 3-15.

King, R.P., A model for the quantitative estimation of mineral liberation by grinding. International Journal of Mineral Processing, 1979, 6(3), 207-220.

King, R.P., Comminution and liberation of minerals. Minerals Engineering, 1993, 7(2-3), 129-140.

King, R.P., Linear stochastic models for mineral liberation. Powder Technology, 1994, 81(3), 217-234.

King, R.P., Schneider, C.L., Mineral liberation and the batch communition equation. Minerals Engineering, 1998a, 11(12), 1143-1160.

King, R.P., Schneider, C.L., Stereological correction of linear grade distributions for mineral liberation. Powder Technology, 1998b, 98(1), 21-37.

Kingman, S., Recent development in microwave processing of minerals. International Materials Reviews, 2006, 51(1), 1-12.

Kingman, S., Bradshaw, S., Rowson, N.A., Jackson, K., Cumbane, A., Greenwood, R., Development of microwave assisted comminution. International Journal of Mineral Processing, 2004a, 74(3), 71-83.

Kingman, S., Vorster, W., Rowson, N.A., 'The effect of microwave radiation on the processing of Palabora copper ore'. J. S. Afr. Inst. Min. Metall., 197-204, 2000a.

Kingman, S.W., Jackson, K., Bradshaw, S.M., Rowson, N.A., Greenwood, R., An investigation into the influence of microwave treatment on mineral ore comminution. Powder Technology, 2004b, 146(3), 176-184.

Kingman, S.W., Jackson, K., Cumbane, A., Bradshaw, S.M., Rowson, N.A., Greenwood, R., Recent developments in microwave-assisted comminution. International Journal of Mineral Processing, 2004c, 74(1-4), 71-83.

Kingman, S.W., Rowson, N.A., Microwave treatment of minerals-a review. Minerals Engineering, 1998, 11(11), 1081-1087.

Kingman, S.W., Vorster, W., Rowson, N.A., The influence of mineralogy on microwave assisted grinding. Minerals Engineering, 2000b, 13(3), 313-327.

Klauber, C., A critical review of the surface chemistry of acidic ferric sulphate dissolution of chalcopyrite with regards to hindered dissolution. International Journal of Mineral Processing, 2008, 86(1), 1-17.

Kobusheshe, J., 2010. Microwave enhanced processing of ores, In *Department of Chemical and Environmental Engineering*. University of Nottingham, Nottingham.

Kodali, P., Dhawan, N., Depci, T., Lin, C.L., Miller, J.D., Particle damage and exposure analysis in HPGR crushing of selected copper ores for column leaching. Minerals Engineering, 2011, 24(13), 1478-1487.

Koyama, T., Jing, L., Effects of model scale and particle size on micro-mechanical properties and failure processes of rocks—A particle mechanics approach. Engineering Analysis with Boundary Elements, 2007, 31(5), 458-472.

Krishnan, K.H., Mohanty, D.B., Sharma, K.D., The effect of microwave irradiations on the leaching of zinc from bulk sulphide concentrates produced from Rampura–Agucha tailings. Hydrometallurgy, 2007, 89(3–4), 332-336.

Krogscheepers, C., Gossel, S.J., Input cost and international demand effects on the production of platinum group metals in South Africa. Resources Policy, 2015, 45, 193-201.

Lama, R., Vutukuri, V., *Handbook of Mechanical Properties of Rocks.* 1978a, Trans Tech Publications (Clausthal, Germany).

Lama, R., Vutukuri, V., *HANDBOOK ON MECHANICAL PROPERTIES OF ROCKS-TESTING TECHNIQUES AND RESULTS. VOLUME 2.* 1978b.

Lätti, D., Adair, B.J.I., An assessment of stereological adjustment procedures. Minerals Engineering, 2001, 14(12), 1579-1587.

Lau, S., Miller, J., Lin, C., 2012. 3D mineralogy, texture and damage analysis of multiphase mineral particles with a high contrast, submicron resolution X-ray tomography system, In *XXVI International Mineral Processing Congress*, pp. 2726-2736.

Leahy, M.J., Schwarz, M.P., Modelling jarosite precipitation in isothermal chalcopyrite bioleaching columns. Hydrometallurgy, 2009, 98(1), 181-191.

Li, Y., Kawashima, N., Li, J., Chandra, A., Gerson, A., A review of the structure, and fundamental mechanisms and kinetics of the leaching of chalcopyrite. Advances in colloid and interface science, 2013, 197, 1-32.

Lin, C., Garcia, C., 2005. Microscale characterization and analysis of particulate systems via cone beam X-ray microtomography (XMT), In *Innovations in Natural Resource Processing, Proceedings of the Jan D., Miller Symposium, SME*, pp. 421-432.

Lin, C., Miller, J., 3D characterization and analysis of particle shape using X-ray microtomography (XMT). Powder Technology, 2005, 154(1), 61-69.

Lin, C.L., Miller, J.D., Hsieh, C.H., 2012. Particle Damage During HPGR Breakage as Described by Specific Surface Area Distribution of Cracks in the Crushed Products, In *XXVI IMPC*, New Delhi, p. paper No. 687.

Liu, J., Schanert, K., Modelling of interparticle breakage. International Journal of Mineral Processing, 1996, 44-45(0), 101-115.

Lotfalian, M., Schaffie, M., Darezereshki, E., Manafi, Z., Ranjbar, M., Column bioleaching of low-grade chalcopyritic ore using moderate thermophile bacteria. Geomicrobiology Journal, 2012, 29(8), 697-703.

Lotter, N., Kormos, L., Oliveira, J., Fragomeni, D., Whiteman, E., Modern process mineralogy: two case studies. Minerals Engineering, 2011, 24(7), 638-650.

Lottering, M., Lorenzen, L., Phala, N., Smit, J., Schalkwyk, G., Mineralogy and uranium leaching response of low grade South African ores. Minerals Engineering, 2008, 21(1), 16-22.

Lundgren, D., Silver, M., Ore leaching by bacteria. Annual Reviews in Microbiology, 1980, 34(1), 263-283.

Lupo, J., Sustainable issues related to heap leaching operations. Journal of the Southern African Institute of Mining and Metallurgy, 2012, 112(12), 1021-1030.

Marland, S., Merchant, A., Rowson, N., Dielectric properties of coal. Fuel, 2001, 80(13), 1839-1849.

McClung, C.R., Viljoen, F., A detailed mineralogical assessment of sphalerites from the Gamsberg zinc deposit, South Africa: The manganese conundrum. Minerals Engineering, 2011, 24(8), 930-938.

McGill, S.L., Walkiewicz, J.W., Smyres, G.A., The Effects of Power Level on the Microwave Heating of Selected Chemicals and Minerals. MRS Online Proceedings Library, 1988, 124.

Meisels, R., Toifl, M., Hartlieb, P., Kuchar, F., Antretter, T., Microwave propagation and absorption and its thermo-mechanical consequences in heterogeneous rocks. International Journal of Mineral Processing, 2015, 135, 40-51.

Meloy, T.P., Clark, N., Liberation of target material from locked particles: a theoretical analysis. Particulate Science and Technology, 1985, 3(1-2), 15-26.

Meredith, R.J., *Engineers' handbook of industrial microwave heating.* 1998, The Institution of Electrical Engineers, London.

Metaxas, A.C., Meredith, R.J., *Industrial microwave heating*. 1983, The Institution of Electrical Engineers.

Middlemiss, S., Surface damage effects in single particle comminution. International Journal of Mineral Processing, 2007, 84(1), 207-220.

Miller, J., Lin, C., 2003. 3D analysis of particulates in mineral processing systems by cone beam X-ray microtomography, In *XXII International Mineral Processing Congress, Cape Town, South Africa*.

Miller, J.D., Lin, C.L., Garcia, C., Arias, H., Ultimate recovery in heap leaching operations as established from mineral exposure analysis by X-ray microtomography. International Journal of Mineral Processing, 2003, 72(1–4), 331-340.

Morley, C., 2006. High-pressure grinding rolls a technology review, In *Advances in Comminution. Society for Mining, Metallurgy, and Exploration (SME)*, ed. Kawatra, K.S., pp. 15-40.

Morley, C., HPGR-FAQ. Journal of the South African Institute of Mining and Metallurgy, 2010, 110(3), 107-115.

Morley, C., Staples, P., 2010. SAG or HPGR?–The Current Dilemma, In *Proceedings of the 42nd Annual Meeting of the Canadian Mineral Processors*, pp. 19-21.

Morrell, S., Predicting the specific energy required for size reduction of relatively coarse feeds in conventional crushers and high pressure grinding rolls. Minerals Engineering, 2010, 23(2), 151-153.

Morrison, R., Cleary, P., Towards a virtual comminution machine. Minerals Engineering, 2008, 21(11), 770-781.

Mousavi, S., Jafari, A., Yaghmaei, S., Vossoughi, M., Roostaazad, R., Bioleaching of low-grade sphalerite using a column reactor. Hydrometallurgy, 2006, 82(1), 75-82.

Mousavi, S., Yaghmaei, S., Vossoughi, M., Roostaazad, R., Jafari, A., Ebrahimi, M., Chabok, O.H., Turunen, I., The effects of Fe (II) and Fe (III) concentration and initial pH on microbial leaching of low-grade sphalerite ore in a column reactor. Bioresource technology, 2008, 99(8), 2840-2845.

Napier-Munn, T., 2005. Preface to 7th Edition, In *Wills' Mineral Processing Technology (Seventh Edition)*. Butterworth-Heinemann, Oxford, pp. ix-ix.

Nelson, S., Lindroth, D., Blake, R., Dielectric properties of selected minerals at 1 to 22 GHz. Geophysics, 1989, 54(10), 1344-1349.

Ogbonna, N., Petersen, J., Laurie, H., An agglomerate scale model for the heap bioleaching of chalcocite. JOURNAL-SOUTH AFRICAN INSTITUTE OF MINING AND METALLURGY, 2006, 106(6), 433.

Olubambi, P.A., Influence of microwave pretreatment on the bioleaching behaviour of low-grade complex sulphide ores. Hydrometallurgy, 2009, 95(1–2), 159-165.

Olubambi, P.A., Potgieter, J.H., Hwang, J.Y., Ndlovu, S., Influence of microwave heating on the processing and dissolution behaviour of low-grade complex sulphide ores. Hydrometallurgy, 2007, 89(1–2), 127-135.

Omran, M., Fabritius, T., Elmahdy, A.M., Abdel-Khalek, N.A., El-Aref, M., Elmanawi, A.E.-H., Effect of microwave pre-treatment on the magnetic properties of iron ore and its implications on magnetic separation. Separation and Purification Technology, 2014, 136, 223-232.

Palm, N.A., Shackleton, N.J., Malysiak, V., O'Connor, C.T., The effect of using different comminution procedures on the flotation of sphalerite. Minerals Engineering, 2010, 23(11-13), 1053-1057.

Parkash, A., Vaid, J., Mansingh, A., Measurement of dielectric parameters at microwave frequencies by cavity-perturbation technique. Microwave Theory and Techniques, IEEE Transactions on, 1979, 27(9), 791-795.

Pascoe, R.D., Power, M.R., Simpson, B., QEMSCAN analysis as a tool for improved understanding of gravity separator performance. Minerals Engineering, 2007, 20(5), 487-495.

Petersen, J., Modelling of bioleach processes: connection between science and engineering. Hydrometallurgy, 2010, 104(3), 404-409.

Petersen, J., Dixon, D.G., Competitive bioleaching of pyrite and chalcopyrite. Hydrometallurgy, 2006, 83(1), 40-49.

Petersen, J., Dixon, D.G., Modelling zinc heap bioleaching. Hydrometallurgy, 2007, 85(2–4), 127-143.

Pickles, C., Mouris, J., Hutcheon, R., High-temperature dielectric properties of goethite from 400 to 3000 MHz. Journal of materials research, 2005, 20(01), 18-29.

Pina, P.d.S., Leão, V.A., Silva, C.A.d., Daman, D., Frenay, J., The effect of ferrous and ferric iron on sphalerite bioleaching with Acidithiobacillus sp. Minerals Engineering, 2005, 18(5), 549-551.

Pirrie, D., Butcher, A.R., Power, M.R., Gottlieb, P., Miller, G.L., Rapid quantitative mineral and phase analysis using automated scanning electron microscopy (QemSCAN); potential applications in forensic geoscience. Geological Society, London, Special Publications, 2004, 232(1), 123-136.

Plumb, J., Muddle, R., Franzmann, P., Effect of pH on rates of iron and sulfur oxidation by bioleaching organisms. Minerals Engineering, 2008, 21(1), 76-82.

Porro, S., Ramirez, S., Reche, C., Curutchet, G., Alonso-Romanowski, S., Donati, E., Bacterial attachment: its role in bioleaching processes. Process biochemistry, 1997, 32(7), 573-578.

Potyondy, D.O., Cundall, P.A., A bonded-particle model for rock. International Journal of Rock Mechanics and Mining Sciences, 2004, 41(8), 1329-1364.

Powell, M.S., Morrison, R.D., The future of comminution modelling. International Journal of Mineral Processing, 2007, 84(1-4), 228-239.

Pradhan, N., Nathsarma, K.C., Srinivasa Rao, K., Sukla, L.B., Mishra, B.K., Heap bioleaching of chalcopyrite: A review. Minerals Engineering, 2008, 21(5), 355-365.

Prior, T., Giurco, D., Mudd, G., Mason, L., Behrisch, J., Resource depletion, peak minerals and the implications for sustainable resource management. Global Environmental Change, 2012, 22(3), 577-587.

Rawlings, D., Industrial practice and the biology of leaching of metals from ores The 1997 Pan Labs Lecture. Journal of industrial microbiology and biotechnology, 1998, 20(5), 268-274.

Rawlings, D.E., Dew, D., du Plessis, C., Biomineralization of metal-containing ores and concentrates. TRENDS in Biotechnology, 2003, 21(1), 38-44.

Rodrigues, W.J., Leal Filho, L.S., Masini, E.A., Hydrodynamic dimensionless parameters and their influence on flotation performance of coarse particles. Minerals Engineering, 2001, 14(9), 1047-1054.

Rodríguez, Y., Ballester, A., Blázquez, M.L., González, F., Muñoz, J.A., Study of bacterial attachment during the bioleaching of pyrite, chalcopyrite, and sphalerite. Geomicrobiology Journal, 2003, 20(2), 131-141.

Rosario, P., Hall, R., Grundy, M., Klein, B., A preliminary investigation into the feasibility of a novel HPGR-based circuit for hard, weathered ores containing clayish material. Minerals Engineering, 2011, 24(3-4), 290-302.

Rule, C.M., Minnaar, D.M., Sauermann, G.M., HPGR-revolution in platinum? Journal of the South African Institute of Mining and Metallurgy, 2009, 109(1), 23-30.

Sadrai, S., Meech, J., Ghomshei, M., Sassani, F., Tromans, D., Influence of impact velocity on fragmentation and the energy efficiency of comminution. International journal of impact engineering, 2006, 33(1), 723-734.

Sahyoun, C., N.A. Rowson, S.W. Kingman, L Groves, J.C. Dorfling, and S.M. Bradshaw, The Influence of Microwave Pre-Treatment on Copper Flotation Plant Performance. Transactions of SAIMM, 2005, 105(1), 7-17.

Salsman, J.B., Williamson, R.L., Tolley, W.K., Rice, D.A., Short-pulse microwave treatment of disseminated sulfide ores. Minerals Engineering, 1996, 9(1), 43-54.

Sand, W., Gerke, T., Hallmann, R., Schippers, A., Sulfur chemistry, biofilm, and the (in) direct attack mechanism—a critical evaluation of bacterial leaching. Applied Microbiology and Biotechnology, 1995, 43(6), 961-966.

Saramak, D., Kleiv, R.A., The effect of feed moisture on the comminution efficiency of HPGR circuits. Minerals Engineering, 2013, 43, 105-111.

Schmuhl, R., Smit, J.T., Marsh, J.H., The influence of microwave pre-treatment of the leach behaviour of disseminated sulphide ore. Hydrometallurgy, 2011, 108(3–4), 157-164.

Scott, G., 2006. Microwave pretreatment of a low grade copper ore to enhance milling perfomance and liberation, In *Department of Process Engineering*. Stellenbosch University, Stellenbosch.

Scott, G., Bradshaw, S.M., Eksteen, J.J., The effect of microwave pretreatment on the liberation of a copper carbonatite ore after milling. International Journal of Mineral Processing, 2008, 85(4), 121-128.

Sokić, M., Marković, B., Matković, V., Živković, D., Štrbac, N., Stojanović, J., Kinetics and mechanism of sphalerite leaching by sodium nitrate in sulphuric acid solution. Journal of Mining and Metallurgy, Section B: Metallurgy, 2012, 48(2), 185-195.

Solomon, N., Becker, M., Mainza, A., Petersen, J., Franzidis, J.P., Understanding the influence of HPGR on PGM flotation behavior using mineralogy. Minerals Engineering, 2011, 24(12), 1370-1377.

Sutton, W.H., 1993. Key issues in microwave process technology, In *Ceramic transactions: Microwaves. Theory and application in materials processing II. Volume 36*.

Sutton, W.H., Brooks, M.H., Chabinsky, I., 1988. Microwave processing of materials. Pittsburgh, PA (USA); Materials Research Society.

Suzuki, I., Microbial leaching of metals from sulfide minerals. Biotechnology advances, 2001, 19(2), 119-132.

Tavares, L.M., Particle weakening in high-pressure roll grinding. Minerals Engineering, 2005, 18(7), 651-657.

Thostenson, E., Chou, T.-W., Microwave processing: fundamentals and applications. Composites Part A: Applied Science and Manufacturing, 1999, 30(9), 1055-1071.

Tromans, D., Mineral comminution: Energy efficiency considerations. Minerals Engineering, 2008, 21(8), 613-620.

Tupikina, O., Ngoma, I., Minnaar, S., Harrison, S., Some aspects of the effect of pH and acid stress in heap bioleaching. Minerals Engineering, 2011, 24(11), 1209-1214.

Uslu, T., Atalay, Ü., Arol, A., Effect of microwave heating on magnetic separation of pyrite. Colloids and Surfaces A: Physicochemical and Engineering Aspects, 2003, 225(1), 161-167.

Veasey, T., Wills, B., Review of methods of improving mineral liberation. Minerals Engineering, 1991, 4(7), 747-752.

VGSTUDIO, 2010. Reference Manual VGStudio Max Release 2.0.

Vizcarra, T.G., Wightman, E.M., Johnson, N.W., Manlapig, E.V., The effect of breakage mechanism on the mineral liberation properties of sulphide ores. Minerals Engineering, 2010, 23(5), 374-382.

Von Hippel, A.R., *Dielectric materials and applications*. 1954, Artech House on Demand.

Vorster, W., Rowson, N., Kingman, S., The effect of microwave radiation upon the processing of Neves Corvo copper ore. International Journal of Mineral Processing, 2001a, 63(1), 29-44.

Vorster, W., Rowson, N.A., Kingman, S.W., The effect of microwave radiation upon the processing of Neves Corvo copper ore. International Journal of Mineral Processing, 2001b, 63(1), 29-44.

Walkiewicz, J., Kazonich, G., McGill, S., Microwave heating characteristics of selected minerals and compounds. Minerals and Metallurgical Processing, 1988, 5(1), 39-42.

Walkiewicz, J.W., Clark, A.E., McGill, S.L., Microwave-assisted grinding. Industry Applications, IEEE Transactions on, 1991, 27(2), 239-243.

Wang, G., Radziszewski, P., Ouellet, J., Particle modeling simulation of thermal effects on ore breakage. Computational Materials Science, 2008, 43(4), 892-901.

Wang, Y., Djordjevic, N., Thermal stress FEM analysis of rock with microwave energy. International Journal of Mineral Processing, 2014, 130, 74-81.

Wanne, T.S., Young, R.P., Bonded-particle modeling of thermally fractured granite. International Journal of Rock Mechanics and Mining Sciences, 2008, 45(5), 789-799.

Waters, K.E., Rowson, N.A., Greenwood, R.W., Williams, A.J., Characterising the effect of microwave radiation on the magnetic properties of pyrite. Separation and Purification Technology, 2007, 56(1), 9-17.

Watling, H., The bioleaching of sulphide minerals with emphasis on copper sulphides—a review. Hydrometallurgy, 2006, 84(1), 81-108.

Wen, S.B., Hsih, C.S., Kuan, C.C., The application of a mineral exposure model in a gold leaching operation. International Journal of Mineral Processing, 1996, 46(3–4), 215-230.

Whittles, D.N., Kingman, S.W., Reddish, D.J., Application of numerical modelling for prediction of the influence of power density on microwave-assisted breakage. International Journal of Mineral Processing, 2003, 68(1-4), 71-91.

Wills, B.A., *Wills' mineral processing technology: an introduction to the practical aspects of ore treatment and mineral recovery*. 2011, Butterworth-Heinemann.

Wills, B.A., Atkinson, K., Some observations on the fracture and liberation of mineral assemblies. Minerals Engineering, 1993, 6(7), 697-706.

Wong, L., Zhang, X.-P., Size Effects on Cracking Behavior of Flaw-Containing Specimens Under Compressive Loading. Rock Mechanics and Rock Engineering, 2013, 1-10.

Xingyu, L., Rongbo, S., Bowei, C., Biao, W., Jiankang, W., Bacterial community structure change during pyrite bioleaching process: effect of pH and aeration. Hydrometallurgy, 2009, 95(3), 267-272.

Xu, W., Dhawan, N., Lin, C.-L., Miller, J.D., Further study of grain boundary fracture in the breakage of single multiphase particles using X-ray microtomography procedures. Minerals Engineering, 2013, 46, 89-94.

Zhai, X., Fu, Y., Zhang, X., Ma, L., Xie, F., Intensification of sulphation and pressure acid leaching of nickel laterite by microwave radiation. Hydrometallurgy, 2009, 99(3–4), 189-193.

Zheng, Y., Wang, S., Feng, J., Ouyang, Z., Li, X., Measurement of the complex permittivity of dry rocks and minerals: application of polythene dilution method and Lichtenecker's mixture formulae. Geophysical Journal International, 2005, 163(3), 1195-1202.

Znamenáčková, I., Lovas, M., Mockovčiaková, A., Jakabský, Š., Briančin, J., Modification of magnetic properties of siderite ore by microwave energy. Separation and Purification Technology, 2005, 43(2), 169-174.

APPENDICES

Appendix A: List of publications and presentations arising from this study

1. Charikinya, E., Bradshaw, S., Becker, M., Characterising and quantifying microwave induced damage in coarse sphalerite ore particles. Minerals Engineering, 2015, 82, 14-24.
2. Charikinya, E., Bradshaw, S.M., Becker, M., 2014, Characterising and quantifying microwave induced damage in coarse sphalerite ore rocks, Process Mineralogy Conference, 9-11 November, Cape Town, South Africa
3. Charikinya, E., Bradshaw, S.M., 2014, Use of X-ray computed tomography to investigate microwave induced cracks in sphalerite ore particles, XXVII International Mineral Processing Congress, 20-14 October, Santiago, Chile, (229-238)
4. Charikinya, E., Bradshaw, S.M., Akdogan, G., 2014, Effects of model resolution on Bonded Particle Modelling of microwave induced cracks in sulphide ore particles, 9th South African Conference on Computational and Applied Mechanics, 21-24 September, Cape Town, South Africa,(s.a),ISBN: 978-0-620-58994-9
5. Charikinya, E., Bradshaw, S.M., du Plessis, A., 2014, X-ray computed tomography visualisation and quantification of microwave induced cracks in particles, The 21st General Meeting of the International Mineralogical Association, 1-5 September, Johannesburg, South Africa.
6. Charikinya, E., Bradshaw, S.M., Akdogan, G., 2013, Bonded particle modelling of microwave induced fracture: PFC3D/ PFC2D simulations, Southern African Institute of Mining & Metallurgy (SAIMM) Mineral Processing Conference, 6-8 August, Cape Town.
7. Charikinya, E., Bradshaw, S.M., Akdogan, G., 2014, Bonded particle modelling of microwave induced fracture: study of effects of model resolution on microwave induced particle damage, SAIMM Mineral Processing Conference, 4-6 August, Cape Town.
8. Charikinya, E., Bradshaw, S.M., 2014, Use of X-ray computed tomography to investigate the potential application of microwave assisted preparation of heap leaching feed ore, SAIMM Mineral Processing Conference, 4-6 August, Cape Town.
9. Charikinya, E., Bradshaw, S.M., 2015, Particle damage and exposure analysis of microwave treated ores for bio-heap leaching, SAIMM Mineral Processing Conference, 6-7 August, Cape Town.
10. Charikinya, E., Bradshaw, S.M., 2015, Microwave assisted preparation of bio-heap leaching feed ore: modelling and experimental studies, South Africa National Imaging with Radiation conference (IMGRAD), 10-11 September, Stellenbosch

Appendix B: Power density and Energy input calculation examples

Minerals	%	Densities (kg/m^3)
Pyrite	39%	5010
Sphalerite	16%	4050
Quartz	46%	2620
	100%	

Mass of microwave treated ore sample = 0.06kg

Absorbent phase percentage = 54%

Mass of absorbing phase = 0.0324 kg

Forward power = 6.00 kW

Reflected power = 1.12 kW

$$Power\ density\ \left(\frac{W}{m^3}\right) = \frac{(Forward\ power - Reflected\ power)}{Volume\ of\ abs\ sample}$$

$$Avg\ density\ of\ abs\ phase\ \left(\frac{kg}{m^3_{abs}}\right) = (71\%(Py).5010 \times 29\%(Sph).4050)\left(\frac{kg}{m^3}\right)$$

$$Volme\ of\ absorbent\ phase\ (m^3) = \frac{Absorbent\ phase\ (kg)}{Average\ density\ of\ absorbent\ phase\ (kg/m^3_{abs})}$$

$$= 6.85 \times 10^{-6}(m^3_{abs})$$

$$Power\ density\ \left(\frac{W}{m^3_{abs}}\right) = \frac{4.87\ \times 1000W}{6.85\ \times\ 10^{-6}m^3_{abs}} =\ 7.11\ \times\ 10^8\left(\frac{W}{m^3_{abs}}\right)$$

The specific energy input is then calculated as:

$$P_{in} = 4.87\ kW$$

$$t = 1.00\ s$$

$$\rho_{ore} = \frac{mass\ of\ ore\ sample}{Volume\ of\ sample\ holder}$$

$$Volume\ of\ sample\ holder = 0.0000385\ m^3$$

$$E_{in\ (ore)} = \left(\frac{P_{in} \times t}{3600\ s \times Volume_{ore} \times\ \rho_{ore}}\right)\left(\frac{kWh}{ton}\right) =\ 2.82\ \left(\frac{kWh}{ton}\right)$$

Appendix C: VG Studio Max 2.1 defect analysis algorithm

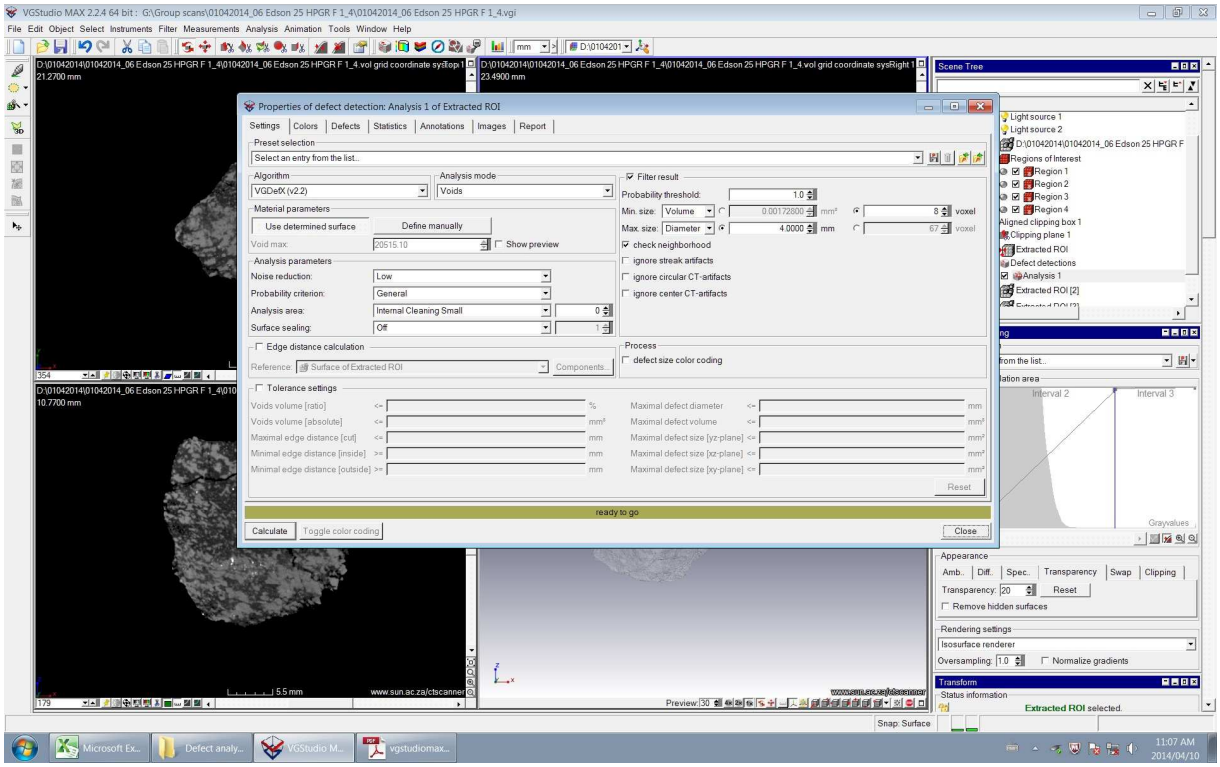

Screen shot of defect analysis algorithm input parameters required in VG Studio Max

Appendix D: Solution concentrations of the metals from gangue minerals

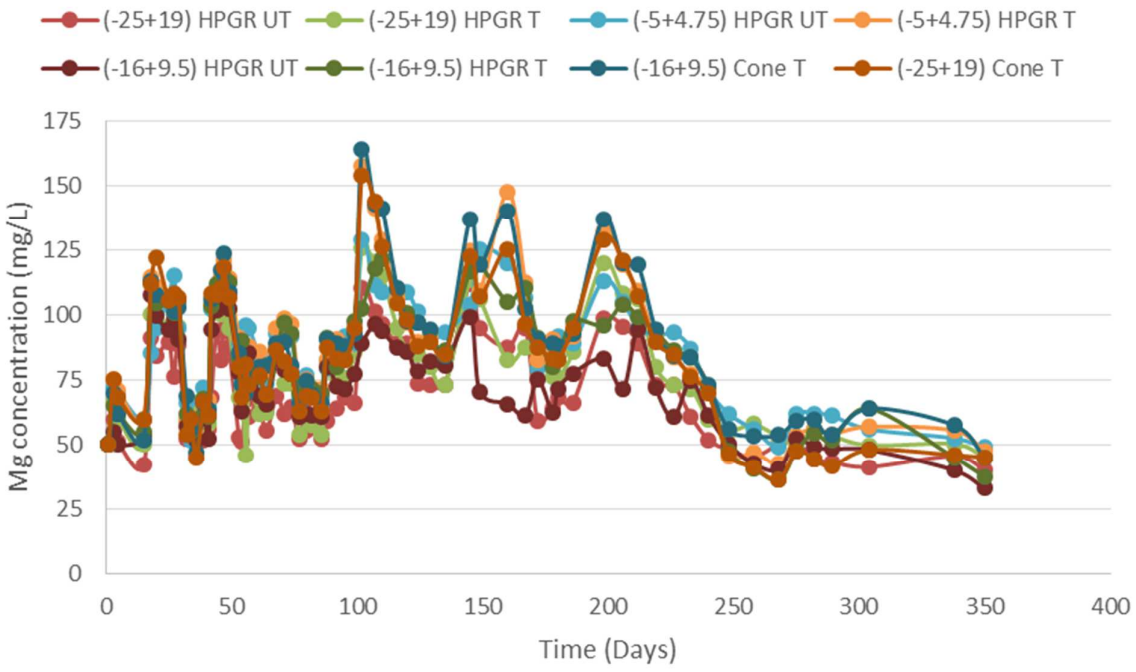

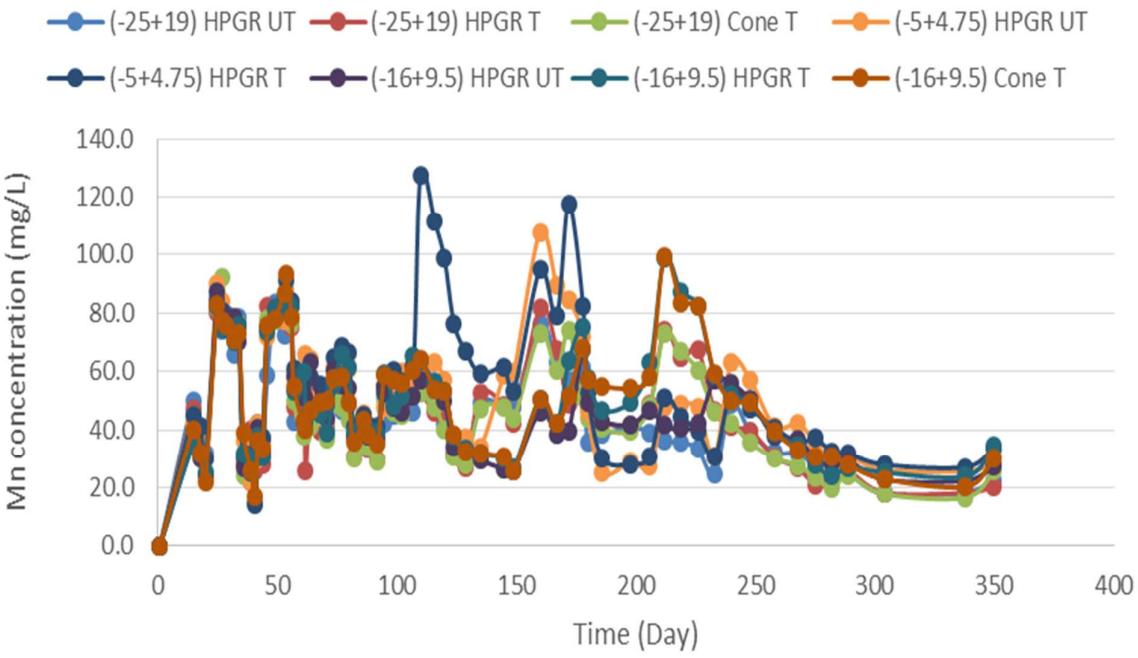

Solution concentrations of the metals from gangue minerals, a. Magnesium, b. Manganate, in the PLS from all reactors

Appendix E: QEMSCAN and SEM images of leach residue

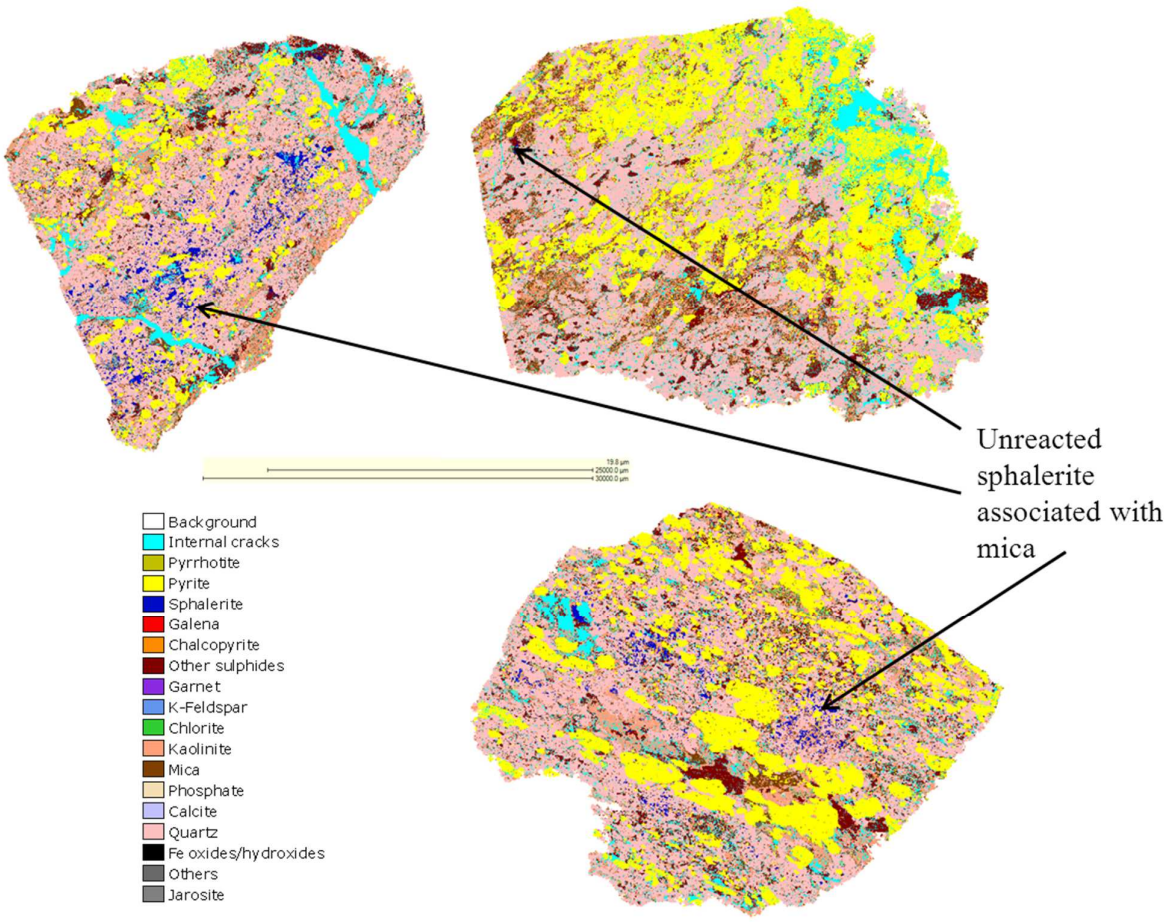

QEMSCAN image of three HPGR (-25+19) mm microwave treated leached particles showing unreacted sphalerite grains

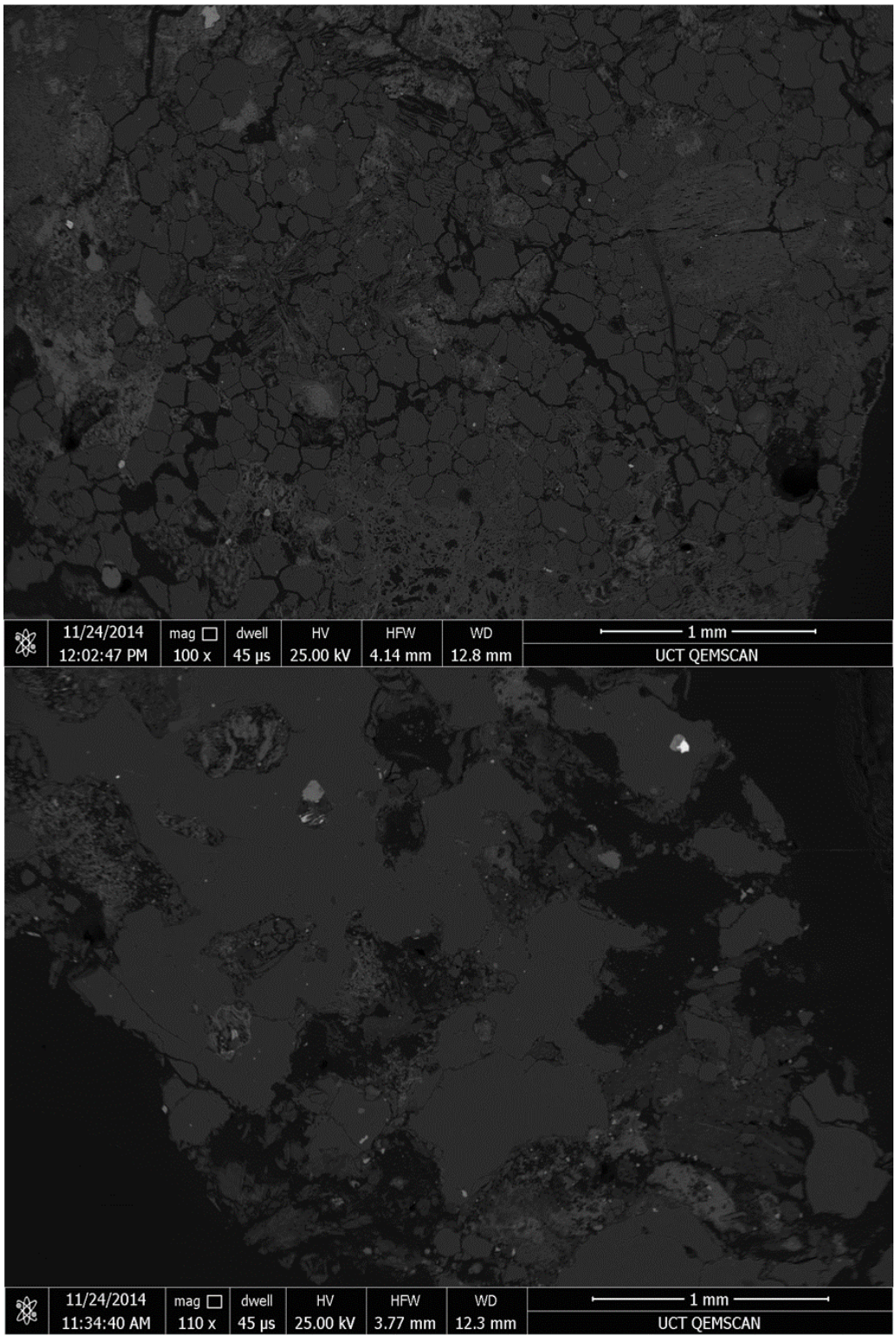

SEM microphotographs showing leached microwave treated small HPGR (-5+4.75) mm particles

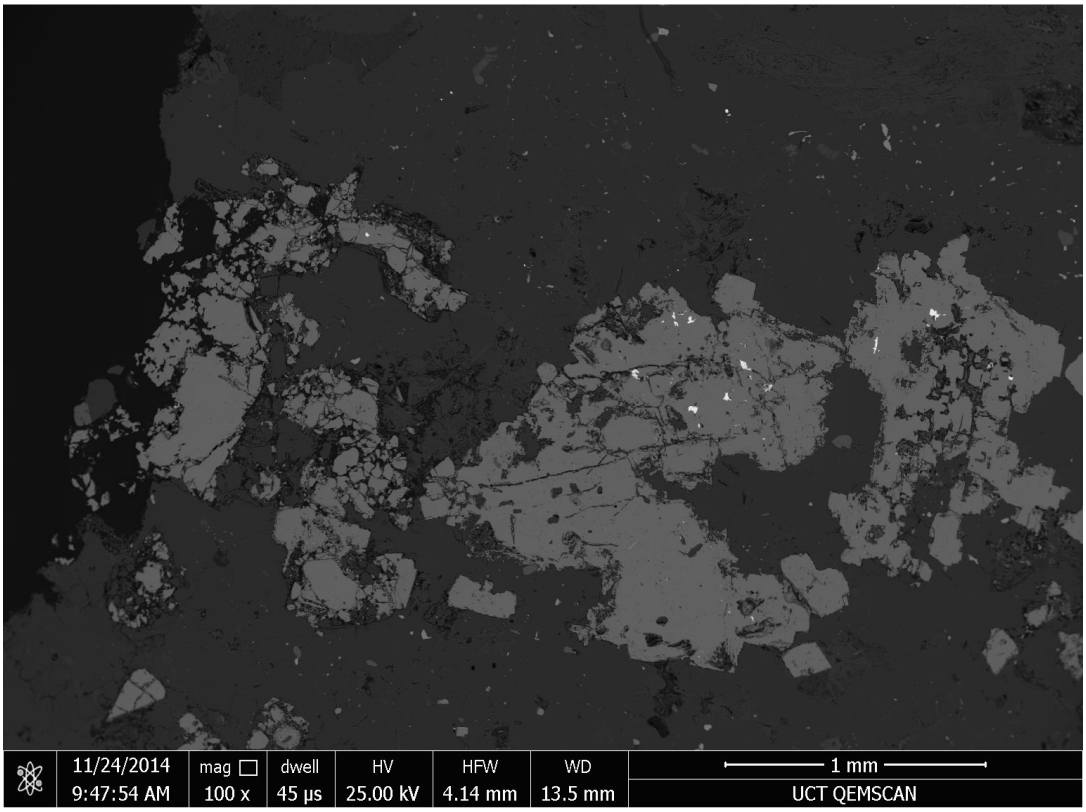

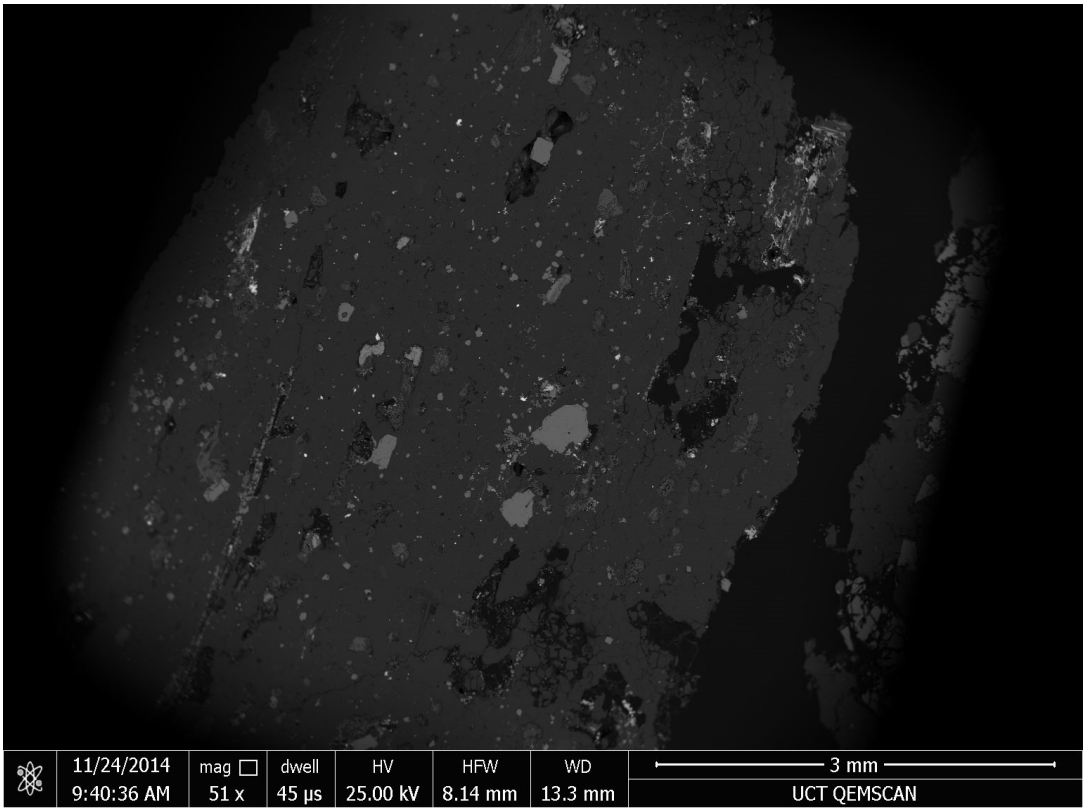

SEM microphotographs showing leached microwave untreated small HPGR (-5+4.75) mm particles

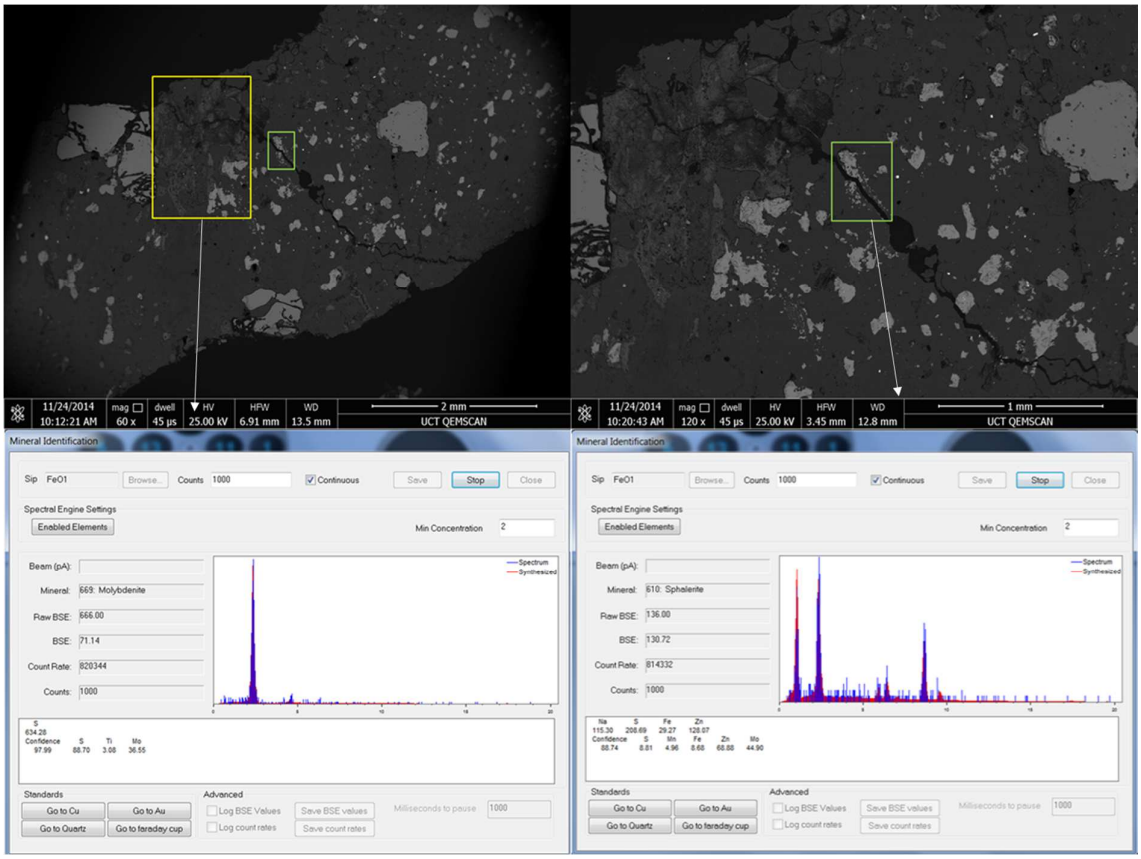

SEM images of leach residue with elemental maps of highlighted sections

Appendix F: Statistical analysis of effect of absorbent phase content on crack damage

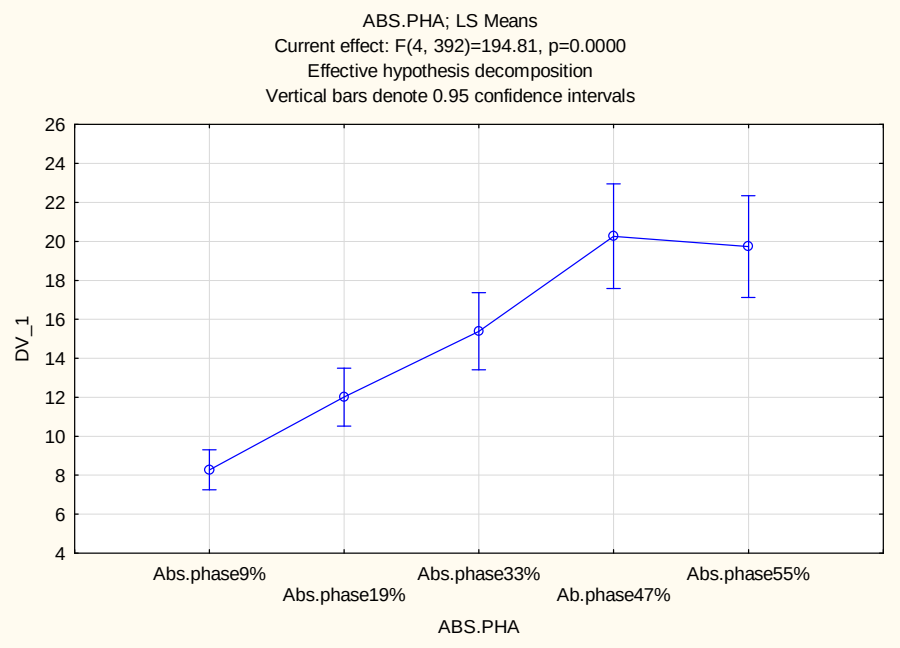

Least squares mean of crack damage over absorbent phase content (power density of 1 x 10^{10} W/m^3_{abs})

Crack damage unweighted means

Cell No.	ABS.PHA; Unweighted Means (PFC2D Results-summary) Current effect: F(4, 392)=194.81, p=0.0000 Effective hypothesis decomposition ABS.PHA	DV_1 Mean	DV_1 Std.Err.	DV_1 -95.00%	DV_1 +95.00%	N
1	Abs.phase9%	8.27714	0.515727	7.25370	9.30058	99
2	Abs.phase19%	12.00888	0.749662	10.52120	13.49655	99
3	Abs.phase33%	15.38711	0.995098	13.41237	17.36185	99
4	Ab.phase47%	20.25812	1.352136	17.57486	22.94139	99
5	Abs.phase55%	19.73365	1.315996	17.12210	22.34520	99

Repeated measures analysis of variance

Effect	Repeated Measures Analysis of Variance (PFC2D Results-summary) Sigma-restricted parameterization Effective hypothesis decomposition SS	Degr. of Freedom	MS	F	p
Intercept	113358.5	1	113358.5	236.4260	0.00
Error	46987.8	98	479.5		
ABS_PHAS	10321.8	4	2580.4	194.8060	0.00
Error	5192.5	392	13.2		

Benferroni test results

Cell No.	Bonferroni test; variable DV_1 (PFC2D Results-summary) Probabilities for Post Hoc Tests Error: Within MS = 13.246, df = 392.00 ABS.PHA	{1} 8.2771	{2} 12.009	{3} 15.387	{4} 20.258	{5} 19.734
1	Abs.phase9%		0.000000	0.000000	0.000000	0.000000
2	Abs.phase19%	0.000000		0.000000	0.000000	0.000000
3	Abs.phase33%	0.000000	0.000000		0.000000	0.000000
4	Ab.phase47%	0.000000	0.000000	0.000000		1.000000
5	Abs.phase55%	0.000000	0.000000	0.000000	1.000000	